Design of Photo-Switchable Self-Assembled Monolayers for the Study of Protein-Receptor Interactions

by

Scott Charlesworth

9/27/2011

A thesis submitted to

The University of Birmingham

For the degree of

Doctor of Philosophy

School of Chemistry

College of Physical Sciences and Engineering

September 2011

This thesis is dedicated to my mother who taught me the value of education. Without her influence my PhD would not have happened. Mum - this is your PhD as much as it is mine, thank you so much...

Acknowledgements

First and foremost I would like to thank Professor Jon Preece and Dr Paula Mendes for giving me the chance to do my PhD and for all their help, guidance and patience, for which I am deeply grateful.

I would also like to thank all members of the Preece and Mendes research groups, past and present, In particular I would like to mention: James Bowen, Parvez Iqbal and Manikam who were there for me throughout my research; Simon Leigh, Coen van den Brom, Brenda Long and Sara Diegoli who helped me starting out and last but no means least Paul Yeung whom I have known since being a undergraduate. All of you have contributed considerably to my progress for which I'm deeply grateful, Thank you all very much.

I would also like to thank all the people behind the scenes: Peter Ashton, Nick May and Leanne Hill (Mass Spectroscopy and Elemental Analysis), Neil Spencer (NMR Spectroscopy), Graham Burns (HPLC) Danny Long, Graham Beamson (XPS) Stuart Arkless, Pam Marshall, Lyn Blake, Sarah Horswell and Anna Walkiewicz for all their help.

Abstract

Nano-biotechnology combines recent advances in nanotechnology with biology. It is a relatively new discipline and full of promise. One such promise is the elucidation of complex bio-molecular reactions and interactions, the elucidation of which requires the development of reliable *in-vitro* models. Such models could be developed through the use of self-assembled monolayer's (SAMs). Research into this competitive field has already started and there is currently a call to develop SAMs which present specific bio-molecules in a switchable fashion; switchable SAMs can have their surface properties switched between two states, *i.e.* they can be switched *'on'* or *'off'*. Such switch-ability would help such models mimic the real time changes of the bodies' bio-chemistry and is a vital development. This thesis addresses this current research need, through the employment of azobenzene based SAMs.

Currently the switch-ability (isomerisation) of numerous azobenzene SAMs has been shown to be hindered by a lack of inter-surfactant space. This hindrance to isomerisation is addressed in Chapter 4. While Chapter 5 explores the design of an azobenzene based photo-switchable SAM, for use as *in-vitro* model for the study of bio-molecular interactions. The two chapters are not directly related and future work would aim to bring the findings together.

The thesis is split into 6 chapters: Chapter one provides an introduction giving a detailed description of SAMs; Chapter two gives details of the surface characterisation techniques employed throughout this research (Ellipsometry, contact angle, X-ray photoelectron spectroscopy, UV/Vis spectroscopy and Surface Plasmon resonance spectroscopy); Chapter three discusses the synthetic routes used to synthesis SAM surfactants; Chapter four, explores the effect that a novel head group has upon the isomerisation of azobenzene within SAMs; Chapter five presents progress with respect to the development of an azobenzene based photoswitchable SAM, as an *in-vitro* model for the study of bio-molecular interactions; Finally Chapter six list the details of experimental procedures.

1.0 Introduction: Nano-science: a short history

Nano-science[1] concerns the study and manipulation of systems or objects in which at least one dimension is between 1-100 nm in length. This relatively new discipline was initially discussed in 1959 by Richard Feynman, when he delivered a lecture[2] entitled *'There's plenty of room at the bottom'*. In this famous lecture, Feynman postulated that the manipulation of matter on the atomic scale was possible and he used physical calculations to illustrate, for example, that it is theoretically possible to rewrite the world's literature on a piece of dust:

"It turns out that all of the information that man has carefully accumulated in all the books in the world can be written in this form (information content in a code of dots and dashes) in a cube of material one two-hundredth of an inch wide, which is the barest piece of dust that can be made out by the human eye. So there is plenty of room at the bottom!"[2]

Although Feynman did not suggest how this might be achieved, his famous lecture inaugurated a new area of scientific research. To facilitate the study of this new area of research, Feynman stressed that the precision of existing analytical techniques, such as the electron microscope, must be improved. He postulated that such improvements to analytical tools would be made by physicists and in turn tested by scientists of other disciplines. This interdisciplinary collaboration was used to illustrate the requirement of a multidisciplinary team based approach to nanoscientific research. He also highlighted the need to consider potential challenges of scale, which he correctly envisaged would arise in the study of such small systems,[3] since defects or deviations from the bulk structure would logically become much more prominent.

It has been fifty-two years since Feynman's famous lecture and great progress, within this multidisciplinary field, has been achieved. The multidisciplinary research area of nanoscience is now well established and supported by governments worldwide. Governments of many European countries as well as America, China, Japan, Korea and others have funded national centres of excellence to support nano scientific research.[4] Furthermore thanks to nanoscientific research, a nanotechnological revolution is upon us. Evidence can be seen through simple comparison of the advances in electronic consumables over the last 5-10 years: from cassette tape Walkmans to 80 GB I-Pods; from mobile phones to smart phones and from 16 to 122 bit video games consoles. Such technological advances are huge and its all fundamentally thanks to nanoscientific research, which underpins advances in nanotechnology.

It is worth mentioning that well before Feynman's speech sparked a surge of interest in research into the area of nanoscience, nanoscientific phenomena had been observed, exploited, and reported long before his speech; for example in western literature, as early as the 18th century, Benjamin Franklin observed the calming effect of oil on water[5] Then nearly a century later Lord Rayleigh calculated Franklin's oil layers to be 1.6 nm thick.[6] Shortly after this Agnes Pockles studied the variation of surface tension, with the work being published by Rayleigh in Nature, in 1891.[7] This early monolayer work laid the ground for discovery of Langmuir-Blodgett layers,[8] the predecessors of self-assembled monolayers (SAMs).

1.1 Self-assembled monolayers (SAMs)

1.1.1 A brief history self-assembled monolayers

Observations of SAMs were first recorded in the literature mid 20th century.[9, 10, 11] However, it was not until the early 1980s[9,1,12,13] that research into SAMs really began.

Initially, most literature focused on the formation of organosulphur SAMs on gold or silver. This early work established the basic structural models, formation thermodynamics and preparation protocols of SAMs. The majority of this early research was published between 1983-93.[1] Post 1993, research branched out to the study of both new and non-planar substrates,[1] as well as new surfactant systems. One new class of surfactants, which has emerged over the last decade or so, are those which contain switchable units. Switchable units react to some external stimuli[14] which switches the SAM surfactants between two different chemical states. These two different chemical states give the SAM different surface properties.

1.1.2 A detailed account of self-assembled monolayers

SAMs[1,6,15] (**Figure 1.1**) are formed from the spontaneous adsorption of surfactant molecules on the plane of a solid substrate, to give a two-dimensional (2D) molecular assembly.[10, 15, 16, 17] The assembly is a densely packed quasi crystalline array of surfactant molecules. Surfactants lie at a tilt angle from the surface normal and are chemically bound to the substrate through chemisorption. Relatively strong chemisorption, can make modified surfaces relatively durable under ambient conditions. Furthermore, careful design of the surfactant molecules allows for the tailoring of SAM properties, such as thickness, structure, surface energy and stability.[15,18,19]

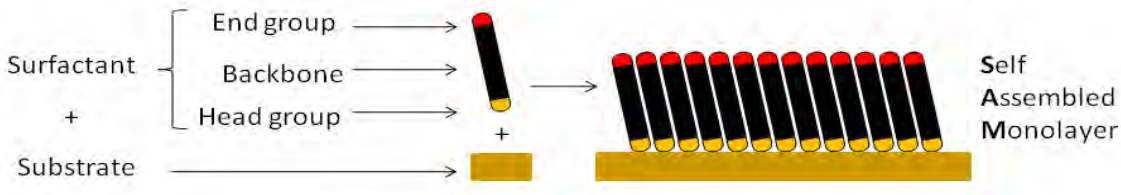

Figure 1.1 A cartoon representation of a self-assembled monolayer (SAM) which are composed of a 2D molecular assembly of surfactant molecules chemically adsorbed, in a perpendicular fashion, on top of a solid substrate. The surfactant is composed of three parts: end group, backbone and head group.

1.1.2.1 SAM components

SAMs are composed of surfactant molecules and a solid substrate (**Figure 1.1**). Both the substrate and surfactant nature influence SAM properties. Particular substrates are generally used to make SAMs from a particular class of surfactants. Various substrate-surfactant systems exist. The two (model) substrate-surfactant systems that have been the most widely studied are, thiol surfactants on gold (Au)[15] and silane surfactants on silica (SiO_2)[15] These two substrate-surfactant systems have become archetypal. Other common substrate/surfactant systems include: silanes on indium tin oxide;[20] amines[21] on platinum and carboxylic acids on both aluminium oxide[22] and silver.[23]

1.1.2.2 Surfactant

SAM surfactants[15] consist of three domains: 1) head group, 2) backbone, 3) end group. These domains are explained below, along with their effect on SAM structure. Generally surfactants are classified by the nature of the head group and backbone, for example alkyl thiols and alkyl silanes.

1.1.2.3 Surfactant head group

The head group '*anchors*' the surfactant to the substrate surface through chemisorption.[8, 9, 15] Chemisorption is exothermic and may be either covalent or ionic depending on the head group's nature. Common head groups include sulphur and silanes.[15] Different head groups have varied affinities for particular substrates.

Head groups have been shown to effect the overall molecular ordering within SAMs. For example, the use of thioacetates[24] reduces order, resulting in a striped phase SAM

(backbone parallel to surface) while the use of selenium,[25] instead of thiol, has been shown to increase order of aromatic SAMs.

1.1.2.4 Surfactant backbone

The backbone is the middle part of the surfactant and separates the head group from the end group. The backbone orientation (**Figure 1.2**) is defined by three angles.[9, 15] Firstly the backbone lies at a tilt angle (α) normal to the plane of the substrate surface, further to this tilt there is an angular twist (β) of the backbone plane about the surfactants molecular axis and thirdly there is an angle of precession (ω) which defines the direction of molecular tilt.

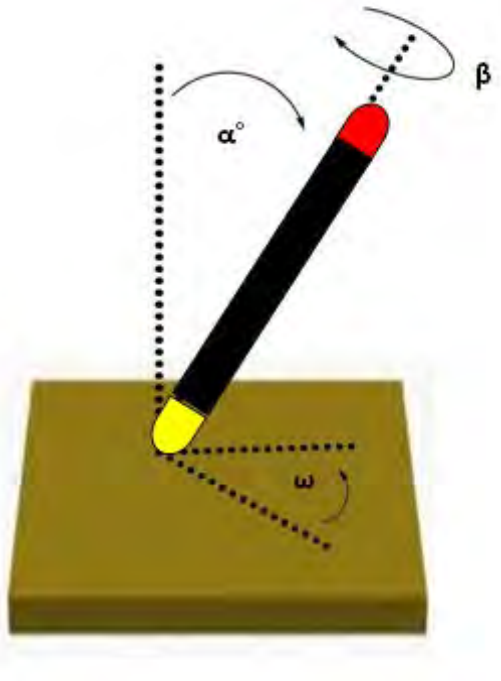

Figure 1.2 Cartoon representation of backbone orientation angles of SAM surfactants. The backbone orientation can be described by three different angles: α - The tilt angle from the surface normal; β - The angular twist of the backbone and ω - The direction of the tilt.

The backbone can be either hydrophobic or hydrophilic in nature. The nature and length of the backbone depends upon the target SAM and its application. The nature and length[26] of the surfactant can profoundly influence the molecular ordering and thermal stability[27] of SAMs. Molecular ordering within SAMs is promoted, mainly but not exclusively, by intermolecular backbone interactions, which generally produce a quasi crystalline structure. Intermolecular interactions and hence the crystallinity of the SAM are dependent on the length and nature of surfactant backbone. Intermolecular van der Waals forces are typically the most common and important of these intermolecular interactions. Due to these van der Waals forces, alkyl backbone chains with a length ≥ 10 carbon units, have been shown to have crystal like periodicity[28] in gold-thiol SAMs. Depending on the nature of the backbone other, non van der Waals, intermolecular interactions (*e.g.* electrostatics, π-π interactions, etc) may be present.[25] Inevitably all intermolecular forces present have an effect on the SAMs stability and molecular ordering. For example, the incorporation of bulky polar substituents such as oxygen leads to adoption of relatively disordered molecular conformations.[29]

The backbone is also important in the isolation of the end group from the influence of the substrate. Substrate isolation requires that the backbone be of sufficient length. For example, a length of more than 10 carbon units for alkyl thiols on gold[30] is sufficient to ensure isolation of the end group wettabilty from the substrate.

1.1.2.5 Surfactant end group

The end group lies at the SAM/air interface and its functionality generally defines the SAM surface properties. End group functionalities depend on the SAM application. The exact effect of end groups on the overall molecular ordering of SAMs is still unclear.[31] Although generally, the introduction of end groups other than methylene decreases the overall order of the structure. However, end groups that are able to form hydrogen

bonds (COOH and OH) have been shown to promote order when the backbone is small.[31]

The ordering of the end group domain itself has been shown to depend upon their nature. Some end groups have been shown to form ordered structures, for example azobenzene, within alkyl thiols.[32] However, within such SAMs the ordering of the end groups results in a disordering of the underlying backbone structure. Furthermore, end group order can be effected by SAM preparation conditions and even solvent washing post SAM formation, as is the case of thioctic acid SAMs[33] made in the presence of acetic acid. Post formation of these SAMs the carboxyl group planes lie at 38° from the surface plane, however, upon washing with aqueous KOH the carboxyl group deprotonates and adopts a more upright conformation in which the carboxyl planes lie at 66° to the surface plane.

In recent years, SAMs have been developed with switchable chemical functionalities.[34] Such functional switchability (usually '*on*' and '*off*') often, but not exclusively, depends on switching the end group between two states. Switching between these two states is initiated by some external stimuli such as light, temperature, pH, chemical or electrical charge, which either changes the molecular conformation or part of the chemical nature of the SAM surfactants.[34] Such switchable chemical functionalities have also been applied to research areas other than SAMs.[35]

1.1.2.6 Substrate

The natureof the substrate can affect the properties of SAMs.[36] The substrate presents valence sites for the chemisorption of the surfactants head group. Valence sites are

defined by both the topography and nature of the substrate.[37] Both the substrate nature and topology can affect the intermolecular structure of SAMs.[37]

For example, SAMs formed from identical surfactants on Au and Ag can have different intermolecular structures.[38, 39, 40] Differences in intermolecular structure are seen for n-alkylthiol SAMs on Au and Ag. On Au the C-S bond is almost parallel to the Au surface[40] and the tilt angle is ≈ 30°.[39] However, on Ag the C-S bond is perpendicular to the Ag surface,[40] and the tilt angle of surfactants is ≈ 12°.[39] These differences are caused by differences in the S-metal bonding which in turn affects the tilt. Furthermore, the packing density of SAMs on Ag is higher than Au.[38]

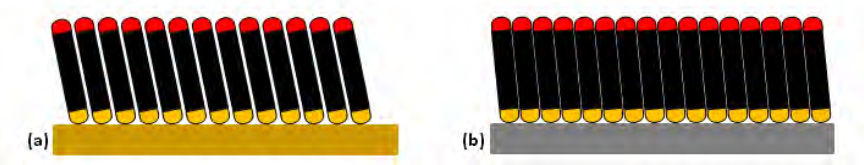

Figure 1.3 Cartoon representation of the influence of substrate on the tilt angel of alkane thiol SAMs (**a**) Au substrate on which alkyl thiol SAM surfactants lie tilted 30° from the surface normal (**b**) Ag substrate on which alkyl thiol SAM surfactants lie tilted at 12° to the surface normal.

The difference in the tilt angle of SAMs, between the two substrates influences the orientation of the surface end group, which can effects the surface properties. For example, with Oligo(ethyleneglycol) (OEG) thiol SAMs on Au and Ag. On Au OEG SAMs have been widely shown to resist non-specific protein adsorption.[41] However, OEG SAMs on Ag do not resist non-specific protein adsorption owing to the close packing intermolecular structure of such SAMs.[42] On Ag the surfactants sit normal to the substrate in an all trans conformation, whereas on gold the backbone adopts a helical

amorphous structure[42] which resists protein absorption much more effectively, due to the absorption of water.[43]

However and despite the above examples, differences between SAMs on different substrates do not always occur. SAMs with identical intermolecular structures can be formed on Au and Ag if packing is determined by the surfactant nature, as is the case for some aromatic surfactants.[38]

1.1.2.6.1 Gold (Au) as a substrate

Sulphur compounds have been found to bind strongly to Au, Ag Cu and Pt substrates.[15] Of these substrates, Au has received the most attention for several reasons: SAMs on Au are highly organised, easy to prepare and easy to analyse.[44] Atomically flat Au substrates can be easily prepared, thus allowing the use of a vast number of analytical surface techniques.[44] In addition Au desirably 'lacks' a stable oxide, remaining in a oxidation state of (0), thus pre-prepared surfaces (cleaned) can be handled in ambient conditions.[44] Under ambient conditions other metal substrates form oxide layers, thus complicating SAM preparation on such surfaces.

1.1.2.6.2 Silica (SiO_2) as a substrate

Silane compounds form strong bonds with hydroxylated surfaces. The most widely studied system is silanes on SiO_2 due, mainly, because SiO_2 is the base material of the microelectronics industry which itself was a major contributor to early SAM research.[45] SAMs of silanes have also been formed on gold[46] although are not widely studied.

Relative to thiols on Au, silane SAMs on SiO_2 are stronger bound[47] to the substrate, but less ordered.[47] These contrasts are due to the irreversible cross-polymerisation of silanes at the substrate-surfactant interface. The structural order of silane SAMs is defined by the degree of polymerisation of silane head groups at the substrate surface.[48] The substrate does not directly affect order, however, the degree of substrate hydration can limit the degree of polymerisation.[48] Polymerisation makes silane SAMs on SiO_2 generally more chemically, thermally and mechanically stable[47] relative to thiol SAMs on Au. Increased stability allows for extensive synthetic modification, post SAM formation.[47]

Despite the increased stability of silane SAMs, their formation is complicated by the inherent instability of silanes. Silanes are much more reactive than sulphur compounds. For example, silanes are prone to water induced polymerisation,[15] thus making the preparation of silane SAMs more challenging than thiol SAMs.

1.1.3 Self-assembled monolayer formation of thiol based SAMs

The discussion now focuses on the formation of sulphur based SAMs. Sulphur based SAMs can be formed from surfactants in either solution or vapour phase.[49] The formation process is the same regardless of the phase. Prior to SAM formation surfactants must diffuse to the substrate surface. Post diffusion SAM formation is initiated. Formation is generally thought to be a four step process (**Figure 1.4**) which ultimately equilibrates in the formation of a stable and relatively ordered closely packed molecular assembly:[15]

1. The first step of SAM formation (post diffusion of surfactant to surface) is physisorption of surfactants. The surfactant molecules now lie parallel to the substrate due to attractive physical forces.
2. Secondly, chemisorption occurs as the surfactant head group forms a chemical bond (covalent or ionic) with the substrate. As a result, the surfactants start to '*stand up'*.
3. Thirdly, as the fraction of chemisorbed surfactants increases adsorbates start to reorganise forming islands. Reorganisation and island formation is promoted by intermolecular interactions of surfactants, such as van der Waals and other electrostatic forces. This process eventually leads to the formation of a fully formed SAM.
4. Finally, after initial SAM formation, more ordering may take place over days or even months.

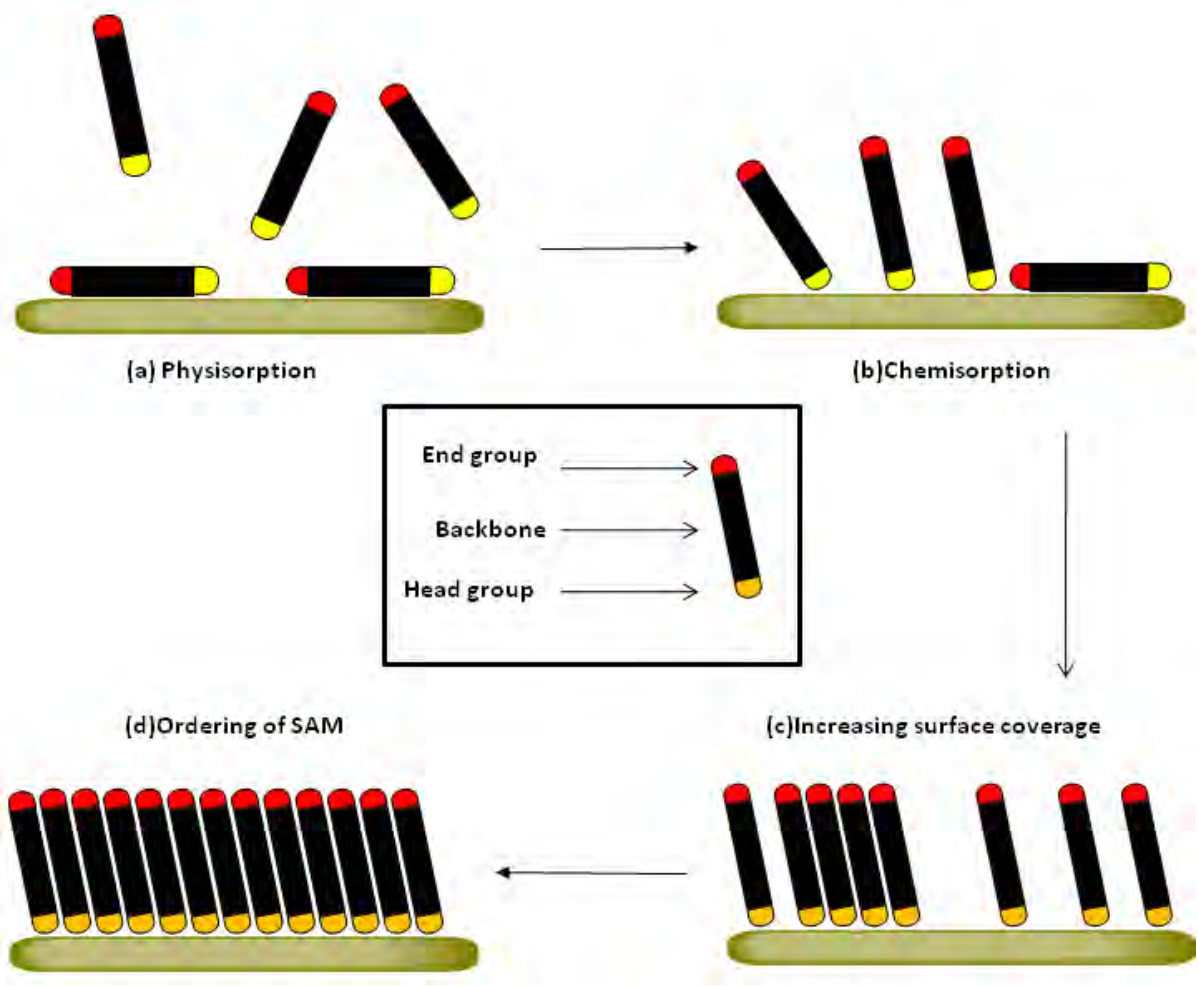

Figure 1.4 A cartoon representation of SAM formation involving the four steps described above (a) Physisorption of surfactants to the substrates surface (b) Chemisoprtion of head group to the substrate (c) Increasing surface coverage of surfactants, which ultimately results in them standing up, owing to intermolecular interactions (d) Final ordering of fully formed SAM.

1.1.3.1 Formation energetics of thiol based SAMs

For a full description of SAM formation, it is important also to consider the associated energy changes.[9] These energy changes are shown in a schematic in **Figure 1.5**. The schematic shows that the absorption (ΔE_{ads}) of the surfactant onto the substrate surface is the main change in energy. This large energy change is dependent upon both the surfactant physisorption energy and chemisorption energy. Post chemisorption, surfactants have some surface motility, importantly the energy barrier (ΔE_{corr}) to this motility is low (at least on a relatively flat surface) thus facilitating the close packing of surfactants. As packing of surfactants increases (due to increasing concentration of surfactants on surface) the backbones come into close enough proximity for the manifestation of a 3rd energy change ($\Delta E_{IM} = \Delta E_{vdW}$ + other intermolecular interactions) which occurs through intermolecular interactions. Of these intermolecular interactions van der Waals forces are the most common. However, others may operate depending on the nature of the backbone. Finally there is some energy changes associated with defects such as gauche conformations (ΔEg) within surfactants.

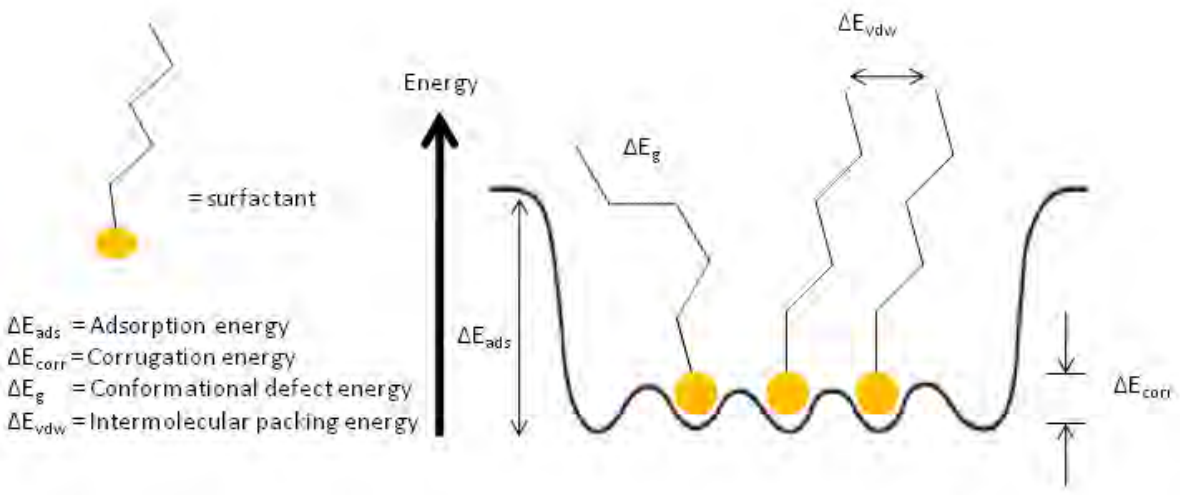

Figure 1.5. Schematic of some energetic changes associated with SAM formation. The biggest energy change is the adsorption energy (ΔEads) associated with the physisorption and chemisoprtion energies. The van der Waals energy (ΔE_{vdW}) contributes to the intermolecular energy (ΔE_{IM}) between SAM surfactants and in the case of alkane thiols is the biggest contributor. The corrugation energy (ΔE_{corr}) is the energy required for SAMs to move between valence sites, its relatively low value allows for the close packing of surfactants as surface concentration increases. The conformational defect energy (ΔE_g) reduces the Gibbs free energy of the system.

SAM formation and the associated energy changes are also dependent on experimental parameters such as: temperature,[50] solvent,[51] acidity,[52] surfactant nature,[53] surfactant concentration,[50] substrate nature,[54] substrate topology,[54] substrate immersion time,[55] substrate cleaning method,[56] and preparation protocol.[53]

The above explanation of SAM formation and associated energy changes are applicable to SAMs in general, however, the actual mechanism maybe more complicated and various mathematical models of formation have been devised.[9] The most simple and well known is the Langmuir model.[9] Other formation models exist, such as the Kisliuk and Frumkin mechanisms,[9] which are both modifications of the Langmuir model taking adsorbate-adsorbate interactions into account. For example, azobenzene SAMs have

been suggested to form through the Frumkin mechanism, as surfactants interact through π-π interactions which affect the formation process.

1.1.3.2 The Gold-Thiolate Bond

Post physisorption of the surfactant to the gold surface, chemisorptions occurs resulting in the formation of a strong, covalent gold-thiolate bond. However, the exact mechanism of this bond formation is not yet understood.[57] Despite this gap in our understanding, it is believed that for thiols the reaction occurs via oxidative adsorption, of R-SH to the metallic surface. However, it is not known if the reaction involves an ion, radical or other species,[57] and furthermore, the fate of hydrogen is yet to be established.

For organosulphur SAMs on gold, a variety of gold-thiolate lattices have been observed.[63] Lattices may be effected by surfactant nature[58] and/or the quality of underlying gold.[59] Despite this variety of lattices, there is a general consensus that, for the majority of SAMs on Au (111) the bonding results in a (√3 X √3) R30° lattice (**Figure 1.6a**). This (√3 X √3) R30° can transform to a c(4 x 2) super lattice (**Figure 1.6a**) due to the secondary ordering, promoted by inter-surfactant interactions.[60] Several c(4x2) super lattice phases are known to co-exist and depend up on chain length and surface defects.[61]

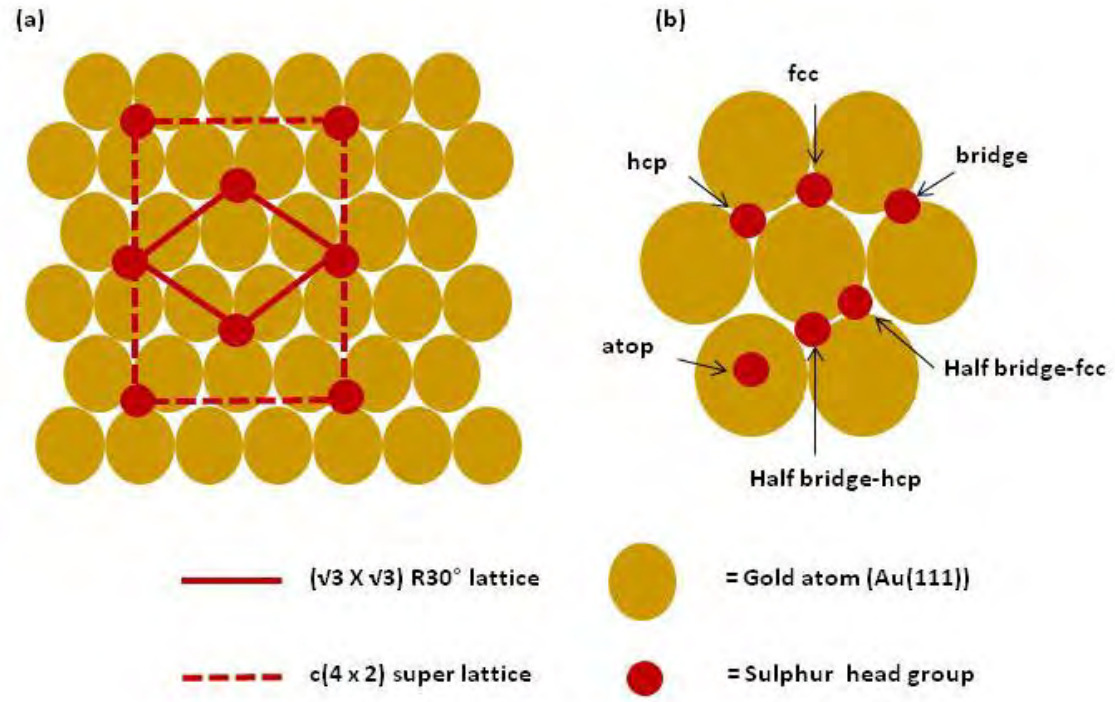

Figure 1.6 (a) schematic showing the (√3 X √3) R30° lattice and the c(4 x 2) super lattice on a Au(111) surface (**b)** Diagram showing the possible positions of sulphur on the Au(111) surface. Note sulphur atoms are not drawn to scale.

Although this general consensus - with respect to lattice structure - has been reached the actual position of the thiolate species on the Au surface is not clear and the binding models of both lattices remain speculative.[62] Possible binding positions are shown in **Figure 1.6b**. Within the (√3 X √3) R30° lattice on unreconstructed Au(111) it has been traditionally assumed that sulphur occupies a three-fold coordinate hollow site (fcc) however, there has been an increasing amount of literature that has exhibited contrary evidence. This contrary evidence has resulted in new models. Some of these new models show adaptations where the c(4 x 2) super lattice is composed of a distorted (√3 X √3) R30° lattice, in which some sulphurs occupy two different sites, the traditional three fold hollow and a bridged site. Other new models involve reconstruction of the Au (111) surface[62] in a variety of different ways.[63] The similarities in bond strength between the

thiolate-Au and Au-Au bonds is important in facilitating this reconstruction.[62] In summary, the exact binding mode(s) is yet to be established and in recent years several new binding modes have been proposed[62] (**Figure 1.7**).

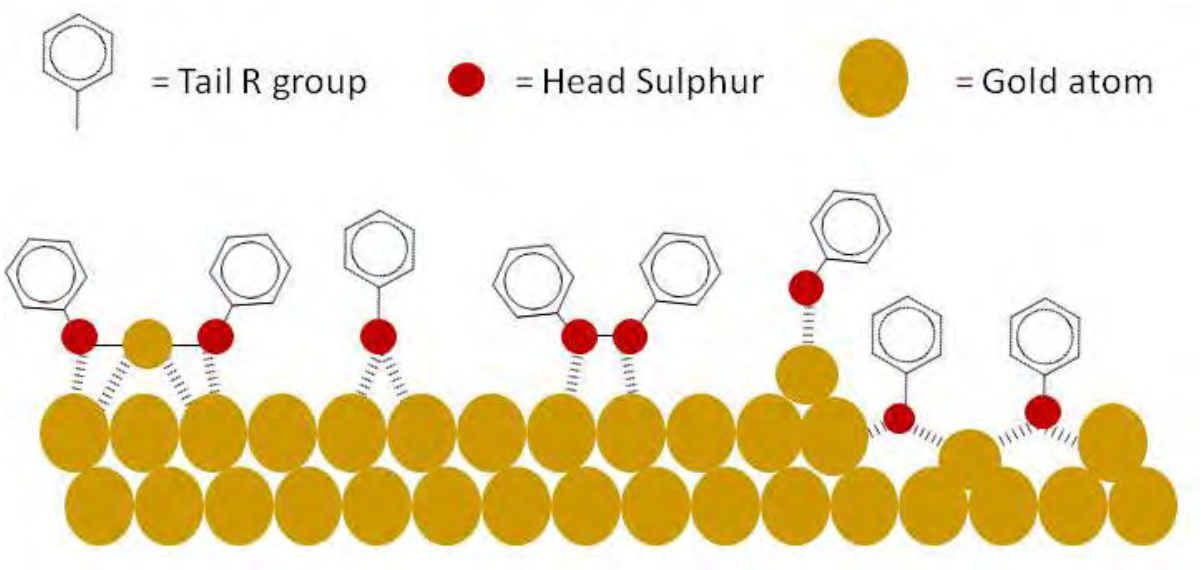

Figure 1.7, Several new binding modes have been proposed for the binding of thiolates to Au.[62]

1.1.4 Defects/long range order

Despite the quasi crystalline and ordered nature of thiol based SAMs, long range molecular ordering is disrupted by defects. Defects (**Figure 1.8**) occur due to several factors:[63,64] substrate topology/morphology; formation parameters (time, temperature, concentration, solvent, deposition method); cleanliness of ambient formation environment; purity and conformational distortions of surfactants. Furthermore several types of defects exist: (**Figure 1.8**) i) domain/island boundaries,[36] ii) pinhole defects due to missing surfactants/uncovered sites,[64] iii) pit defects[31] due to ad-atom

rearrangement and iv) low density/disordered phases due to conformational gauche defects.

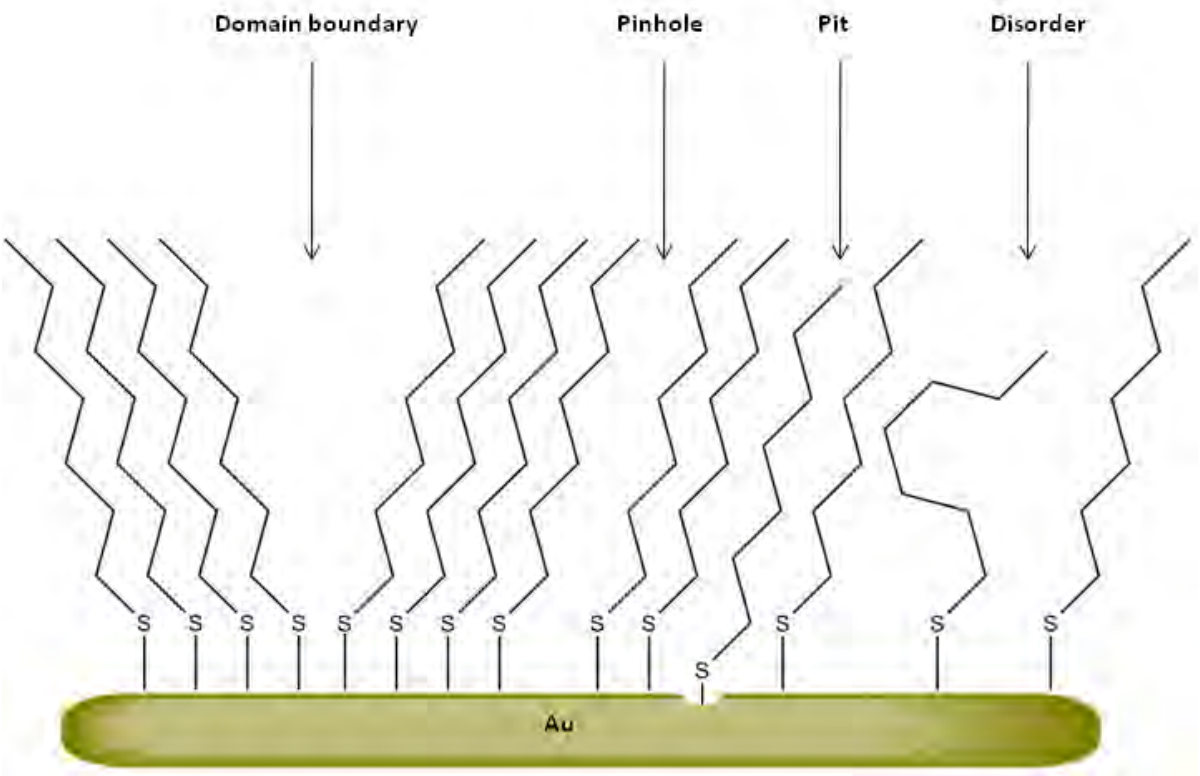

Figure 1.8 A cartoon representation of possible SAM defects which are described above: domain boundaries, pinhole defects, pit defects and disorder induced defects.

Defects can act as nucleation sites of chemical or electrochemical degradation. Furthermore, the behaviour of defected SAMs is generally unpredictable, erratic and non-reproducible.[63] The elimination of defects and furthermore, the creation of long range order, are important in the technological application of SAMs. Due to this technological demand for defect free SAMs, attempts have been made to eliminate defects and introduce long range order. For example, filling in defects with polymers.[64] More sophisticated approaches attempt to form defect free SAMs with long range order,

such strategies include: the use of novel surfactants such as those with selenium[25] or phospolipids[65] head groups and the development of sophisticated formation techniques, such as: the growth of monolayers (on nanoparticles) in the presence of an electrical field;[65] use of masks to allow for selective deposition of surfactants within the correct orientation,[66] and also the use of elevated temperatures. Elevated temperature (75°C) has been shown to drive the formation of long range ordered domains of pentafluorobenzenethiol SAMs on Au,[68] which form disordered domains at normal temperatures.

1.1.5 Mixed self-assembled monolayers

SAMs that are constituted of two or more different types of surfactants are known as mixed SAMs.[69] Mixed SAMs can be formed in one of three ways, either by selectively changing the end group functionality of a SAM, post formation,[70] during SAM formation by co-adsorbing two or more species onto the substrate,[71] or finally through using asymmetrically substituted disulphides.[69]

Co-adsorption of two or more species is the route generally employed.[71] Importantly, with co-adsorption there is control over the final molecular composition and order of the SAM. However, formation of co-adsorbed SAMs is more complicated than single component systems. For example, the composition of mixed co-adsorbed SAMs does not reflect the relative surfactant concentrations in solution.[72] The composition of mixed SAMs depends on adsorbate-solvent, backbone-backbone and backbone-substrate interactions, that occur during SAM formation. The solvent can have a drastic effect on composition, independent of surfactant concentration.[69] Moreover, longer backbones are favourable absorbed due to increased cohesive interactions of hydrocarbon

chains.[69] Despite these draw backs mixed SAMs have been used extensively. Furthermore, recently their structural complexity has been systematically investigated[73] and a method of control over local structure been suggested.

An important application of mixed SAMs is in the study of bio-molecular interactions.[74] In such SAMs bio-active surfactants are presented within a protein inert matrix, which allows a controlled study of the desired bio-molecular interaction. These mixed SAMs have overcome the problems associated with traditional *in-vitro* substrates and have been extensively applied to the study of bio-molecular interactions. An account of protein inert SAMs is given below.

1.1.6 Protein inert SAMs

Protein inert SAMs prevent undesired non-specific binding to the surface. Non-specific protein binding, occurs through three mechanisms: electrostatic interaction, hydrogen bonding and hydrophobic interactions.[75] Several protein-inert SAMs have been developed[76,77] (**Figure 1.9**). However, it is OEG SAMs that have received, by far, the most attention in the literature.[74]

Oligo(ethyleneglycol) (OEG) alkyl thiolates on Au have been widely shown to resist non-specific protein adsorption.[74] The protein inert nature of OEG SAMs, is dependent on the SAMs ability to stabilise an interfacial water layer.[75] The interfacial water layer prevents, direct contact between the surface and protein. The stability of the interfacial water layer, is dependent on several factors; an internal hydrophilic structure; a relaxed/disordered lateral packing density, with helical conformations preferred over *trans*; terminal hydrophilicity. All these aforementioned factors, help to promote the adsorption and coordination of the SAM to water. Consequently any factors, reducing

the degree of adsorption and coordination of water to the SAM, reduce the protein inert nature of the surface. For example, OEG SAMs on silver are not protein resistant.[42] This loss in protein resistance is due to a high packing density characterised by an all *trans* conformation in which molecules lie normal to the surface. Whereas on gold the backbone adopts a helical amorphous structure[78] which repels protein absorption much more effectively.

Protein inert surfactants are used as a bio-inert spacer groups which allow desirable control over the surface density of bioactive surfactants.[79] Surface density is important in the development of biomolecule immobilisation.[79] If the surface density is too high biomolecules will be immobilised in a fashion that brings them in to contact with each other, resulting in the denaturing of their bioactive structure. Furthermore, when switching is dependent on some conformational change, the use of protein inert surfactants can provide space.

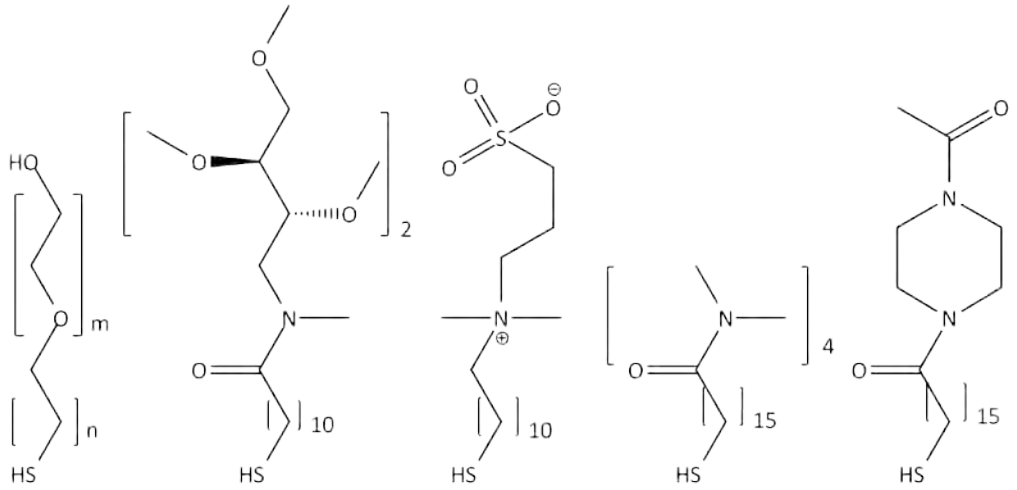

Figure 1.9 Surfactants that give protein inert SAMs. The most widely studied of which is the glycol based surfactant, which is the on the far left.

1.2 Switchable SAMS

Several switchable SAM systems are currently in development.[80] Current examples use a variety of different response units and stimuli. Stimuli induce some chemical response to surfactants within the SAM. This chemical response changes the surfaces chemical functionality thus altering the surfaces properties. Switching stimuli currently exploited include heat,[81-85] chemical,[86,87] electrical charge[88-100] and light.[101-116] The following discussion concentrates on illustrating the different types of switchable SAM systems, evident within the literature and as defined by the different stimuli mentioned above. Emphasis is placed on their application in bio-nanotechnological research.

1.2.1 Heat as a stimulus

Resistance of pure oglioethyleneglycol (OEG) SAMs to protein absorption has been shown to deplete with temperature.[81] The critical temperature of this transition, however, is not convenient for the study of bio-molecular interactions,[82,83] as bio-molecules denature above physiological temperatures. However, in mixed SAMs [83,84] made from alkyl and OEG surfactants (**Figure 1.10**) SAMs cyclical[83] transitions between a protein-inert to a protein-reactive surface, close to physiological temperatures, have been observed. The temperature induced differences in non-specific adhesion are related to conformational changes of the SAM surfactants, between the two temperature ranges. The system has been developed[85] to reversibly control the surfaces affinity for the specific adhesion of streptavidin to the biotin containing SAMs.

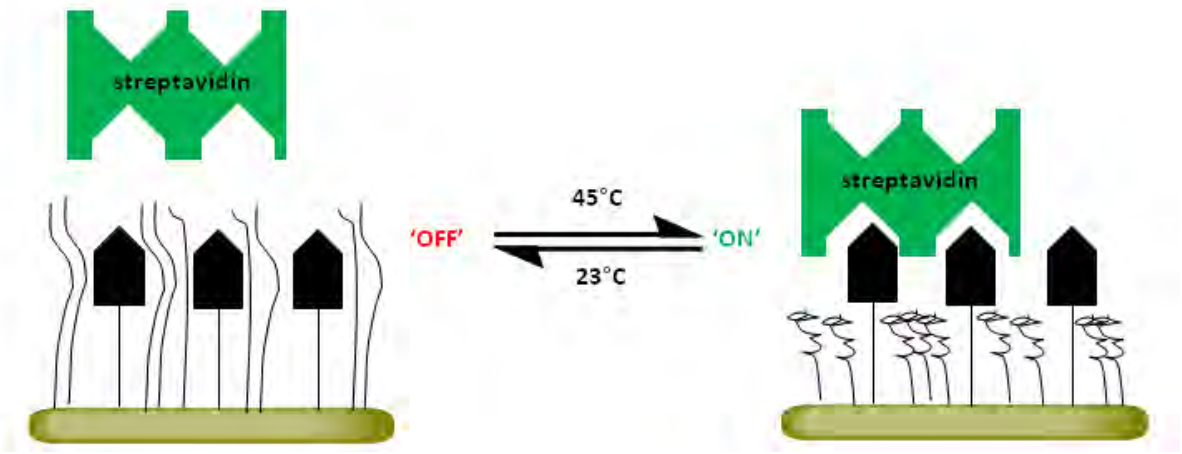

Figure 1.10 Example of a temperature based switchable mixed SAM made from OEG thiols and avidin terminated alkyl thiols. At low temperatures the surface is inert to protein absorption as the OEG surfactants shadow the biotin. However, upon heating to 45°C the OEG surfactants compact and expose the biotin to which streptavidin is able to bind. [85]

1.2.2 pH as a stimulus

Change in pH, in the presence of a solution of bis-benzyl-amine, has been shown to switch a carboxylic acid terminated SAM between a bio-inert to bio-reactive surface.[86] At pH 8.7 bis-guanidinium electrostaticly binds to the carboxylate, giving a positively charged surface, which can selectively absorb negatively charged biomolecules such as ATP. If the pH is then reduced to 3 the bis-guanidinium-biomolecule complex is released from the surface, which itself is returned to its original carboxylic acid state. (**Figure 1.11**)

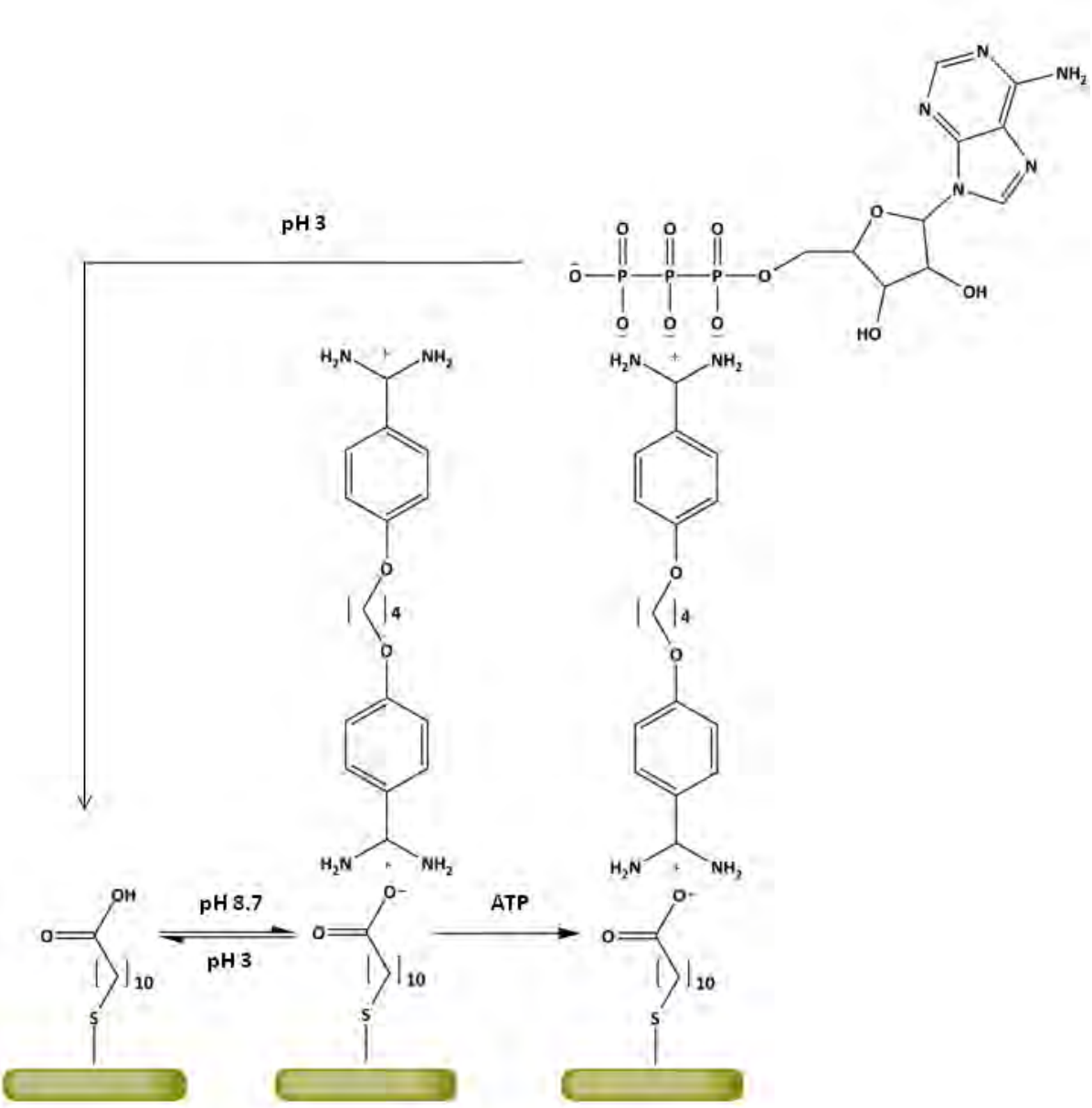

Figure 1.11 Example of a pH stimulated switchable SAM. At a low pH (3) the SAM is terminated with a carboxyl group, however, increasing the pH to 8.7 deprotonates the carboxyl to give a carboxylate. bis- guanidinium is then added and binds to the surface through electrostatic interactions. The protonated bis- guanidinium surface can immobilse negatively charged ATP. The system can then be restored to its original state by reducing the pH to 3. .[86]

1.2.3 Bio-chemical stimulus

Bio-chemical induced switching of a SAM has been achieved through employment of an engineered cell, containing the non-mammalian enzyme cutinase.[87] Cutinase induces hydrolysis of an aromatic ester terminated SAM to a produce a hydroquinone (**Figure 1.12**). The hydroquinone can be oxidised to the quinone by cyclic voltammetry. Measuring the voltametric response allows measurement of the degree of cellular activity. Such a system has future applications as a SAM based cell sensor.

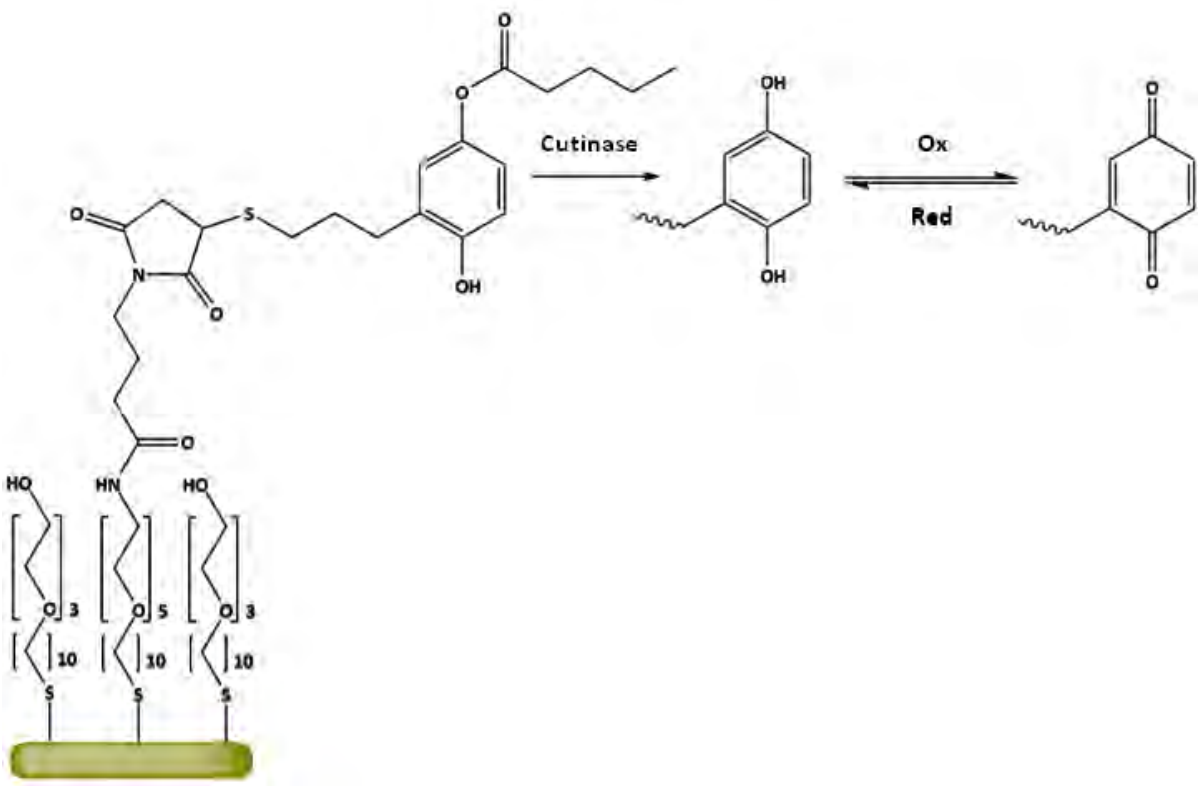

Figure 1.12. Example of a biochemical stimulated switchable SAM. The enzyme cutinase, present in an engineered cell, cleaves the aromatic ester to give a hydroquinone. The hydroquinone is part of a redox pair and can be cycled, via cyclic voltammetery, between itself and the quinine. Measuring the cyclo-voltametric response allows derivation of the degree of cellular activity.[87]

1.2.4 Electrical stimulius

The use of electrical potential to induce chemical switchability has resulted in the development of several different systems which can be broadly split into two categories, i) electrically induced redox reactions and ii) electrically induced conformational changes

1.2.4.1 Electrically induced redox reactions

Electrical inducement of a redox reaction in SAM end groups, has been shown to switch surfaces between a bio-inert and bio-reactive state.[88, 89, 90] More than one system has been reported in the literature. For example, SAMs terminated with aromatic nitro (NO_2) groups can be electrically switched to aromatic amines (NH_2). The amine surface can be further modified in order to immobilise both DNA and proteins.[88] Another system depends upon the electro-induced oxidation of a 4-H-benzo[1,3]dioxinol end group (presented within mixed SAMs) to produce an aldehyde, which can immobilise hydrazide/ammino tagged ligands.[89] A final example and perhaps the most extensively studied system, exploits a mixed SAM made from OEG and an OEG derviative (**Figure 1.13**).[90-96] The OEG derivative has a hydroquinone end group that forms a redox pair with quinone. The hydroquinone is electrically oxidised to the quinone upon the application of a positive potential to the substrate surface. The reaction is reversible through the application of a negative potential.

The redox active hydroquinone/quinone system is suitable for the study of cell migration and has been exploited in several different ways, all of which exploit some electrocative tether between the SAM and a bio-molecule. For example, the quinone is able to bind to the cyclo-pentadiene (C_p) tethered to the protein motif RGD[90] (**Figure 1.10**) for the study of cell adhesion or biotin[91] for the study of immobilisation of the protein strepatavidin. Attachment of the cyclo-pentadiene to the quinone occurs through a Diels-Alder reaction.[91] The RGD-Cp system has been exploited as a mask for the patterning of a substrate with two different cell populations.[92] In another example, RGD tethered to the quinone through an electroactive ester.[93] Upon the application of a negative potential the quinone is reduced to the hydroquinone ensuing an intra-molecular cyclicisation reaction to give a lactone and release of RGD. Other electrocative tethers include thiols[94] and amino-oxy groups.[95] Furthermore, the system has also been developed to form a SAM with RGD attached to the hydroquinone, through a silyl

ether tether[96] RGD is released from the surface through hydrolysis, by the electrochemical oxidation of the hydroquinone to the quinone.

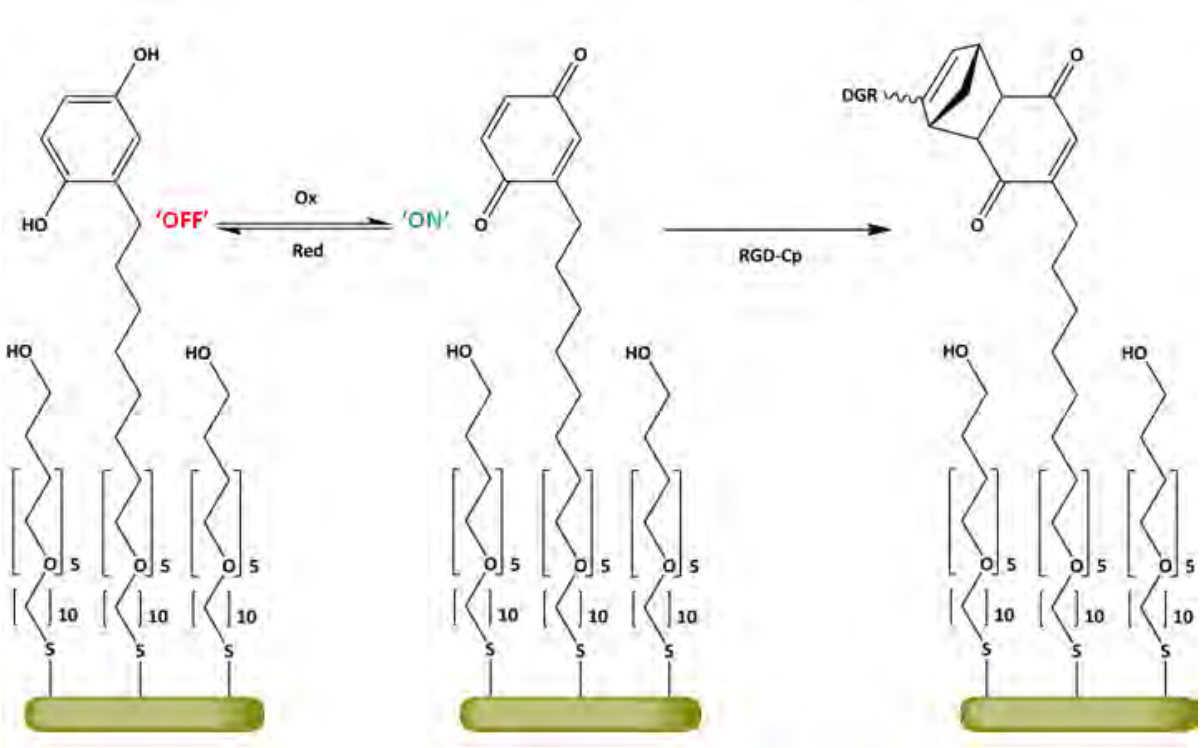

Figure 1.13 Example of a redox switchable SAM, for the study of cell migration. Redox reaction is stimulated applying a potential to the underlying gold substrate, oxisising the terminal hydroquinone to the quinone. The quinone terminated SAM is able to bind to cyclopentene-RGD which can be used to study cell migration. Furthermore and as described above, the system has also been used to present bio-molecules other than RGD.

1.2.4.2 Electrically induced conformational reactions

Electrical potentials have been used to reversibly switch the conformation of charged SAM surfactants, between an *'on'* and *'off'* state.[97,98] In the *'on'* state charged end groups immobilise biomolecules through electrostatic interactions (**Figure 1.14**). The change in conformation which gives rise to the *'on/off'* states is due to the electrostatic attraction of polarised end groups to the electrically charged gold substrate. End groups

exploited are carboxylates (COO^-)[97,98] and protonated amines (NH_3^+)[98] that change conformation to the 'off' state upon application of positive or negative potential, respectively. Such conformational change requires space and so SAMs must be of low density. One method of achieving low density SAMs is through making the SAMs with globular end groups that can be removed post formation[97] or from from cyclodextrin-surfactant complexes,[98] from which the cyclodextrin can be washed away. Such electro-active surfaces have been shown to control protein adhesion and release in-vitro.[98] Furthermore the system has recently been expanded by our group in order to bend peptides within mixed SAMs of OEG and peptides.[99]

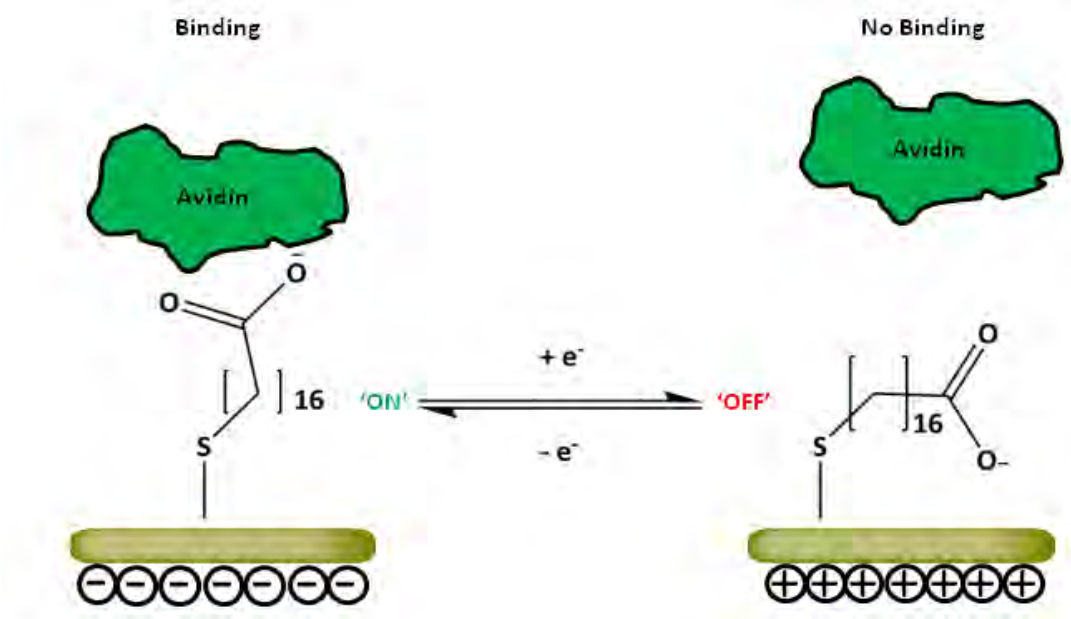

Figure 1.14 Example of electro induced conformational switch. Application of a negative potential to the surface repels and exposes the negatively charged surfactants, the SAM is switched *'on'* and can covalently bind to positively charged avidin. Upon application of a positive potential to the surface the negatively charged surfactants are attracted to Au substrate, releasing avidin and/or turning the SAM *'off'*. Furthermore and as decribed above the system has been applied to other surfactants and bio-molecules.[92]

Electrically induced conformational changes have also been exploited to switch SAMs with DNA-based end groups.[100] DNA contains phosphates which are negatively charged, thus application of a positive charge to the gold substrate of a DNA-terminated SAM pulls the DNA to the surface. While the application of a negative potential to the gold surface results in the DNA 'standing up'.

1.2.5 Light as a stimulus

Light-stimulated switching of SAMs may induce photo-chemical reactions or photo-physical conformational changes.

1.2.5.1 Switching by photo-reaction

Light has been used to reversibly switch a SAM[101] between a bio-inert and bio-reactive state (**Figure 1.15**). In the bio-reactive state the surface is able to produce gluconoic acid from glucose, where as in the bio-inert state it cannot. Glucononic acid production is facilitated by a flavoenzyme immobilised on the SAM. The flavoenzyme requires a FAD-cofactor to work. In this SAM system the natural-FAD-cofactor is replaced by a semi-synthetic-FAD-cofactor, that can be turned 'on/off' by inducement of a reversible photochemical reaction.

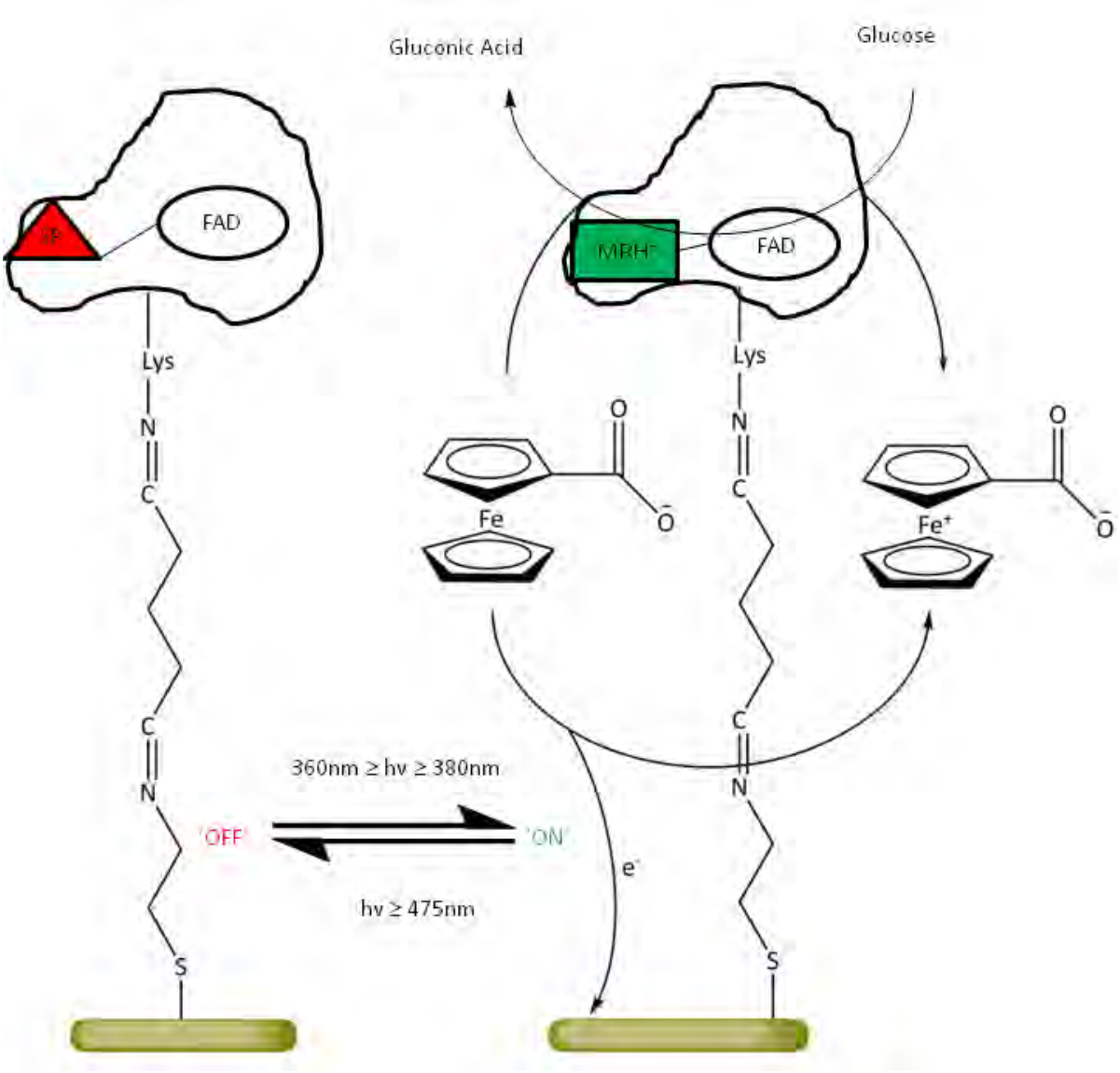

Figure 1.15. Example of photochemical reaction switch. The SAM is terminated with a flavoenzyme containing a semi-synthetic-FAD-Cofactor. The semi-synthetic-FAD-Cofactor responds to *UV* and *Vis* light turning the flavoenzyme *'on'* and *'off'* respectively through a photochemical reaction.

1.2.5.2 Switching by photo-isomerisation

Light is known to induce geometric isomerisation in many functional groups, some of which have been exploited in photoswitchable self-assembled monolayers. Photoswitchable SAMs have been made from both diarylethenes,[102] stilbenes[103] and azobenzenes.[104-116]

1.3 Azobenzene SAMs

1.3.1 Azobenzene a brief history

Studied for over 70[117] years, azobenzene was first popularised due to its optical absorption which gives it an intense colour. This intense colour lead to its widespread use, as a textile and leather dye, in the 1960s. Since its early popularity, it has been found to decompose into carcinogenic aromatic amines and as a result is now illegal to use as a dye within the European union.[118] Despite its now legally restricted use as a dye, azobenzene is now being applied in new areas of research. Over the last couple of decades, there has been an increasing number of reports on the use of azobenzenes in photo switchable systems. For example, azobenzene has been used in switchable chemical systems that influence things such as peptide conformation,[117] binding affinity[117] and molecular motion.[119] Such switchable chemical systems exploit the different physical[120] and/or chemical properties[119] of azobenzenes two geometric isomers (discussed below). It is the substantial differences between the two isomers (**Figure 1.16**) that makes them attractive in chemically switchable systems.[117]

1.3.2 Azobenzene isomerisation

The Geometric isomerisation of azobenzene is induced by light (*UV* and *Vis*) which switches it between its *trans* and *cis* states. In its ground state, azobenzene predomimately resides in its thermally stable *trans* conformation. Upon photoirradtion with *UV* light (≈360 nm) isomerisation to the *cis* conformation occurs, steady state conditions are reached quicky and the cis isomer becomes the most populated state. There is an approximate 50 KJ mol^{-1} energy difference between the two isomers.[104,117] The *cis* state is only meta-stable and relaxation to the ground state (*trans* isomer) can occur, either instantaneously by photoirradtion with visible light (≈440 nm) or over a longer time period through thermal relaxation.[117,108]

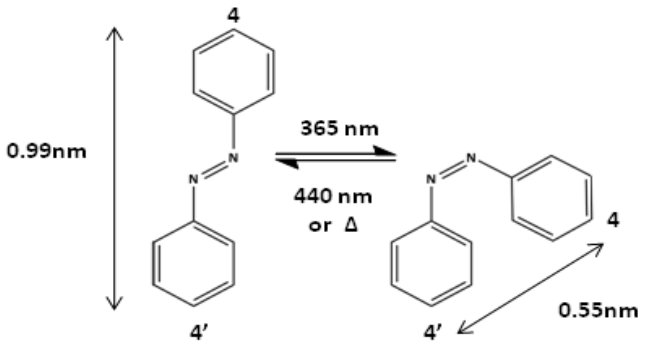

Figure 1.16. illustration of azobenzene isomerisation. In its ground state azobenzene adopts the *trans* conformation and the distance between the 4 and 4' positions is 0.99 nm. Upon irradiation with *UV* light of wavelength 365 nm it isomerises to the *cis* conformation, in which the distance between the 4 and 4' positions is 0.54 nm. The *cis* state is only meta-stable and relaxation back to the trans state occurs thermally over time or instantaneously through irradiation with *Vis* light at 440 nm.

Importantly, for its application as a chemical switch, the photoisomerisation of azobenzene does not generate any detectable side products making it one of the cleanest photoreactions known.[117] The reaction kinetics are on the order of a hundred

fs to one ps, therefore offering real time switching. Such real time switching has important implications in the study of interfacial biomolecular interactions.[74]

1.3.2.1 Physical changes

Isomerisation induces a change in azobenzenes geometrical conformation. In the *cis* state there is a change, relative to the trans state, of the phenyl rings about the C-N=N-C plane. The distance between the 4 and 4' positions is reduced from 0.99 nm for the *trans* to 0.54 nm for the cis isomer (**Figure 1.16**).[117] Consequently, the cis isomer has a higher free volume requirement than the *trans*. The exploitation of dramatic shape change caused by photo-isomerisation can be used to selectively expose or conceal functional groups attached to azobenzene. Furthermore, the actual shape change can be finely tuned through substitution.[121]

1.3.2.2 Chemical changes

Isomerisation induces a change in azobenzenes dipole moment (μ): for the *trans* isomer μ ≈ 0 D and for the *cis* μ = 3.1 D.[117] These changes in the dipole moment can be used to induce reversible changes in wettability of surfaces, inducing movement of liquids.[120] In the *trans* conformer the SAM surface is hydrophobic. Upon irradiation with UV light the *trans* isomer is excited to the *cis* and the surface becomes slightly less hydrophobic with changes in the contact angle of an olive oil droplet from 15° ± 2 to 20° ± 2 upon 5 mins exposure to *UV* (335 nm) and *Vis* (442 nm) light, respectively. Furthermore, and useful to future developments of the azobenzene SAMs the actual change in dipole moments can be tuned through substitution.[121]

1.3.2.3 Excited state lifetime

When using azobenzene in switchable systems it is important to consider the excited state's lifetime. Typically the thermodynamic (i.e. in the dark) lifetime of the excited *cis* isomer is on the timescale of hours. However, timescales of relaxation (as well as absorption maxima) may be be effected by substitution patterns: for example lifetimes from seconds to sixty days have been observed for some derivatives [117] functionalised with bulky pendant groups; down to seconds for 4,4'disubsituted pseudo-stilbenes (**Figure 1.17**). This potentially large effect of substitution on the lifetime of excited states (and absorption maxima) has lead to three classifications[111] of azobenzene derivatives (**Figure 1.17**).

a.Azobenzene classification: these molecules have substitutions to the benzene rings, however, they have similar absorption properties to unsubstituted azobenzene, with prominent absorption occurring in *UV* region.

b.Aminoazobenzene classification: Azobenzene derivatives substituted at the ortho or para positions with electrodonating groups (e.g. amino, NH_2). Such substitution shifts absorption into the visible-blue region

c.Pseudo-stilbenes classification: These mimic the absorption pattern of stilbenes. They are characterised by substitution at the 4,4' positions with an electron donating and an electron-withdrawing group giving a push/pull substitution pattern. This push/pull substitution pattern results in a strong asymmetric electron distribution. Such asymmetric electron distribution gives this class strong and broad absorption in the visible region.

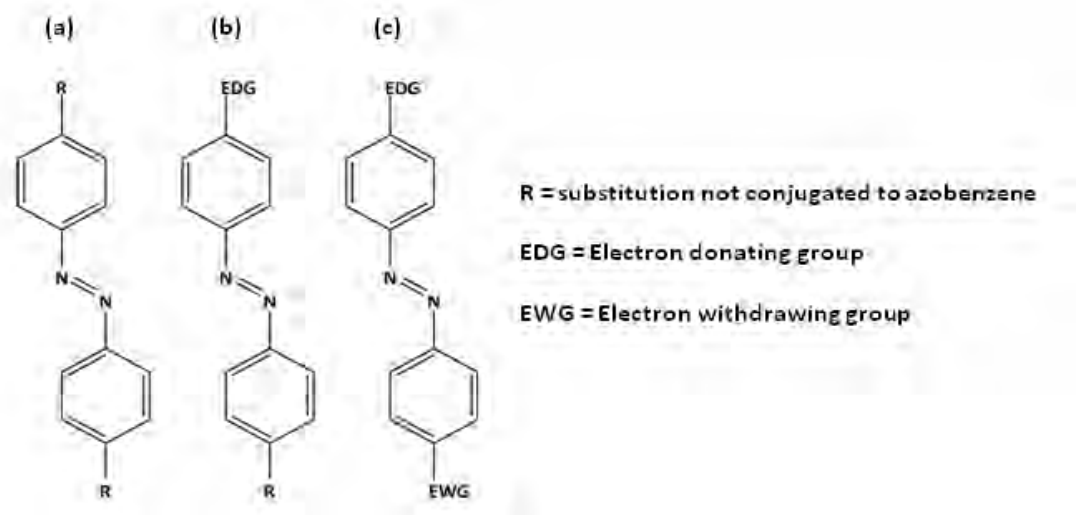

Figure 1.17. Classes of azobenzene as defined by substitution pattern (a) azobenzene type, substitutions to azobenzene have no to little effect on λmax and excited state lifetime (b) Aminoazobenzene type are substituted by an electron donating group which shifts λmax into the visible-blue region (c) Pseudo-stilbenes are substituted by electron donating and electron withdrawing groups shifting λmax into visible region.[117]

1.3.2.4 Mechanism of azobenzene isomerisation

The mechanistic details of *trans* to *cis* photoisomerisation of azobenzene is currently a subject of debate.[122] In this debate two main mechanisms have been proposed, rotation *Vs.* inversion (**Figure 1.18**) about the diazo bond,[123] other mechanisms have also been proposed.[124] Both inversion and rotation mechanisms have been shown to operate through relaxation from excited states.[125-127] The two mechanisms of isomerisation require different free volumes.[117] Inversion requires an estimated free volume of 0.12 nm^3, whereas the rotation mechanism requires an estimated free volume of 0.28 nm^3. The required free volume of isomerisation and hence the mechanism of isomerisation, has important implications on the isomerisation of azobenzene within SAMs which is known to be restricted by spatial constraints.

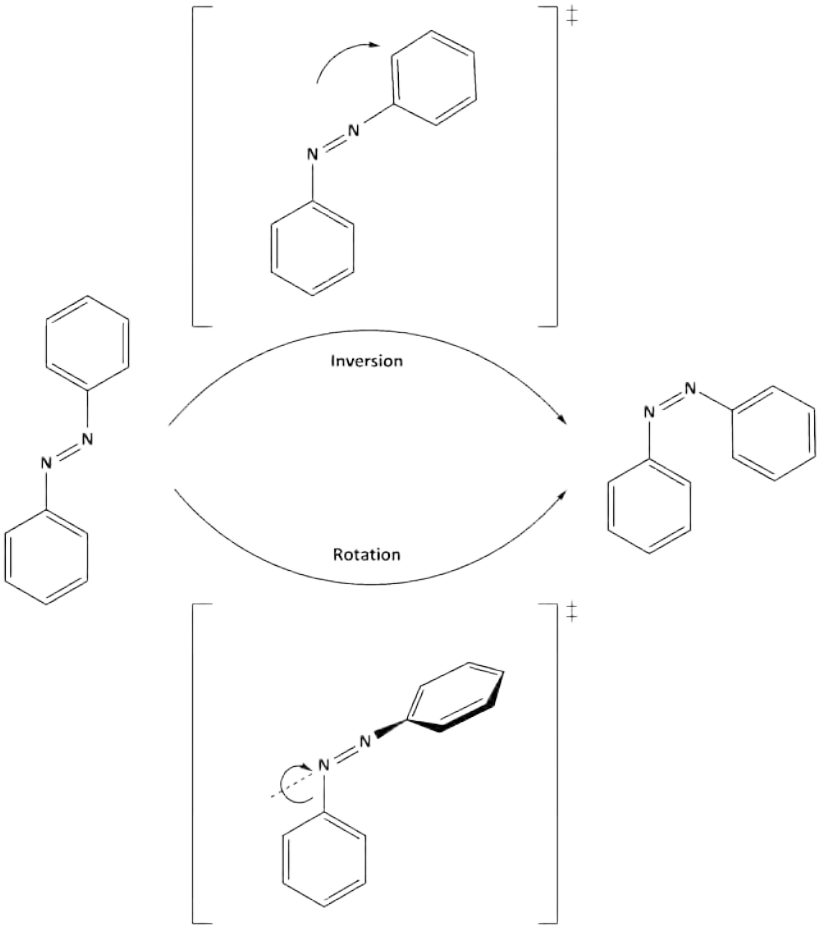

Figure 1.18. Illustration of the two main proposed mechanisms of isomerisation. Isomerisation by inversion about the diazo-bond can be simply described as proceeding by a bending of the bond. Rotation can be simply described as proceeding by a turning about the diazo bond.

1.3.2.5 Photochemistry of isomerisation

The photochemistry of azobenzene is complex and despite it being studied for 50 years it is still not fully understood, however, various important features are known.[122] Isomerisation is known to occur on the pico-second timescale and involves $\pi - \pi^*$ and/or n - π^* transitions, depending on the wavelength of excitation.[122] The $\pi - \pi^*$ for

trans azobenzene occurs between 320 – 350 nm and is much more intense than that of the *cis* absorption which occurs between 260 – 300 nm. The n - π* excitation occurs as nitrogen contains a lone pair of electrons and is formally forbidden from the *trans* state, but allowed from the *cis* state occurring at approximately 440nm.[123] The spectra of the *trans* and *cis* isomers can be easily distinguished due to the difference in intensities of absorption between the two isomers.[123] Furthermore, the exact wavelength of absorption is dependent on the substitution pattern.

The photochemistry of the π – π* excitation is the more complicated and involves a three step mechanism. In the first or ground state (S_0) of the trans isomer the electron is promoted, through excitation, to the second singlet state (S_2); some other states (S_3, S_4, T_1 , T_2) may also become populated.[124, 125] The excited electron then relaxes to the first singlet state (S_1) through non-radiative decay. Finally the excited electron can relax back to the ground state through either radiative decay or non-radiative decay *via* the intersection of the S_1/S_0 states. Isomerisation itself occurs mainly from the S_1 potential energy surface.[124] Some literature points towards a more complicated isomerisation mechanism using other singlet and triple states.

The photo-chemistry of the n - π* transition is much simpler and only involves the S_1 state.[122] Isomerisation also occurs from the S_1 potential energy surface, but at a different point to that of the π – π* isomerisation.

The quantum yield of isomerisation depend not only on the excited state (S_n,T_n) but also the isomeric transition, as well as the substitution pattern of the chromophore.[125] For *trans – cis* isomerisation the quantum yields are generally in the range of 0.20 – 0.36 for the symmetry forbidden n - π* and 0.09 – 0.20 for the π – π* transition.[125,126] For *cis – trans* isomerisation the quantum yields are generally in the range of 0.4 – 0.75 for the n - π* and 0.27 – 0.44 for the π – π* transition.[125]

1.3.3 Azobenzene SAMs

Since the early 1990s there has been an increasing number of reports of SAMs made from azobenzene containing surfactants.[104-116] Azobenzene containing SAMs made from traditional silane surfactants have shown a degree of isomerisation.[133] However, isomerisation of azobenzene SAMs made from traditional thiol surfactants has been shown to be hindered.[134,135]

1.3.3.1 Thiol based azobenzne SAMs

There are mixed reports[133] with respect to the photo-response of azobenzene thiol SAMs. The use of conventional thiol surfactants in azobenzene SAMs has resulted in a lack or low[139] degree of photoisomerisation. Photoisomerisation of thiol based azobenzene SAMs has been shown to be inhibited by two factors, aggregation (**Figure 1.19**)[134] and/or spatial constraints.[137] Inhibition to isomerisation has been shown to be overcome by modifications to traditional sulphur based surfactants (**Figure 1.20**).

When aggregated within SAMs, azobenzene is unable to geometrically isomerise.[134] Two types of aggregation can occur, namely H and J aggregation. Both types of aggregation are manifested through π - π electron stacking interactions and result in a shift in λ_{max} of the *trans* isomers π-π* transition, relative to the non-aggregated state. In H-aggregation π - π stacking occurs in a symmetrical fashion (**Figure 1.19b**) which results in a hyposochromic shift of λ_{max}. In J-aggregation π - π electron stacking occurs in an asymmetrical fashion (**Figure 1.19c**) and results in a bathochromic shift of λ_{max}.

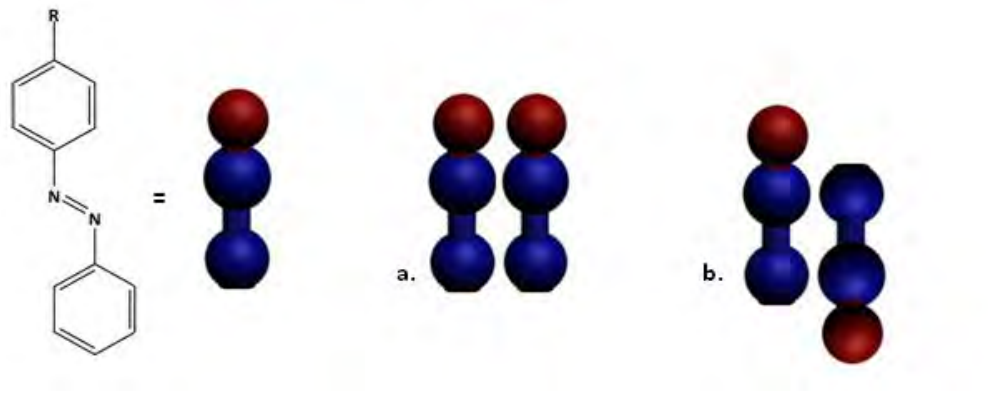

Figure 1.19. Azobenzene is known to form two types of aggregates in solution as shown by the diagram a. H-aggrgation where azobenzene units line up in a parallel and symmetrical fashion and results in a hypsochromic shift of λ_{max}, such aggregation has also been seen in SAMs and has been blamed for optical inactivity of such SAMs b. J-Aggregation where azobenzene units align in a parallel but asymmetrical fashion, which results in a bathochromic shift of λ_{max}, such aggregates have not been found in SAMs.

1.3.3.1.1 Novel thiol based azobenzene surfactants

Several groups have created sulphur based surfactants that form non-aggregated SAMs (**Figure 1.20**). Some of these surfactants are based on existing sulphur surfactants, for example asymmetrically substituted disulfides[105] (**Figure 1.20 a**) and asymmetrically substituted thiol ethers[106] (**Figure 1.20 b**) have been shown to undergo isomerisation. Other examples of non-aggregating surfactants are based novel modifications of traditional surfactants. For example, improvement to the degree of isomerisation has been made with the introduction of alkyl substitutions to the benzene ring (**Figure 1.20 c**).[107] More extravagant surfactants modifications include: the use of novel head groups such as alpha lipoic,[119] asparagusic acid[110] (**Figure 1.20 d**) and a an adamantane core[111] (**Figure 1.20 e**); Or the spacing out of backbones by inclusion of a bulky Carborane[112] para to the diazo functionality. Furthermore, cyclodextrin complexed to azobenzene surfactants through electrostatic interactions has been shown to promote

photoisomeristion in SAMs on Au nanoparticles, with the SAM remaining as a CD-surfactant inclusion complex.[113]

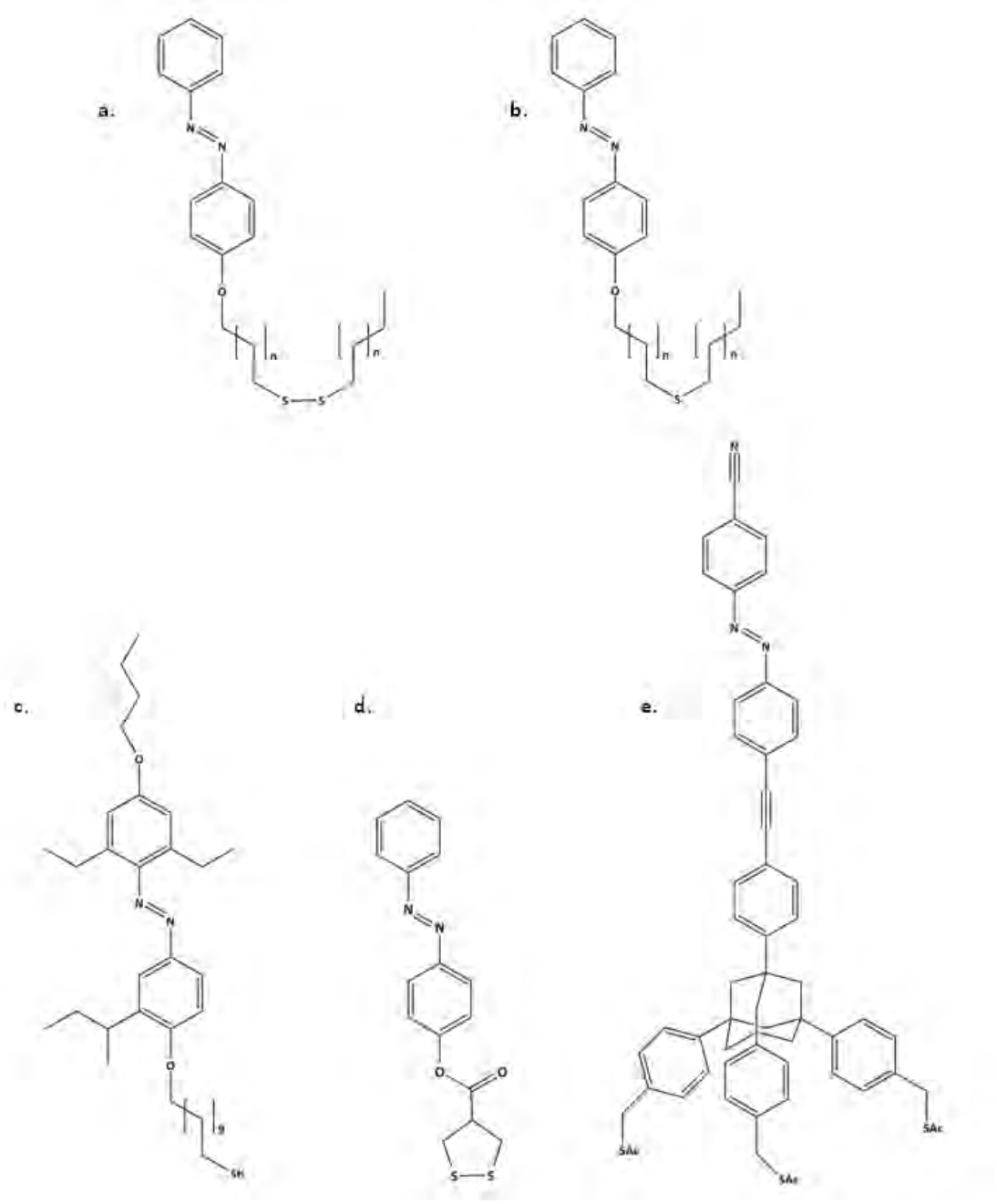

Figure 1.20. Examples of some some sulphur based surfactants which undergo isomersiation within SAMs (a) asymmetrically substituted dithiol (b) asymmetrically substituted thiol ether (c) Alkyl substitution on benzene ring (d) use of asparagusic as a head group (e) use of a tripodal adamantane head group.

1.3.3.1.2 Azobenzene SAMs for biological application

Photoswitchable azobenzene SAMs[106] made from asymmetrically substituted thiol-ethers functionalised with a cationic group have been exploited in the study of porphyrins[114] and DNA.[115] Porphyrins or DNA bind to the azobenzene SAM when in its *trans* state and are released upon isomerisation of azobenzene to its *cis* isomer. However, the authours do not mention any attempt to reattach the DNA and hence we are skeptical of whether or not the realse is due to, either, the isomerisation of azobenzene or the photochemical cleavage of the tertiary amine-DNA complex from the SAM.

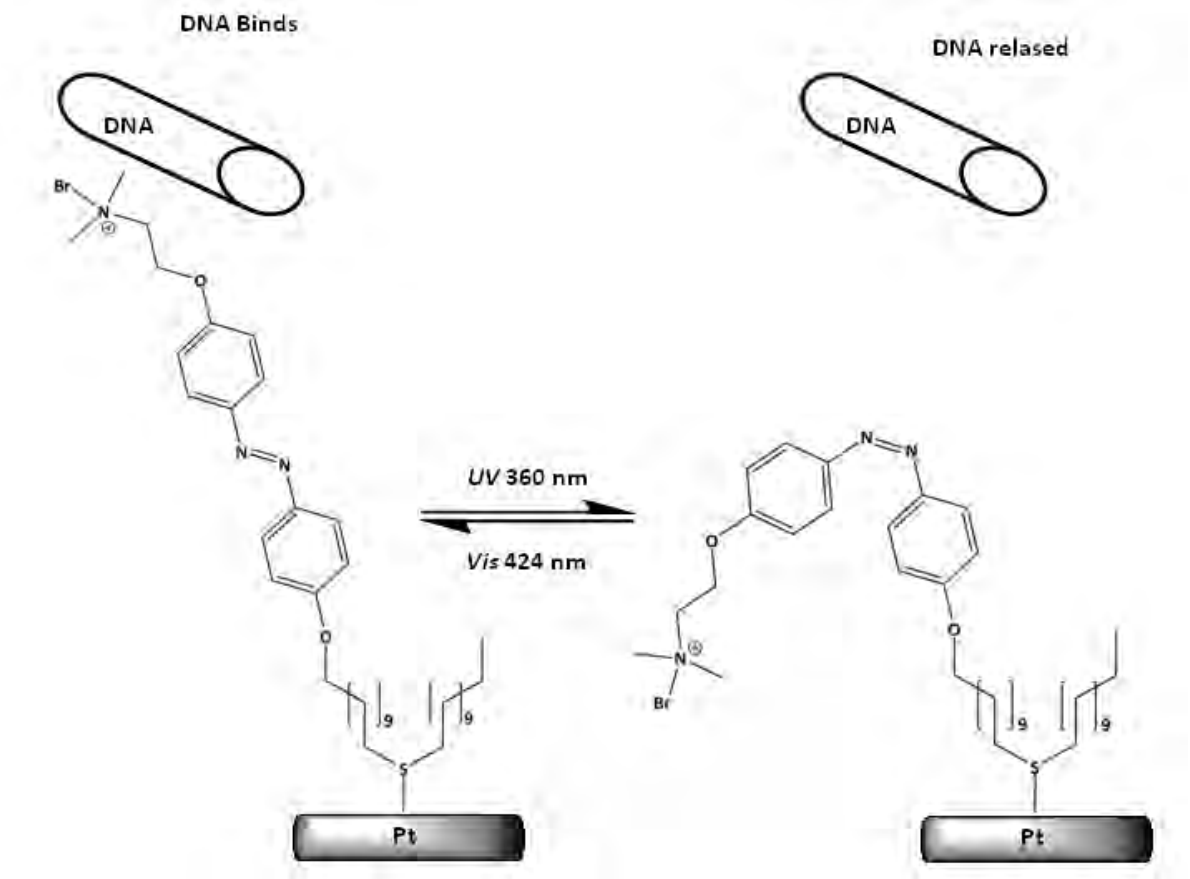

Figure 1.21 Photo-switchable SAM for *'catch and release'* of DNA based on asymmetrical thiolether SAMs on platinum substrates. The same system has also been used with porphyrins instead of DNA.

Photoswitchable azobenzene SAMs, made from amide containing azobenzene glycol surfactants, have been shown to switch a terminal RGD protein motif *'on'* and *'off'* (**Figure 1.22**).[116] The system is *'on'* in the *trans* state, due to exposure the terminal RGD and '*off*' in the *cis* state, due to concealment of the terminal RGD group. Switching RGD *'on'* and *'off'* allows reversible control over cell adhesion.

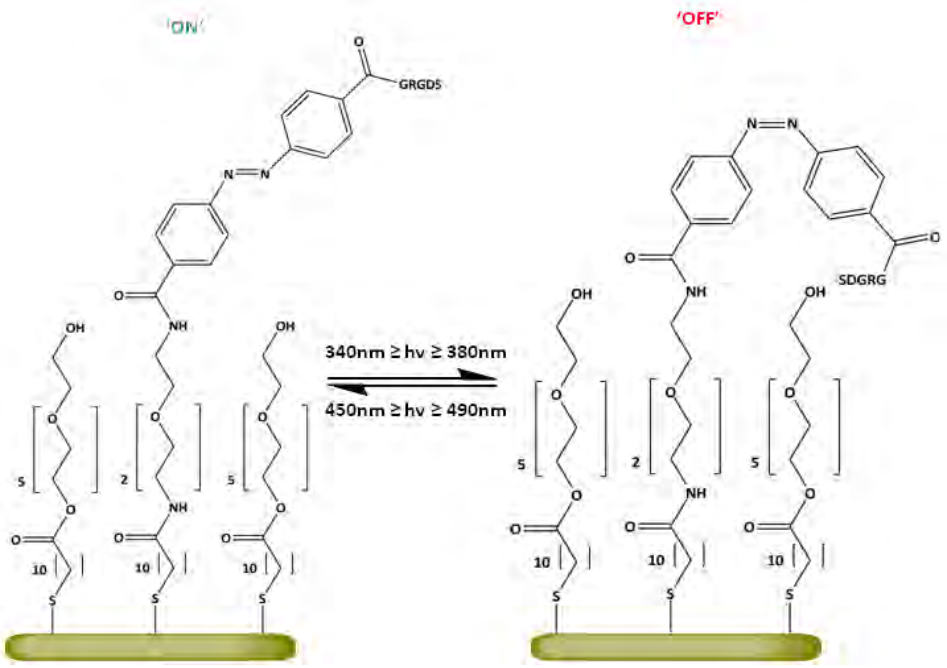

Figure 1.22. Presence of an amide increases isomerisation with SAMs, such a method has been applied to reversibly control cell adhesion

1.4 Concluding remarks

Self-assembled monolayer research has been extensive. Over the past decade there has been an increasing number of reports on both SAMs with switchable functionalities and

SAMs for application as *in-vitro* models of biochemical phenomena. Current development of SAMs as *in-vitro* models, needs to focus on switchability of the surface, as this will recreate the real time signalling of the body.

The use of azobenzene based glycol thiol SAMs is an attractive system, for the creation of *in-vitro* models, from switchable SAMs. Despite this attractiveness the application of glycol thiol based azobenzene SAMs to the study of bio molecular interactions is not widely researched and only one example has been found in the literature. Research is complicated as azobenzene within SAMs made from traditional alkyl thiol surfactants, are prone to aggregation. Some current research efforts focus[109-119] on removal of aggregation through surfactant design with future application for the study of bio molecular interactions.

1.5 Objectives

There are two main objectives to this thesis. Firstly, a novel surfactant is investigated as a non-aggregating sulphur based azobenzene surfactant as shown in **Figure 1.23**. Secondly, a glycol based mixed SAM system was investigated as shown in **Figure 1.24**

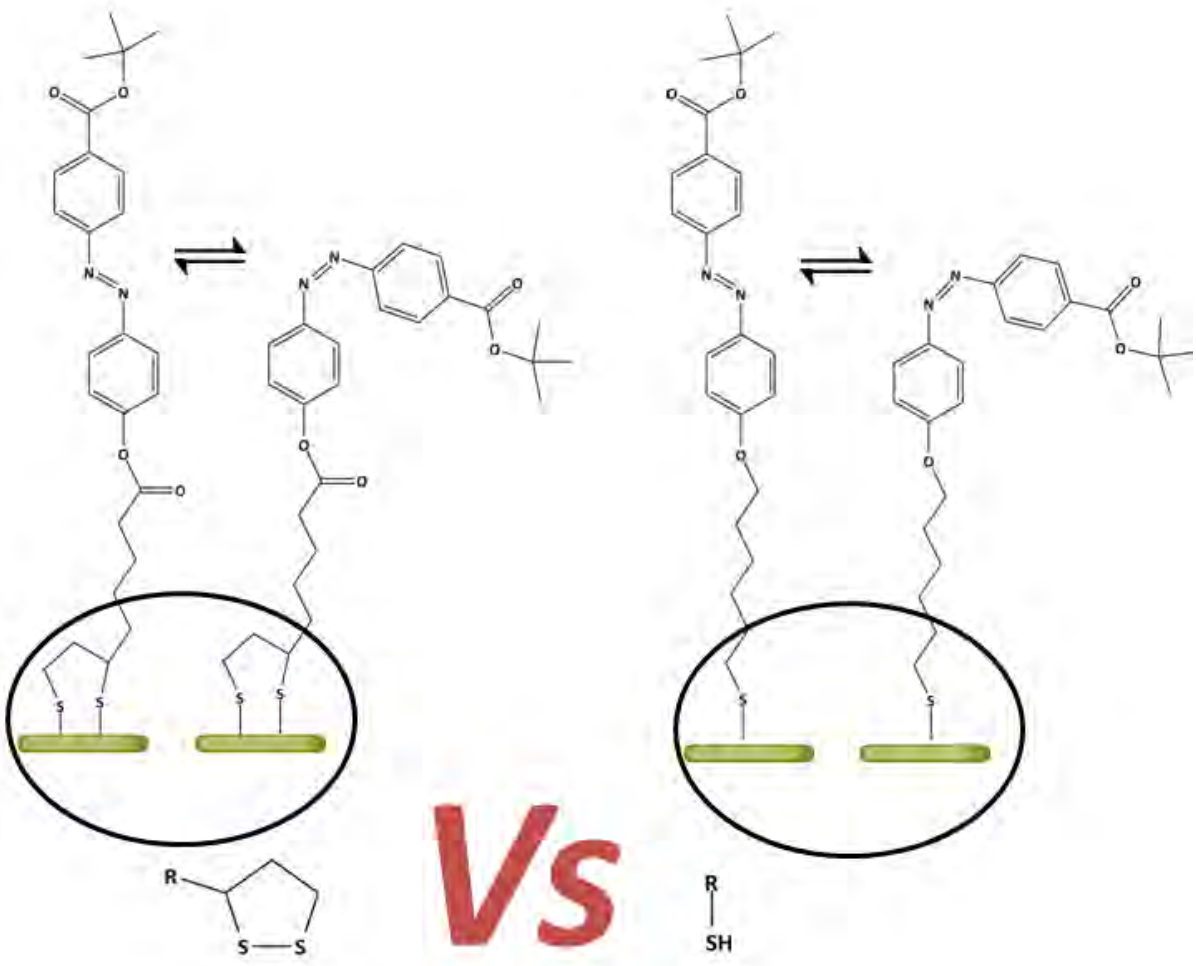

Figure 1.23. Schematic of research presented in chapter 4, which investigates the geometric isomerisation of a surfactant with a cyclic 1,2-dithopentane head group, relative to a traditional thiol head group. Note, for SAM the surfactants are drawn standing upright for convienence and clarity, in reality they will be tilted.

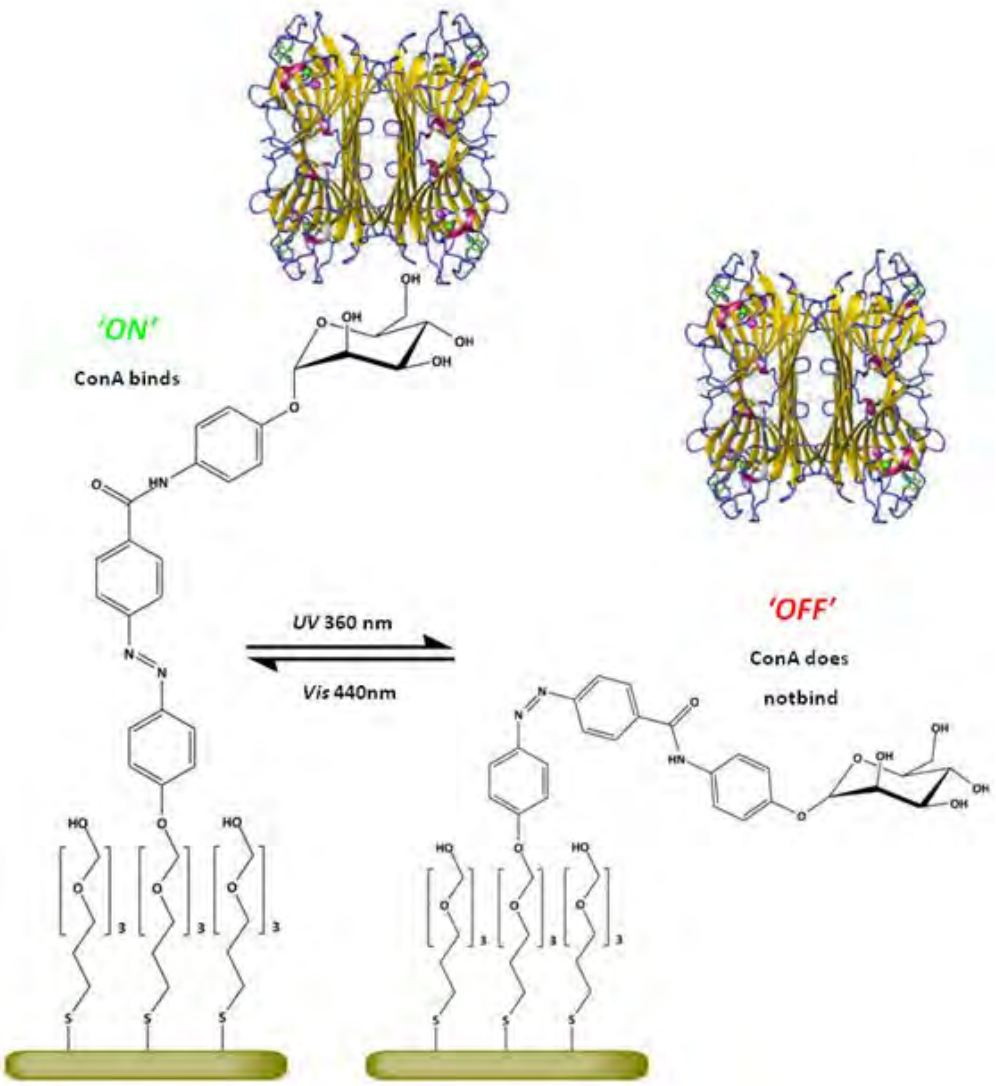

Figure 1.24 The *'on'/'off'* switcahability of 1:1 GAZ1:TEGT SAMs with respect to ConA immobilisation is investigated in chapter 5. Note, the surfactants are drawn standing upright for convienence and clarity, in reality they will be tilted.

1.6 PhD Overview

Herein, the aim of this PhD is to design and synthesise azobenzene-based surfactants, which will be used to develop photo-switchable SAM systems as shown above. The research is discussed over five chapters. Chapter two gives an introduction to the analytical techniques used. Chapter three reports the synthesis of the azobenzene-based surfactants, working in collaboration with a post doctoral researcher, Dr Parvez Iqbal. Chapter four reports the formation of SAMs from an azobenzene surfactant with a novel head group, which is investigated as a non aggregating SAM. Chapter five reports the investigation of a mixed SAM, for use as a photo-switchable SAM for the investigation of biochemical interactions. Finally chapter six reports the experimental techniques. A breakdown of research in chapters' three to five is given below.

In Chapter three, the synthesis of the five surfactants (**Figure 1.25**) is discussed. These surfacatnats were used to make SAMs in Chapters four and five. Chapter four uses the surfactants 4,4'(benzoicacid-*tert*-butyl-ester)(thiocticester)azobenzene (TAZ1), 4,4'(benzoicacid-*tert*-butyl-ester)(hexathiol)azobenzene (SAZ1) and thioctic methyl ether (TME). Chapter five uses 4,4'(benzoicacid)((triethyleneglycol)- propylthiol)azobenzene (GAZ1) and triethylene glycol thiol (TEGT).

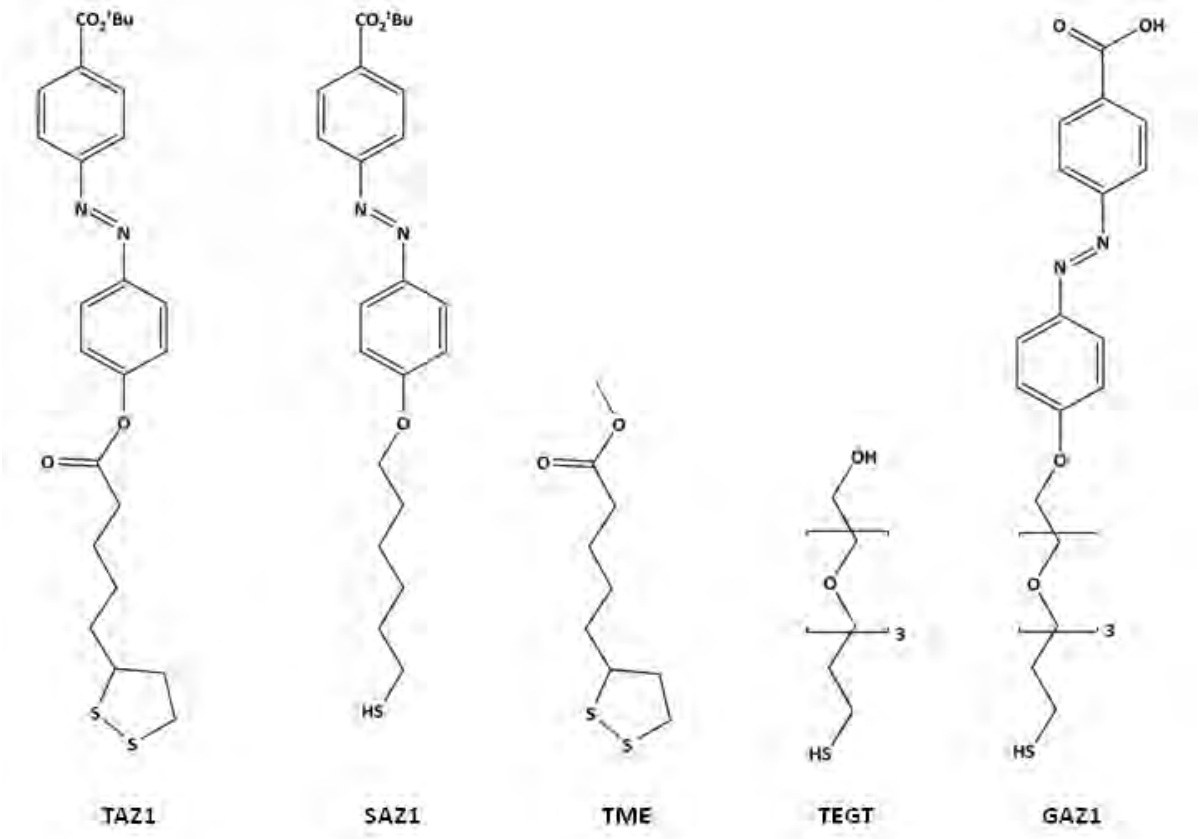

Figure 1.25 Surfactants used to make SAMs in chapters four and five. Chapter 4 compares isomerisation of pure TAZ1 to pure SAZ1 SAMs and uses TME to interpret XPS results. Chapter five investigates mixed SAMs of GAZ1 and TEGT.

Chapter four (**Figure 1.23**) is split into three parts. Firstly TAZ1 SAM formation was investigated with respect to time using contact angle, ellipsometry, *UV*/*Vis* and XPS. Secondly the isomerisation was investigated using *UV*/*Vis* spectroscopy, the isomerisation was then compared to SAMs made from the thiol based SAZ1 surfactant Finally the hydrolysis of the TAZ1 SAMs was investigated, in order to introduce chemical functionality to the SAM.

Chapter five (**Figure 1.24**) is split into three parts. Firstly GAZ1:TEGT mixed SAM formation was investigated with respect to time using contact angle, ellipsometry and

UV/*Vis* spectroscopy. Secondly (**Figure 1.24**) the immobilisation of the lectin Concavalin A on mixed SAMs, functionalised with mannose, was investigated by surface Plasmon resonance (SPR) and ellipsometry. Finally (**Figure 1.324**) the *'on'*/*'off'* switchability of 1:1 GAZ1:TEGT SAMs with respect to ConA immobilisation was investigated by SPR, ellipsometry and *UV*/*Vis* spectroscopy.

2.0 Surface characterisation techniques

SAMs can be analysed using a range of different analytical techniques.[15] The analytical techniques used to analyse SAMs in this PhD are ellipsometry, contact angle, X-ray photo-electron spectroscopy (XPS), surface UV/VIS spectroscopy and surface plasom resonance (SPR).

Ellipsometry was used to determine SAM thickness and probe formation time. Contact angle was used to determine SAM wettability, probe formation time and surface roughness. XPS was used to determine the surface composition. Surface UV/VIS spectroscopy was used to probe isomerisation of azobenzene within SAMs. SPR was used to study the binding of biomolecules to the surface in real time. Each of these techniques are described in detail below. Details of experimental protocols and the specific make/model of analytical equipment can be found in chapter 6.

2.1 Ellipsometry

Ellipsometry was first invented in the late 1800s but was not popularised until the 1960s.[138] Ellipsometry is a non-destructive optical technique usually preformed under ambient conditions, although it can also be done in a vacuum.[138] The technique can be used to analyse various properties of thin films, such as dielectric constant, refractive index and thickness.[138] Furthermore, ellipsometry has recently been applied to detect the isomerisation of azobenzene SAMs,[104] however, this requires an ellipsometer with monochromatic light source.

Ellipsometry depends upon the interaction of the surface with polarised light.[138] Polarised light is defined by its polarisation state (phase and amplitude) and is composed of two components, s and p which are parallel (p) and perpendicular (s) to direction of propagation.[138] In the experimental setup (**Figure 2.1**) linear polarised light

is reflected off a surface at an angle of incidence. Linear polarised light is characterised by either in phase or opposite phase, s and p components. Interaction of linear polarised light with the surface changes its polarisation state, due to the differences in the refractive indices of the two mediums. The change in polarisation causes the light to become elliptically polarised. Elliptically polarised light is characterised by out of phase s and p components. The detector measures the changes in the polarisation state, between incident and reflected light, allowing establishment of the phase shift and relative change in amplitude, which can be explained by the Fresnel equations. From establishment of the phase shift and relative change in amplitude the properties mentioned above, maybe calculated [139]

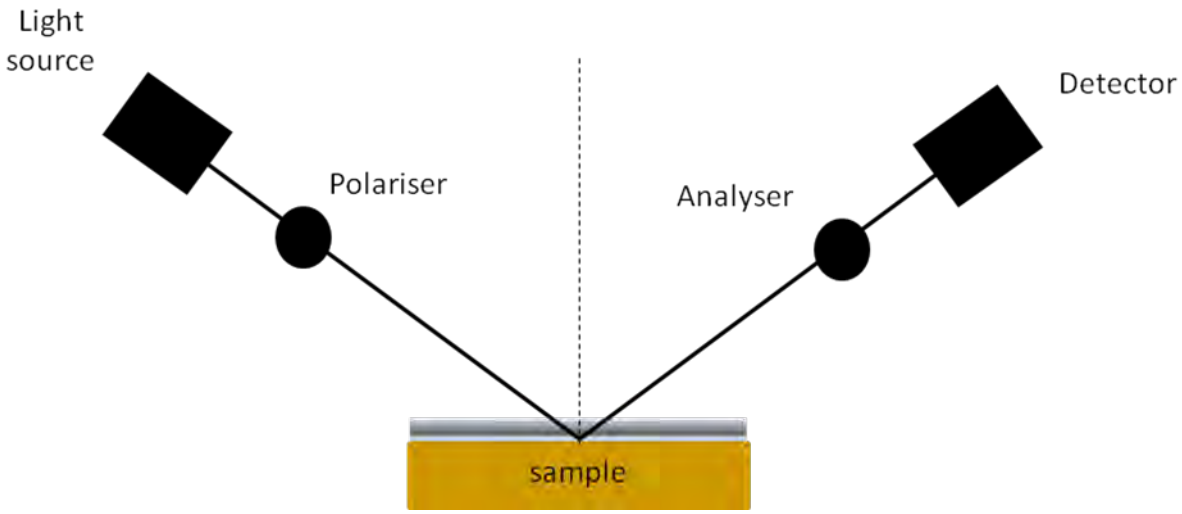

Figure 2.1 Schematic of ellipsometer setup

Calculation of properties is done computationally and requires complicated mathematical modelling of the air/film/solid interface. The model assumes the film to be homogenous and requires assignment of refractive index (usually 1.5 for organic films). Models are tested for validity using standard SAM systems for example tetra-,

hexa-, and octadecane thiol SAMs. These model SAMs from well packed homogenous structures of known thickness.

2.2 Contact angle

The analytical technique of contact angle measures the angle a drop of liquid makes on a surface at the three phase interface (solid/liquid/gas)(**Figure 2.2**).[140] Contact angle measurements give information on a surface's wettability.[140]

Wettability of a surface, with respect to a liquid droplet, is a function of all the forces acting at the three phase interface.[140] The forces at the three phase interface are mathematically explained by various surface tension theories, such as Young's equation (**Equation 1**).[140] Young's equation, defines the contact angle when all three interfacial forces are in equilibrium. At equilibrium the chemical potential of the phase boundaries is minimised.

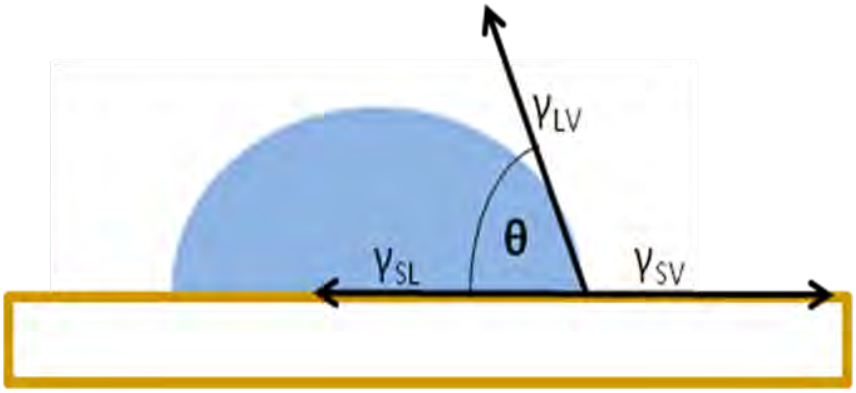

Figure 2.2 Schematic of contact angle and the associated forces acting at the 3 phase boundary

$$\gamma_{SV} = \gamma_{SL} + \gamma_{LV}\text{Cos}\theta \quad \textbf{(Equation 1)}$$

γ_{SV} = Free energy between solid and vapour

γ_{SL} = Free energy between solid and liquid

γ_{LV} = Free energy between liquid and vapour

θ = Contact angle

Young's equation and other surface tension theories must be used with caution due to the assumptions of each model.[142] For example, Young's equation defines the equilibrium contact angle of an ideal surface.[140, 141] Ideal surfaces are atomically smooth, heterogeneous and do not interact with the probing liquid.[140, 141] In reality ideal surfaces are very rare, except in some examples of polymers. Deviations of contact angles, from the values predicted for ideal surfaces, may be described by more complicated surface tension theories, such as the Wenzel and Cassie-Baxter models.[142]

Contact angle measurements may be either static or dynamic.[141] The static contact angle is the equilibrium angle that a static drop of liquid makes at the three phase boundary. However, it has been reported that this angle shouldn't be used if the surface exhibits a hysteresis (explained below) between the advancing and receding angles of the dynamic contact angle.[141]

The dynamic contact angle is composed of two values, the advancing contact angle (θ_{Adv}) and the receding contact angle (θ_{Rec}).[141] The advancing contact angle is the maximum angle made by a droplet of liquid advancing over a previously un-wetted surface. The receding contact angle is the minimum angle that the droplet makes as the

droplet is retracted from the previously wetted surface. The difference between these two angles ($\Delta\theta = \theta_{Adv} - \theta_{Rec}$) is known as the contact angle hysteresis.

The contact angle hysteresis can be either kinetic or thermodynamic.[141] Kinetic hysteresis changes with time and is due to either the liquid penetrating the surface, and/or the reorientation of surface groups.[141] Thermodynamic hysteresis is determined by surface roughness and chemical heterogeneity of the surface.[141] With respect to surface roughness, the hysteresis is only zero when the surface is ideal. A smooth homogenous and crystalline SAM will exhibit a hysteresis < 5°. The change in thermodynamic hysteresis over time can be used to probe the formation kinetics of SAM formation, as once the SAM is fully formed the hysteresis plateaus. It is the thermodynamic hysteresis that is usually reported.[141]

There are four different approaches[142] to measuring contact angles of planar surfaces (Figure 2.3): Visually through employment of the sessile drop method (Figure 2.3a) or tilting plate method (Figure 2.3b) both of which require the use of a goniometer; through the direct measure of associated forces using the Wilhelmy balance approach (Figure 2.3c); Finally, contact angle can be determined through the use of the captive bubble technique (Figure 2.3d). All three approaches can be used for static and dynamic contact angles and furthermore each technique has its advantages and disadvantages.[142]

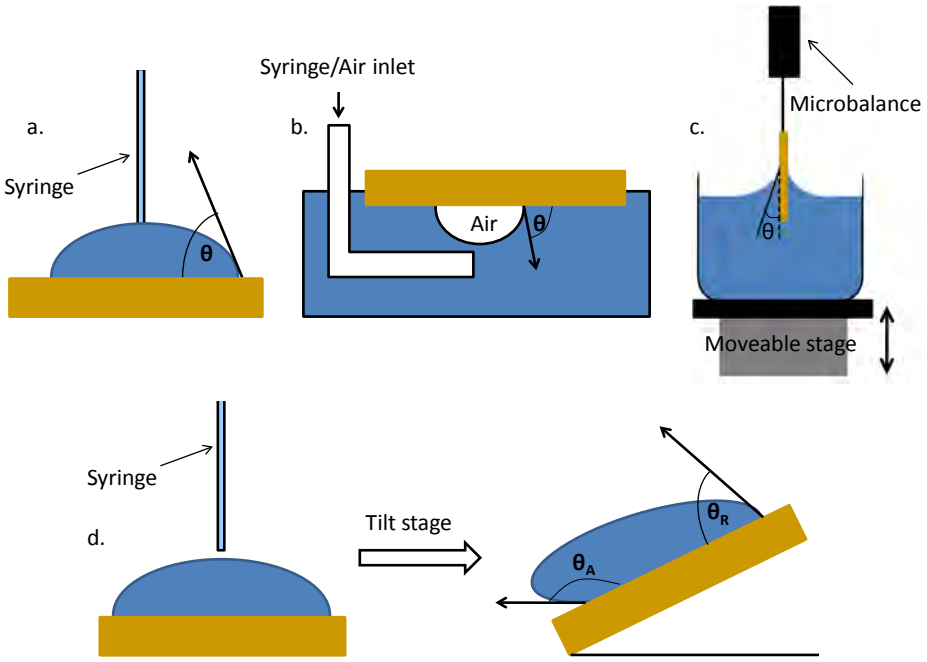

Figure 2.3 Cartoon representations of the different contact angle techniques (a) sessile drop (b) captive bubble (c) Wilhelmy balance (d) tilting plate.

The sessile drop method is more versatile and so is often the preferred method of analysis.[142] Samples used in the sessile drop methods, as well as adaptations of the technique (i.e. dynamic sessile drop method) can be used to gain several results from one sample, giving a measure of surface homogeneity.[142] However, the calculation of surface tensions using the sessile drop method is subjective. Subjectivity arises from both operator error (when using manual machines) and the two dimensional nature of photos used in contact angle analysis.[142] Analysis is preformed computationally, on a picture of the liquid droplet. However, such a two dimensional analysis may not always be truly representative of the whole surface, particularly if the droplet doesn't spread homogenously.[142] The dynamic sessile drop method tends to give a more accurate θ_{Adv} than θ_{Rec}.[142]

The captive bubble technique can be used to give a more accurate θ_{Rec}.[142] However, as a consequence the captive bubble technique gives less reliable θ_{Adv}.[142] The contact angle has also been shown to be dependent on bubble size[143]

The tilting plate method can be used to simultaneously obtain both θ_{Adv} and θ_{Rec}, making it useful for measuring the hysteresis.[142] Furthermore, the technique removes any interference that the needle, used in the dynamic sessile drop, may have.[142] However, the technique must be used with caution as angles have been shown to depend heavily on drop size.[142]

The main advantages of the Wilhelmy balance method is the removal of operator error and accurate establishment of surface tensions.[142] It has also been shown to be the best technique for measuring hysteresis.[144] However, disadvantages include the requirement of large volumes of liquids and the preparation of relatively large two sided samples, which can be difficult or impractical.[142]

2.3 X-Ray photoelectron spectroscopy

X-Ray photo-electron spectroscopy (XPS) is an ultra high vacuum (UHV) and surface sensitive technique. XPS can be used to analyse the elemental composition of surfaces[145] including self assembled monolayers.[146]

The technique depends on the interaction of X-rays with matter (**Figure 2.4**).[145] When X-ray light interacts with matter it can excite core electrons, ejecting them from the sphere of influence of the nucleus.[145] XPS measures the kinetic energy of the photo-

ejected electrons. Electrons are ejected from core orbitals of species at the surface, through their bombardment with soft X-rays, of fixed energy *hv*.[145] The kinetic energy of ejected electrons is measured by an analyser, according to **Equation 2**.[145] The kinetic energy of ejected electrons is relatively low, thus the profile depth of XPS is also low, making it a surface (i.e. not bulk) technique.[145]

$$\mathbf{E_B = hv - (Ke + Ø)} \quad \textbf{(Equation 2)}$$

$\mathbf{E_B}$ = Binding energy of the ejected electron

hv = energy of incident radiation

Ke = Kinetic energy of ejected electron

Ø = work function of spectrometer

XPS exploits the quantisation of electrons within atomic species.[147] Each elemental species has its own range of quantised electron energies. Quantised electron energies in heterogeneous molecular bonds are slightly shifted relative to the atomic species. The shift is in dependent on the local bonding environment, thus allowing the user to probe not only the nature but also the chemical state of the surface bound species.[145]

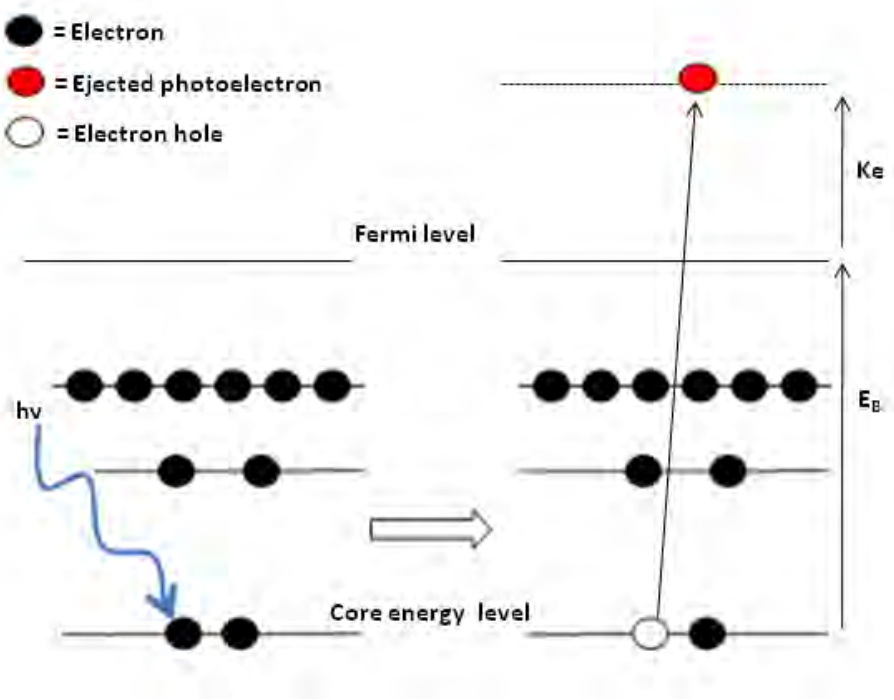

Figure 2.4 Cartoon representation of photo-electron ejection exploited in XPS

1.4 *UV/VIS* spectroscopy

UV/Vis spectroscopy can be used to assert the existence of chemical species, which absorb light in the near ultra-violet and/or visible range.[148] Commonly the technique is used to identify a reaction product,[149] follow a reactions progress,[149] determine the concentration of an absorbing species[150] or study photo- isomerisation within samples.[151] The interaction of samples with *UV/Vis* light is determined, for a range of frequencies (**Figure 2.5**). Samples can be analysed within all mediums: solution,[149-151] solid[152] or gaseous.[153] Furthermore and recently, the technique has been used on azobenzene self assembled monolayers. However, due to the low concentrations of surfactants on the surface the signal is low,[136] complicating the study of such surfaces.

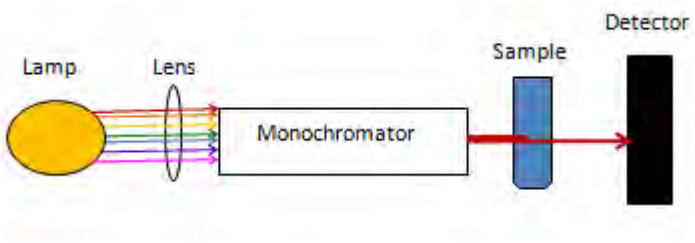

Figure 2.5 Cartoon representation of *UV/VIS* spectrometer experimental setup.

The technique of *UV/VIS* spectroscopy exploits the phenomena of outer shell electronic excitation (**Figure 2.6**) which is induced in molecules through the absorption of near *UV* and/or *visible* light.[148] Absorbing species generally have a degree of π conjugation, which shifts the energy gap, between the bonding and excited state orbitals, into the near *UV* or *VIS* range.[148] This range of *UV* is 200-380 nm and visible is 380-780 nm.

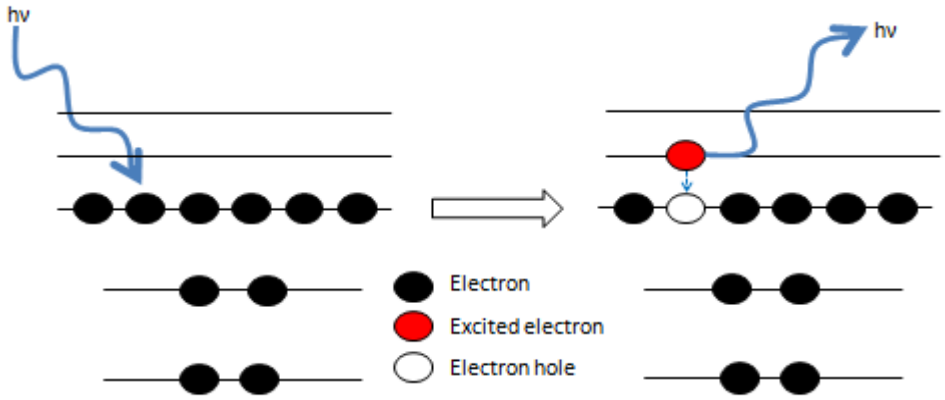

Figure 2.6 Cartoon representation of the Interaction of *UV/VIS* light with molecular orbitals. Outer electrons are able to absorb incoming light, exciting them to a higher enrgy state. The higher energy state is unstable and decays through either radiative decay (emission of UV/Vis) or non-radiative decay (emission of heat, through relaxation of vibrational modes).

The wavelength of maximum absorption (λ_{max}) corresponds to the predominant electronic transition between the ground and excited state.[148] Excited states are unstable and the electron falls back to the ground state, through a process known as relaxation. During relaxation the excess energy is emitted as the excited state decays.[148] Several decay routes may be possible, including the combination of electronic relaxation with both vibrational and rotational relaxation.[148] Existence of vibrational and rotational relaxation pathways leads to the broadening of measured absorption peaks.[148]

The Beer Lambert law (**Equation 3**) is commonly used in the quantitative analysis of analytes.[148] The Beer Lambert law states that an analytes degree of absorption (extinction or optical density in older literature) of monochromatic light is directly proportional to the concentration of the analyte.[148] A graph of the law that plots absorption *vs* wavelength gives a straight line, with a gradient equal to the Molar absorption coefficient (ε). However, the law is limited to homogenous isotropic mediums in which absorbing species are independent of each other.[154] This limitation makes the Beer Lambert law inappropriate for use at high concentrations or in SAMs, where absorbing species interact.

$A=c\lambda L$ (**Equation 3**)

A=absorption

c= concentration

λ= wavelength of absorbed light (maximum)

L=path length of cell/sample

2.4 Surface Plasmon Resonance spectroscopy

Surface Plasmon Resonance spectroscopy (SPR) is a non-destructive optical technique. SPR probes the absorption of species in solution to surfaces, in real time.[155] SPR allows the quantification of bio-molecular interactions[155] and recently conformational changes of azobenzene SAMs.[155] Surface interactions typically studied are ligand-receptor interactions between bio-molecules. Bio-molecules are typically studied due to their large size, although recent technological advancements and innovations are increasing the techniques precision.[157]

The technique depends upon the interaction of plane polarised light with a surface interface, when the angle of incidence is above the critical angle.[158] The critical angle of incidence is the angle at which total internal reflection of incident light occurs, below this angle there is both reflection and refraction.[158] Total internal reflection of light requires that the interface is from a dense to less dense medium. Total internal reflection creates an evanescent field, which propagates from the surface normal of the interface.[158] If the surface interface is coated with a thin layer of a conducting material, such as a noble metal film, the field is enhanced and penetrates a depth of 200-300nm from the metallic surface.[158]

Photons of incident light are able to excite the metal's delocalised electrons.[158] Excited electrons propagate across the evanescent field, giving a surface plasmon.[158] The relative size of the surface plasmon is dependent on the angle at which it occurs.[158] The angle which gives the maximum surface plasmon is known as the surface plasmon resonance angle (θ_{spr}).[158] θ_{spr} is above the critical angle of incidence and is the angle that gives the lowest degree of reflectivity.

θ_{spr} is dependent on the refractive index of the metallic films adsorbate (i.e. SAM).[158] The refractive index of the adsorbate layer changes with absorption of molecules.[158] Absorption mass may be determined through detecting changes in the θ_{spr}.[158] The change in θ_{spr} can be measured by the change in responsive units (RU) which can be converted into mass absorbed on the surface (1µRU = 1 ng cm^{-2}).[158]

There are various SPR spectrometer designs: fibre optic sensors; Diffraction grating coupled sensors (GC); optical wave guide sensors and prism coupled sensor.[155] Prism coupled sensors are employed in this research. Several experimental setups exist for prism coupled sensors: The Otto setup, the resonant mirror setup and the Kretschmann setup.[155] The kretschmann setup is the most popular and useful for solution studies. Studies in this PhD employ an SPR with the Kretschmann setup (**Figure 2.7**).[155]

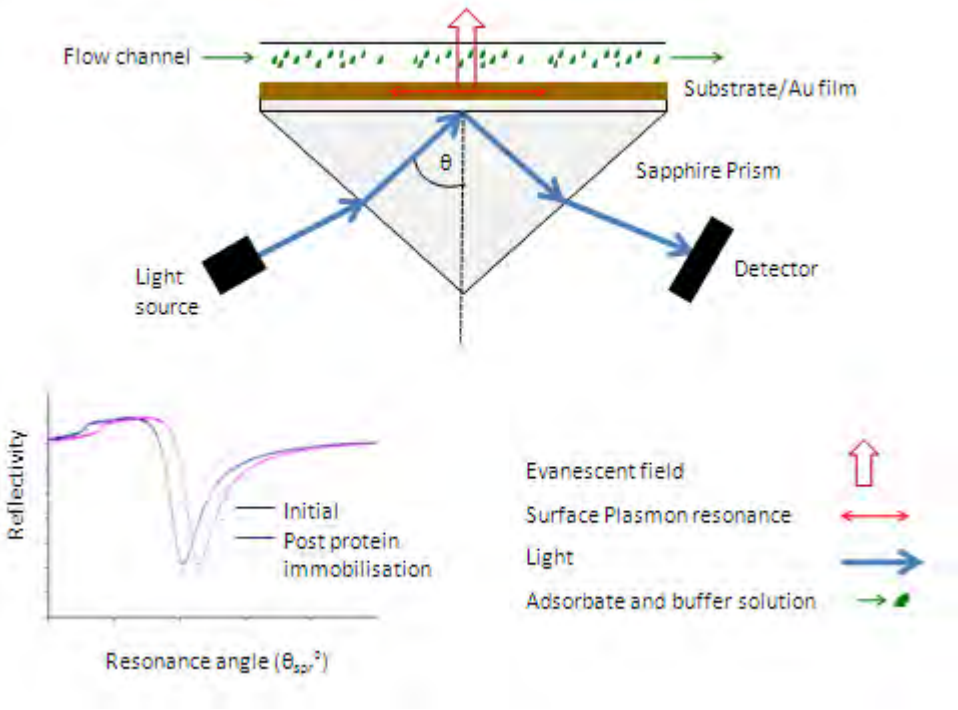

Figure 2.7 SPR schematic of the Kretschmann and change in resonance angle post protein adsorption

Further to the different experimental setups there are also several different ways to take the measurement:[155] scanning angle SPR (SPR scanning angle shift) is the method most commonly employed, it uses a single wavelength of incident light and measures % reflectance (%R) *Vs* incident angle. The SPR angle is the angle above the critical angle at which %R is least; SPR wavelength shift is another method it uses a fixed angle of incidence and measures the reflectivity as a function of wavelength, reflectivity is lowest at a certain wavelength; SPR imaging is a third method.

3.0 Synthesis of surfactants used to makie SAMs

3.1 Aims

The aim of the research presented in this chapter is to design and synthesise the SAM surfactants used throughout the rest of the research (**Figure 3.1**). Five different surfactants were synthesised, three of them in collaboration with Dr. Parvez Iqbal, School of Chemistry, University of Birmingham. The synthesied surfactants were:

- **TAZ1** - 4,4'(benzoicacid-*tert*-butyl-ester)(thiocticester)azobenzene
- **SAZ1** - 4,4'(benzoicacid-*tert*-butyl-ester)(hexathiol)azobenzene
- **TE** - Thioctic methyl ester
- **TEGT** - triethylene glycol thiol
- **GAZ1** - 4,4'(benzoicacid)((triethyleneglycol)- propylthiol)azobenzene

SAMs made from compounds **TAZ1**, **SAZ1** and **TE** are investigated in Chapter four. SAMs made from compounds **TEGT** and **GAZ1** are investigated in Chapter five.

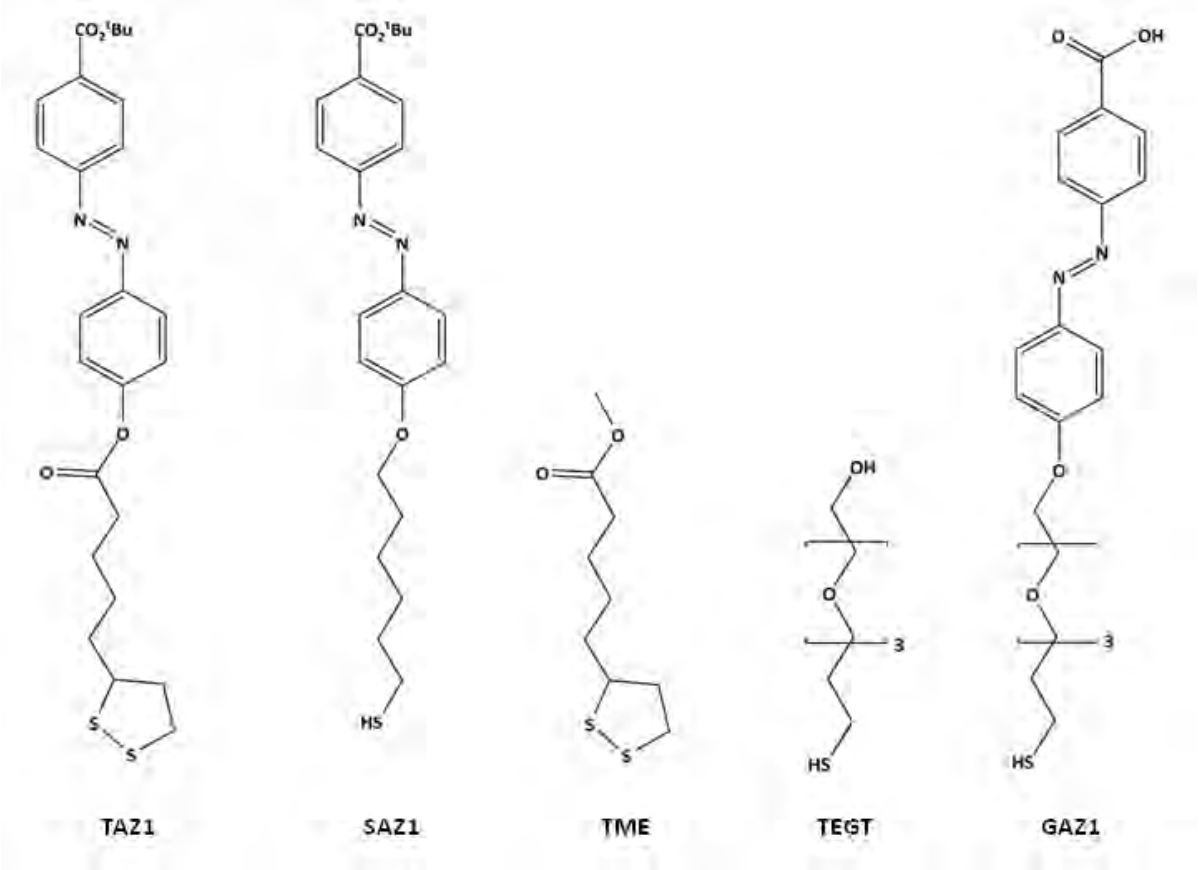

Figure 3.1 Structures of five surfactants synthesised as SAM surfactants. Surfactants TAZ1, SAZ1 and TME were are studied in chapter 4, where we investigate the effect that the ditholane head group of TAZ1 has on the isomerisation of azobenzne, within the fully formed SAM. Surfactants TEGT and GAZ1 are investigated in chapter 5. Importantly GAZ1 has a carboxyl head group, which is important in the attachment of bio-active mannose to the surface. Also both surfactants contain triethylene glycol components in their backbone which is important with respect to the controlled immobilisation of bio-molecules.

3.2 Synthesis

3.2.1 TAZ1

TAZ1 was synthesised through a two step procedure (**Figure 3.2**). The synthesis of compound **1** followed a literature procedure.[59] The procedure involved the diazotisation of 4-aminobenzoicacid-*tert*-butyl-ester followed by the addition of de-protonated phenol. Compound **1** was afforded in good yield (85 %). **TAZ1** was then obtained from **1** using an adapted literature procedure.[160] The procedure involved the Steglich esterification of **1**, with commercially available α-lipoic acid. The steglich esterification is commonly employed for the hydrolysis of the tert-butyl ester of compound 1. The reaction requires dicyclohexylcarbodiimide (DCC) is preformed at room temperature, overnight, under anhydrous conditions and in the presence of a catalyst **4-Dimethylaminopyridine** (DMAP). TAZ1 was afforded in a reasonable yield (70 %) and purified by column chromatography.

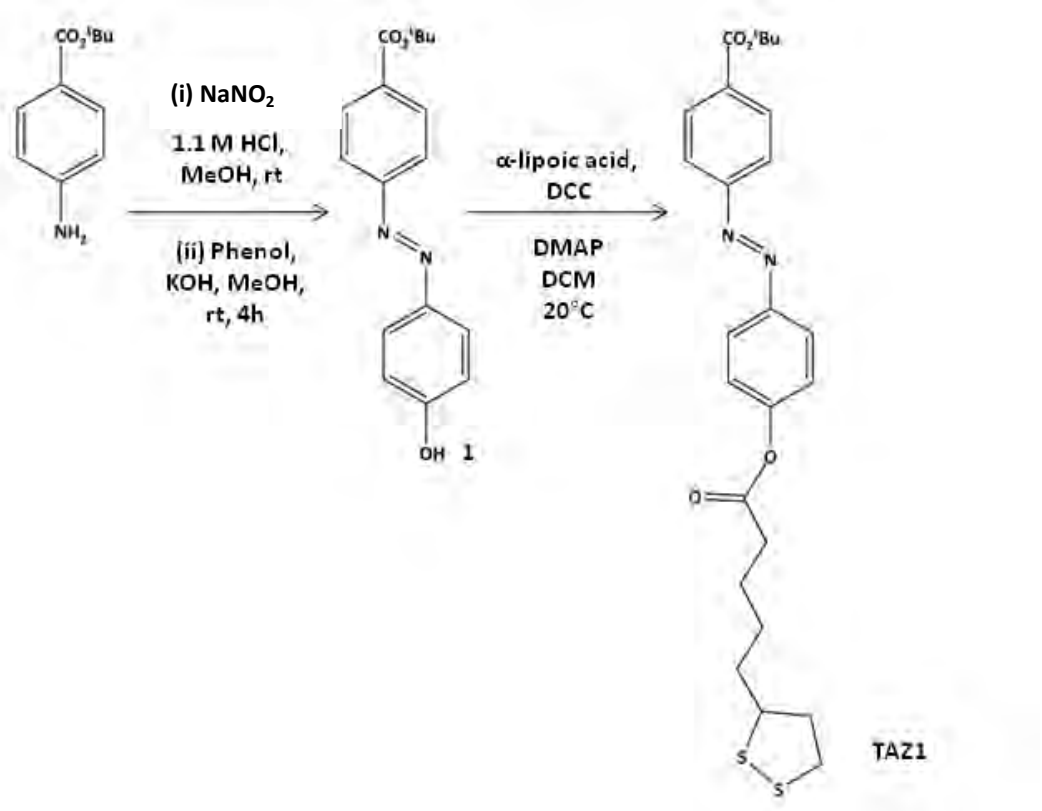

Figure 3.2 scheme for the synthesis of TAZ1.

3.2.2 TME

The synthesis of TME was followed the same procedure as the synthesis of **TAZ1** from compound **1**. However, compound **1** was replaced by methanol to afford **TE** in good yield (70 %). The crude mixture was purified using column chromatography.

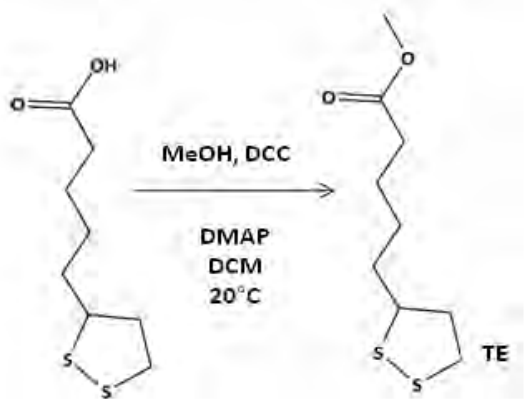

Figure 3.3 Scheme for the synthesis TME

3.2.3 SAZ1

SAZ1 all the following surfactants were synthesized n collaboration with Dr. Parvez Iqbal, School of Chemistry, University of Birmingham, through a multi step procedure (**Figure 3.4**). The synthesis of compound **1** is described above. Compound **2** was synthesized from commercially available 6-bromo-hex-1-ene through thioacetylation at reflux, for 2 hrs and in the presence of azobisisobutyronitrile (AIBN). Compound **2** was afforded in good yield (76 %). Compound **3** was obtained by alkylation of **1** by addition **2**, at reflux, overnight and under basic conditions. Compound **3** was afforded in good yield (66 %). **SAZ1** was obtained by de-protection of **3** through hydrolysis, at reflux, for 2 hrs, under acidic and anhydrous conditions. **SAZ1** was afforded in good yield (71 %).

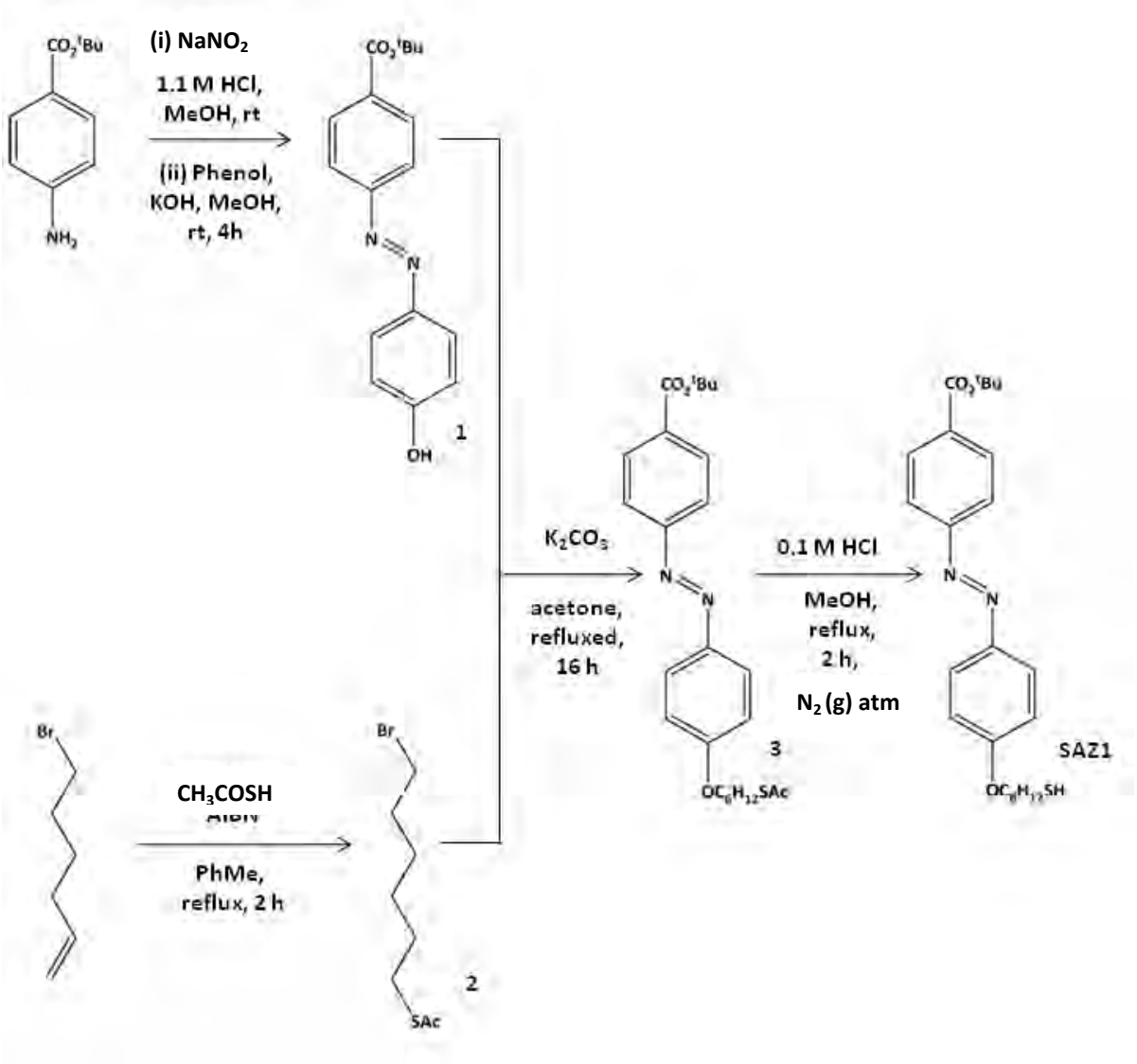

Figure 3.4 Scheme for the synthesis of SAZ1

3.2.4 TEGT

TEGT was synthesized through a three step procedure (**Figure 3.5**). Commercially available tri-ethylene-glycol was alkylated through the addition of 3-bromo-prop-1-ene, at reflux, overnight and under basic conditions. Compound 4 was afforded in good yield (60 %) and was converted into 5 through thioacetylation at reflux, for 1 hr, in the presence of azobisisobutyronitrile (AIBN). Compound 5 was afforded in good yield (79%). Compound 5 was converted to TEGT through de-protection of the thioacetate at reflux, for 4hrs under acidic conditions. TEGT was afforded in good yield (90%).

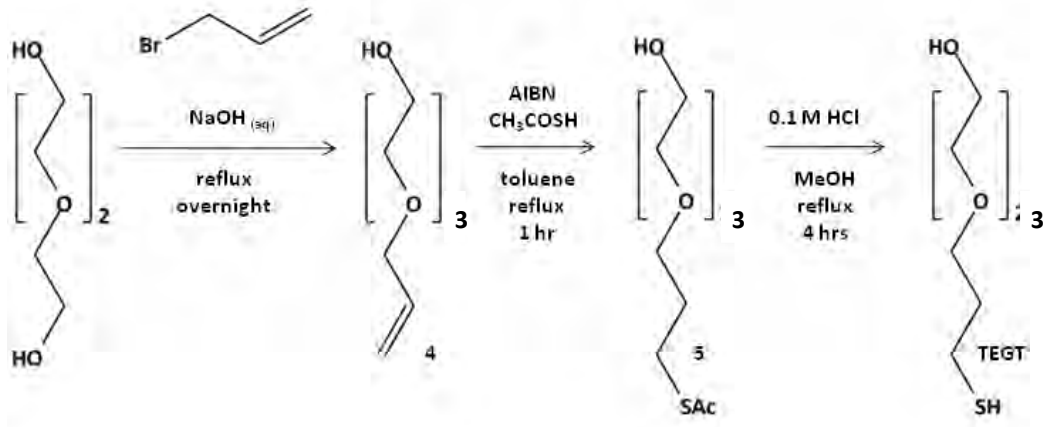

Figure 3.5 Scheme for the synthesis of TEGT

3.2.5 GAZ1

GAZ1 was synthesized through a multi step procedure (**Figure 3.6**). The synthesis of compound **6** is the same as described above for **1** but using 4-aminobenzoicacid instead of 4-aminobenzoicacid-*tert*-butyl-ester. Compound **6** was obtained in good yield (90 %). Compound **7** was obtained from the esterification of **6** at reflux, overnight and under acidic conditions. Compound **7** was afforded in good yield (76 %). Compound **8** was obtained from tosylation of **5** in the presence of triethylamine at room temperature, in DCM, overnight and under anhydrous conditions. Compound **8** was afforded in good

yield (75 %). Next compound **9** was obtained by the alkylation of **7** by the addition of **8** at reflux, overnight under basic and anhydrous conditions. Compound **9** was afforded in good yield (94 %). Compound **10** was obtained from **9** by de-protection of the thiol by hydrolysis of the acetyl group at reflux for 16 hrs, under acidic and anhydrous conditions. Compound **10** was afforded in good yield (83 %). Finally **GAZ1** was obtained from **10** by hydrolysis of the methyl ester, at reflux for 16 hrs, under basic and anhydrous conditions. **GAZ1** was afforded in a satisfactory yield (52 %).

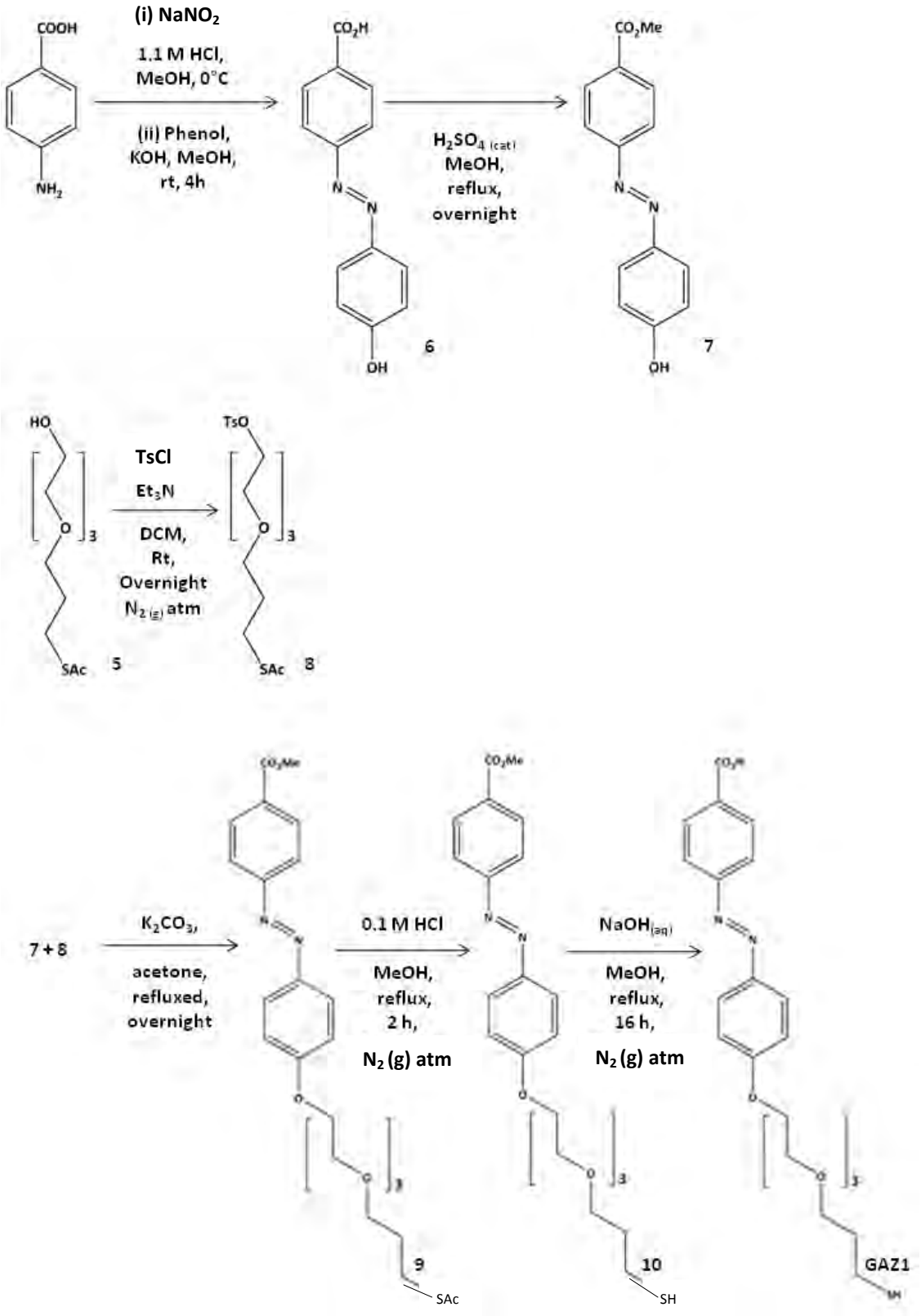

Figure 3.6 Scheme for the synthesis of GAZ1

4.0 Making space for azobenzene isomerisation within SAMs

In recent years, there has been an increasing number of reports in the literature on the development of switchable SAMs.[80] These SAMs are switched between two different states, through the application of an external stimulus, such as heat,[81-85] chemical,[86, 87] electrical potential[88-100] and light.[101-116] Light is the most attractive of stimuli,[161] as it holds several advantages over other stimuli: switching can be stimulated from far a field;[161] response times can be of the order of pico seconds[120, 161] and furthermore, light is compatible with a number of different solvent, electrolyte and gas media.[161]

Several photo-chromic molecules have been investigated as switchable SAMs, including diarylenes,[102] stilbenes[103] and azobenzenes.[101-116] Azobenzene is particularly attractive as it shows the most dramatic shape change between its two photochromic isomers.[117] Azobenzene undergoes photo-isomerisation, between its *trans* and *cis* isomers, upon the application of *UV* or *Vis* light.

Silane SAMs made from azobenzene based surfactants have been shown to undergo photo-isomerisation.[162] However, photo-switching of thiol SAMs made from azobenzene containing surfactants is hindered.[134] Hindrance to photo-isomerisation of thiol based azobenzene SAMs occurs through two mechanisms, which are chromophore aggregation[134] and spatial constraints.[137] In recent years, research has focused on overcoming these hindrances, through design of surfactants with novel modifications, such as different sulphur based head groups, [105, 106, 109 - 111] substitution on azobenzene rings with alkyl functionalities[107] and the inclusion of bulky groups such as carborane[112] and hydrogen bonding amides[117] within the surfactants backbone. A further discussion of these systems can be found in chapter 1. Herein we report on the design of a novel azobenzene containing surfactant with a cyclic 1,2-dithiolan-3-yl head group.

4.1 Aims

The research presented in this chapter is aimed to overcome the optical inactivity[134, 137] of azobenzene thiol SAMs. Optical inactivity will be overcome by the development of a non-aggregating photo-switchable SAM, with sufficient space for the isomerisation of azobenzene. The system is based upon an azobenzene containing surfactant, TAZ1 (**Figure 4.1a**) synthesised in chapter 3. TAZ1 is a thioctic acid derivative and so has a bulkier cyclic 1, 2-dithiolan-3-yl head group, relative to the conventional thiol head group (e.g. SAZ1)

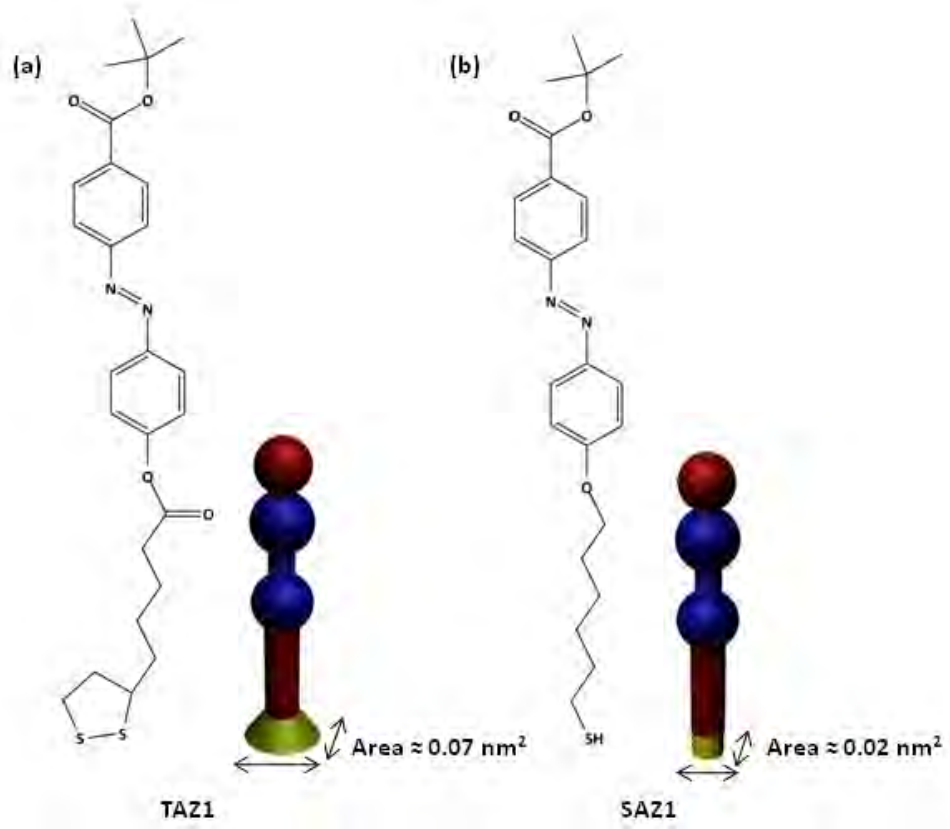

Figure 4.1 Chemical structure and cartoon representation of surfactants used in this chapter (a) TAZ1 (b) SAZ1 control.

It is hypothesised that TAZ1s bulky cyclic 1, 2-dithiolan-3-yl head group will prevent aggregation, as well as creating some space for azobenzene isomerisation, relative to the alkyl thiol head group control, SAZ1 (**Figure 4.1b**). This difference is hypothesised due to the differences in the molecular foot prints of the head groups of the two surfactants (**Figure 4.2**).

TAZ1s end group is a *tert*-butyl ester, which is chemically inert under ambient conditions. Once the SAM has been shown to undergo isomerisation, its *tert*-butyl end group will be hydrolysed in order to reveal the carboxylic acid.[150]

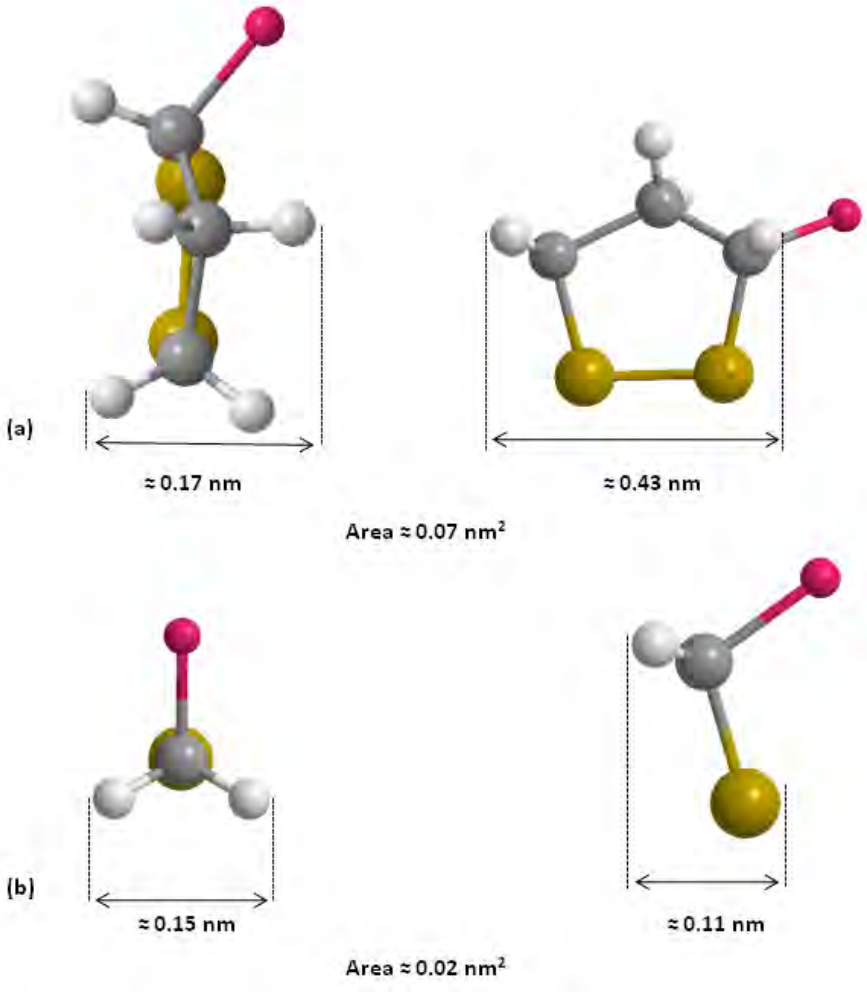

Figure 4.2 Calculated molecular footprints of (a) TAZ1 (b) SAZ1

4.1.1 Objectives

There are three research objectives in this chapter:

1. Investigate the formation of SAMs from TAZ1.
2. Compare the photo-isomerisation of TAZ1 SAM to the control SAZ1 SAM.
3. Hydrolyse the TAZ1 SAM's *tert*-butyl end group to produce an acid.[160]

4.1.1.1 Objective 1

The formation of TAZ1 SAMs on Au (**Figure 4.3**) was investigated as a function of time and concentration by contact angle, ellipsometry and X-ray photo electron spectroscopy (XPS).

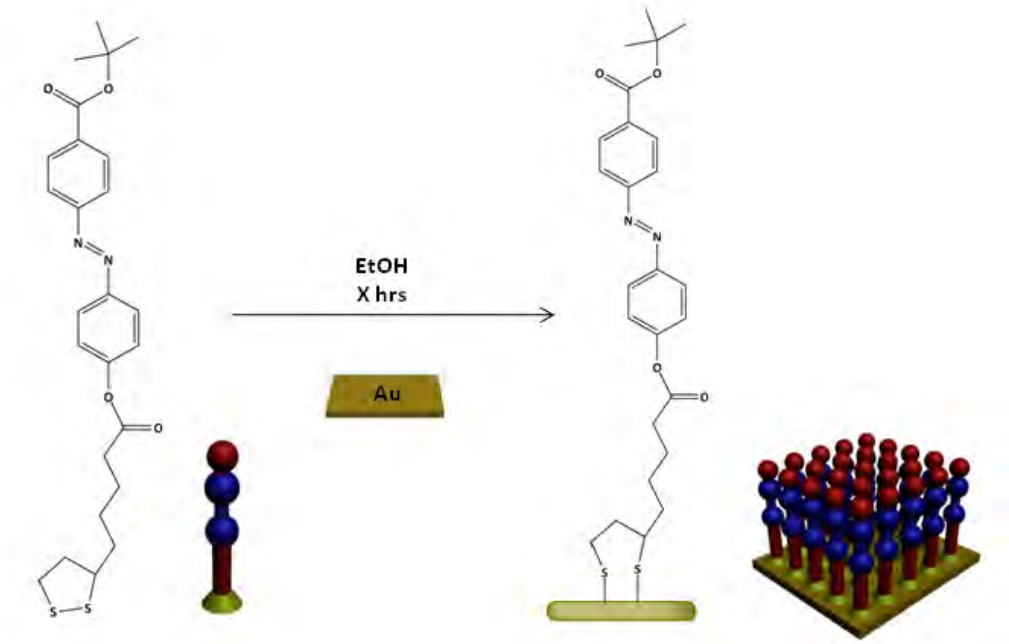

Figure 4.3 illustration of objective 1, TAZ1 SAM formation showing both the chemical structure of the cartoon representations. SAMs were formed in ethanol (EtOH) over

different time scales (X hrs). Note, for TAZ1 SAM the surfactant is drawn standing upright for convienence and clarity, in reality they will be tilted.

4.1.1.2 Objective 2

The photo-isomerisation of TAZ1 SAMs was investigated by ultraviolet/visible light (*UV/VIS)* spectroscopy. The isomerisation was compared to SAZ1 SAMs. SAZ1 was used as a control because of its thiol head group. Thiol based azobenzene SAMs are known to form aggregated SAMs.[134] The proposed difference in isomerisation is due to the differences in the head groups foot print. The molecular footprint of the cyclic 1, 2-dithiolan-3-yl head group of TAZ1 is 0.07 nm^2, whereas the thiol head group of SAZ1 has a molecular footprint of 0.02 nm^2 (**Figure 4.4**).

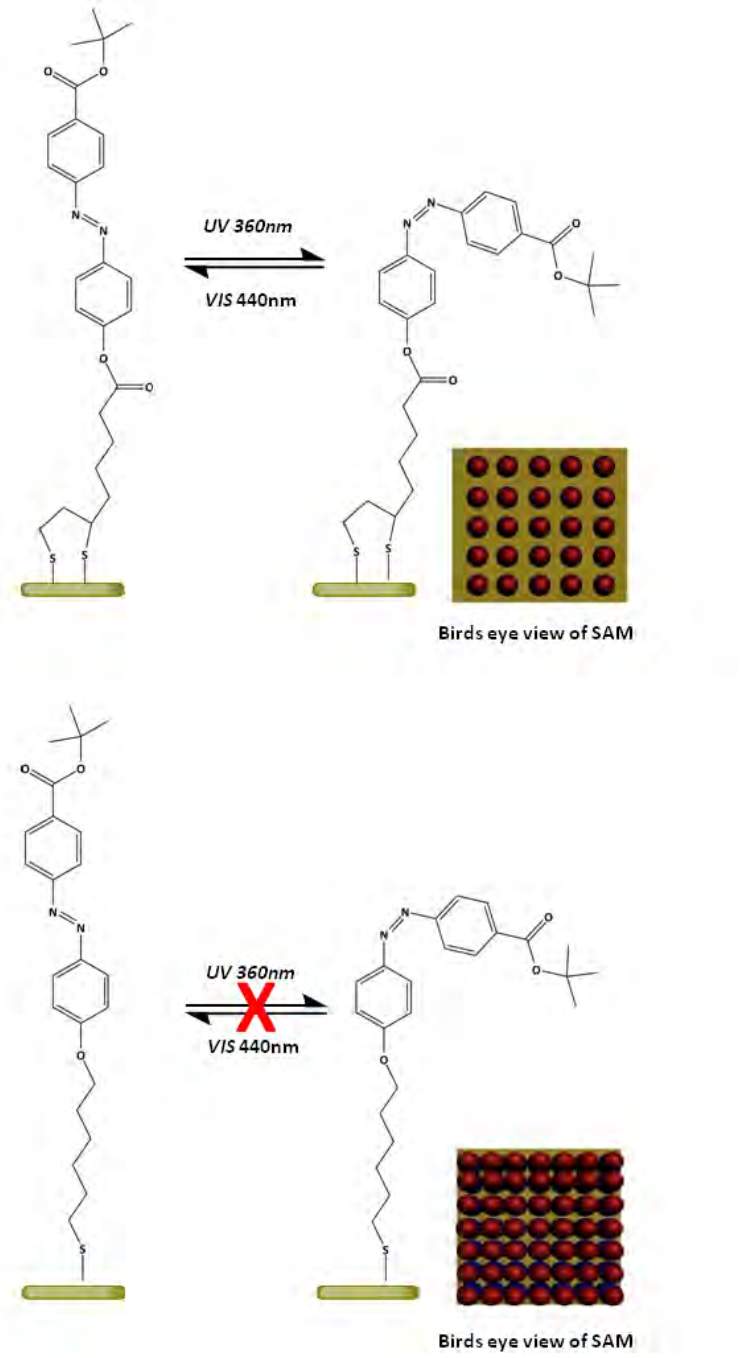

Figure 4.4 Illustration of objective 2, comparison of isomerisation of TAZ1 and SAZ1 SAMs. We propose that TAZ1 SAMs should isomerise while SAZ1 SAMs should not as the large footprint of the TAZ1 head group, relative to SAZ1, inhibits azobeneze aggregation by spacing azobenzene out. Note, molecules are drawn standing upright for convienence and clarity, in reality they will be tilted.

4.1.1.3 Objective 3

The hydrolysis of TAZ1 SAMs *tert*-butyl ester end group, to the carboxylic acid (**Figure 4.5**) was to be investigated, using contact angle and XPS. The aim of hydrolysis is to introduce chemical activity to the surface. The hydrolysed SAM was to be used to study the *'on'/'off'* switching behaviour of the SAM, with respect to the immobilisation of carboxylic acid terminated polystyrene nano-particles. Previous work within our group[160] studied the immobilisation of carboxylic acid terminated polystyrene nano-particles onto hydrolysed aromatic *tert*-butyl ester SAMs.

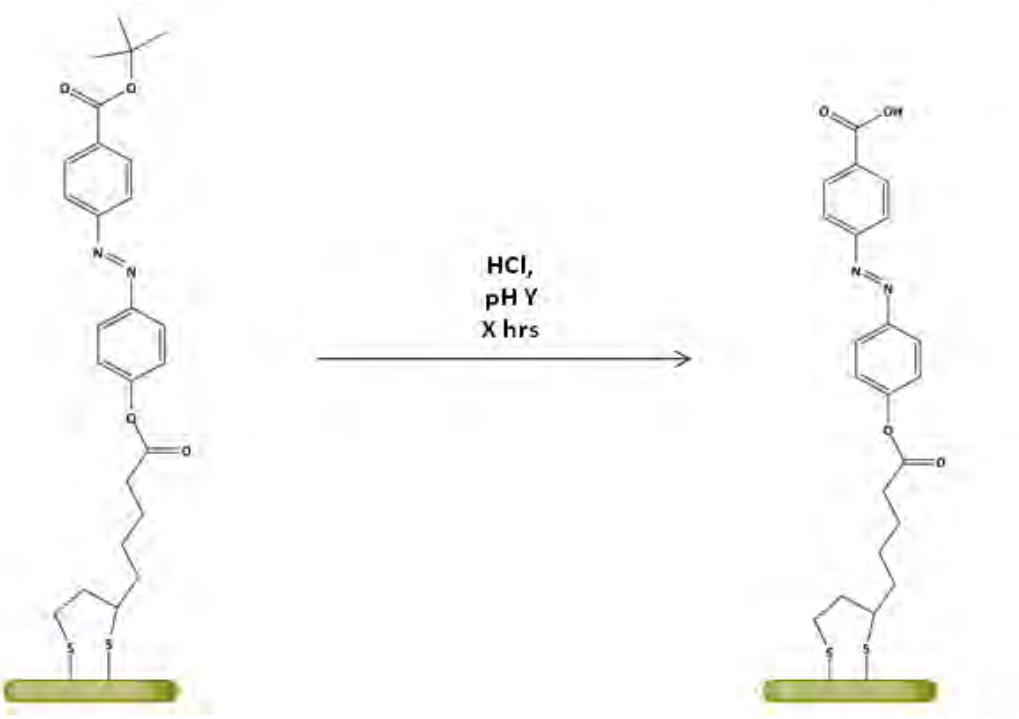

Figure 4.5 illustration of objective 3, hydrolysis of TAZ1 SAM. Synthetic procedure will follow the method for hydrolysis of an aromatic *tert*-butyl ester. Hydrolysis was preformed in hydrochloric acid at different pHs (Y) and over different time scales (X hrs). Note, the surfactants are drawn standing upright for convienence and clarity, in reality they will be tilted.

4.2 Results and discussion

4.2.1 Objective 1 -TAZ1 SAM Formation Studies

The formation of TAZ1 SAMs was investigated. The analytical techniques used were ellipsometry, contact angle, and X-ray photoelectron spectroscopy (XPS). All glassware and Au substrates were piranha cleaned prior to use. SAMs were formed by immersion of freshly cleaned Au substrates in ethanolic solutions of TAZ1, after which SAMs were washed, dried and analysed (see experimental section). Details of sample preparation and analytical protocols can be found in the experimental section (**Chapter 6**).

4.2.1.1 Ellipsometry

4.2.1.1.1 TAZ1 SAM formation as a function of solution concentration

The thickness of TAZ1 SAMs formed over 24 hours, from ethanolic solutions, was measured as a function of TAZ1 solution concentration, as shown in **Figure 4.6**. At higher concentrations (0.5 to 0.125 mM) the SAM thickness is ≈ 3.2 nm, which is greater than the molecular length of TAZ1, which is estimated to be 2.5 nm, as determined by Chem Draw 3D software. At the lowest concentration (0.0625 mM) the ellipsometric thickness is ≈ 1.8 nm, in keeping with the modelled molecular length and a tilt of 44° in the SAM.

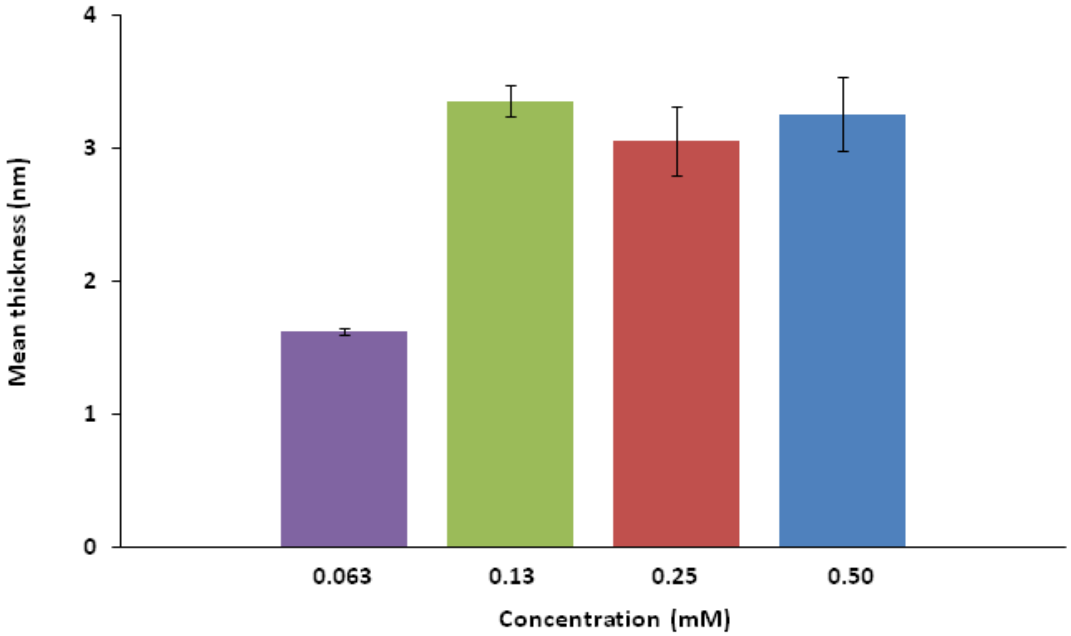

Figure 4.6 TAZ1 SAMs, Ellipsometric thickness *vs*. concentration at a formation time of 24 hours, concentration is given to two significant figures.

The higher than expected thickness, at higher concentrations (≥ 0.125 mM) could suggest multi-layer formation, promoted through the aggregation of surfactants. Aggregation occurs through non-covalent interactions and results in the formation of dimers or higher aggregates.[163] Two types of aggregation, J- and H, are known to occur in both solution[163] and on surfaces[164] of azobenzene derivatives, including SAMs[137, 165]

We propose a model of either a bi-layer or multilayer, both promoted through aggregation (**Figure 4.7**). An aggregated bi-layer would have the same thickness that we observed (**Figure 4.7a**). However, an aggregated multilayer is also plausible (**Figure 4.7b**). Indeed n-alkylthiol surfactants have been shown to form such a transient multilayer during SAM formation.[166] Furthermore, relative to n-alkylthiols, TAZ1s ability to form a transient multilayer is theoretically higher, due to azobenzenes ability to form

aggregates, as well as its increased physisorption energy on Au (6.2 KJmol^{-1} per linear CH_2 unit; 8.1 per cyclic CH_2 unit [167] and 61.8[168] per azobenzene unit). Stronger physisorption and aggregation will inevitably provide a higher energy barrier to SAM formation, post multilayer formation. The phenomenon was not investigated further. All further formation studies were carried out with a surfactant concentration of 0.0625 mM.

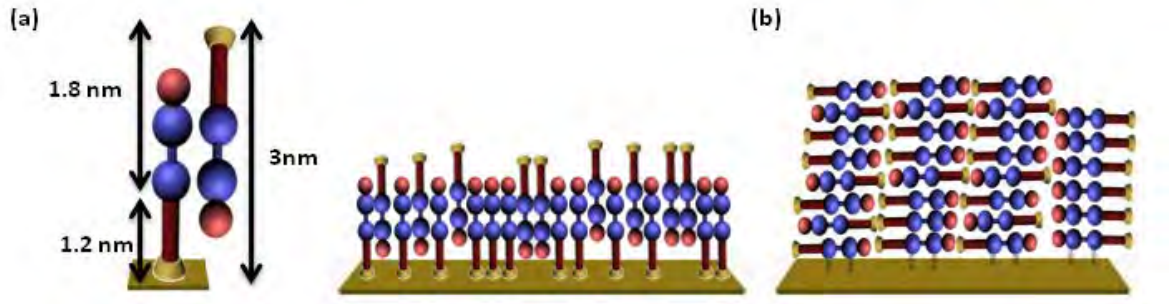

Figure 4.7 proposed models of TAZ1 multilayer at concentrations ≥ 0.125 mM (a) aggregated bi-layer (b) aggregated multilayer. These models were arrived at considering available literature on transient multilayer's during SAM formation as well as the ability of azobenzene to form aggregates, see above.

4.2.1.1.2 Formation of TAZ1 and SAZ1 SAMs as a function of time

Ellipsometry was further used to investigate the formation of TAZ1 SAMs, formed from a 0.0625 mM ethanolic solution, as a function of time (**Figure 4.8**). We also investigated both (**Figure 4.8**) the thickness of SAZ1 SAMs at 0.0625 mM as well as the thickness of bare gold, the rationale for which is explained on page 69.

What was striking about the TAZ1 SAM (**Figure 4.8**, blue diamonds) was that formation can be split into three regions. Region I occurring between 0 – 6 hrs, region II between 6 - 21 hrs and region III after 21 hrs.

Region I: The thickness has rises to ≈ 2.4 nm in 0.5 hr and then drops to 1.2 nm after 6 hrs.

Region II: Over the next 15 hrs, the SAM undergoes a growth in thickness, as might be expected for SAM formation.

Region III: After 21 hrs the thickness plateaus at ≈ 1.8 nm, indicating that the SAM is fully formed.

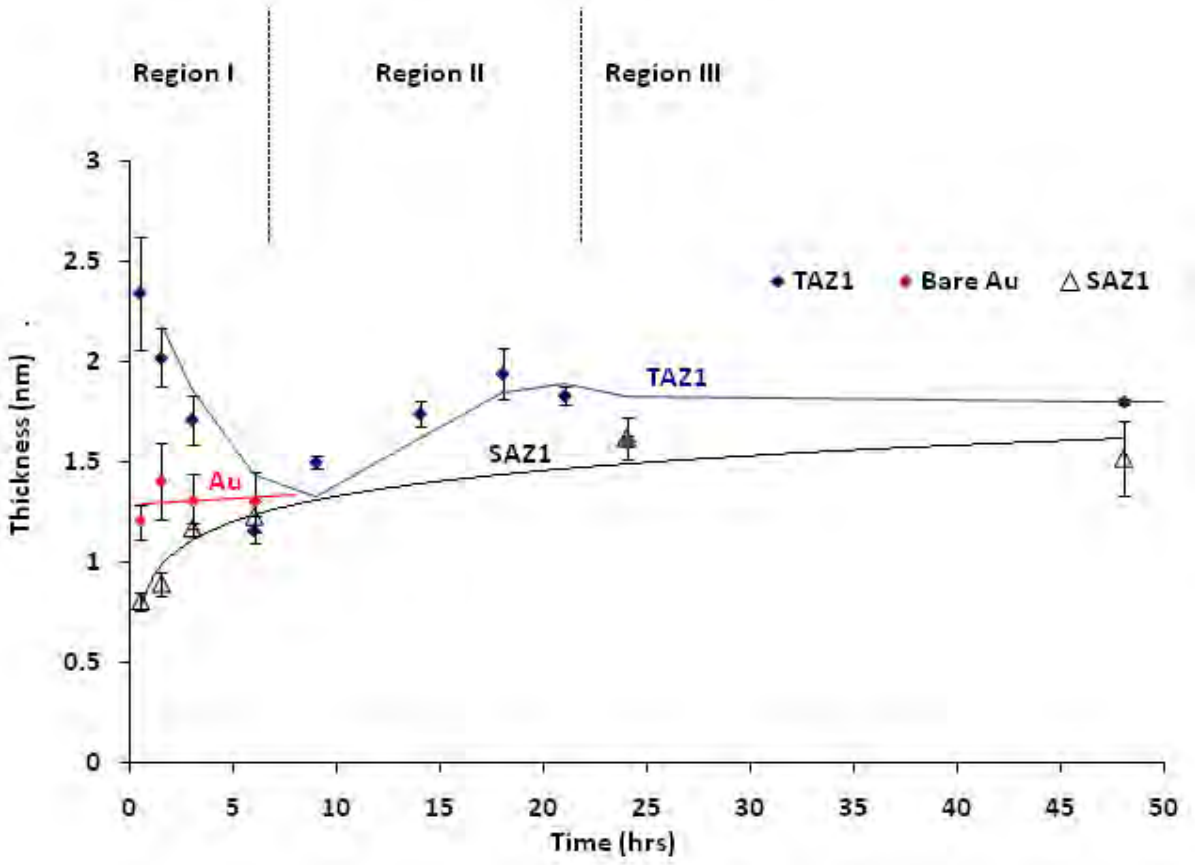

Figure 4.8 ellipsometry kinetic study, thickness against formation time for TAZ1, SAZ1 (formed from a solution concentration of 0.0625 mM) and bare Au, immersed in pure ethanol.

The pattern observed for SAZ1 SAMs (**Figure 4.8**, clear triangles) followed traditional formation kinetics, as expected, in that over the first 6 hrs there was no region I as for TAZ1. The thickness of SAZ1 SAMs had risen to ≈ 0.80 nm in 0.5 hrs and then rose to ≈ 1.2 nm by 6 hrs (region I for TAZ1 SAMs) and reached a plateau of ≈ 1.6 nm by 24 hrs, giving a calculated tilt angle ≈ 50°. This suggests that the strange behaviour of region I, in the curve of TAZ1, is a phenomenon of TAZ1s molecular structure.

The ellipsometric thickness of both fully formed SAMs, is less than the molecular length of the molecules (both 2.5 nm, **Figure 4.9**). This discrepancy, between molecular length

and SAM thickness, is expected and in agreement with the literature and is attributble to both the tilt angle and density of the SAM surfactants.[15, 169] The tilt angle of azobenzene SAMs has been shown to vary, depending on the chain lengths and nature of the 4 4' substitutions.[169] In the literature, a wide variation in the tilt angle has been found from 14°[165] to 34°[169] for azobenzne SAMs with alkyl based backbones and thiol head groups. However, the head group of TAZ1 SAMs is based on the cyclic 1, 2-dithiolan-3-yl of thioctic acid. Thioctic acid based SAMs, have been shown to have a tilt angle between 35-45°.[170] We calculated the tilt angle of TAZ1 SAMs to be 44°, and therefore is in accordance with the literature value for thioctic acid SAMs. The high tilt angle in SAZ1 has been attributed to the small length of the alkyl chain.[171]

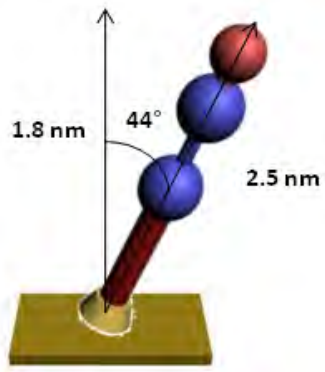

Figure 4.9 Schematic of calculated molecular length and tilt angle of TAZ1 SAM surfactants. SAZ1 has the same molecular length as TAZ1.

The high thickness, of TAZ1 SAMs, at lower formation times (region I) was further investigated. It was envisaged that TAZ1s molecular structure may give rise to slow formation kinetics that exposed bare Au. Bare Au is a relatively high energy surface and is prone to the physisorption of air borne contaminants.[172] However, ellipsometry showed the thickness of the contaminant layer on bare Au to be ≈ 1.24 nm, irrespective of immersion time (**Figure 4.8**, red circles). This thickness is lower than the high values

observed at low formation times, for TAZ1 and hence region I in the curve cannot be attributed to the non-specific physisorption of airborne contaminants.

It is hypothesised that the high thickness of TAZ1 SAMs at low formation times (region I) relative to bare Au and SAZ1, could be explained by a transient multilayer (**Figure 4.10a**) similar to that of n-alkyl thiol SAMs.[163] Furthermore, this fits with thickness observations at high concentrations (≥ 0.125 mM, page 72) where we have suggested such a multilayer exists. At high concentrations it is hypothesised that this multilayer cannot be displaced by SAM formation (**Figure 4.10b**) whereas at lower concentrations the multilayer is thinner, and therefore, can be displaced by SAM formation. This model was not investigated further, however, it will be the subject of future work through the employment of Electrochemical Quartz-Crystal Microbalance (EQCM) which is the same technique used to show the existence of transient multilayer's in the formation of n-alkane thiol SAMs.[163] .

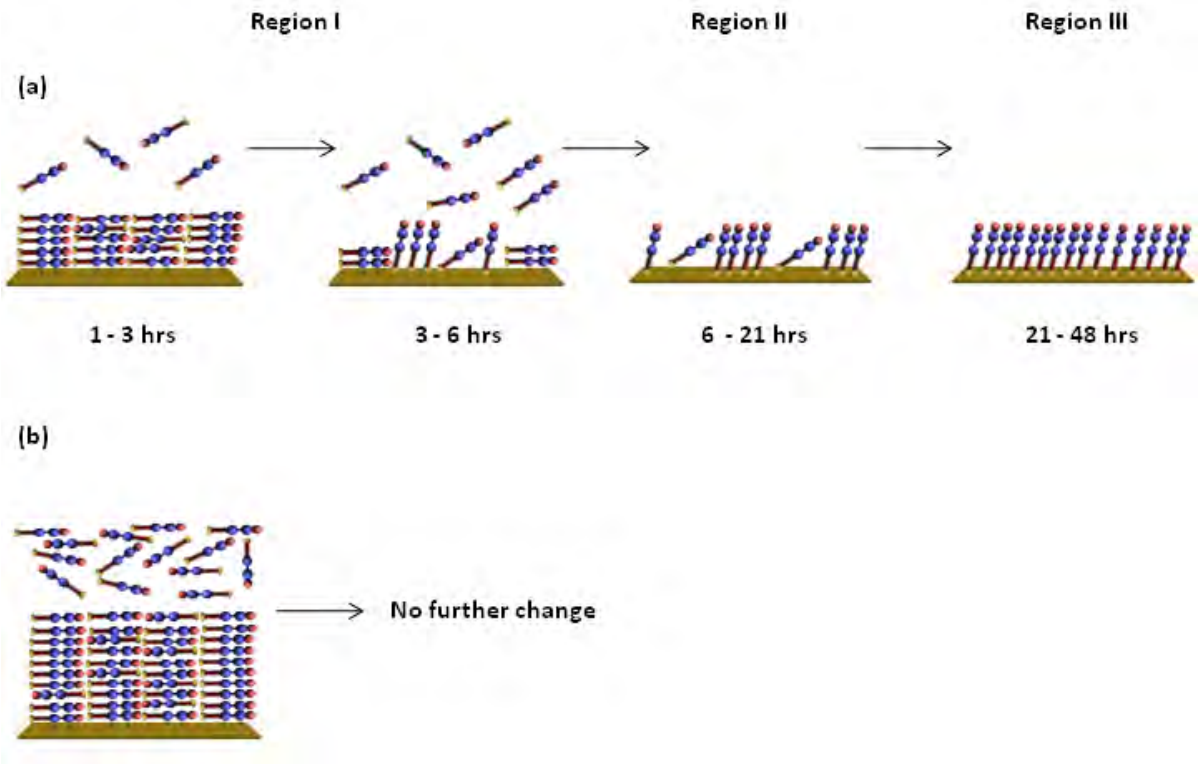

Figure 4.10 Cartoon representation of aggregated multilayer hypothesis (a) low concentration (< 0.0625 mM) aggregated multilayer is thinner and displaced by SAM formation (b) high concentrations (0.5 – 0.125 mM) the aggregated multilayer is thick and consequently stable, so is not displaced by SAM formation.

In summary, ellipsometry data suggests a formation time of ≈ 21 hrs for TAZ1 SAMs at a concentration of 0.0625 mM, giving a SAM of thickness 1.8nm, with a calculated tilt angle of 44°, this angle is in accordance to the literature values for thioctic acid SAMs. At low formation times we hypothesise that a transient aggregated multilayer exists. Furthermore, above concentrations of 0.0625 mM an aggregated multilayer forms, which cannot be displaced by SAM formation.

4.2.1.2 Contact Angle

The dynamic advancing (θ_{Adv}) and receding (θ_{rec}) contact angles were recorded as a function of time for TAZ1 SAMs made from 0.0625 mM ethanolic solutions (**Figure 4.11**).

The advancing contact angle was approximately constant over the times investigated and was ≈ 90°. However, the receding contact angle changed with time. The observed pattern is similar to that observed for ellipsometry and three formation regions seem apparent: region I = 0 - 6 hrs; region II = 6 - 21 hrs and region III = 21 + hrs.

Region I: The receding contact angle started at ≈ 64° at 0.5 hrs, it dropped to ≈ 36° at 1.5 hrs, then rose to ≈ 64° over the following 4.5 hrs.

Region 2: The receding contact angle showed little change over the next 15 hrs.

Region 3: By 21 hrs the receding contact angle had reached a plateau at ≈ 72° (region III).

Similarly the contact angle hysteresis started at ≈ 25° at 0.5 hrs, increased to ≈ 45° at 1.5 hrs then decreased to ≈ 19° over the following 4.5 hrs (region I). Hysteresis changed little over the next 12 hrs (region II) and by 21 hrs had reached at plateau at 21 hrs ≈ 15° (region III).

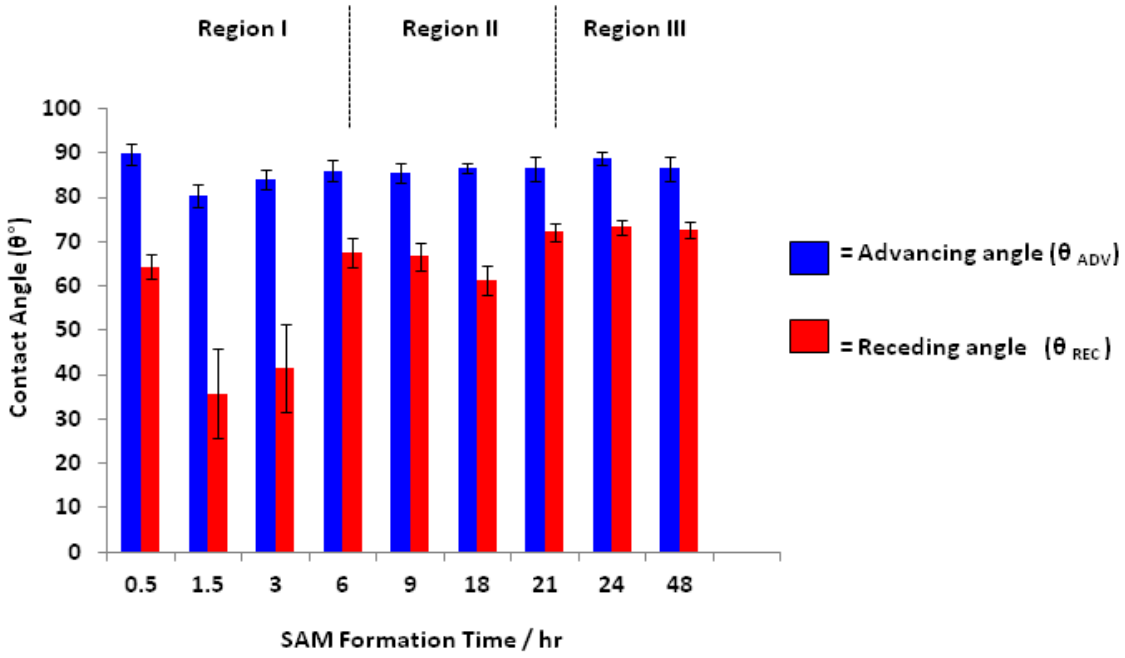

Figure 4.11 Contact angle kinetics of TAZ1 SAM formed from 0.0625 mM surfactant solution.

The advancing angle was in agreement to the static contact angle (89° ± 2) for a *tert*-butyl ester terminated azobenzene alkyl thiol SAM.[159] Furthermore, the dynamic contact angles (θ_{Adv} = 89 ° ± 1.5 θ_{Rec} = 73° ± 1.8) were in accordance with the literature for aromatic *tert*-butyl ester SAMs (θ_{Adv} = 89 ° ± 1 θ_{Rec} = 78° ± 1).[160] The high hysteresis in region one is believed to correspond to disorder, due to the tranisinet multilayer propsed in **Figure 4.10**.

In summary, contact angle data suggests a formation time of 21 hrs for TAZ1 SAMs made from a 0.0625 mM ethanolic solution. This result is in accordance with ellipsometry results. Furthermore, the values of the dynamic contact angles are in accordance to the literature values for aromatic *tert*-butyl thiols. However, interestingly the contact angle data at low SAM formation times supports the hypothesis of an

unusual phenomena, which we hypothesized (**section 4.3.1.1.2**) as an initial multilayer formation.

4.2.1.3 XPS

XPS was used to determine the elemental composition of TAZ1 SAMs, formed over 24 hours. TAZ1 SAMs contain sulphur, nitrogen, carbon, oxygen and gold, each of these regions were scanned individually and a survey scan of the SAM was also taken. The de-convoluted high resolution XPS spectra, of each binding region, are shown below (**Figure 4.12 - 4.16**). The spectra confirmed the presence of elemental species Au, S, O, C and N as was expected.

The gold Au 4f region was scanned and de-convoluted to show two peaks characteristic of Au $4f_{7/2}$ (84.01 eV) and $4f_{5/2}$ (87.68 eV).[145] The Au $4f_{7/2}$ peak was used as a reference/calibration for all other peaks. No oxidised gold[173] was apparent (**Figure 4.12**).

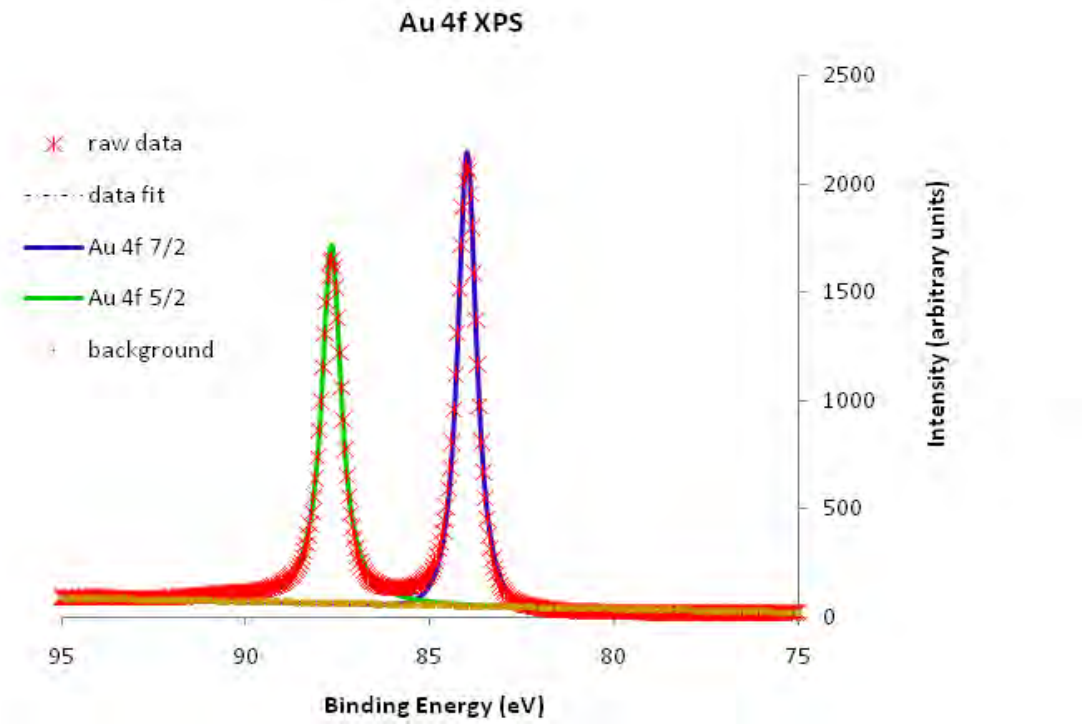

Figure 4.12 De-convoluted XPS spectra of gold 4f region of TAZ1 SAM

The carbon 1s spectra was de-convoluted into 3 separate peaks, attributed to five different binding environments (**Figure 4.13**). The main, predominant peak (284.8 eV) was attributed to C-C bonds[145] within both the alkyl chains and phenyl rings. The first of the two smaller peaks (286.6 eV) was attributed to C1s of the three binding environments[145] of C-S, C-N and C-O-C. Unambiguous de-convolution of these three peaks was not possible, due to the overlap of the binding environments. The third and final peak (288.9 eV) was attributed to the C1s photoelectron of the carbonyl C=O.[145]

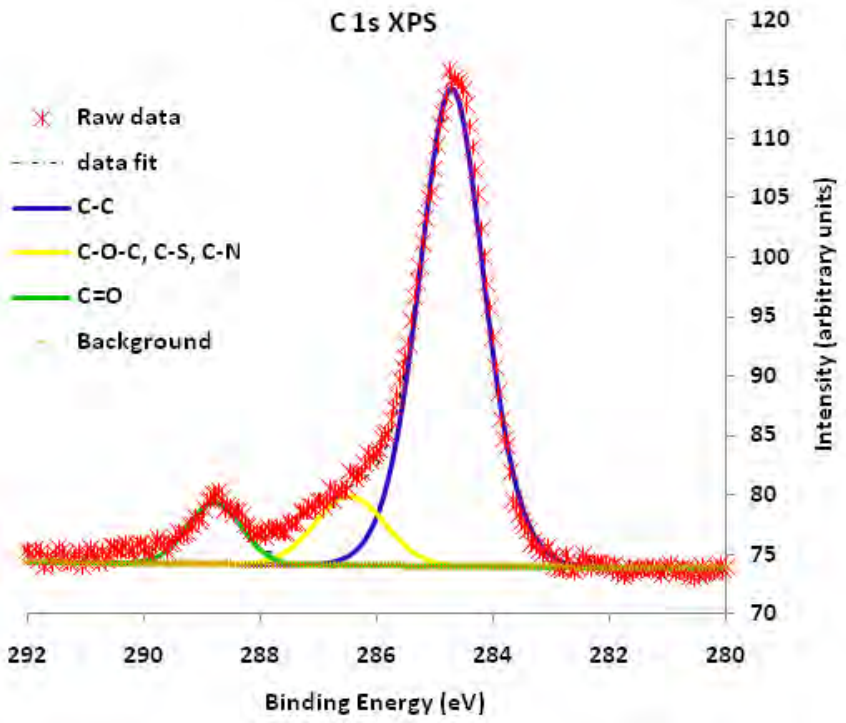

Figure 4.13 De-convoluted XPS spectra of carbon 1s region of TAZ1 SAM

The oxygen 1s spectra was de-convoluted into two different peaks, corresponding to two different binding environments,[145] arising from the ester moieties, C-O-C (533.45 eV) and the carbonyl oxygen C=O (531.95 eV) (**Figure 4.14**).

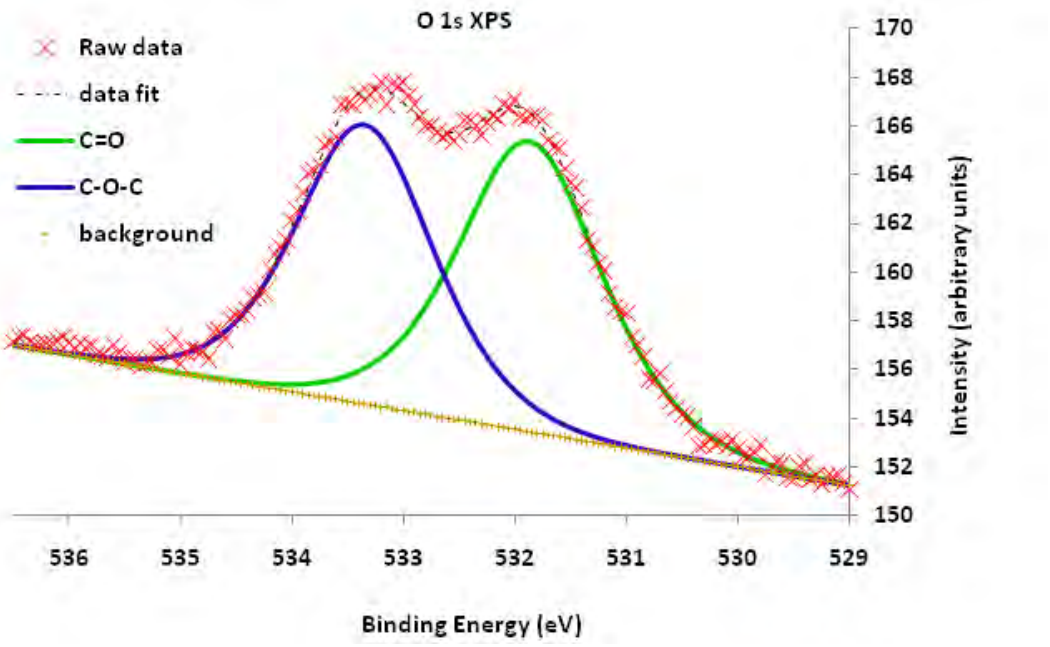

Figure 4.14 De-convoluted XPS spectra of oxygen 1s region of TAZ1 SAM

The nitrogen 1s spectra was de-convoluted into one peak (399.95 eV) corresponding to N=N of the azobenzene bond[174] (**Figure 4.15**).

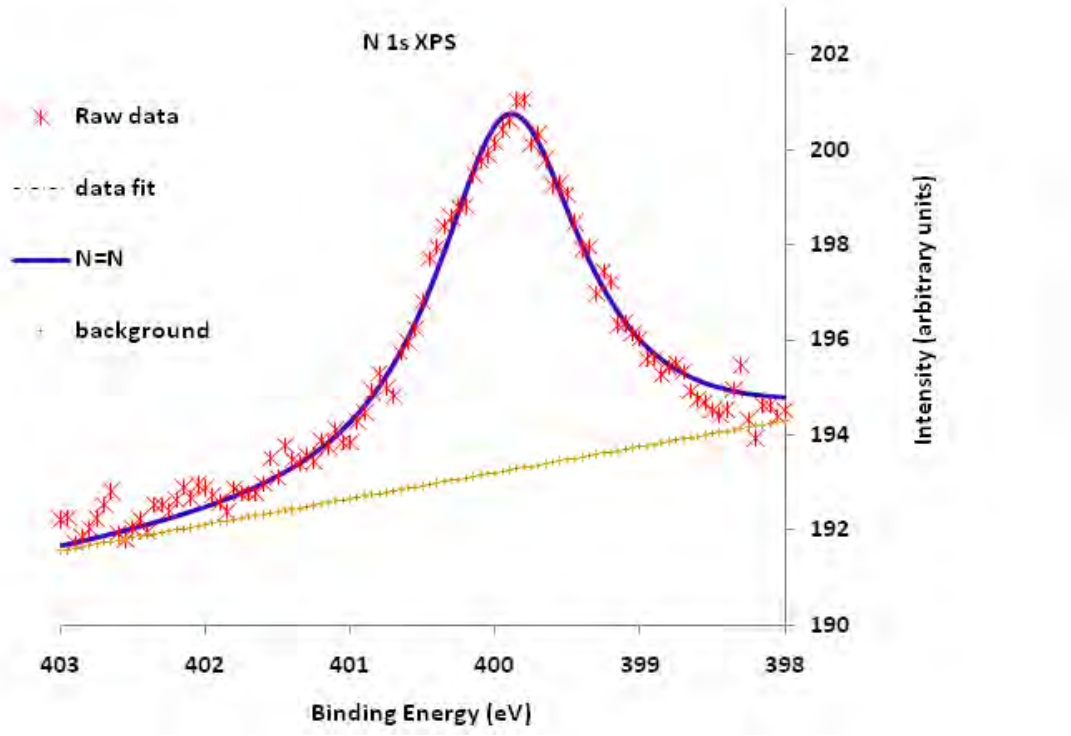

Figure 4.15 De-convoluted XPS spectra of nitrogen 1s region of TAZ1 SAM

The sulphur 2p spectra was de-convoluted with the characteristic branching ratio of 2:1 for the $2p_{3/2}$ and the $2p_{1/2}$ peaks, respectively (**Figure 4.16**). Deconvolution revealed two species to be predominant on the surface: gold bound thiolate, with S $2p_{3/2}$ (161.9 eV) S $2p_{1/2}$ (163.1 eV), and a disulphide,[175] with $S2p_{3/2}$ (163.3 eV) $S2p_{1/2}$ (164.5 eV). The disulphide peak has been reported[175] in thioctic acid based SAMs, and has been attributed to surfactants not bound to Au through the thiolate. Unbound surfactant is present due to the carboxylic acid end group, which either forms a H-bonded bi-layer or binds to the gold. However, TAZ1 contains no carboxylic acid and so the rational used to explain the disulphide peak in thioctic acid SAMs cannot explain the same observation in TAZ1 SAMs. The origin of the peak is investigated further below.

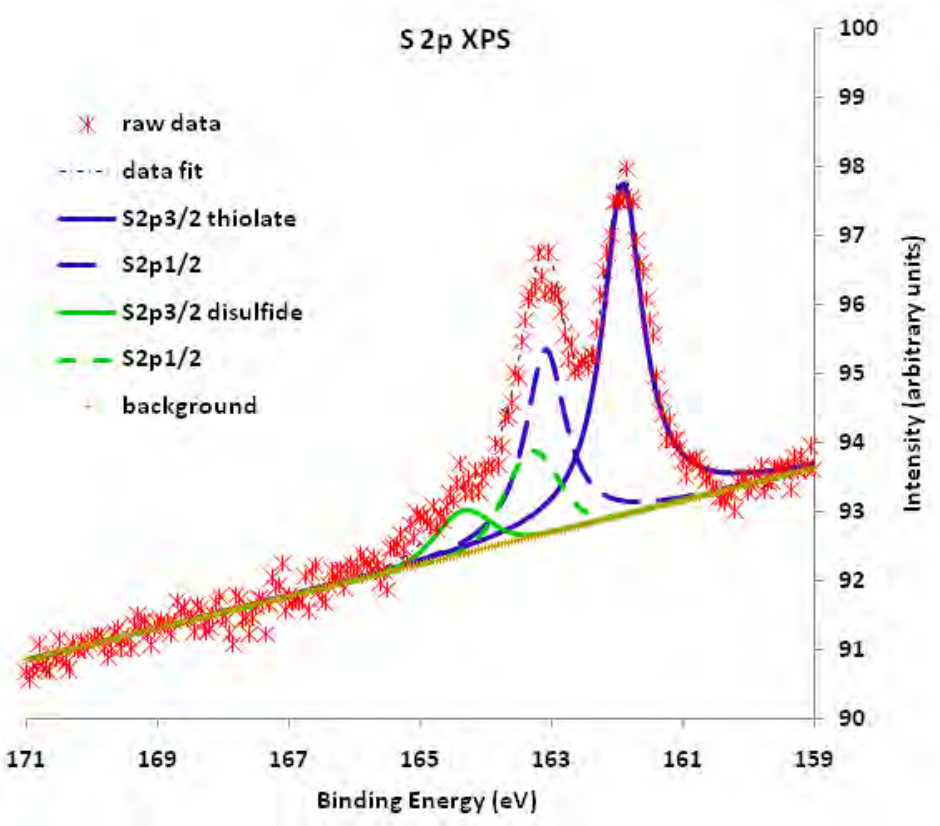

Figure 4.16 De-convoluted XPS spectra of Sulphur 2p region of TAZ1 SAM

In summary, XPS data shows the elemental composition of TAZ1 SAMs to be in accordance with the elemental species present. However, a disulphide peak was also observed and is investigated further below.

4.2.1.4 Further investigation of disulphide peak

The origin of the disulphide peak seen in the XPS spectra of TAZ1 SAMs was investigated further. Five hypothesises on the nature of this disulphide peak were made and each one investigated. These hypothesis are:

1. An artefact created by XPS photo-irradiation,[174, 176]

2. An intermediate species of SAM formation,
3. A feature of a bi-layer,[175]
4. Presence of unbound surfactants within a fully formed SAM and
5. A feature of the fully formed SAM

1. An artefact created by XPS photo-irradiation

XPS is a chemically invasive technique[145] and is known to induce photochemical changes in SAMs.[174, 176-178] Such photochemical changes include both desirable[176] reactions and undesirable photodecomposition of both alkyl[176, 178] and azobenzene[174] based thiol SAMs on gold. In a study by Lahio *et al.*[178] a disulphide peak (163.3 eV) was shown to emerge and grow, when thiol SAMs were subjected to the invasive irradiation of the XPS technique.

To investigate if the disulphide peak was an artefact of XPS irradiation five consecutive scans of the S_{2p} region were preformed. These scans were of 10 iterations each compared to the normal 20 iterations per scan of used for other S_{2p} XPS spectra. If the disulphide peak was an artefact of XPS its intensity, relative to Au, would increase with each scan.[178] No significant change was seen in the disulphide($2p_{3/2}$) to gold($4f_{7/2}$) ratio (**figure 4.17**) between scans. This result suggests that the disulphide peak is not a product of XPS irradiation.

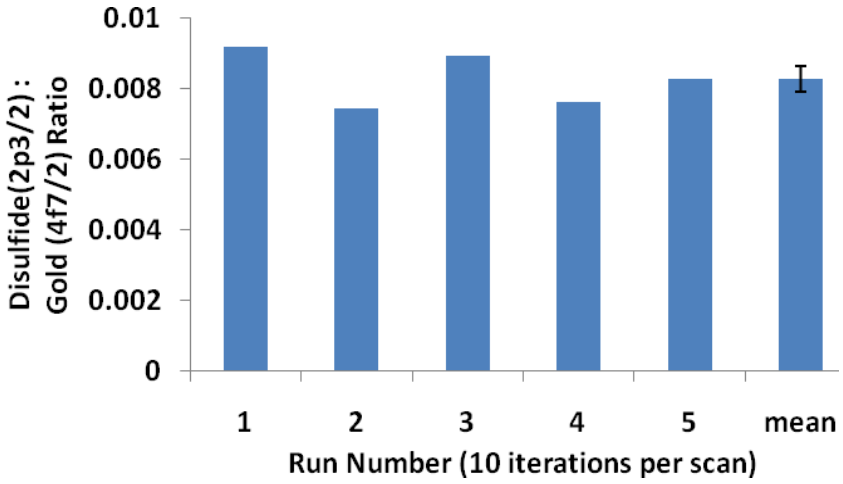

Figure 4.17 Disulphide:Gold ratio of 5 consecutive scans of the sulphur 2p binding environment.

2. An intermediate species of SAM formation

It was considered that the unexpected peak (163.3 eV) could be a feature of SAM formation, either as an unbound disulphide or possibly due to $R\text{-}S^-$, present as an intermediate of SAM formation.[179] The proposed model is shown below (**figure 4.18**).

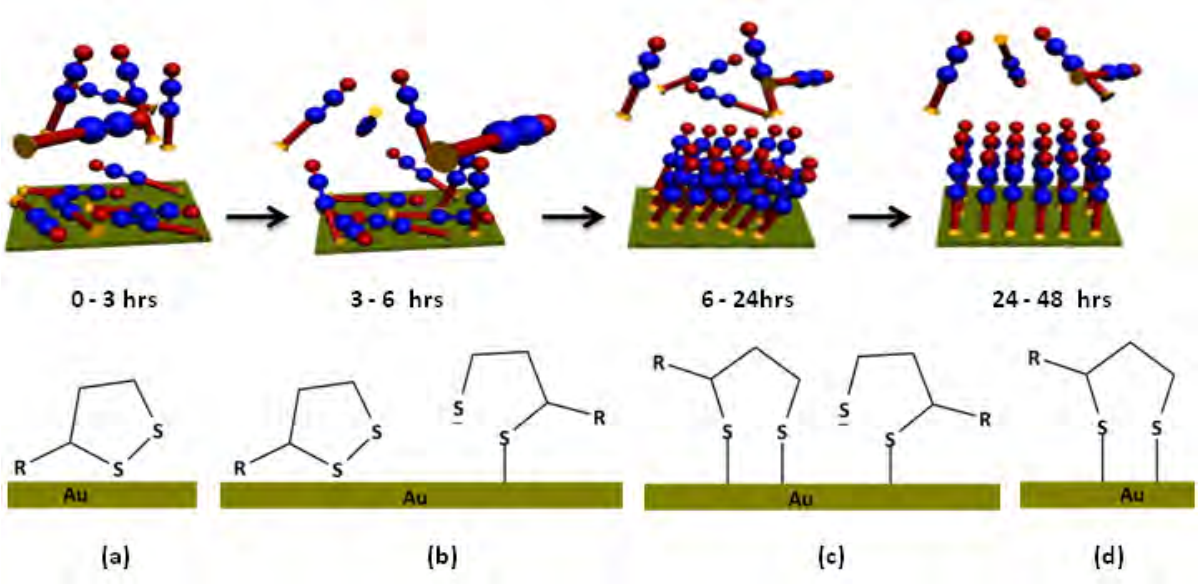

Figure 4.18 Proposed model of SAM formation. (a) Between 0-3 hours surfactants physisorb on the gold substrate, (b) Between 3-6 hours some disuphides start to chemisorb to the substrate, chemisorptions occurring by the breaking of the disulphide which generates the $R\text{-}S^-$ species, (c) between 6 -24 hours all surfactants have started to chemisorb and some have bound through both sulphurs, and (d) between 24-48 hours all surfactants have chemisorbed through both sulphurs.

If the above model were correct, we would expect the disulphide peak to be predominant at 2 hrs and then decrease or disappear between 2 – 48 hrs. To test the above model (**Figure 4.18**) XPS spectra were taken as a function of SAM formation time, in order to probe for a decrease in the intensity of disulphide and an increase in intensity of the thiolate (**Figure 4.19**).

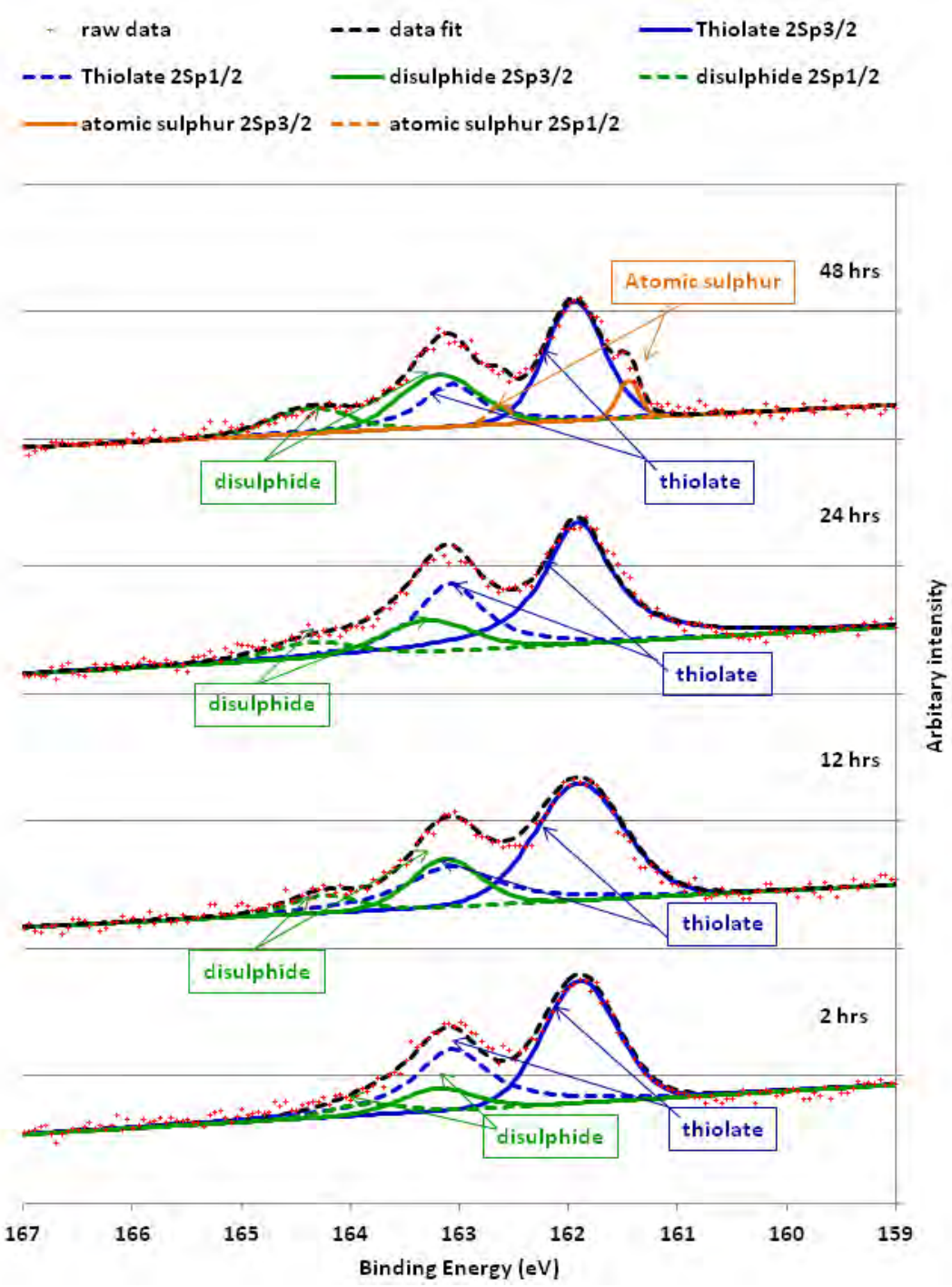

Figure 4.19 XPS spectra of TAZ1 SAMs Sulphur 2p region, measured at different SAM formation times. All formations times show the presence of both the thiolate and disulphide species.

At all formation times, the XPS spectra of TAZ1 SAMs showed the presence of both the thiolate and disulphide species. Furthermore, the total sulphur:gold ratio was constant over all formation times (**Figure 4.20**) suggesting that the surface was saturated with surfactants within 2 hrs. Interestingly at 48 hrs a peak attributable to atomic sulphur was apparent.

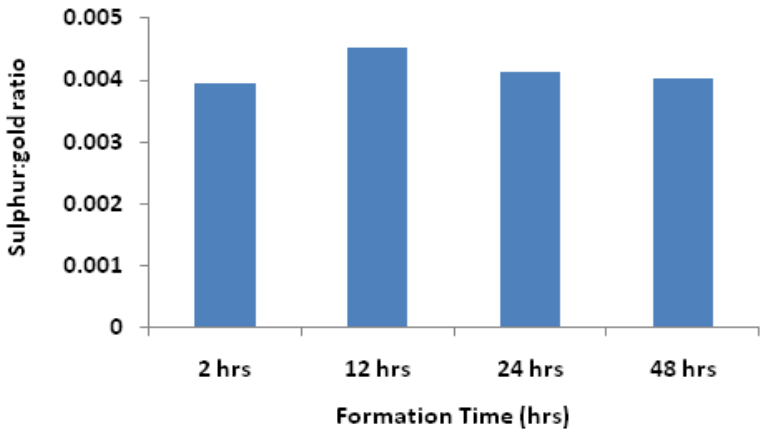

Figure 4.20 Total sulphur:gold ratio for TAZ1 SAMs as a function of formation time.

In summary, XPS spectra of TAZ1 SAMs measured as a function of time shows that the presence of the disulphide peak is not dependent on SAM formation time. Thus the hypothesis that the disulphide is present due to incomplete SAM formation is not correct.

3. A feature of a bi-layer

Next we proposed that the disulphide could be attributed to the formation of a partial bi-layer, formed through the J-aggregation of TAZ1, which exposes the disulphide at the SAM/air interface (**Figure 4.21a**). A similar partial bi-layer has been suggested to be responsible for the presence of the disulphide peak in the XPS spectra of thioctic acid SAMs[175] (**Figure 4.21b**). Bi-layer formation, being manifested *via* hydrogen bonding, between the carboxylic acid end groups of the surfactants, exposing disulphide at the SAM/air interface. In order to investigate bi-layer formation we used two different experiments. Firstly we used angle resolved XPS, in order to determine if the disulphide peak is at the Au/SAM or SAM/air interface. Secondly we made SAMs from the thioctic-methyl-ester (TME) synthesised in chapter 3 (page 53) which could not form a bi-layer through either of the models described in **Figure 4.21**.

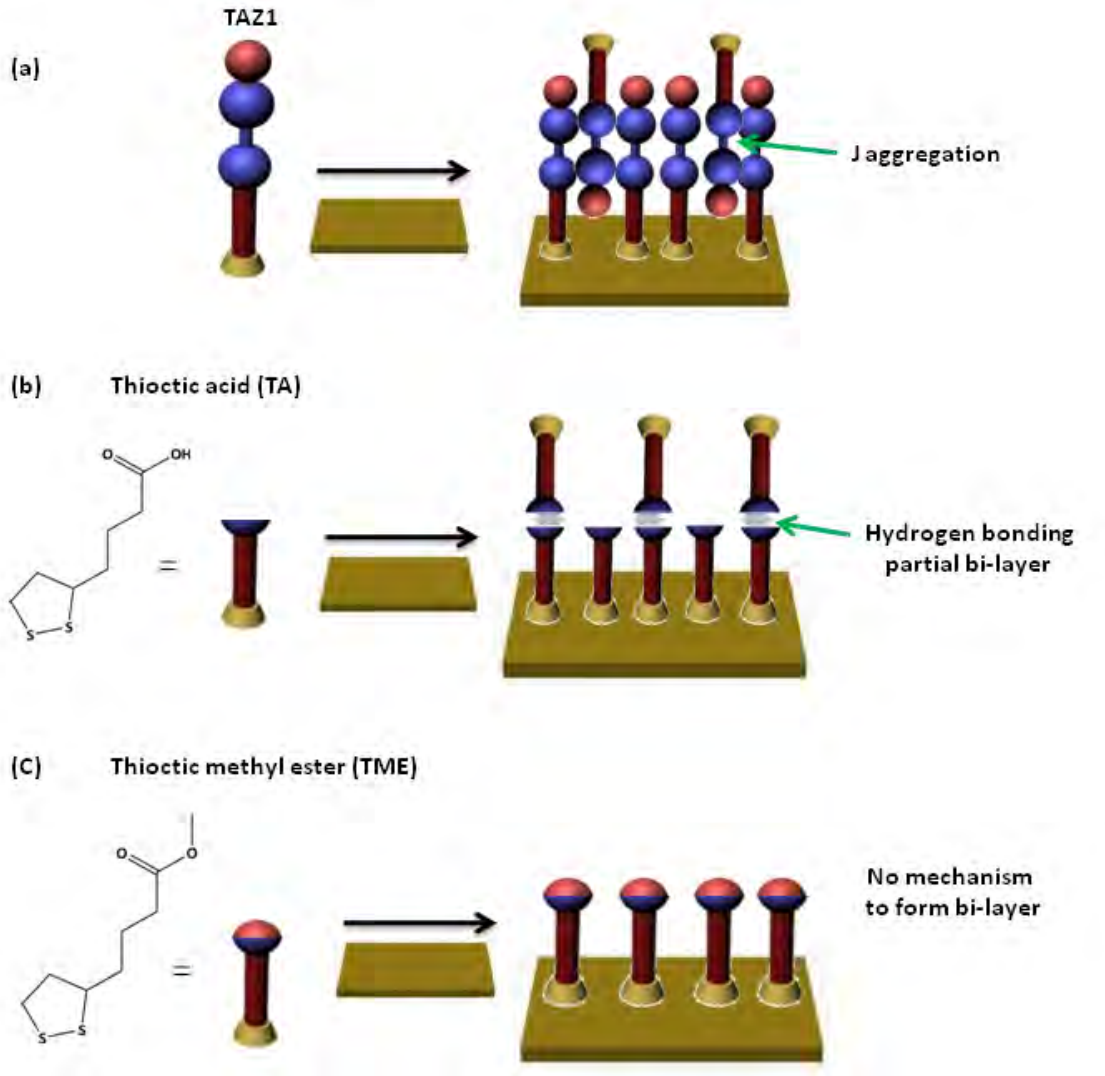

Figure 4.21 Formation of bi-layers from (a) TAZ1, manifested through J-aggregation (proposed) (b) Thioctic acid, manifested through Hydrogen bonding (from literature) (c) TME can not form a bi-layer through either aggregation or H-bonding.

Angle resolved XPS was employed to test the hypothesis that the disulphide peak of TAZ1 SAMs was due to J-aggregation. As a consequence of a J-aggregated bilayer, the disulphide peak intensity (relative to Au) would be greatest at high angles of incidence.[180]

Angle resolved XPS showed the disulphide:gold ratio of TAZ1 SAMs to be lowest at high angles (**figure 4.22**). This result suggests that the disulphide peak is located at the SAM/Au interface, opposed to being located at the SAM/air interface.

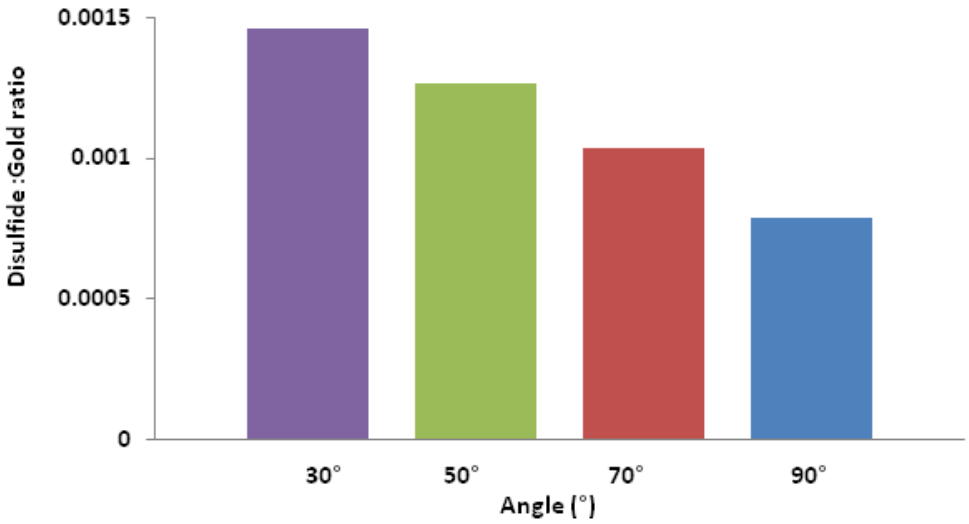

Figure 4.22 Angle resolved disulphide ($2p_{3/2}$):gold ($4f_{7/2}$) ratio of TAZ1 SAMs shows disulphide peak to be located at the surfactant-gold interface.

In order to corroborate the above result we made a SAM from a synthesised thioctic methyl ester (TME, **figure 4.23**). TME, synthesised in chapter 3, contains no carboxylic acid group or azobenzene group and so could not form bi-layers through either models discussed above. Hence if these models were correct the XPS of TME would not exhibit the disulphide peak.

XPS of the TE SAM also exhibited the disulphide peak. This suggests that the disulphide peak is a characteristic of sulphur-gold bonding of thioctic acid based surfactants (see **Figure 4.2.6**)

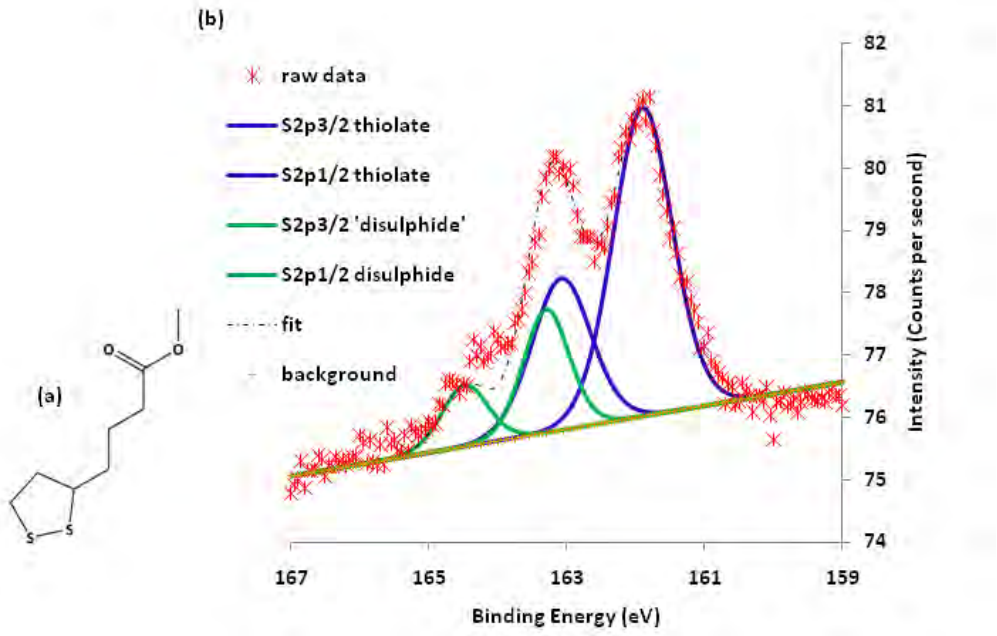

Figure 4.23 (a) synthesised thioctic-ester TME **(b)** De-convoluted XPS spectra of sulphur 2p region of TME SAM formed over 24 hours.

4. Disulphide present as physisorbed surfactants within SAM

The hypothesis that the disulphide peak could be the result of physisorbed surfactant, loosely bound by a weak disulphide-gold interaction (**figure 4.24**) is supported by the angle resolved XPS which shows the peak to be located at the surface (**figure 4.22**).

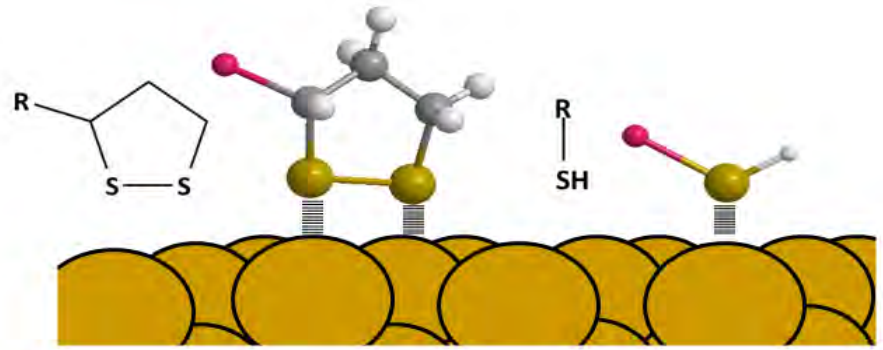

Figure 4.24 physisorbed disulphide and thiol on Au.

However, when TAZ1 SAMs were subjected to hydrolysis conditions (discussed in objective 3, in keeping with the context of discussion) the disulphide peak not only remained, but furthermore, increased in ratio, relative to the thiolate (**figure 4.25**). Physisorbed molecules are less strongly bound than chemisorbed thiolates.[181] With this in mind, it is reasonable to assume that under the conditions employed for hydrolysis, physisorbed surfactants would be preferentially removed over chemisorbed ones. Thus, this result suggests that the disulphide is not present as a physisorbed contaminant.

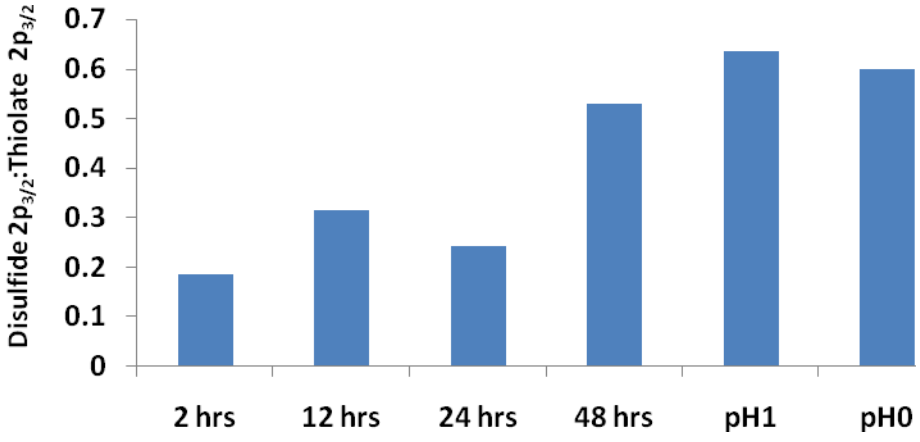

Figure 4.25 XPS disulphide($2p_{3/2}$):thiolate($2p_{3/2}$) ratio *Vs* formation time and post hydrolysis of 24 hr SAM.

5. Disulphide bond a feature of fully formed SAM

Considering both the research discussed above and the literature discussed below, it is believed that the disulphide is a feature of the fully formed SAM, two models are proposed. Firstly, the disulphide bond maybe attributed to chemical bonding of the intact disulphide, to the gold surface (**Figure 4.26**). Secondly it may be attributed to a more complicated bonding model, involving intermolecular binding of surfactants, through sulphur disulphide bond formation (**Figure 4.27**).

Chemical bonding of the intact disulphide, to the gold surface is supported by the literature. Dialkyl sulphides have been shown to adsorb in a non destructive way, that shows no apparent differences in the XPS spectra, relative to thiols binding through the gold thiolate.[182] There is also evidence in the literature that points to disulphides binding in equilibrium, between the disulphide and the thiolate.[183] Furthermore, it has been suggested in the literature that SAMs formed from thiols can give rise to S-S dimers with a 0.22nm bond distance.[184] Such bonding occurs when surfactants have gauche defects, in the C-S bond. The C-S bonds in thioctic acid are part of a strained 5 member ring with a S-S bond distance of 0.22nm, giving the ring pseudo-gauche features, due to the conformational restrictions, imposed by the ring.

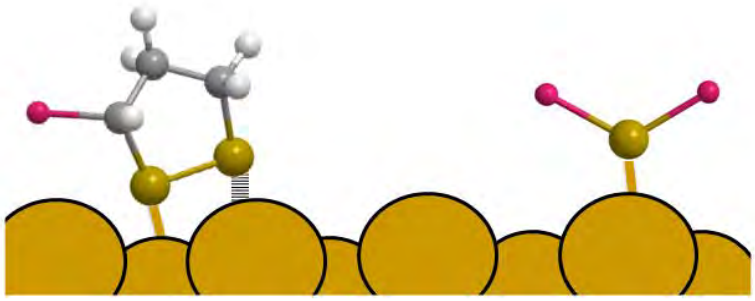

Figure 4.26 Schematic of possible binding mode of TAZ1 compared to a known binding mode of thioether.

The second hypothesised model, is the formation of a disulphide bond between surfactants. A proposed mechanism of the reaction is in **Figure 4.27**. This hypothesis fits with XPS results of SAMs exposed to hydrolysis conditions which are discussed in detail later (objective 3, section 4.3.3). Importantly, post hydrolysis the disulphide remains, and furthermore, the disulphide:thiolate ratio increases, suggesting that inter-surfactant binding might be promoted by acidic conditions or elevated temperatures. Further support comes from the XPS of TAZ1 SAMs at 48 hours which also show a disulphide:thiolate ratio greater than 0.5 and the presence of monatomic sulphur not seen in any previous spectra, (page 23, **Figure 4.19**) which maybe a product of the proposed inter-surfactant reaction.

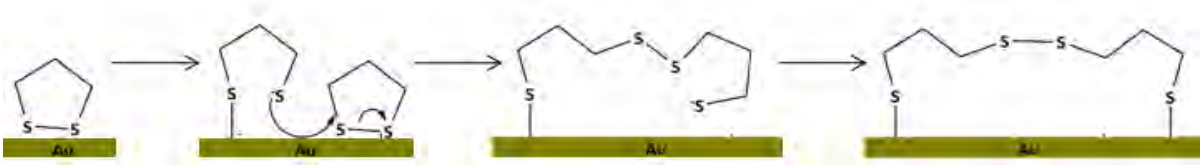

Figure 4.27 Schematic of possible disulphide bonding between surfactants.

In summary, it has been shown that the unexpected disulphide peak is probably not an artefact of XPS irradiation, or incomplete SAM formation, neither is it due to bi-layer formation or physisorbed surfactant. Furthermore, data shows that it is present at the gold surface and is likely to be a feature of the fully formed SAM.

4.2.1.5 UV/Vis spectroscopy

The *UV/Vis* spectra of both TAZ1 (**Figure 4.28**) and SAZ1 (**Figure 4.29**) SAMs were investigated as a function of time. Post SAM formation samples were washed and dried, then immediately analysed by *UV/Vis* absorption spectroscopy. Three samples were analysed at each formation time. All SAMs exhibited optical absorbance attributed to azobenzene and are discussed below.

The *UV/Vis* spectra of TAZ1 SAMs showed the three formation regions (I - III) which are described below. These regions (I - III) are defined by formation time, in accordance to those seen in ellipsometry and contact angle, and are labelled on **Figure 4.28**. The λ_{max} of all TAZ1 SAM samples corresponding to the spectra can be seen below in **Table 4.1**, the mean λ_{max} and and the standard error are also given. The surface *UV/Vis* spectra fitted with the solution spectra which can be seen in **appendix I**.

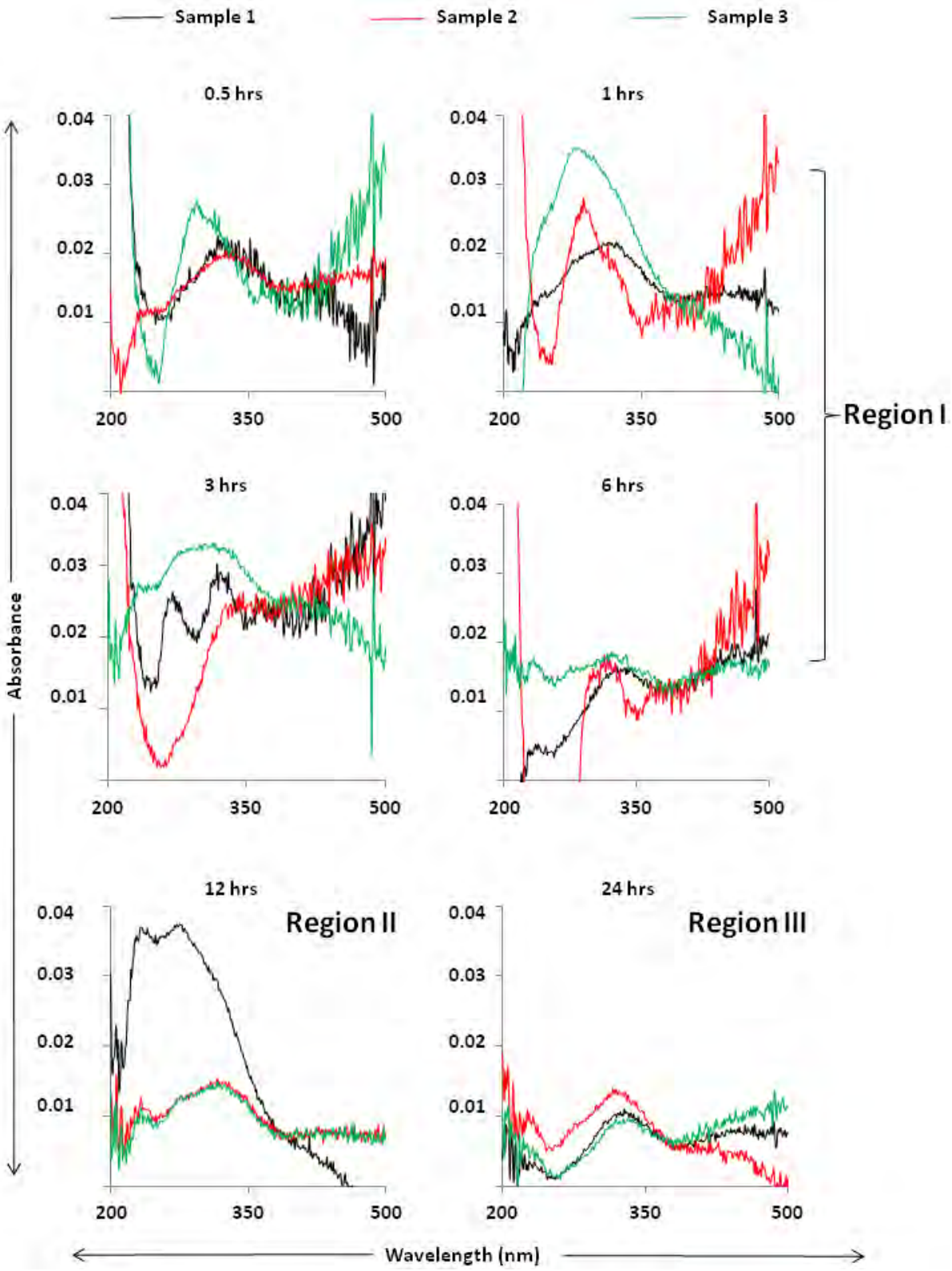

Figure 4.28 *UV/Vis* spectra of TAZ1 SAMs (x3 samples) at different formation times

Table 4.1 λ_{max} of TAZ1 SAM samples at different formation times and the mean.

Region	Time (hrs)	Sample 1 (nm)	Sample 2 (nm)	Sample 3 (nm)	Mean (nm)
	0.5	294	315	326	312 ± 9
	1	276	287	318	293 ± 13
I	**3**	318	346	313	326 ± 10
	6	322	314	331	322 ± 5
II	**12**	275	316	316	302 ± 14
III	**24**	328	328	327	328 ± 0.3

Region I: Corresponds to the formation times 0.5 – 6 hrs. At these low formation times both λ_{max} and the shape of the spectra were generally inconsistent between samples. Furthermore, λ_{max} of all samples, in region I, is generally hypsochromicaly shifted, with respect to the solution value (328 nm **appendix I**) suggesting that the azobenzene within the SAMs are aggregated.

Region II: Corresponds to the formation times 6 - 21 hrs. Three spectra were recorded at 12hrs. Between two of these samples the shape of the spectra and λ_{max} was consistent, with $\lambda_{max} \approx 316$ nm, which is hypsochromicaly shifted indicating a degree of H-aggregation. The third sample, however, had a different shaped curve and a strongly hypsochromicaly shifted $\lambda_{max} \approx 275$ nm. Overall λ_{max} is generally hypsochromicaly shifted with respect to the solution value (328 nm **appendix I**) suggesting that SAMs are still aggregated. However, the hypsochromic shifts are generally not as large as region I, suggesting the degree of aggregation is reduced with increasing formation time.

Region III: Corresponds to the formation time over 21 hrs. Three spectra were recorded at 24 hrs, both the shape of the spectra and λ_{max} were consistent between samples.

Furthermore, $\lambda_{max} \approx 328$ nm which is in agreement with the solution value (328 nm **appendix I**) therefore indicating that azobenzene is not aggregated.

Overall for TAZ1 SAMs λ_{max} generally increases with respect to formation time, from a mean $\lambda_{max} = 312$ nm ± 9 nm at 0.5 hrs, to a mean $\lambda_{max} = 328 \pm 0.3$ nm by 24 hrs which is in agreement with the solution value (328nm **appendix I**). As with ellipsometry and contact angle the formation can be split into three regions. In regions I and II λ_{max} is generally hypsochromicaly shifted from the solution value, suggesting that theses SAMs have a degree of H-aggregation. The degree of H-aggregation decreases to zero with increasing formation time, as shown by a general increase in λ_{max}. Region III exhibits a λ_{max} equal to the solution value indicating that the SAMs are no longer aggregated. Furthermore, the degree of aggregation reported above is reflected in the isomerisation studies (discussed below in objective 2).

In summary, azobenzene within TAZ1 SAMs is aggregated at low formation times. The degree of aggregation decreases with increasing formation time, until non-aggregated SAMs are formed after 24 hrs.

About 50% of the *UV/Vis* spectra (**Figure 4.29**) of SAZ1 SAMs exhibited two peaks and there did not seem to be consistency between samples of the same formation time. The spectra of SAZ1 SAMs are discussed below. The λ_{max} of all SAZ1 SAM samples corresponding to the spectra can be seen below in **Table 4.2**, the mean λ_{max} and the standard error are also given.

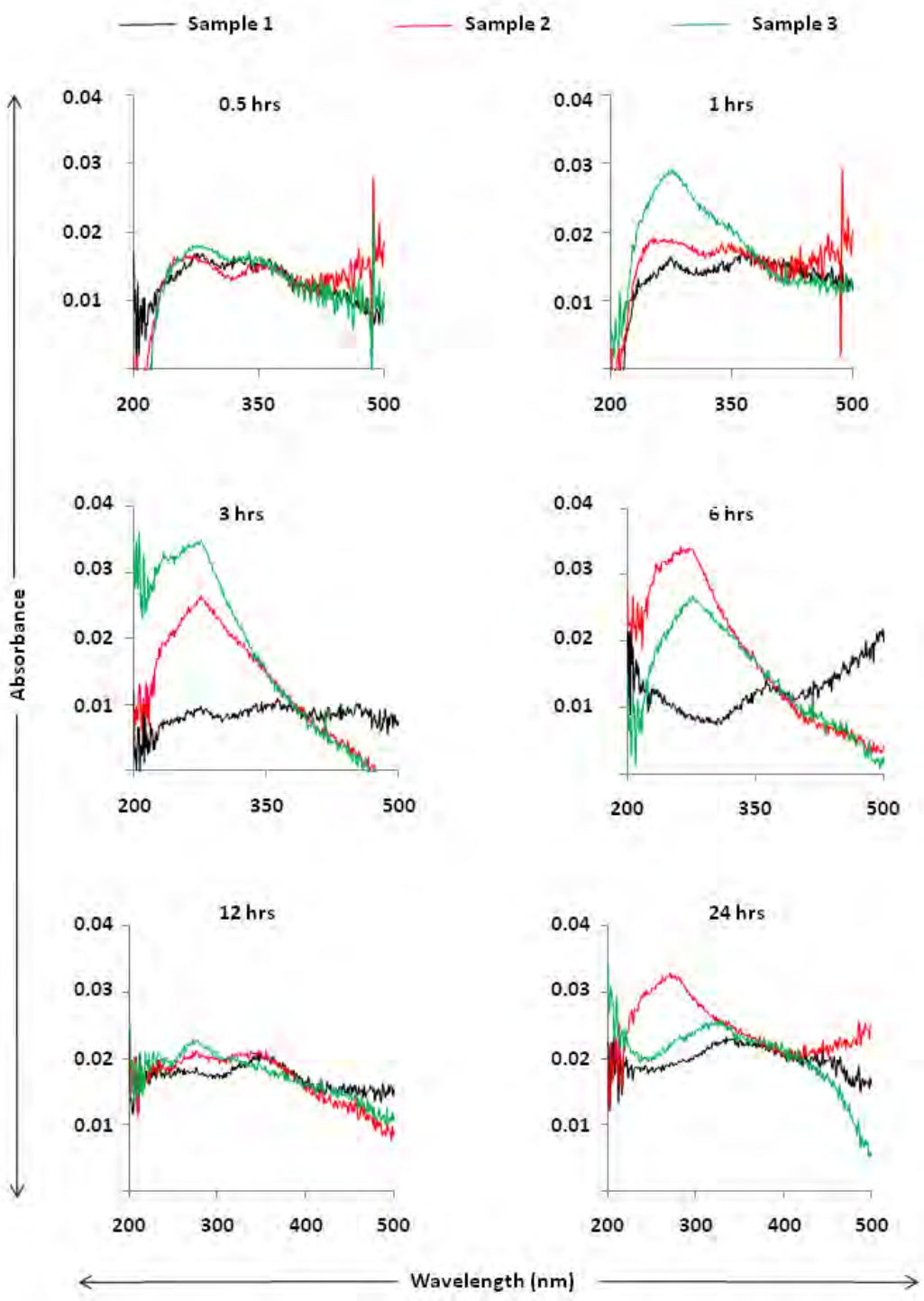

Figure 4.29 *UV/Vis* spectra of SAZ1 SAMs (x3 samples) at different formation times

Table 4.2 λ_{max} of SAZ1 SAM samples at different formation times and the mean.

Time (hrs)	Sample 1 (nm)	Sample 2 (nm)	Sample 3 (nm)	Mean (nm)
0.5	275	276	261	271 ± 5
1	360	252	276	296 ± 33
3	363	276	275	304 ± 30
6	360	275	262	299 ± 31
12	346	272	275	298 ± 24
24	271	327	335	324 ± 20

Overall λ_{max} of all SAZ1 SAM samples is generally strongly hypsochromically shifted from the solution value (358 nm **appendix I**). Some samples do exhibit λ_{max} close to the solution value. However, they are also often accompanied by the second hypsochromically shifted peak which corresponds to the aggregated SAM. Furthermore, when irradiated with *UV* light (discussed next) the hypsochromically shifted peak increases in intensity becoming λ_{max}. In summary SAZ1 generally forms aggregated SAMs, relative to TAZ1.

In conclusion, azobenzene within TAZ1 SAMs are aggregated at low formation times, the degree of aggregation decreases with increasing formation time, until after 24 hrs SAMs are not aggregated. Azobenzene, within SAZ1 SAMs are generally H-aggregated, irrespective of formation time. These results prove our initial hypothesis that TAZ1's cyclic 1, 2-dithiolan-3-yl head group prevents aggregation of azobenzene, relative to the alkyl thiol head group control of SAZ1.

4.2.2 Objective 2 - *UV/VIS* studies

The photo-isomerisation of both TAZ1 and SAZ1 SAMs was investigated as a function of SAM formation time, using the samples discussed above. SAMs were subjected to irradiation cycles of 3 mins *UV* followed by 3 mins *Vis*. It was found that 3 mins was sufficient an irradiation time to induce isomerisation (**appendix II**). A representative spectra for both TAZ1 and SAZ1 SAMs, formed over 24 hrs, are shown in **Figures 4.30** and **4.31** respectively (The other 24 hr spectra are shown in **appendix III** as well as the spectra of lower formation times).

Overall TAZ1 SAMs show a different pattern from SAZ1 SAMs. For TAZ1 SAMs isomerisation behaviour was different between the three formation regions that were identified and described above in formation studies. Overall the optical activity of TAZ1 SAMs increases with increasing formation time. Increase in optical activity is accompanied by a loss of aggregation, as is reflected in the shifts in λ_{max}.

For SAZ1 such regions were not apparent, this is in agreement with the ellipsometry results of SAZ1 SAMs. The SAZ1 *UV/Vis* spectra generally exhibit two absorption peaks one corresponding to the aggregated surfactants, and another corresponding to non-aggregated surfactants. Any non-aggregated surfactants seemed to aggregate upon exposure of the SAMs to *UV* at 360 nm.

A full discussion of early formation spectra, as well as the spectra can be found in **appendix III**. The discussion below focuses on the isomerisation of TAZ1 (**Figure 4.30**) and SAZ1 (**Figure 4.31**) SAMs formed over 24 hrs.

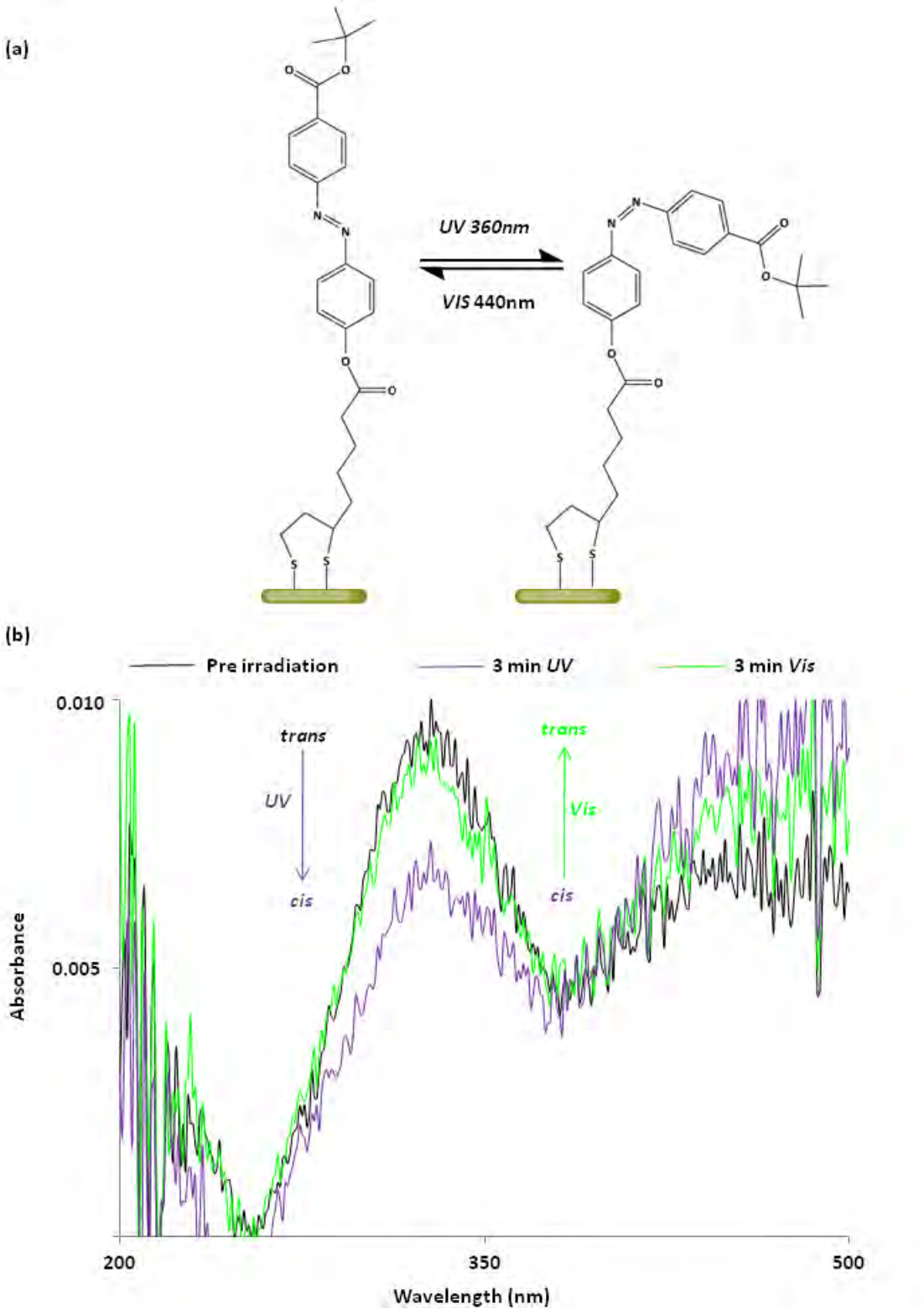

Figure 4.30 *UV/Vis* spectra of TAZ1 SAM exposed to a *UV* and *Vis* irradiation, at formation time 24 hrs

At 24 hrs TAZ1 SAMs (**Figure 4.30**) show reversible isomerisation typical of azobenzene. Furthermore, λ_{max} is ≈ 328 nm, which is in agreement with the solution value, suggesting that azobenzene within the SAMs is not aggregated. However, despite no aggregation not all surfactants are able to isomerise, something probably due to remaining spatial constraints, which inhibit isomerisation.

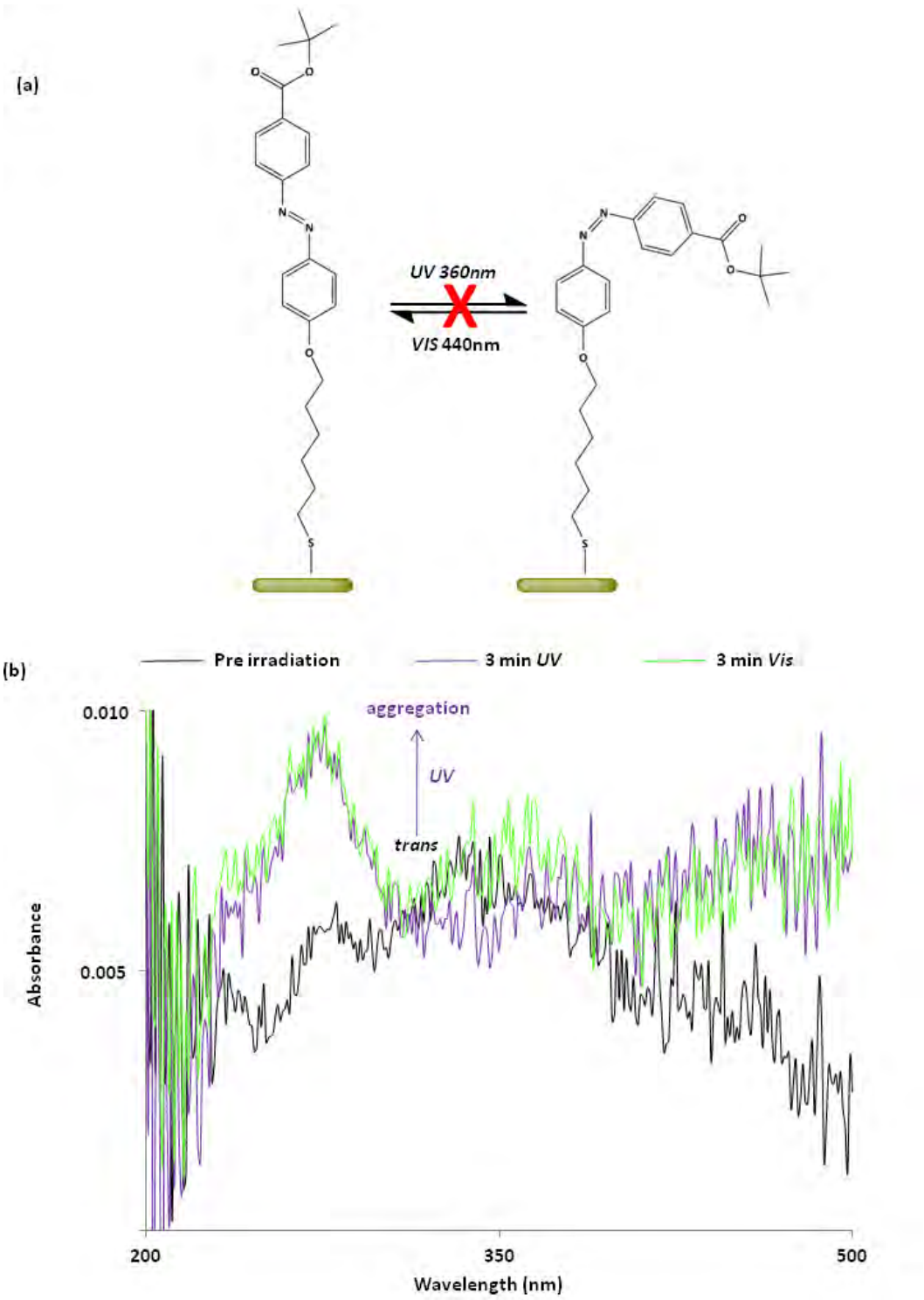

Figure 4.31 *UV/Vis* spectra of SAZ1 SAM exposed to a *UV* and *Vis* irradiation, at formation time 24 hrs, showing that azobenzene aggregates, rather than isomerises upon exposure to *UV* light

At 24 hrs SAZ1 SAMs (**Figure 4.31**) the *UV/Vis* absorption spectra exhibited two peaks, one corresponding to the aggregated surfactants and another corresponding to non-aggregated surfactants. Generally exposure to *UV* resulted in an increase in the intensity of the peak corresponding to aggregated surfactants and didn't seem to have much effect on the non-aggregated peak.

In summary, the cyclic 1, 2-dithiolan-3-yl head group of TAZ1 seems to not only decrease aggregation within fully formed SAMs but also provides space for isomerisation, relative to the alkyl of SAZ1 SAMs. However, not all TAZ1 surfactants isomerise suggesting there are still spatial constraints hindering complete isomerisation.

4.2.3 Objective 3 - Surface hydrolysis

The hydrolysis of TAZ1 SAMs *tert* butyl ester end group (**Figure 4.32**) was investigated by contact angle and XPS. The reaction employed a procedure developed in our group, for the hydrolysis of aromatic tert-butyl ester terminated thiol SAMs, to the aromatic acid.[160] The conditions employed were pH 1, 80°C for 5hrs.[160]

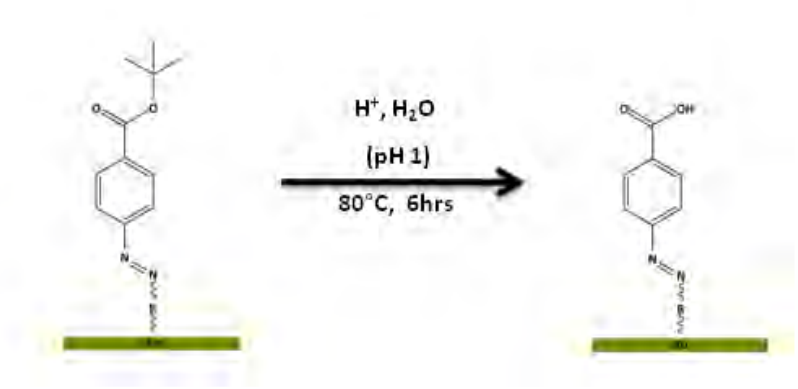

Figure 4.32 Schematic of attempted TAZ1 SAM hydrolysis

4.2.3.1 Contact angle of SAM hydrolysis

The contact angle results are shown in **Figure 4.33**. The advancing contact angle remained approximately constant at ≈ 90°. The receding angle reduced within 2 hrs, from ≈ 70° to ≈ 45°, it continued to fall over the next 4 hrs to ≈ 25°, with no further decrease when left overnight.

This is not as expected,[160] as the advancing angle should also reduce in accordance to the change from a hydrophobic (*tert*-butyl) surface to a hydrophilic (acid) surface. This result indicates that the conditions described for hydrolysis[160] are insufficient to hydrolyse TAZ1 SAMs, even when the reaction time is extended to overnight.

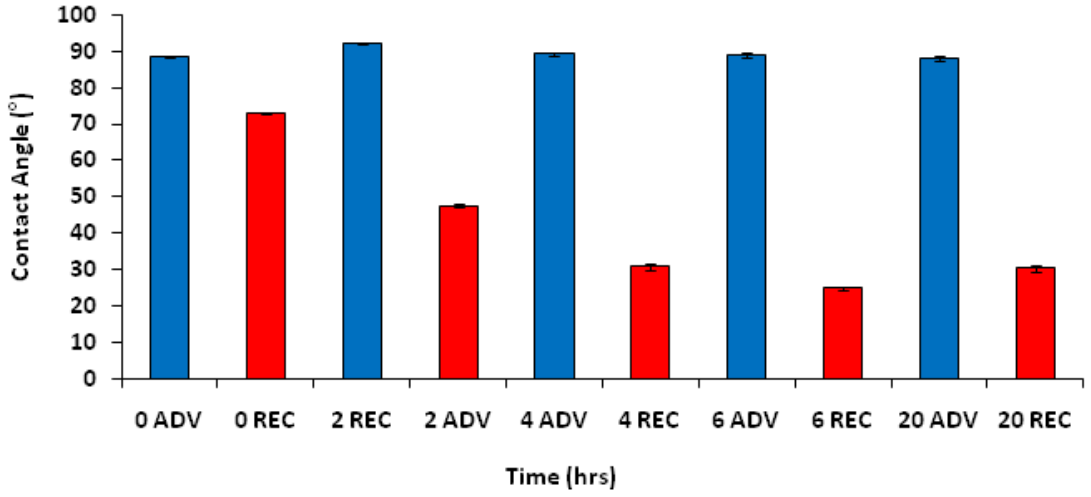

Figure 4.33 TAZ1 SAM hydrolysis contact angle Vs time at pH1, 80°C.

The hydrolysis was further investigated at the same temperature but a lower pH (0) as a function of time. The result was similar to above with the advancing angle showing no decrease and the receding angle decreasing to ≈ 30°. Indicating that these conditions are also insufficient to induce hydrolysis.

4.2.3.2 XPS of SAM hydrolysis

Next we used XPS to determine if the conditions of *'hydrolysis'* were detrimental to the SAM. Sulphur XPS spectra **(figure 4.34a)** of the SAM 'hydrolysed' for 6 hours, at both pH 1 and pH 0, showed peaks attributed to both the gold thiolate and the disulphide.

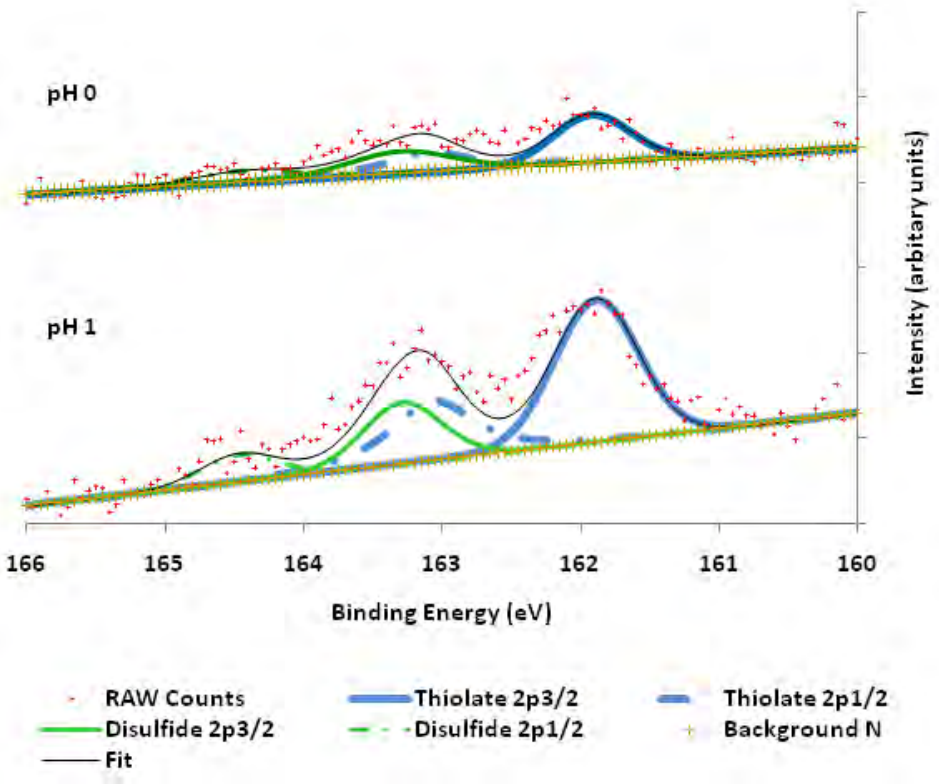

Figure 4.34 XPS spectra post exposure of TAZ1 SAM to hydrolysis conditions of 6 hrs, 80°C, (a) pH 0 (b) pH 1.

Furthermore, there was a sizeable reduction in the overall S:Au ratio **(figure 4.35a)** suggesting the conditions were detrimental to the SAM. However and interestingly, the disulphide:thiolate ratio increases from ≈ 0.3 to 0.6 **(figure 4.35b)**. Suggesting that

either, surfactants giving rise to the disulphide peak are more strongly bound than thiolates or that the disulphide peak is induced at the surface by these conditions.

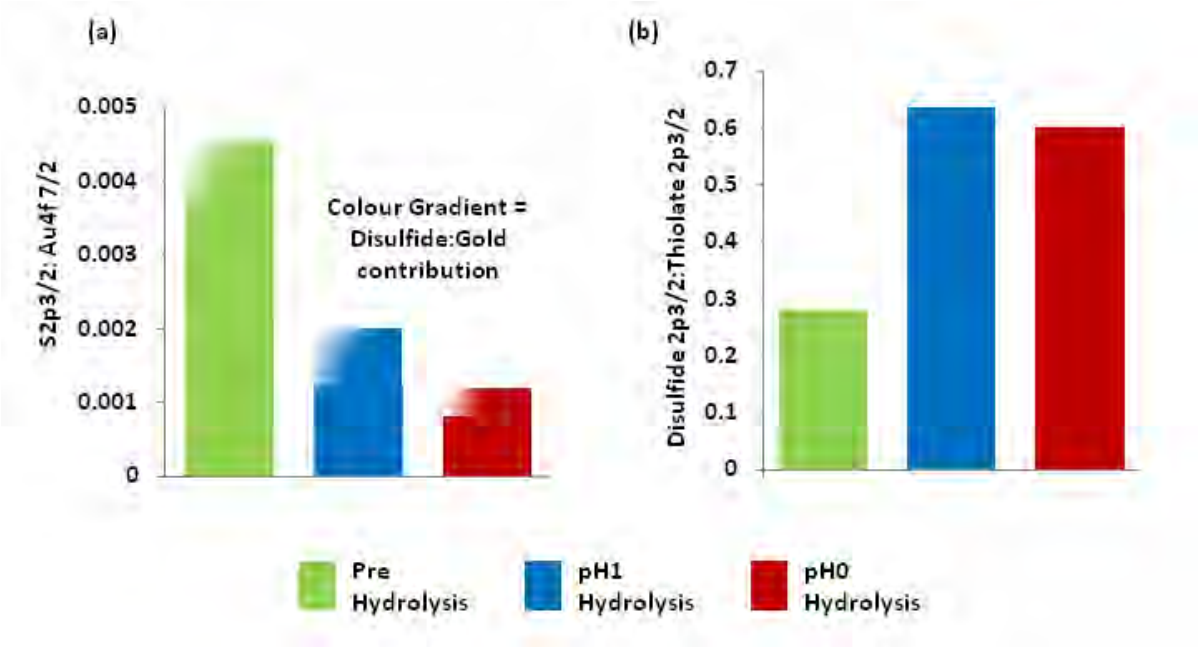

Figure 4.35 XPS ratios pre and post hydrolysis (a) Overall sulphur:gold (b) Disulphide:gold.

4.2.3.3 Further discussion of hydrolysis.

Lack of hydrolysis could be attributed to steric hindrance; however, in the literature[160] successful hydrolysis of an aromatic *tert*-butyl ester is attributed to the lack of steric hindrance to the reactions $A_{AL}1$ mechanism (**Figure 4.36a**). A rationale which was given considering that the hydrolysis of the corresponding methyl ester is inert to hydrolysis because it proceeds through the more sterically demanding $A_{AC}1$ mechanism, which requires the attack of the inaccessible carbonyl carbocation by water (**Figure 4.36b**). It is concluded that the lack of hydrolysis can be attributed to the azobenzene moiety of the

surfactant, stabilising the surfactant due to the electron withdrawing nature of the para ester.

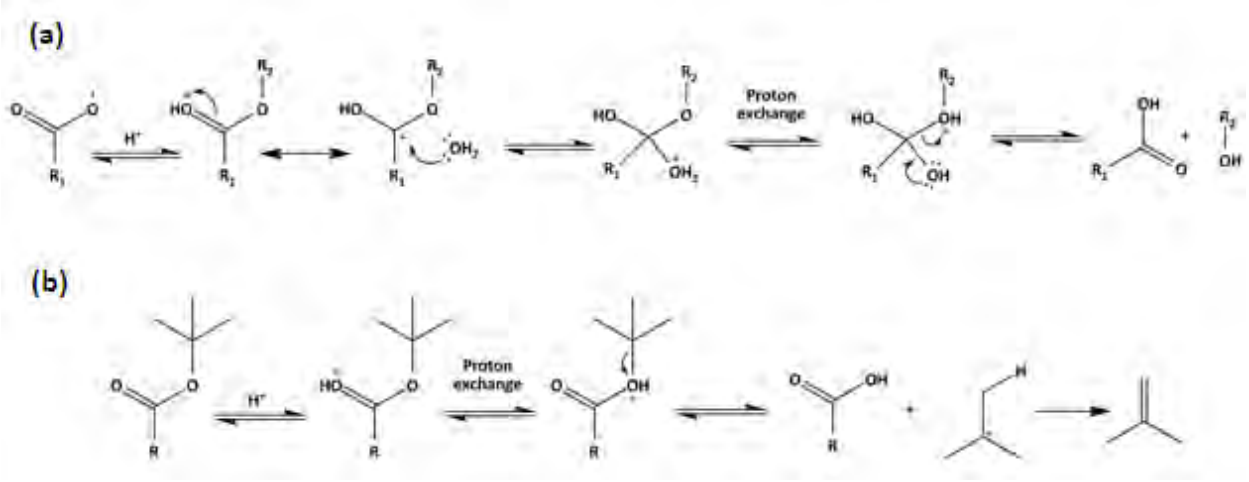

Figure 4.36 Different hydrolysis mechanisms for hydrolysis of (a) aryl or alkyl esters ($A_{AC}1$) Vs (b) tert-butyl esters ($A_{AL}1$).

In summary, the conditions employed were unsuccessful in the hydrolysis of the *tert*-butyl TAZ1 surface, as indicated by the contact angle results. Furthermore, the conditions were detrimental to the SAM as indicated by the XPS results. The inertness of the *tert*-butyl ester terminated TAZ1 surface is believed to be attributed to the azobenzene moiety of the surfactant.

4.3 Conclusions

The formation of SAMs from TAZ1 SAMs has been investigated along with the isomerisation of azobenzene within SAMs, which has been compared to SAZ1 control. The hydrolysis of TAZ1 SAMs was also investigated.

Overall TAZ1 did reduce aggregation and facilitate isomerisation, relative to SAZ1. This result proves our initial hypothesis. Conclusions drawn from each objective are listed below.

4.3.1 Objective 1 conclusions

With respect to formation of TAZ1 SAMs, ellipsometry and contact angle suggested formation to be complete within 21 hrs. *UV/Vis* suggested SAMs were formed between by 24hrs and XPS showed that the surface reached surfactant saturation within 2 hrs. Interestingly ellipsometry, contact angle and *UV/Vis* showed three regions of SAM formation.

4.3.2 Objective 2 conclusions

The response of TAZ1 SAMs to *UV* and *Vis* irradiation was shown to depend on formation time. At low formation times TAZ1 SAMs were aggregated as reflected in the hypsochromic shift of λ_{max} and inconsistent shape of the absorption curve. As aggregation decreased λ_{max} increased as did optical activity of SAMs upon exposure to *UV* and *Vis* irradiation. The control, SAZ1 was shown to form aggregated SAMs, with the degree of aggregation increasing with *UV* and *Vis* irradiation.

4.3.3 Objective 3 conclusions

TAZ1 SAMs were inert to the conditions employed for surface hydrolysis, it is concluded that this is because of the electron withdrawing nature of the para ester.

4.4 Future work

Through the research reported in this chapter two hypothesis have been formed which warrant further investigation.

4.4.1 Transient multilayer of TAZ1 SAM formation

The hypothesised formation of transient aggregated azobenzene multilayer (**Figure 4.10**) could be investigated by QCM, which has shown the presence of similar[166] multilayers in SAM formation from n-alkyl thiols.

4.4.2 S-Au binding mode of TAZ1 SAMs

It has been hypothesised that the sulphurs of the cyclic 1, 2-dithiolan-3-yl head group of TAZ1 may form inter surfactant bonds with the sulphurs of neighbouring surfactants. This binding mode could be further investigated using a model based on TAZ1 SAMs using Au nano-particles as substrates, which will allow the use of SERS FTIR, which enhances the signal at the Au/SAM interface.

5.0 Azobenzene SAMs for the *in-vitro* study of bio-molecular interactions

Many biological reactions occur at interfaces.[185] In recent years, SAMs have been used to mimic such interfacial, bio-molecular reactions.[74, 185, 186] Study of biomolecules on SAMs has yielded important results, providing information on the interactions of biomolecules with their surroundings.[74] However, many of these surfaces present bio-molecule binding sites in a static fashion, which limits their potential.[186] Thus there is a demand to develop switchable SAMs,[186] in which the binding sites presented at the surface can be turned *'on'* and *'off'*, between a bio-active and bio-inert surface, in response to some external stimuli. Such surfaces would mimic the real time changes of biological systems[74] and prove useful to the future study of biological phenomena, such as cell migration. [74, 185, 186]

The application of switchable SAMs to the study of bio-molecular interactions is a relatively new field, and some examples have been reported in the literature. Some examples are discussed in chapter 1. Examples include the use of heat,[81-85] pH,[86] bio-chemicals,[87] electrical potential,[88-99] and light.[101-116] However, most of the examples in the literature study non-specific bio-molecular interactions of biomolecules with the surface. This non-specificity limits their potential use.[187] The development of switchable surfaces, that facilitate the study of specific bio-molecular interactions, is an important future development.[188] There are currently some examples of switchable SAMs being applied to the study of specific bio-molecular interactions. For example, RGD terminated switchable SAMs[90, 92, 116] have been successfully applied to the study of cell adhesion. As another example, biotin terminated switchable SAMs have been used for the specific binding of streptavidin.[85] As a final example, recent work within our group has investigated the specific binding of neutravidin to electrically switchable biotin-terminated SAMs.[99]

Other recent and ongoing work within our group has investigated the binding of the lectin, Concavalin A (described below in section 5.0.1) to mannose-terminated SAMs. However, mannose is presented statically at the SAM surface. The next stage of this research and subject of this chapter is to make this system photo-switchable. Such a photo-switchable SAM would mimic the dynamic changes within the body.

5.1 Concanavalin A and its binding to Mannose

Lectins are a protein class that specifically bind to carbohydrates.[189] Carbohydrates are present on the surface of most cells and are important in molecular recognition,[190] as well playing roles in many cellular functions such as cell growth,[191] immune response,[192, 193] inflammation,[193] cell-cell signalling[192] and metastasis.[192, 193] Carbohydrate-terminated SAMs are promising *in-vitro* models for the study of carbohydrate-lectin and other carbohydrate-protein interactions,[190] the study of which has important health implications.

Concanavalin A (ConA) (**Figure 5.1**) is a widely researched lectin that binds specifically to mannose containing molecules. ConA requires Ca^{2+} and Mn^{2+} ions for binding activity[189] and exists as a tetramer between pH 5.8–7.0. At pH < 5.6 ConA dissociates to a dimer and at pH > 7.0 it aggregates.[190] ConA has important implications in the prevention of diseases. For example, it is known to inhibit strains of human immunodeficiency virus type 1 (HIV-1). Research into the exact mechanism of such inhibition will provide useful information and potentially enable the development of HIV vaccines.[194]

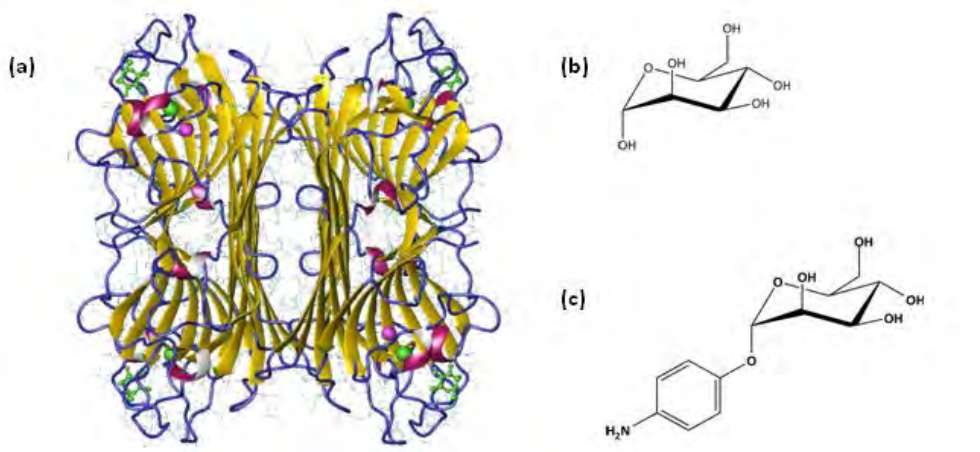

Figure 5.1. Illustration of (a) ConA tetramer crystal structure (b) mannose (c) the mannose derivative 4-aminophenyl α-D-mannopyranoside (ADM) used in this chapter, to present mannose at the SAM surface.

5.2 Aims

The research presented in this chapter is aimed at the development of a photo-switchable SAM system, for the study of specific bio-molecular interactions. The system is based upon the photo-isomerisation of an azobenzene containing surfactant, terminated with mannose. Mannose binds to ConA in a specific manner[189] and will be effectively switched *'on'* and *'off'* by light induced isomerisation of azobenzene. The azobenzene surfactant is presented within a mixed SAM on Au.

Mixed SAMs will be made from GAZ1 and TEGT (**Figure 5.2**). GAZ1 has a carboxylic acid head group which, post SAM formation, will be functionalised with 4-aminophenyl α-D-mannopyranoside (ADM) (**Figure 5.1**) in order to present mannose at the surface. TEGT will be present as a bio-inert spacer group, not only providing space for azobenzene isomerisation, but also facilitating desirable control over the surface density of ADM.[79]

5.2.1 Objectives

There are three research objectives investigated in this chapter:

1. Formation and characterisation of mixed SAMs from the surfactants TEGT and GAZ1.
2. Functionalisation of SAMs (specifically GAZ1 surfactants) with ADM, followed by the investigation of ConA immobilisation on the surface.
3. Investigate *'on'/'off'* switchability of ADM terminated SAMs with respect to ConA immobilisation.

5.2.1.1 Objective 1

The formation of mixed SAMs on Au from GAZ1 and TEGT was investigated at different ratios (GAZ1:TEGT 1:0, 1:1, 1:10, 1:100 and 0:1) as a function of time, by contact angle, ellipsometry and UV/Vis spectroscopy (**Figure 5.2**).

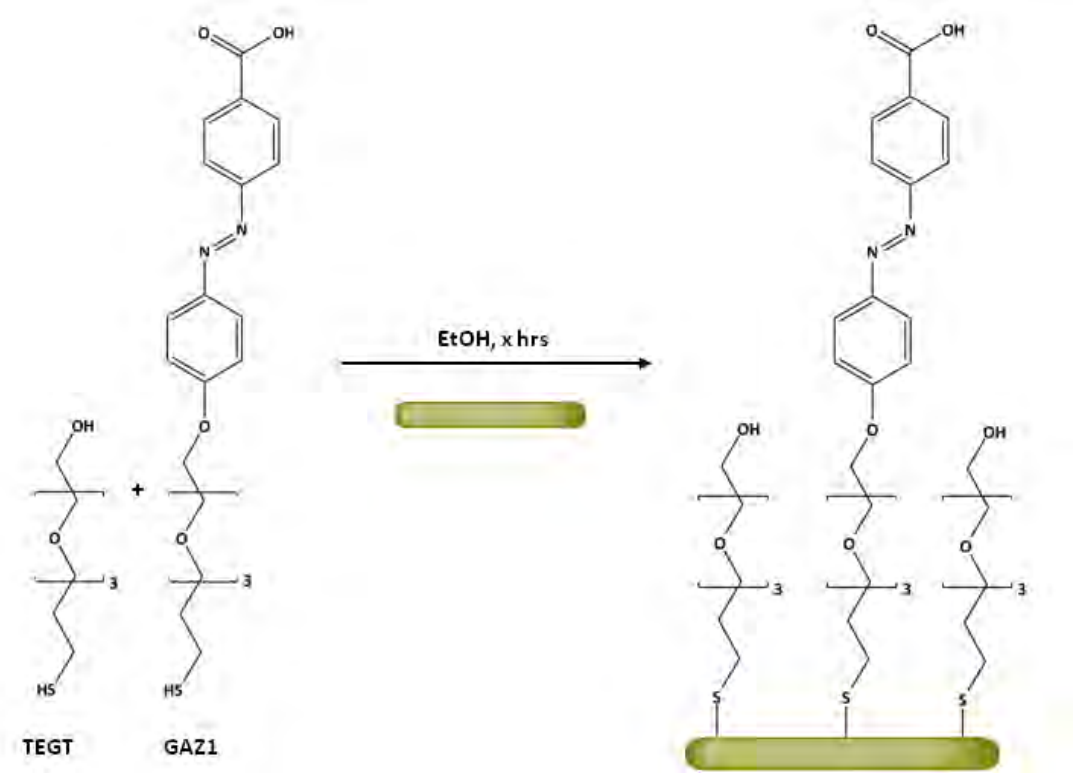

Figure 5.2. Illustration of objective 1: Formation of mixed SAMs from TEGT and GAZ1 surfactants, investigated by contact angle, ellipsometry and *UV/Vis* spectroscopy.

5.2.1.2 Objective 2

After the formation of mixed SAMs in objective 1, they will be functionalised with ADM (**Figure 5.3**). After functionalisation with ADM, the specific immobilisation of ConA to the SAMs will be investigated by surface plasmon resonance (SPR) and ellipsometry.

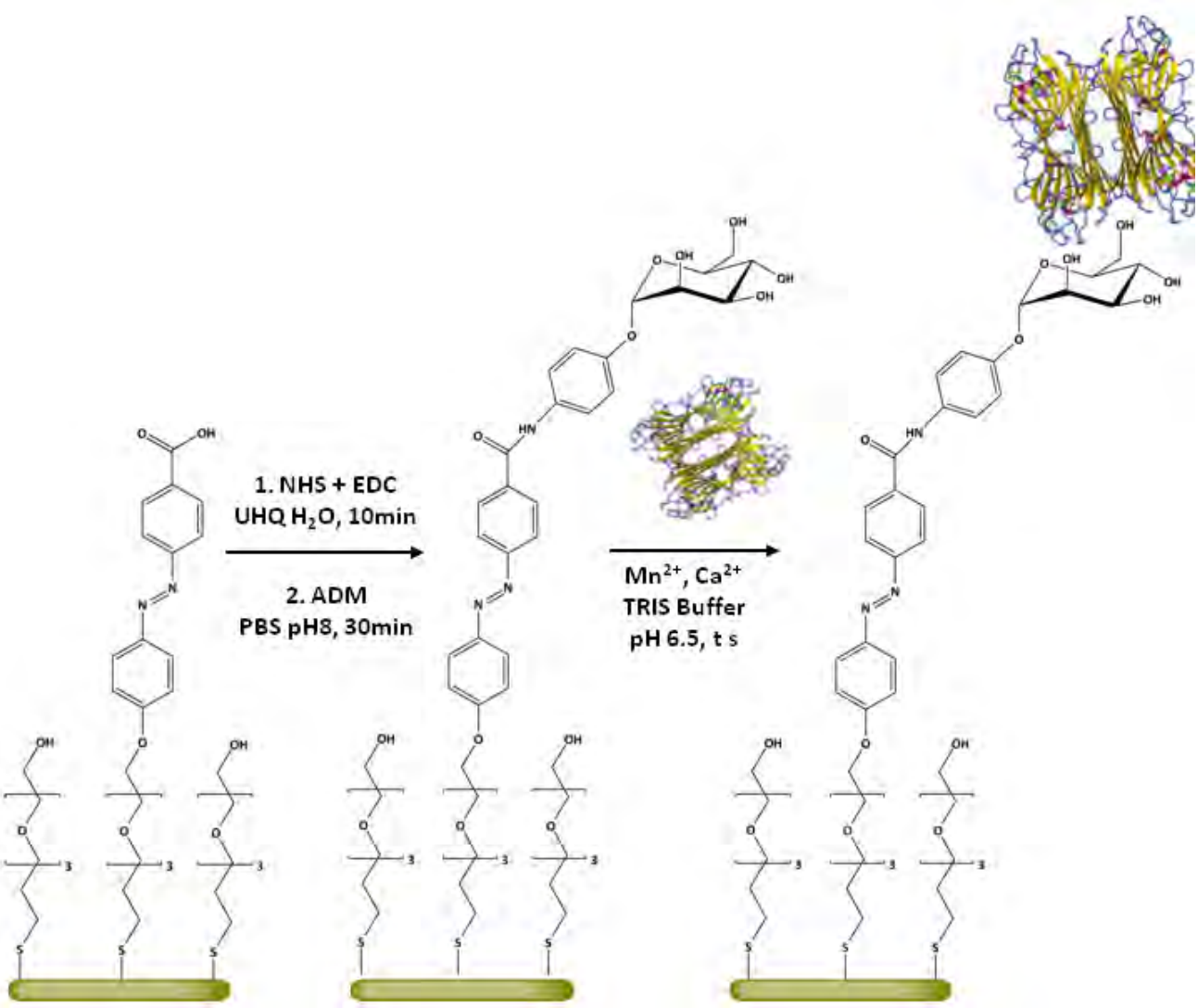

Figure 5.3 Illustration of objective 2: Functionalisation of mixed GAZ1:TEGT SAMs with ADM, followed by investigation of ConA immobilisation by SPR and ellipsometry.

5.2.1.3 Objective 3

Finally, the reversible isomerisation, or *'on'/'off'* switching of the ADM functionalised SAMs will be investigated. ConA will be used to test the isomerisation/switchability of the ADM SAM. The analytical techniques used in objective 3 will be ellipsometry, SPR, and surface *UV*/*Vis* spectroscopy (**Figure 5.4**).

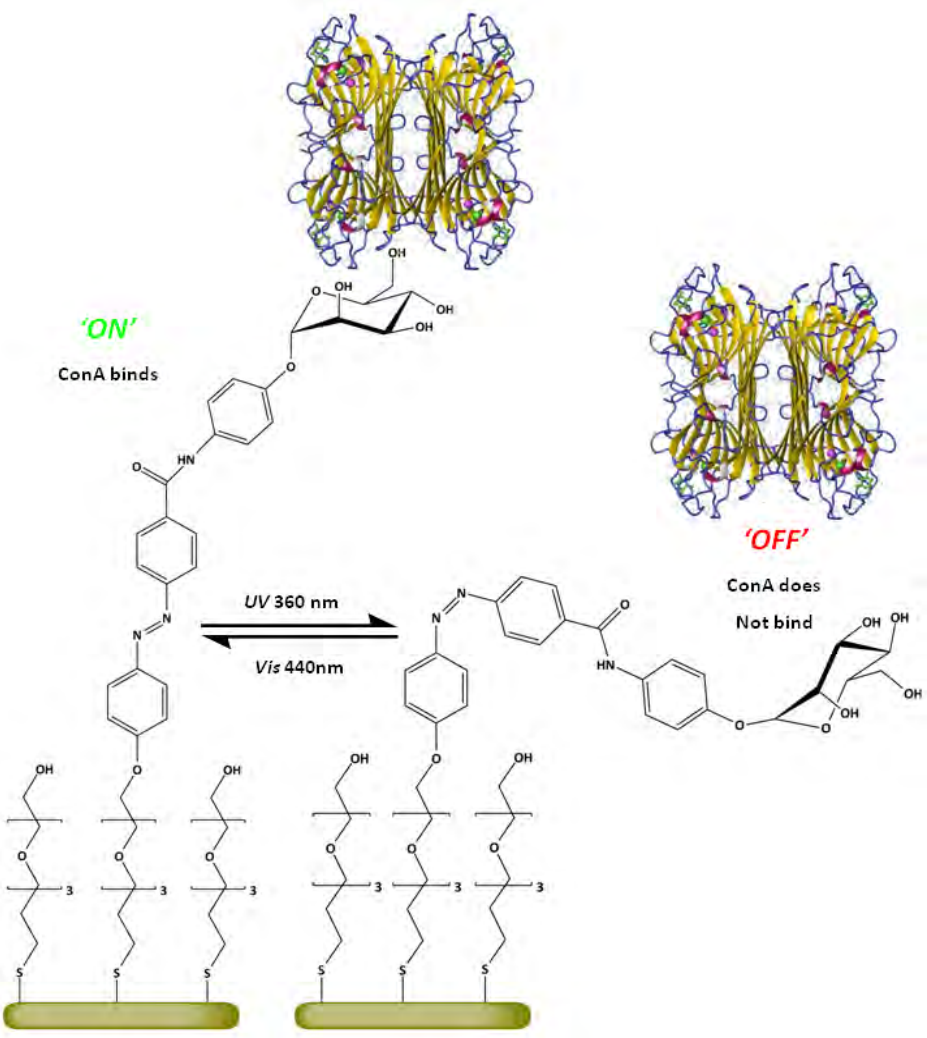

Figure 5.4 Illustration of objective 3: *UV/Vis 'on'/'off'* switching of ADM terminated SAM and the resulting effect on ConA immobilisation investigated by SPR, ellipsometry and *UV/Vis* spectroscopy.

5.3 Results and discussion

5.3.1 Objective 1 - Mixed SAM formation studies

Mixed SAMs were made from the surfactants GAZ1 and TEGT (**Figure 5.2**). The kinetics of SAM formation of five GAZ1:TEGT ratios (1:0, 1:1, 1:10, 1:100 and 0:1) was investigated as a function of time over 24 hr. The solution concentration was 0.0625 mM, of the SAM forming surfactants GAZ1:TEGT, in keeping with Chapter 4.

All glassware and Au substrates were piranha cleaned prior to use. SAMs were formed by immediate immersion of freshly cleaned Au substrates in ethanolic, surfactant solutions of GAZ1:TEGT. After formation, SAMs were washed, dried and analysed, by dynamic contact angle, ellipsometry and *UV/Vis* spectroscopy. Details of sample preparation and analytical protocols can be found in the experimental section (**Chapter 6**).

5.3.1.1 Contact angle of SAM formation

The dynamic advancing (θ_{Adv}) and receding (θ_{Rec}) contact angles were measured for pure GAZ1 SAMs. GAZ1's head group is a carboxylic acid. Surfactants containing carboxylic acid head groups are known to form bi-layers (**Figure 5.5**) through hydrogen bonding.[52, 175] The formation of bi-layers may be suppressed in two different ways:

1. By using a small amount of acetic acid[175] or triflouroacetic acid[52]
2. Use of a bulky end group[195] that can be easily removed post SAM formation.

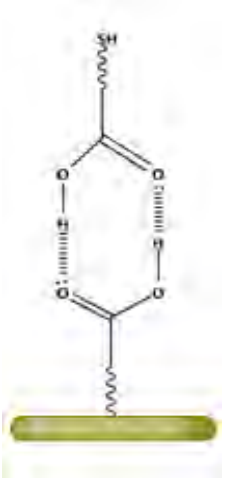

Figure 5.5 Illustration of bi-layer formed by surfactants with carboxylic acid end groups. Hydrogen bonding facilitates bi-layer formation.

Firstly, acetic acid was used to attempt to circumvent bi-layer formation (**Figure 5.6a**).[175] The θ_{Adv} starts at ≈ 49° at 0.25 hr, drops to ≈ 38° by 1 hr. θ_{Adv} then increases back to ≈ 46° by 2 hr, drops to ≈ 34° over the next 2 hr and increases back to ≈ 49° by 12 hr. θ_{Adv} then increases to ≈ 69° by 18 hr and falls to ≈ 40° by 24 hr. The θ_{Rec} remains consistently at ≈ 10° at all formation times.

The θ_{Adv} was seen to fluctuate and did not reach a plateau (**Figure 5.6a**). Furthermore, the hysteresis was large and also did not reach a plateau, indicating that the surface was not functionalised by a homogenous SAM. From this result, it was concluded that acetic acid did not circumvent bi-layer formation.

Next triflouroacetic acid (TFA) was used to circumvent bi-layer formation (**Figure 5.6b**).[52] The θ_{Adv} starts at ≈ 47° at 0.25 hr, rises to ≈ 66° by 0.5 hr. θ_{Adv} then decreases to ≈ 33° by 1 hr, and remains consistent over the next 23 hr. The θ_{Rec} remains

consistently at ≈ 12°. The hysteresis of the dynamic contact angle reached a plateau within 1 hr and was ≈ 20°.

Relative to acetic acid, TFA reduced both θ_{Adv} and θ_{Rec} of the pure GAZ1 SAMs and a hysteresis plateau was reached (**Figure 5.6b**). No examples could be found in the literature for contact angles of COOH terminated PEG or azobenzene thiol SAMs. However, the contact angles for SAMs (made in presence of TFA) are in agreement with COOH terminated alkyl SAMs reported in the literature, which show a wide spread. The value was slightly lower than the literature[196] value for COOH terminated alkyl silanes (θ_{adv} = 48° θ_{rec} = 42°); comparable to alkyl thiols[197] with a value between 30-40° over an acidic pH range (2-5), but higher than alkyl phenyl and some other alkyl thiols where a value as low as θ_{adv} = 10° has been recorded.[160]

The hysteresis of the dynamic contact angle was 20°, indicating a inhomogeneous SAM surface.[140] This is in agreement with the literature,[160] where such a hysteresis is observed for aromatic tert-butyl thiol SAMs. The hysteresis plateau was reached within 1 hr, indicating a SAM formation time of 1 hr.

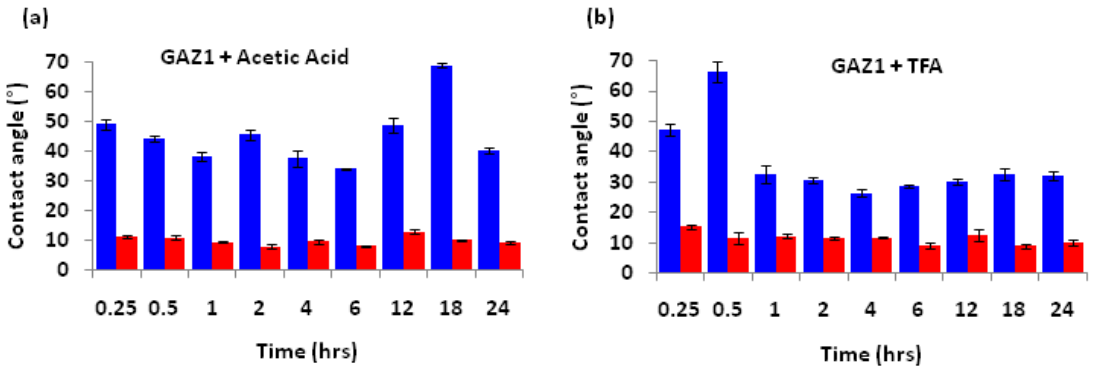

Figure 5.6 Contact angle *Vs* time for pure SAMs made from (a) GAZ1 + acetic acid (b) GAZ1 + triflouroacetic acid.

Next, both θ_{Adv} and θ_{Rec} were measured for pure TEGT SAMs made in the presence of TFA (**Figure 5.7a**). At 1 hr the θ_{Adv} ≈ 44°, falling to ≈ 37° after 2 hr and remaining constant over 24hrs. The receding contact angle remained consistently at ≈ 28°. The hysteresis reached a plateau within 1 hr and was ≈ 10°.

The contact angles are in agreement with the literature, which reports a static contact angle[198] of 32° for TEGT terminated SAMs. The hysteresis of the dynamic contact angle was ≈ 10°, indicating a relatively homogenous SAM. The hysteresis reached a plateau within 2 hr, consequently suggesting a formation time of 2 hr.

Finally, both θ_{Adv} and θ_{Rec} were measured for mixed GAZ1:TEGT SAMs as a function of time, at ratios 1:100, 1:10 and 1:1 (**Figure 5.7 b-c**). The 1:100 GAZ1:TEGT SAMs showed a consistent θ_{adv} ≈ 53° and θ_{rec} ≈ 30° with a hysteresis of ≈ 33° reached within 1 hr. The 1:10 GAZ1:TEGT SAMs showed a consistent θ_{adv} ≈ 58° and θ_{rec} ≈ 26° with a hysteresis of ≈ 34° reached within 1 hr, although 2 and 4 hours showed slightly higher θ_{adv} ≈ 70°. The 1:1 GAZ1:TEGT SAMs showed a consistent θ_{adv} ≈ 52° and θ_{rec} ≈ 14° with a hysteresis of ≈ 40° reached within 1 hr.

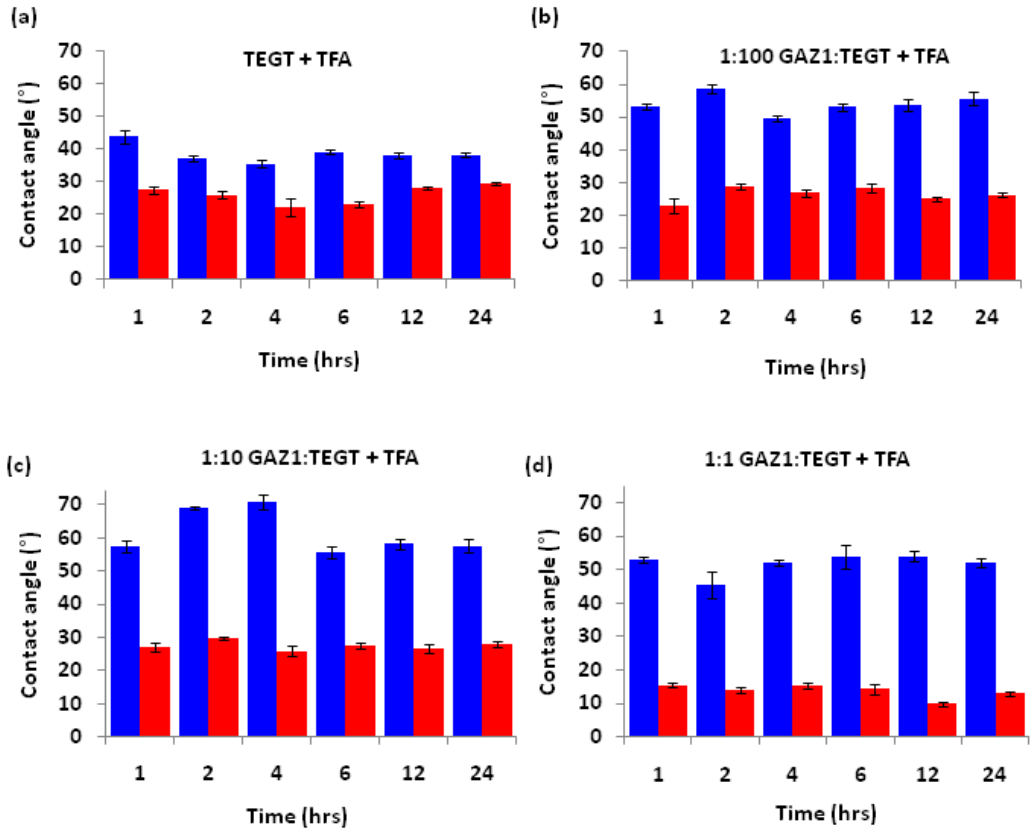

Figure 5.7 Contact angle *Vs* time for mixed SAMs made in the presence of TFA at GAZ1:TEGT ratios (a) 1:1 (b) 1:10 (c) 1:100 (d) 0:1 (TEGT only).

For all mixed GAZ1:TEGT SAMs, both θ_{Adv} and θ_{Rec} as well as the hysteresis were higher than the pure GAZ1 and TEGT SAMs (**Table 5.1**). This result is in agreement with the literature, which suggests that these increases, in the dynamic contact angle hysteresis may be attributed to increased inhomogeneity. Increased inhomogeneity occurs due to the size difference[69] which leads to the formation of a less well-packed monolayer.

The hysteresis of mixed GAZ1:TEGT SAMs decreased in the order 1:1>1:10>1:100, indicating a increase in homogeneity. This increase in homogeneity is as expected, since

GAZ1 becomes a minority surfactant. The hysteresis of all mixed GAZ1:TEGT SAMs had reached a plateau within 1 hr, suggesting a formation time of 1 hr.

5.3.1.2 Ellipsometry of SAM formation

Firstly, the ellipsometric thickness of both pure GAZ1 and pure TEGT SAMs was investigated (in the presence of TFA) as a function of time. Secondly, the ellipsometric thickness of all mixed GAZ1:TEGT SAMs was investigated as a function of time. All the results are presented in **Table 5.1** and plotted **Figure 5.8** in below.

Table 5.1 The Ellipsometric thickness of GAZ1: TEGT SAMs as a function of time. These results are plotted in **Figure 5.8**

SAM thickness / nm					
GAZ1:TEGT.					
Time / hr	**1:0**	**1:1**	**1:10**	**1:100**	**0:1**
0.5	2.32 ± 0.02	1.47 ± 0.05	1.38 ± 0.03	1.39 ± 0.02	1.48 ± 0.04
1	2.03 ± 0.06	1.82 ± 0.02	1.41 ± 0.17	1.36 ± 0.02	1.72 ± 0.10
2	2.34 ± 0.06	2.01 ± 0.03	1.62 ± 0.12	1.83 ± 0.03	1.5 ± 0.04
4	2.25 ± 0.03	2.00 ± 0.04	1.4 ± 0.05	1.67 ± 0.05	1.54 ± 0.04
6	2.12 ± 0.02	2.46 ± 0.05	1.64 ± 0.03	1.55 ± 0.02	1.63 ± 0.04
12	2.41 ± 0.06	2.11 ± 0.04	1.48 ± 0.02	1.74 ± 0.12	1.72 ± 0.09
24	2.33 ± 0.04	2.08 ± 0.06	1.53 ± 0.03	1.66 ± 0.03	1.62 ± 0.07

Pure GAZ1 SAMs appeared to have reached full thickness within 0.5 hr. Pure TEGT SAMs took 1 hr to reach full thickness.

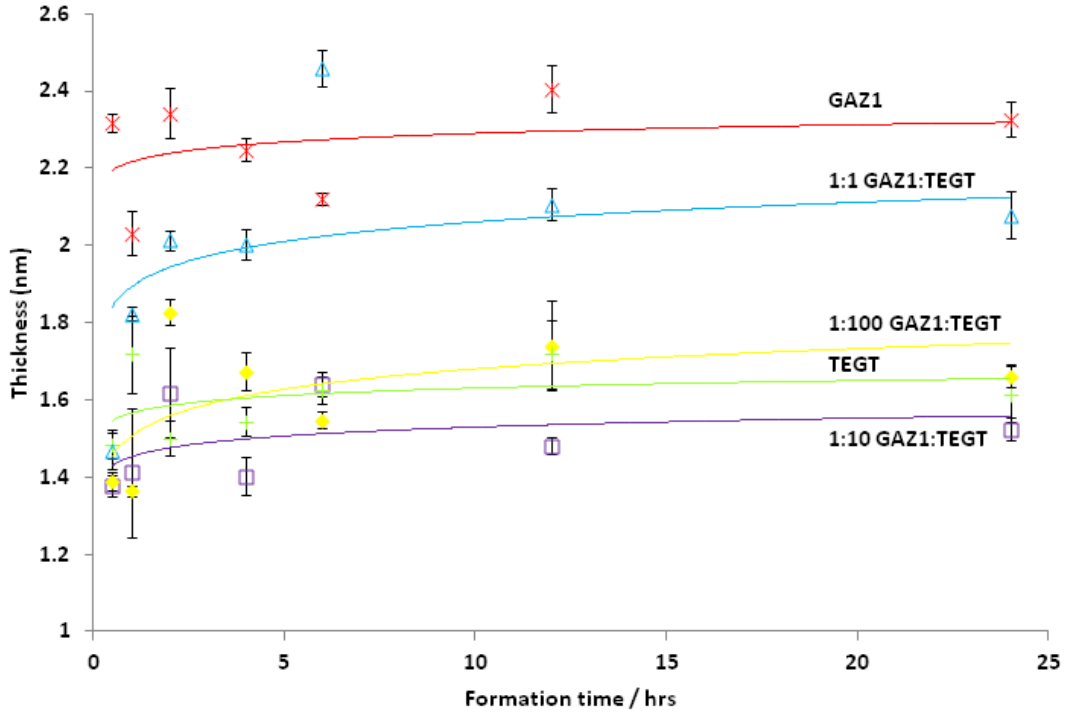

Figure 5.8. Elipsometric thickness *Vs* time of GAZ1:TEGT SAMs made in the presence of TFA at ratios 1:0, 1:1, 1:10, 1:100 and 0:1 with trend lines

The measured ellipsometric thickness obtained for both pure SAMs, was lower than the molecular length of the respective, all *trans* extended molecules (**Figure 5.9**). The molecular lengths were determined by Chem Draw 3D software and are GAZ1 = 2.9 nm and TEGT = 1.7 nm. The discrepancy between molecular length and thickness is in accordance with the literature. The literature reports that the oligo(ethyleneglycol) domain of thiol SAMs (on Au) adopts a helical amorphous structure.[75] Furthermore, there may be a degree of tilt[15, 169] due to the alkyl chain.

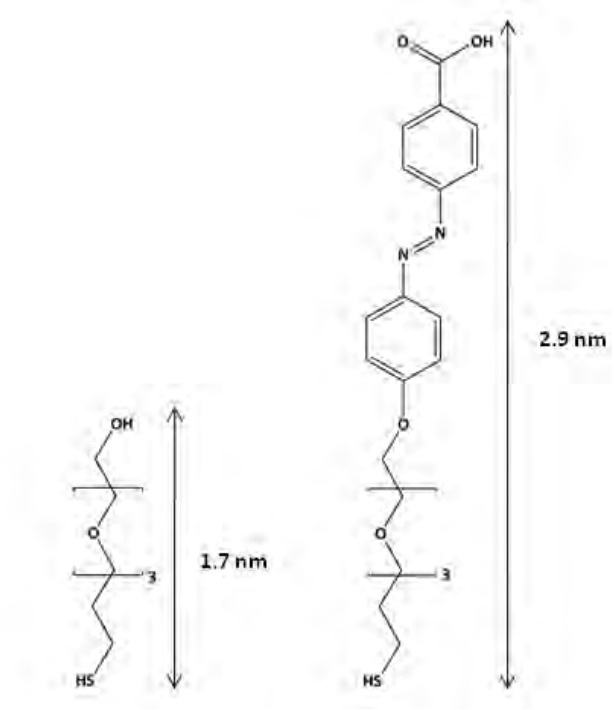

Figure 5.9 molecular lengths of TEGT and GAZ1 as determined by Chem Draw 3D.

The thickness of all mixed GAZ1:TEGT SAMs generally reached a plateau within 2 hr. The thickness of mixed GAZ1:TEGT SAMs generally decreases from the pure GAZ1 to the pure TEGT SAMs. The thicknesses of 1:10 and 1:100 GAZ1:TEGT SAMs were comparable to the pure TEGT SAM.

It is thought that the lower thickness of the 1:10 GAZ1:TEGT SAM relative to the pure TEGT SAM, is due to the increased disorder in the former. Increased disorder decreases the packing density of SAMs, effecting the measured ellipsometric thickness, which is measure of mean thickness.[199] This explanation is in agreement with the contact angle hysteresis results, which indicated that 1:10 GAZ1:TEGT SAMs were more inhomogeneous than the 1:100 GAZ1:TEGT SAMs

5.3.1.3 Surface UV/VIS absorption spectra

5.3.1.3.1 UV/VIS of SAMs as a function of GAZ1:TEGT ratio

Surface *UV/Vis* absorption spectroscopy was used investigate the λ_{max} and isomerisation of pure GAZ1, as well as all mixed GAZ1:TEGT SAMs (**Figure 5.10**) at a formation time of 24 hours. After SAM formation three UV/Vis absorption spectra were recorded. The first spectrum was recorded immediately after SAM formation. The second spectrum was recorded post exposure of SAMs to 3 mins *UV* at 360 nm. The third spectrum was recorded post exposure of SAMs to 3 mins *Vis* at 440 nm. An irradiation time of 3 mins was used.

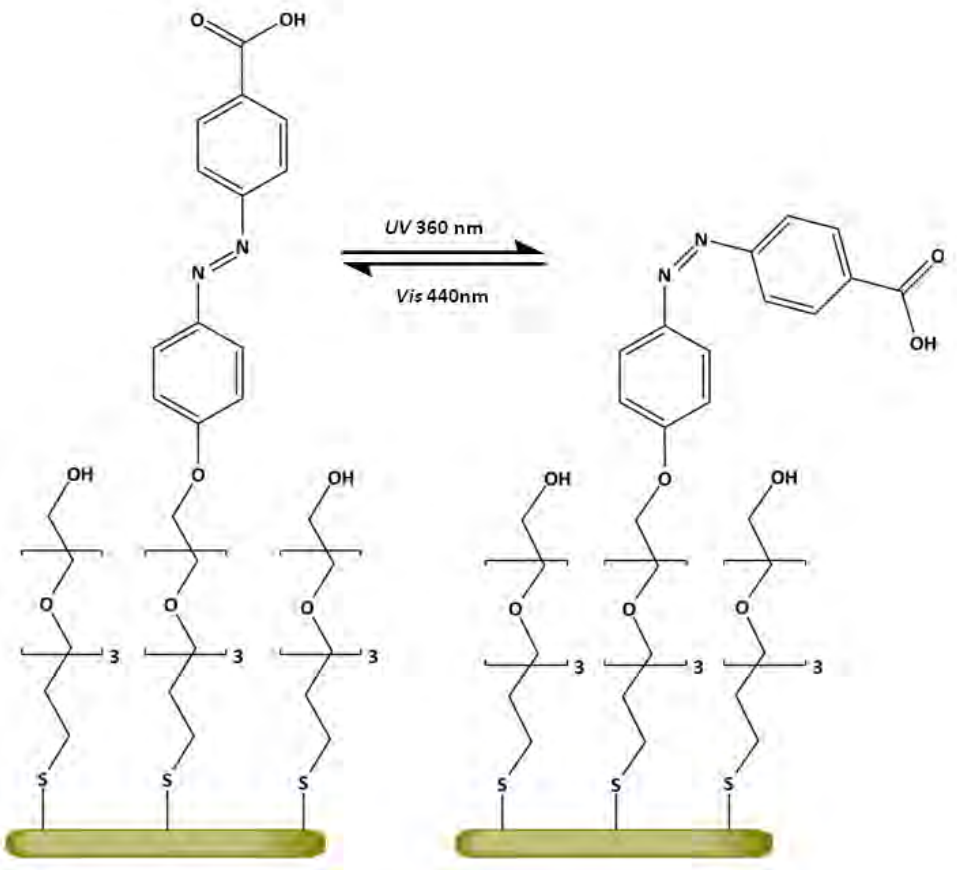

Figure 5.10 Illustration of *UV/VIS* induced isomerisation of mixed GAZ1:TEGT SAMS

The *UV/Vis* absorption spectra of the pure GAZ1 SAM (**Figure 5.11a**) exhibited a λ_{max} ≈ 337 nm. This value is strongly hypsochromicaly shifted with respect to the solution value (λ_{max} = 356 nm **appendix I**). Furthermore, exposure to both *UV* at 360 nm and *Vis* at 440 nm slightly increased absorption, which is not typical of azobenzene isomerisation.

The *UV/Vis* absorption spectra of the 1:1 GAZ1:TEGT SAMs (**Figure 5.11b**) exhibited a λ_{max} ≈ 352 nm. This value is slightly hypsochromicaly shifted with respect to the solution value (356 nm **appendix I**). Furthermore, exposure to *UV* at 360 nm decreased absorption while *Vis* at 440 nm increased absorption, which is typical of azobenzene isomerisation.

The *UV/Vis* absorption spectra of the 1:10 GAZ1:TEGT SAMs (**Figure 5.11c**) exhibited a λ_{max} ≈ 359 nm. This value is in close agreement to the solution value (356 nm). However, the *UV*/*Vis* response is not clear, due to a very low absorption.

The *UV/Vis* absorption spectra of the 1:100 GAZ1:TEGT SAMs (**Figure 5.11d**) was not characteristic of azobenzene and did not exhibit an apparent λ_{max}. Consequently no *UV/Vis* response was observed.

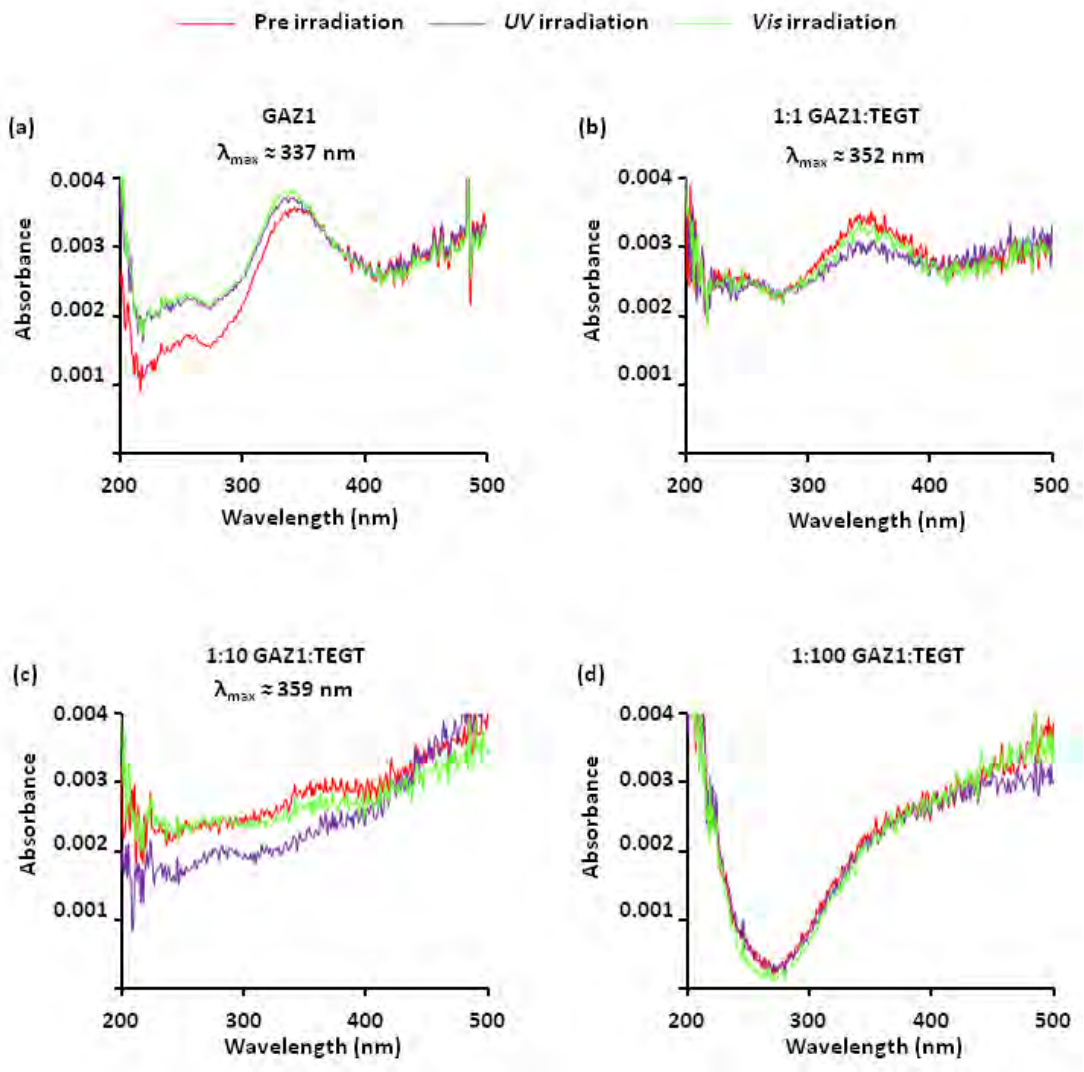

Figure 5.11 *UV/Vis* absorption spectra GAZ1:TEGT SAMs formed over 24 hr at ratios (a) 1:0 (b) 1:1 (c) 1:10 (d) 1:100. Each spectrum shows the SAM pre irradiation, post irradiation with *UV* (3 mins) at 360 nm and post irradiation with *Vis* (3 mins) at 440 nm.

The hypsochromic shifts in λ_{max} of pure GAZ1 (λ_{max} ≈ 337 nm) and 1:1 GAZ1:TEGT (λ_{max} ≈ 352 nm) SAMs suggests a degree of H-aggregation within these SAMs.[134] Pure GAZ1 exhibited the largest degree of aggregation, as shown by the largest shift in λ_{max}. Furthermore, the degree of aggregation was also reflected in the differences between the *UV/Vis* induced response of the two SAMs. Upon exposure to *UV/Vis* GAZ1 shows

behaviour non-typical of azobenzene isomerisation, whereas the 1:1 GAZ1:TEGT SAM shows behaviour typical of isomerisation. However, the azobenzene peak in the 1:1 GAZ1:TEGT SAM would not completely deplete, indicating some inhibition to isomerisation. Inhibited isomerisation could be explained by spatial constraints which are known to inhibit isomerisation[137] of azobenzene within SAMs, isomerisation requiring a free volume of at least 0.12 nm^3.[117]

The λ_{max} of 1:10 GAZ1:TEGT SAMs was similar to the solution value suggesting no, or little H-aggregation. However, the degree of isomerisation was unclear due to the low absorption, which suggests a low concentration of azobenzene within the SAM[136] relative to pure GAZ1 SAMs and 1:1 GAZ1:TEGT, as expected.

The concentration of azobenzene within 1:100 GAZ1:TEGT SAMs was so low no absorption attributable to azobenzene was observed. The literature[136] suggests that SAMs with an azobenzene concentration < 20% cannot be detected by surface *UV/Vis* spectroscopy.

In summary, all SAMs investigated, except 1:100 GAZ1:TEGT, exhibited a *UV/Vis* absorption spectra characteristic of azobenzene. The value of λ_{max} increases in the order GAZ1 < 1:1 GAZ1:TEGT < 1:10 GAZ1:TEGT, which can be explained in terms of the reduction in H-aggregation. Absorption decreases in the order GAZ1 > 1:1 GAZ1:TEGT > 1:10 GAZ1:TEGT > 1:100 GAZ1:TEGT, which can be explained by the decreasing concentration of GAZ1 in the SAM. With respect to the isomerisation: The non-typical isomerisation behaviour of pure GAZ1 can be explained by close packing which results in H-aggregation. The typical but limited isomerisation behaviour of 1:1 GAZ1:TEGT SAMs can be explained in terms of spatial constraints. The unclear behaviour of 1:10 GAZ1:TEGT and 1:100 GAZ1:TEGT can be explained in terms of low concentration.

5.3.1.3.2 UV/VIS of 1:1 GAZ1:TEGT SAMs as a function of time

Next surface *UV/Vis* absorption spectroscopy was used investigate the λ_{max} and isomerisation of 1:1 GAZ1:TEGT SAMs as a function of SAM formation time (**Figure 5.12 and 5.13**). The 1:1 GAZ1:TEGT was chosen as it gave the best *UV/Vis* response at 24 hrs and three spectra were recorded as above (**Figure 5.11b**)

At both 1 and 3 hrs λ_{max} is ≈ 312nm (**Figure 5.12**, black and blue lines respectively) this value is strongly hypsochromically shifted with respect to the solution value (356 nm **appendix I**). Upon exposure to *UV/Vis* the SAMs also exhibited behaviour non-typical of azobenzene isomerisation behaviour, with exposure to *UV* at 360 nm depleting the peak which was non-recoverable upon exposure to *Vis* at 440nm.

At 6 hrs λ_{max} is ≈ 334 nm (**Figure 5.12**, green line) which is also is strongly hypsochromically shifted with respect to the solution value (356 nm **appendix I**). Furthermore, upon exposure to *UV/Vis* the SAMs also exhibited behaviour non-typical of azobenzene isomerisation, in the same fashion as 1 and 3 hrs.

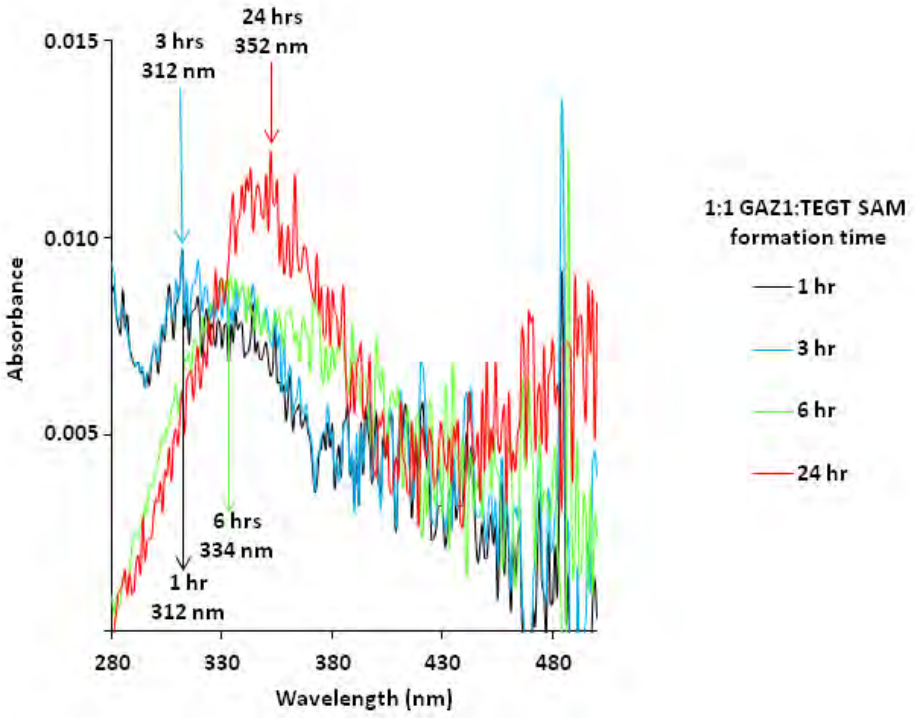

Figure 5.12 *UV/Vis* absorption spectra of 1:1 GAZ1:TEGT SAMs at different SAM formation times.

By 24 hrs λ_{max} is ≈ 352 nm (**Figure 5.12**, red line) which is only slightly hypsochromically shifted with respect to the solution value of 356 nm (**appendix I**). Furthermore, upon exposure to *UV/Vis* the SAMs also exhibited behaviour typical of azobenzene isomerisation.

The *UV/Vis* absorption spectra showed λ_{max} to increase with formation time in the order 1hr = 3 hr < 6 hr < 24 hr. This suggests that at low formation times SAMs are H-aggregated, with the degree of aggregation decreasing with increasing formation time. This decrease in aggregation is also reflected in the degree of isomerisation of mixed SAMs.

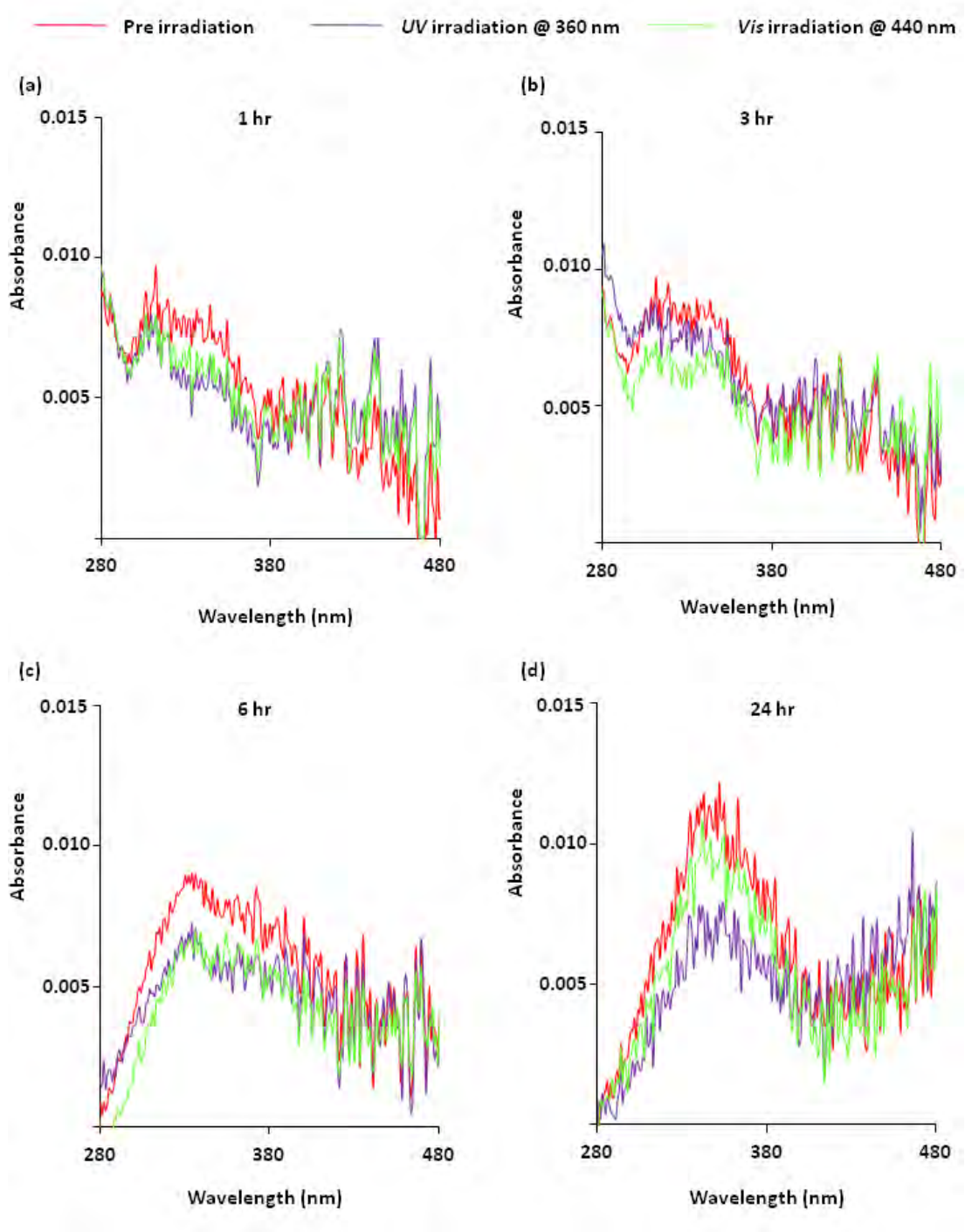

Figure 5.13 *UV/*Vis absorption absorption spectra of 1:1 GAZ1:TEGT SAMS and their response to irradiation with *UV* (3 mins) at 360 nm followed by *Vis* (3 mins) at 440 nm.

The 24 hr SAM was the only one to exhibit reversible isomerisation typical of azobenzene. However, the peak did not completely deplete, which as previously mentioned is probably due to spatial constraints.

5.3.1.4 GAZ1:TEGT SAM formation study conclusions

The formation of mixed GAZ1:TEGT SAMs was investigated as a function of time, at the ratios 1:0, 1:1, 1:10, 1:100 and 0:1. The analytical techniques used were contact angle, ellipsometry and *UV/Vis* spectroscopy.

Contact angle showed that SAM formation required the presence of TFA, in order to circumvent bi-layer formation. SAM formation, of all ratios, was shown to be complete within 1 hr. However, ellipsomtery showed SAM formation of GAZ1 to be complete in 0.5 hrs, 1 hr for pure TEGT and 2 hrs for all GAZ1:TEGT ratios. Whereas, UV/Vis suggested that formation takes place over 24 hrs.

The *UV/Vis* absorption spectra and isomerisation of SAMs was investigated at 24 hr. Pure GAZ1 SAMs were shown to be aggregated and did not show isomerisation. 1:1 GAZ1:TEGT SAMs showed a lower degree of aggregation, and also showed reversible isomerisation. 1:10 GAZ1:TEGT SAMs were not aggregated. However, the isomerisation of 1:10 GAZ1:TEGT SAMs was not clear due to the low concentration of azobenzene within the SAM. The concentration of azobenzene in 1:100 GAZ1:TEGT SAMs was too low to be observed by *UV/Vis.* Hence as the concentration of azobenzene within the SAM decreases as does the degree of aggregation which is consequently accompanied by an increase in *UV/Vis* induced isomerisation.

1:1 GAZ1:TEGT SAMs were shown to have the best *UV/Vis* response at 24 hrs. Hence, the *UV/Vis* absorption spectra of 1:1 GAZ1:TEGT SAMs was investigated as a function of time. The *UV/Vis* absorption spectra were shown to change with respect to time. At low formation times azobenzene surfactants were aggregated and isomerisation inhibited. However, further ordering was shown to occur over 24hr, with both λ_{max} and the degree of isomerisation increasing with respect to time.

Considering all results the following model of mixed 1:1 GAZ1:TEGT SAM formation is proposed. Surfactants are chemisorbed within 2 hr, as suggested by both ellispometry and contact angle. However, surfactants are closely packed and some azobenzene's are aggregated, hence the λ_{max} is hypsochromically shifted as suggested by UV/Vis absorption spectroscopy. Further ordering occurs between 6-24 hrs, as shown by the increase in λ_{max} by 24 hrs. This increase in λ_{max} is also accompanied by an increase in the degree of isomerisation upon exposure of SAMs to UV/Vis irradiation at 360/440 nm, respectively.

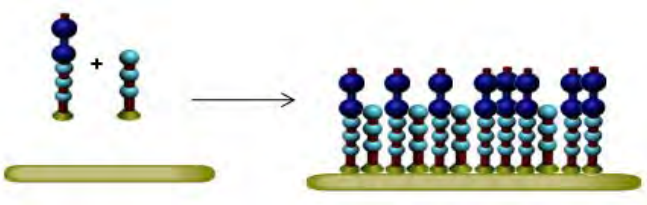

Figure 5.15 Proposed model of 1:1 GAZ1:TEGT SAM formation. At low formation times surfactants are closely packed and some azobenzene's are aggregated. Further ordering occurs between 6 – 24 hrs and at 24 hrs the degree of azobenzene aggregation decreases which is accompanied by an increase in isomerisation upon exposure to *UV/Vis* irradiation at 360/440 nm respectively.

5.3.2 Objective 2 - ConA immobilisation studies

SPR and ellipsometry were used to investigate the specific immobilisation (**Figure 5.3**) of ConA, on mixed GAZ1:TEGT SAMs functionalised with ADM. The GAZ1:TEGT ratios used were 1:0, 1:1, 1:10, 1:100 and 0:1. Firstly, SAMs were formed over 24 hr, in accordance to SAM formation studies, discussed above. Secondly, all ratios of GAZ1:TEGT SAMs were functionalised with ADM giving GAZ1-ADM:TEGT SAMs.[200] Finally, immobilisation of ConA to the ADM functionalised surfaces was investigated.

5.3.2.1 Functionalisation of GAZ1 SAMs with ADM

ADM was chemically bound to GAZ1 containing SAMs through a two step procedure (**Figure 5.16**). The procedure followed a well-established protocol[210] for the functionalisation of an acid surface with an amine to form an amide. This SAM is herein referred to as GAZ1-ADM.

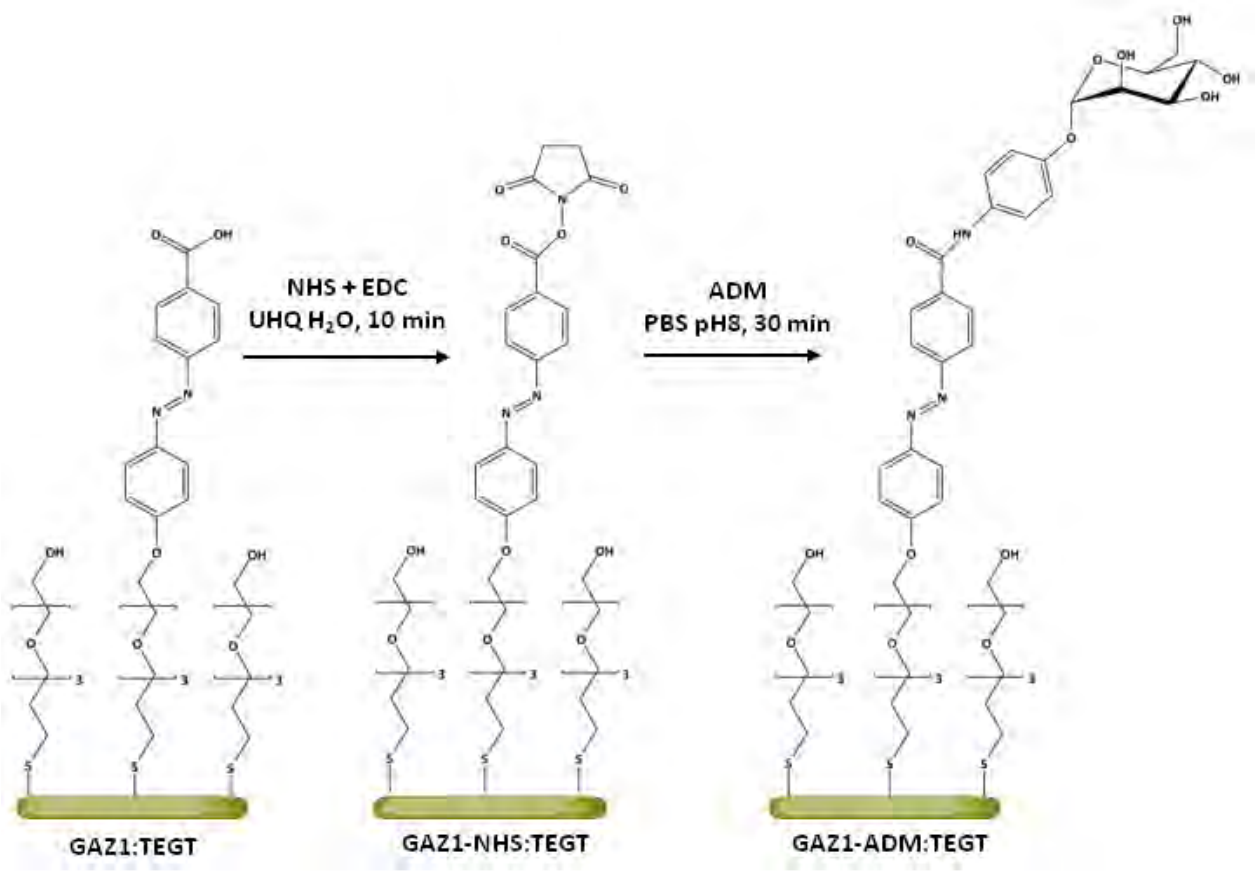

Figure 5.16 Illustration of ADM functionalisation of carboxylic acid-terminated SAMs.

The first step of the procedure, is the activation of the carboxylic acid end group of GAZ1 through addition of N-hydroxy succinimide (NHS) to afford GAZ1-NHS. This activation reaction forms a labile, succinimidyl ester.[200] The reaction was carried out under aqueous conditions for 10 mins with NHS present at a concentration of 0.05 mM. Furthermore, the reaction requires the presence of 1-ethyl-3-(3-dimethylaminopropyl)carbodiimide) (EDC) at a concentration of 0.2 mM.

The second step is the substitution of the labile ester with ADM, producing an amide bond between the carboxylic acid end group of GAZ1 and the aromatic amine of ADM to afford GAZ1-ADM. Substitution by ADM must be preformed immediately after

formation of the labile succinimidyl ester, GAZ1-NHS, in order to prevent hydrolysis of the amine-reactive NHS ester. The reaction is carried out in PBS buffer at pH 8 for 30 mins. ADM is present at a concentration of 0.05 mM.

In order to assert if the reaction was successful we compared the immobilisation of ConA on a pure ADM-GAZ1 SAM to a pure GAZ1 SAM, using SPR. ConA should only bind to the ADM surface so the GAZ1 SAM should show no response. The concentration of ConA to be used was determined first. However, in keeping with the context of the discussion, investigation of ConA concentration is discussed in the next section (**5.3.2.2** page 29).

A typical SPR sensorgram can be seen below **Figure 5.17**. The degree of ConA immobilisation is expressed in micro response units (µRU) which is the difference between the baseline pre-injection and post wash. An increase in µRU represents immobilisation. The size of the increase is relative to the amount of ConA immobilised.

SAMs are placed in the SPR cell, and the cell was purged with ethanol in order to remove any air bubbles. Subsequently ethanol is flushed out with TRIS buffer until a stable baseline is reached. Once the baseline is stabilised a ConA solution is injected and flows across the surface for a time t, at a low flow rate of 50 µL s^{-1}. The ConA solutions were made in TRIS buffer at pH = 6.5, in the presence of Ca^{2+} and Mn^{2+} ions. After exposing the surface to the conA solution for t s the SAM is washed with pure TRIS buffer at a high flow rate (1500 µL s^{-1}) in order to remove any unbound conA.

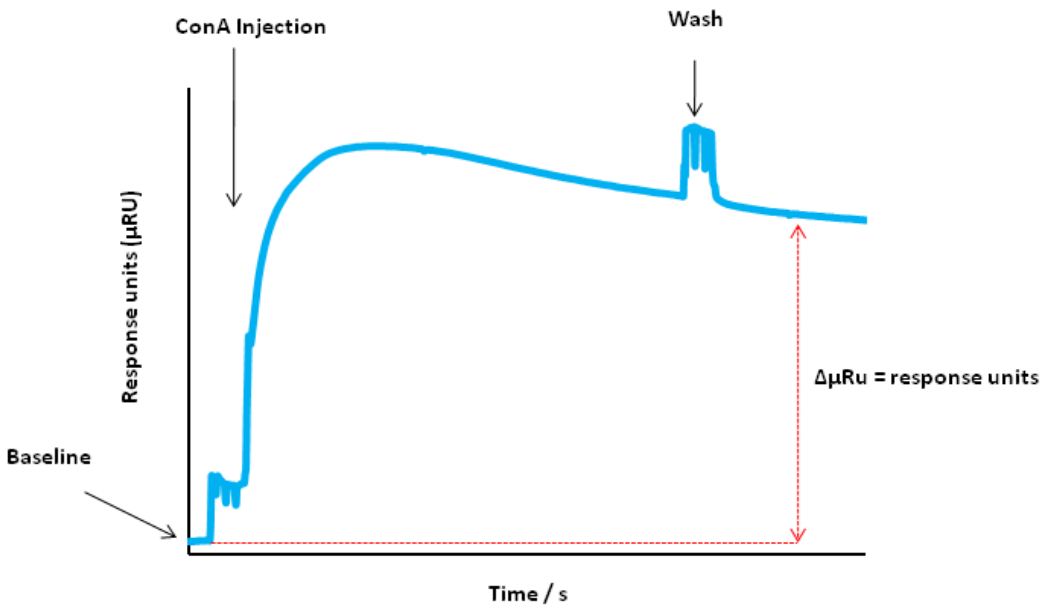

Figure 5.17 Typical SPR sensorgram showing the baseline, ConA injection, wash and the definition of response units, ΔµRu.

The SPR results for ConA immobilisation of GAZ1 SAMs relative to GAZ1-ADM SAMs are reported below in **Figure 5.18**. The SPR response of pure GAZ1 SAMs to ConA was ≈ 200 µRU, whereas pure GAZ1-ADM SAMs have a response of ≈ 1500 µRU. This result suggests that the functionalisation of pure GAZ1 SAMs with ADM was successful.

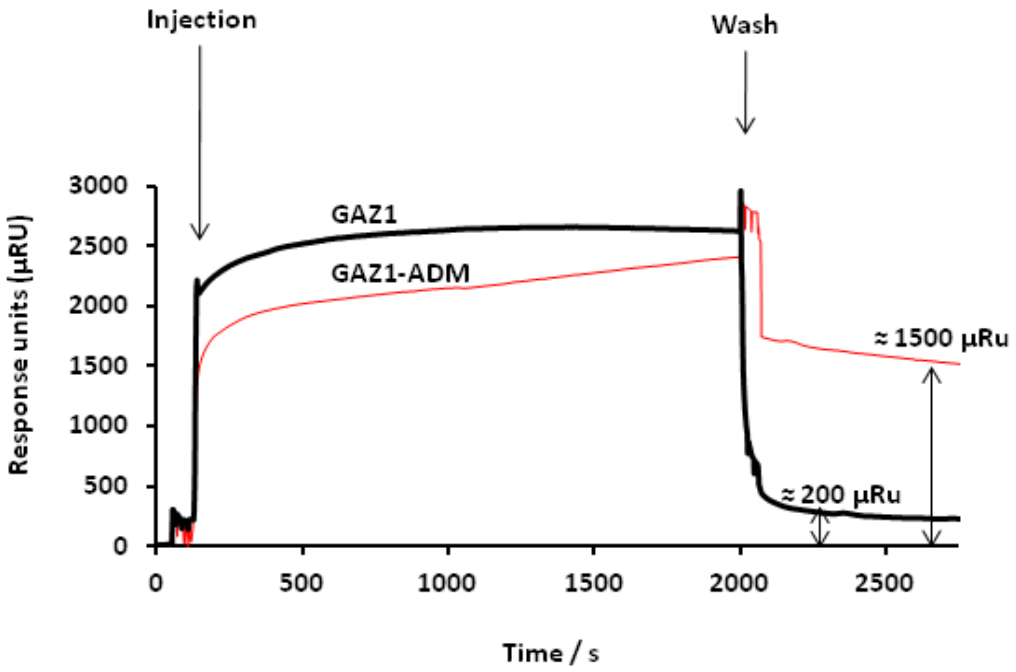

Figure 5.18 SPR sensorgram traces showing the response of pure GAZ1 SAMs with and without ADM to ConA injected over 1800 s at a concentration of 0.005 mg ml^{-1}

However, despite the assertion of the successful functionaliation of the GAZ1 SAM with ADM it was envisaged that the reaction might not have proceeded through the aromatic amine of ADM, as desired (**Figure 5.19a**). This is because the desired reaction is in competition with undesirable reactions of ADM with GAZ1, through the mannose hydroxyls of ADM (**Figure 5.19b**). Indeed the same protocol is used for the functionalisation of acid surfaces with alcohols.

Due to the large differences between the respective pKas and steric hindrances, with respect to the mannose hydroxyls, the reaction would favourably proceed through the aromatic amine, as desired. However, it is still possible that the undesired reaction could proceed, and if it did it would expose the aromatic amine of ADM (**Figure 5.19b**) which could potentially immobilise ConA, in a non-specific manner, therefore distorting

results. An aniline-terminated SAM was used as a model (GAZ1-aniline SAM) to mimic the potential undesired reactions (**Figure 5.19c**) and we investigated the immobilisation of ConA to this model surface.

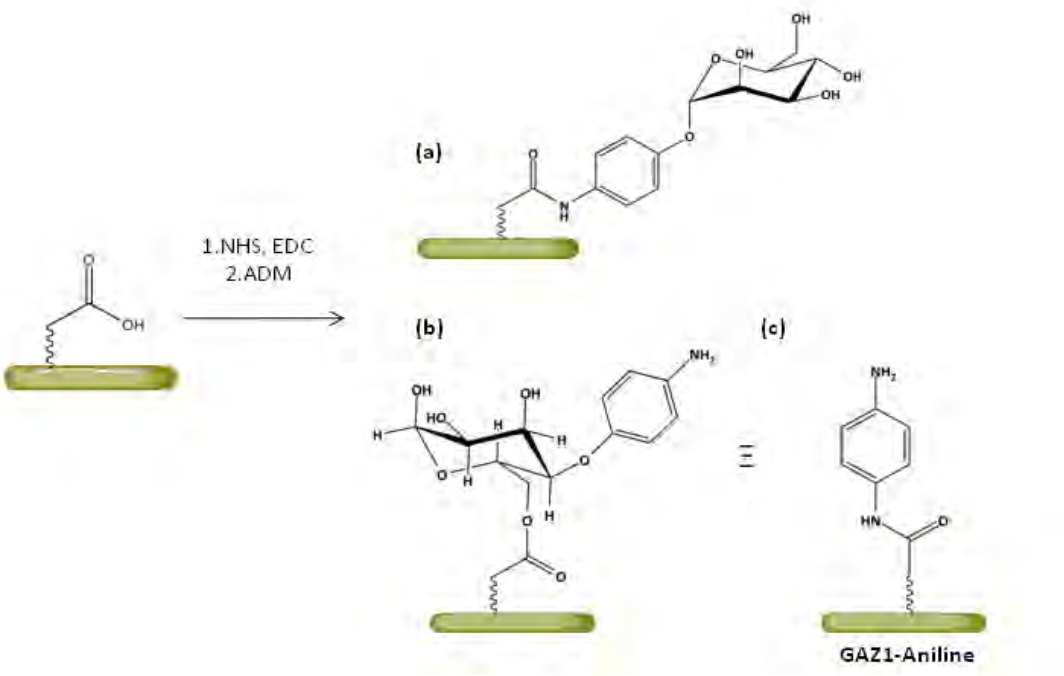

Figure 5.19 illustration of (a) product of ADM functionalisation (b) possible side reaction (c) the model surface used to test if ConA non-specifically binds to aromatic amines.

Functionalisation of a GAZ1 SAM with dianiline used the same procedure as for ADM.[189] The SPR results are reported in **Figure 5.20**. The SPR response of aniline functionalised SAMs was ≈ 500 µRU which is 28 % that of the GAZ1-ADM SAM which was ≈ 1800 µRU (**figure 5.20**).

The small response suggests a degree of non-specific binding does occur on the aniline terminated SAM. However, it also suggests that the majority, if not all the ADM, is attached to GAZ1 through the amine, and not through a hydroxyl of the sugar.

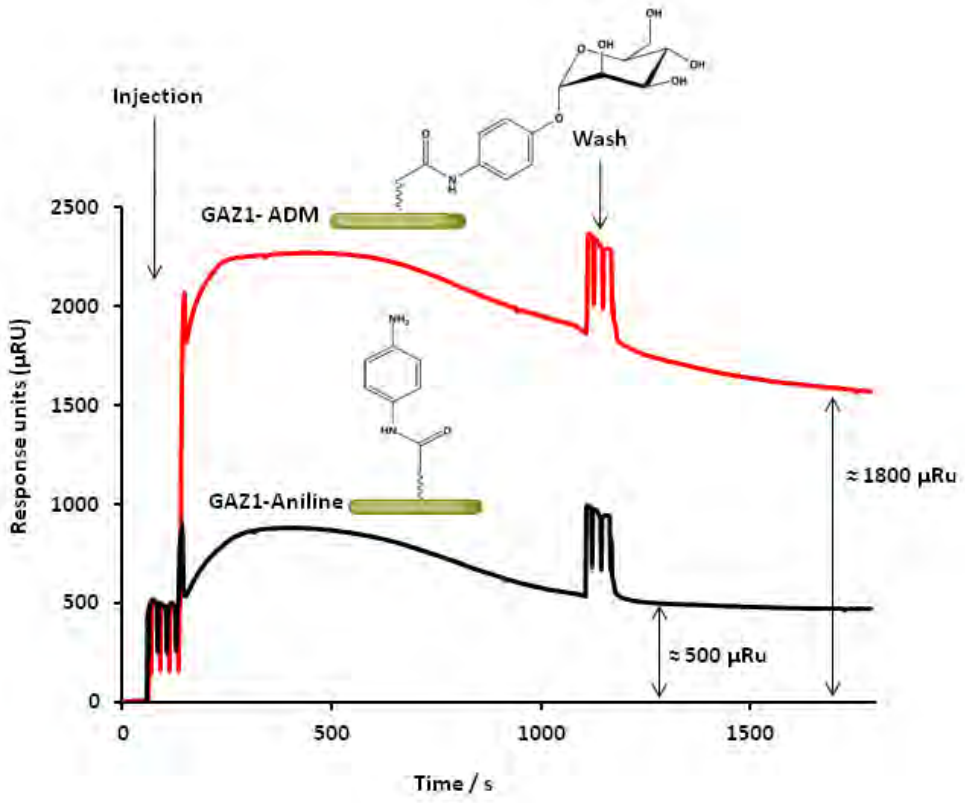

Figure 5.20 SPR sensorgram traces showing the response of GAZ1-ADM and GAZ1-Aniline SAMs to ConA injected at a concentration of 0.005 mg ml^{-1}.

5.3.2.2 Immobilisation of ConA on GAZ1-ADM SAMs by SPR

Following functionalisation of the surface with ADM, both ellispometry and SPR were used to investigate the specific immobilisation of ConA to the GAZ1-ADM SAM (**Figure 5.21**). No protocol could be found for the specific immobilisation of ConA on ADM surfaces. Hence a suitable protocol was devised through investigation, which investigated the experimental parameters of concentration and time.

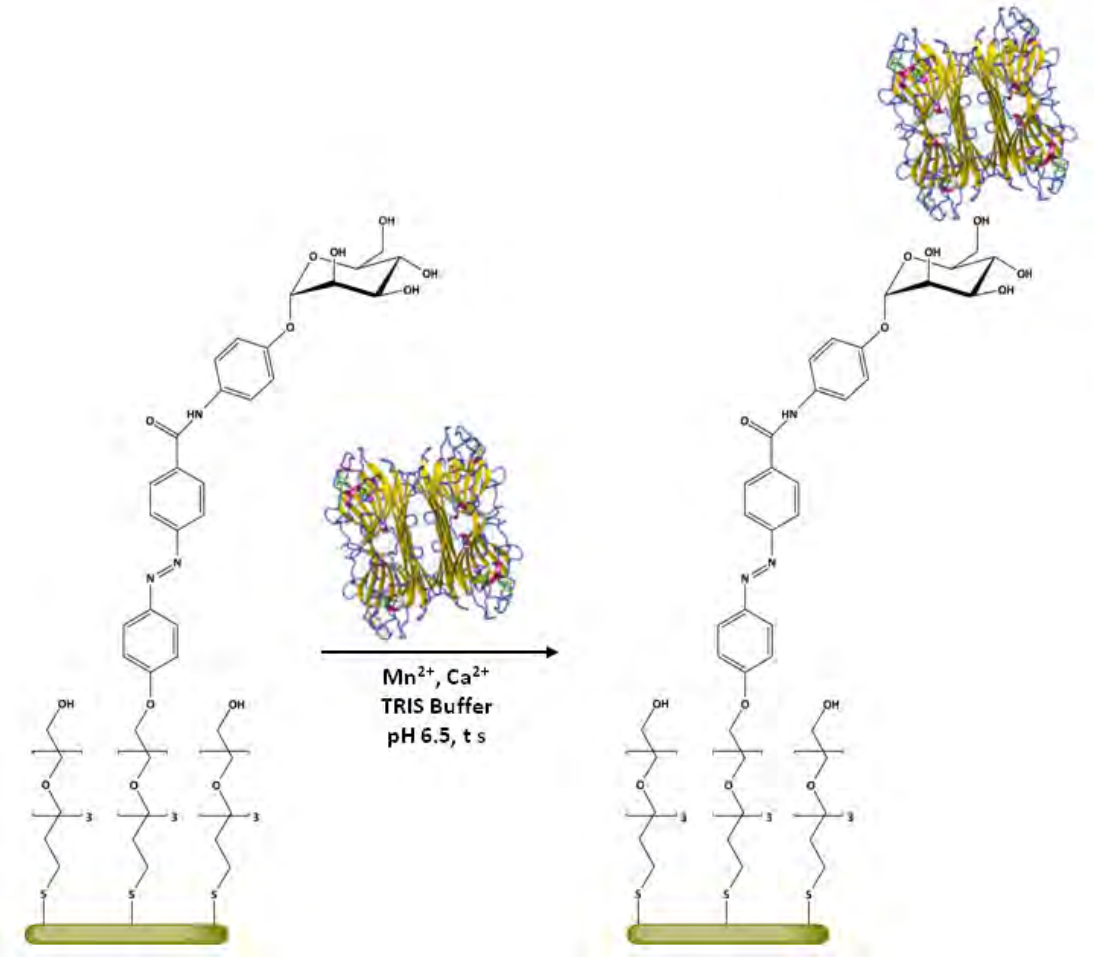

Figure 5.21 Illustration of ConA immobilisation on GAZ1-ADM SAMs.

The following section is split into three parts:

1. The effect of ConA concentration is reported.
2. The immobilisation time is reported.
3. ConA immobilisation at the experimentally determined concentration and time is reported.

5.3.2.2.1 Investigation of ConA immobilisation concentration

The first experimental parameter investigated was ConA concentration. The concentration of ConA needs to be low enough to prevent its non-specific binding to the bio-inert TEGT SAM. Several concentrations of ConA were investigated, the results are reported in **Figure 5.22**. At a concentration of 1 mg ml^{-1} the SPR response was ≈ 600 µRU, at 0.1 mg ml^{-1} the response was ≈ 100 µRU and at concentrations ≤ 0.01 mg ml^{-1} there was no response.

These results show that at concentrations ≥ 0.1 mg ml^{-1} there was a degree of non-specific binding of ConA to TEGT SAMs, as shown by the SPR response.

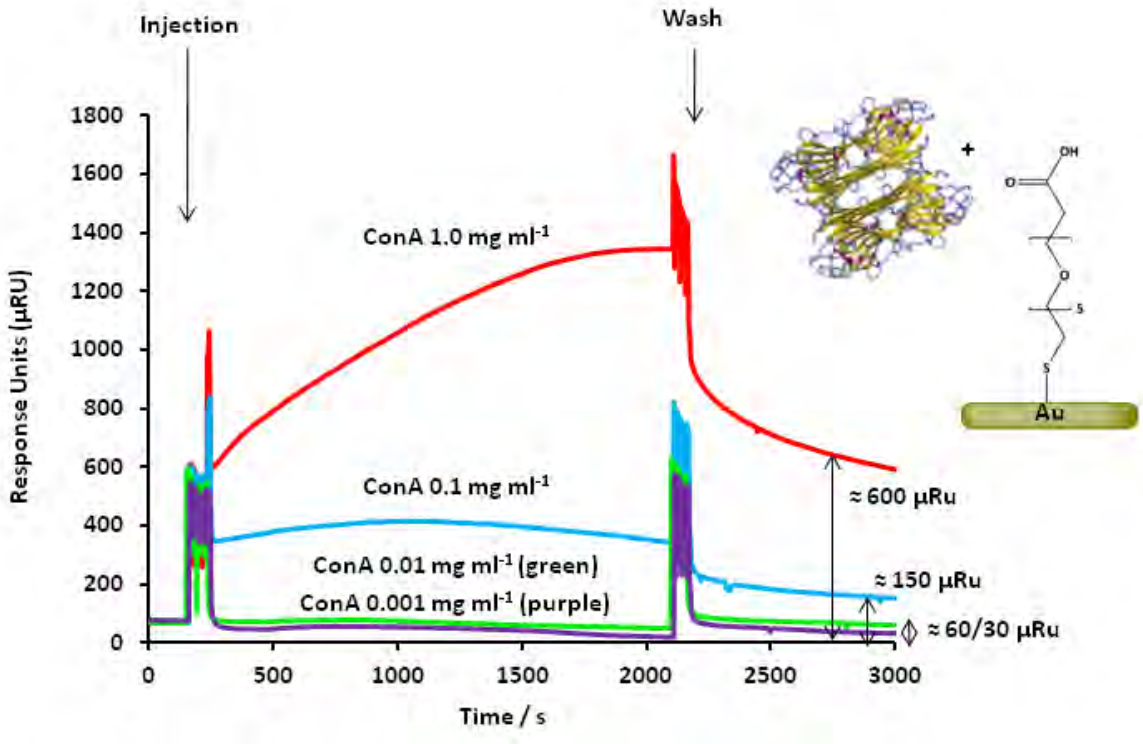

Figure 5.22 SPR sensorgram traces showing the response of pure TEGT SAMs, to ConA injected over 1800 s at different concentrations.

Next the affect of ConA concentration on its binding to pure GAZ1-ADM SAMs was investigated and results are reported in **Figure 5.23**. It was found that at concentrations of 0.01 and 0.005 mg ml^{-1} the SPR responses were similar at ≈ 1500 µRU. As the responses were similar a concentration of 0.005 mg ml^{-1} was chosen for further investigation.

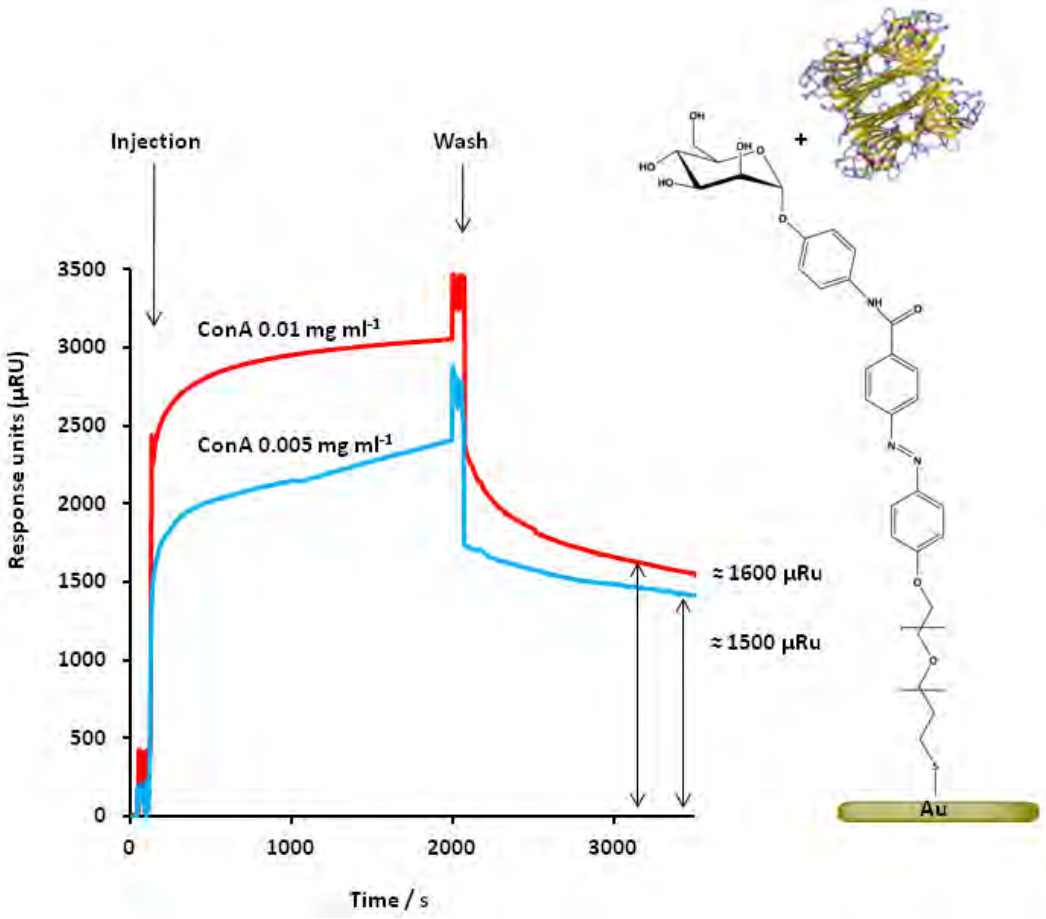

Figure 5.23 SPR sensorgram traces showing the response of ADM functionalised GAZ1 SAMs, exposed to ConA over 1800 s at different concentrations.

In order to determine if previous results were specific to both pure TEGT and pure GAZ1 SAMs we investigated the non-specific immobilisation of ConA on bare Au, at different

concentrations. The results are reported in **Figure 5.24**. The response of bare Au to ConA at a concentration 1.0 mg ml^{-1} was ≈ 280 µRU, 0.10 mg ml^{-1} ≈ 200 µRU and at 0.01 mg ml^{-1} ≈ 180 µRU, suggesting ConA has a degree of non-specific absorption on Au. However, relative to the specific immobilisation of ConA on the GAZ1-ADM surface, it is only a small fraction (13 %). Furthermore, the result asserts that TEGT inhibits ConA immobilisation.

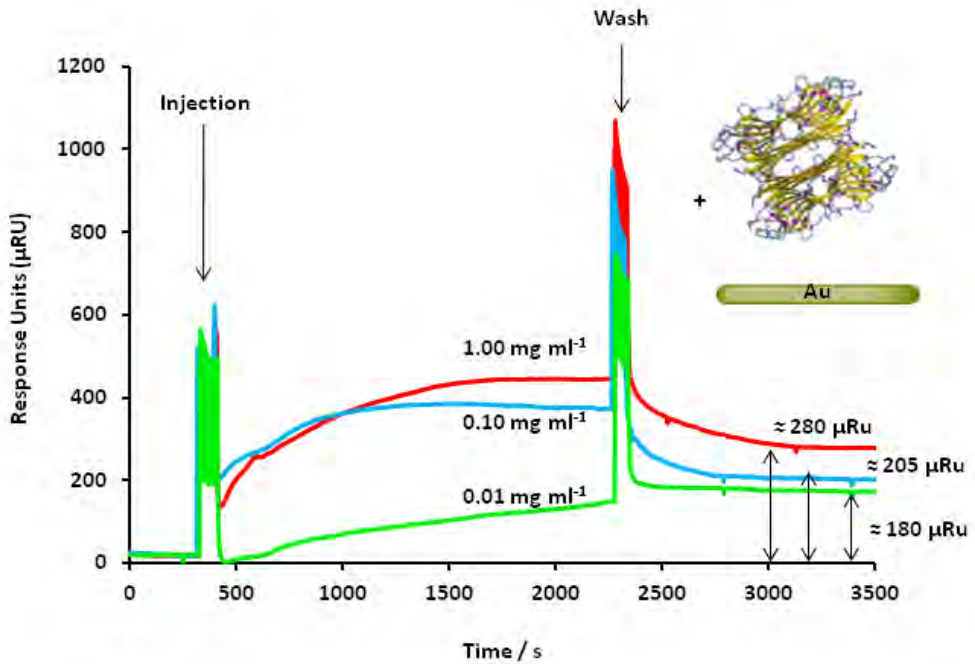

Figure 5.24 SPR sensorgram traces showing the response of bare Au to ConA injected over 1800 s at different concentrations.

After establishing a suitable concentration of ConA, the immobilisation on all ratios of GAZ1-ADM:TEGT SAMs was investigated, and are reported in **Figure 5.26**. We also investigated the immobilisation on a non-azobenzene containing glycol acid SAM functionalised with ADM (**Figure 5.25**, herein referred to as Glycol-ADMSAM) which has been previously studied in our group. The Glycol-ADM SAM gave a SPR response of ≈

2500 µRU, compared to pure GAZ1-ADM ≈ 1500 and to GAZ1-ADM:TEGT ratios 1:1 ≈ 1700 µRU, 1:10 ≈ 1000 µRU, 1:100 ≈ 500 µRU as well as pure TEGT ≈ 0 µRU.

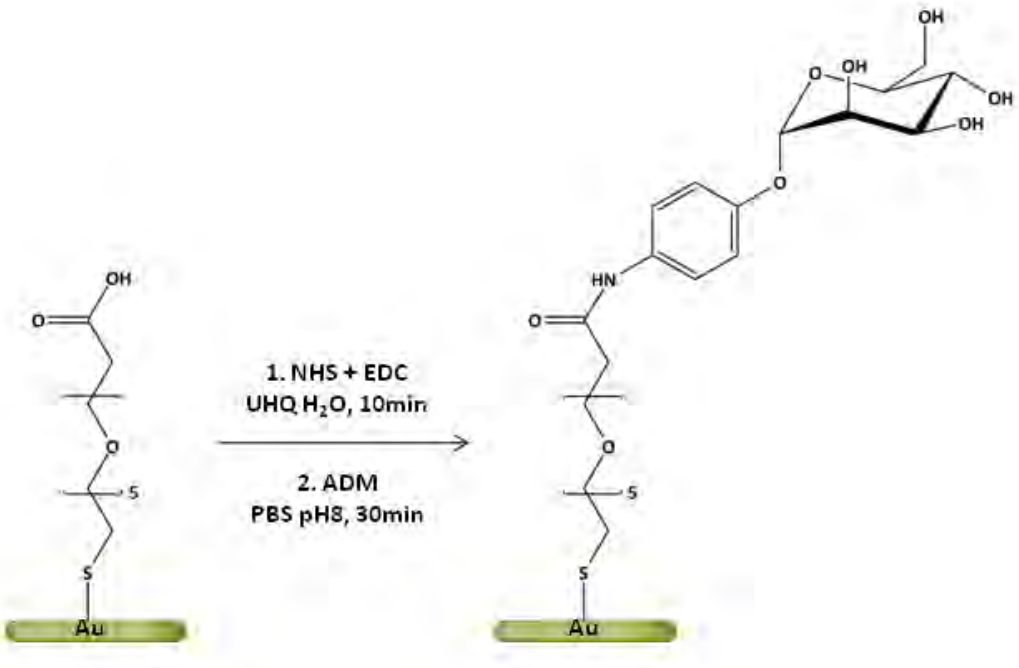

Figure 5.25 Illustration of gylcol acid SAM, functionalised with ADM in order to compare ConA immobilisation with GAZ1.

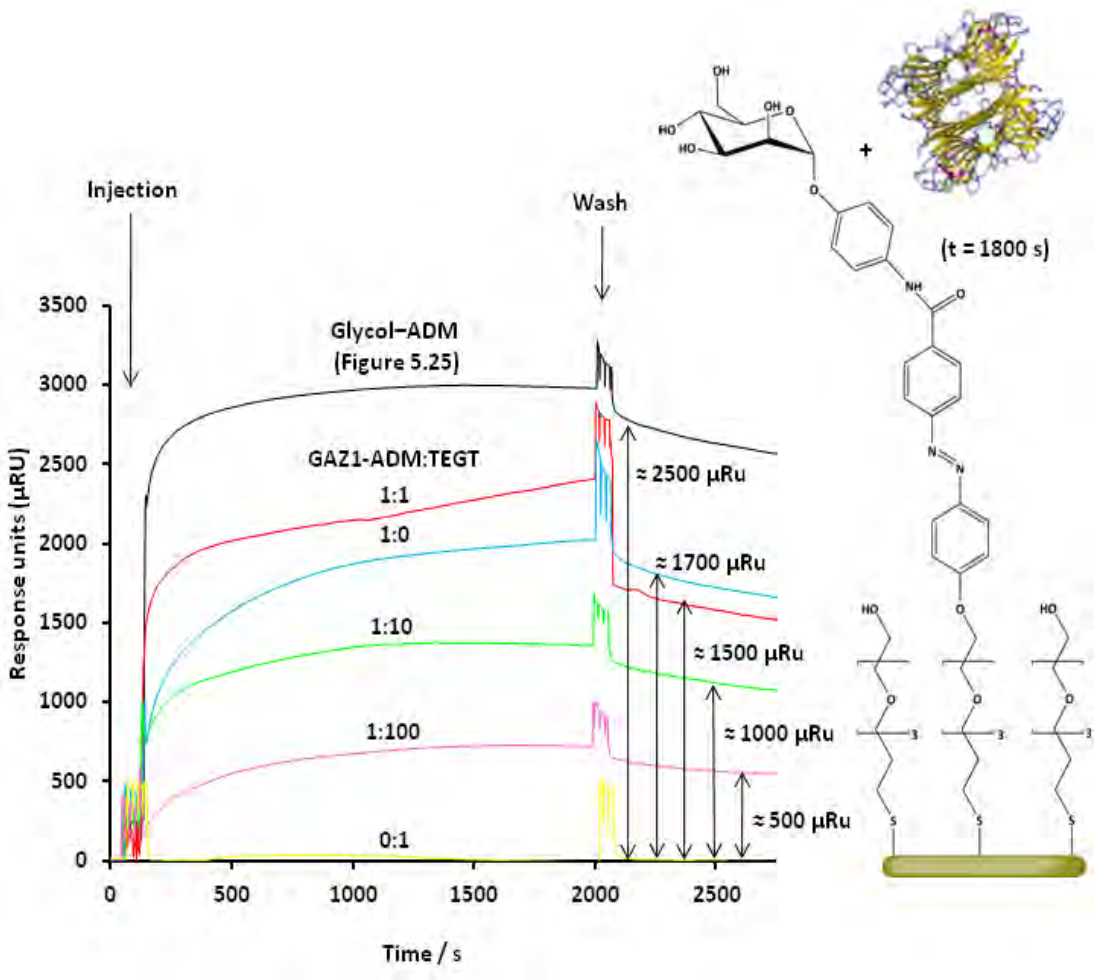

Figure 5.26 SPR sensorgram traces showing the response of different SAMs functionalised with ADM, to ConA injected over 1800 s at a concentration of 0.005 mg ml^{-1}.

The degree of binding was of the order Glycol-ADMSAM> 1:1 ≈ 1:0 > 1:10 > 1:100 > 0:1. The Glycol-ADM SAM had the highest response, this suggests that the presence of the bulky azobenzene group decreases the degree of immobilisation of ConA. Interestingly the GAZ1-ADM:TEGT 1:1 SAM has a bigger response (1700 µRU) relative to the pure GAZ1 SAM response (1500 µRU). This clearly suggests, as one might expected, that the spacing out of GAZ1 with TEGT enhances the binding, presumably due to making the ADM structure more accessible to ConA. However, at 1:10 GAZ1-ADM:TEGT ADM is

spaced out so much that the steric effect is diluted by the low surface concentration of ADM.

5.3.2.2.2 Investigation of ConA immobilisation time

Next we investigated immobilisation as a function of time. A minimisation of the immobilisation time would be advantageous as the cis azobenzene isomer or *'off'* state is unstable, decaying thermally with time.[117]

The SPR response of three pure GAZ1-ADM SAMs to ConA (0.005 mg ml^{-1}) was measured as a function of time over 3000s. The only difference being that the three SAMs were washed at different times (300, 900 and 1800 s). The results are reported in **Figure 5.27**. At 300 s the SPR response was ≈ 1000 µRU which is ≈ 33% less than the response at both 900 and 1800 s, both of which were ≈ 1500 µRU. This suggests that a time scale of 900 s the immobilisation of ConA, at a concentration of 0.005 mg ml^{-1}, has saturated the surface.

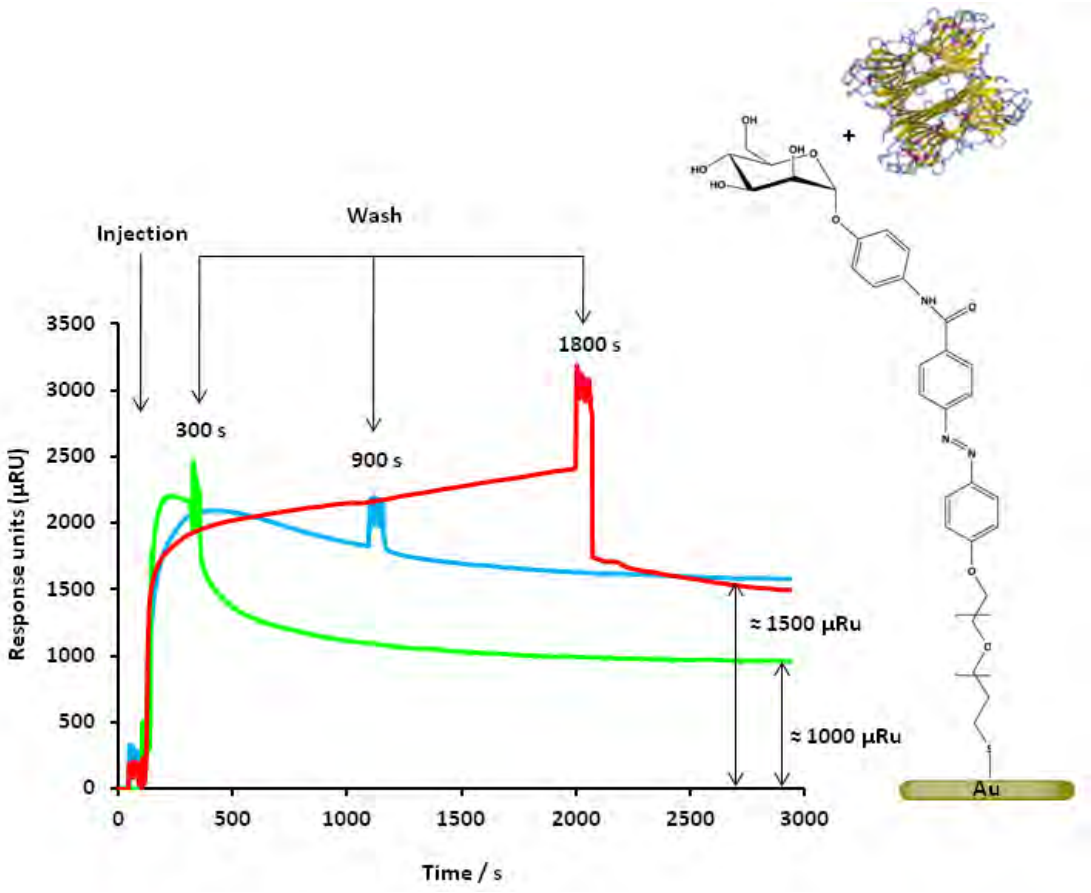

Figure 5.27 SPR sensorgram traces showing the response of GAZ1-ADM SAMs, to ConA, injected at a concentration of 0.005 mg ml^{-1} over different timescales.

5.3.2.3 Immobilisation at determined parameters

5.3.2.3.1 SPR at determined parameters

After establishing sufficient parameters of both ConA concentration (0.005 mg ml^{-1}) and its immobilisation time (900 s), we re-investigated the immobilisation of ConA on all GAZ1-ADM:TEGT ratios (**Figure 5.28**). Pure GAZ1 SAMs gave a SPR response of ≈ 1800 µRU, compared to GAZ1-ADM:TEGT ratios 1:1 ≈ 2100 µRU, 1:10 ≈ 1000 µRU, 1:100 and pure TEGT ≈ 50 µRU.

The degree of binding was of the order GAZ1-ADM:TEGT 1:1 > 1:0 > > 1:10 >> 1:100 ≈ 0:1. The order of binding was in agreement with 1800 s injections at the same ConA concentration. However, the degree of binding for the 1:100 GAZ1-ADM:TEGT SAM at 900 s was less than 1800 s, and furthermore, the degree of binding was comparable to that of pure TEGT. This result suggests that the time required for the saturation of the surface with ConA is dependent on the concentration of ADM at the surface, which is as expected.

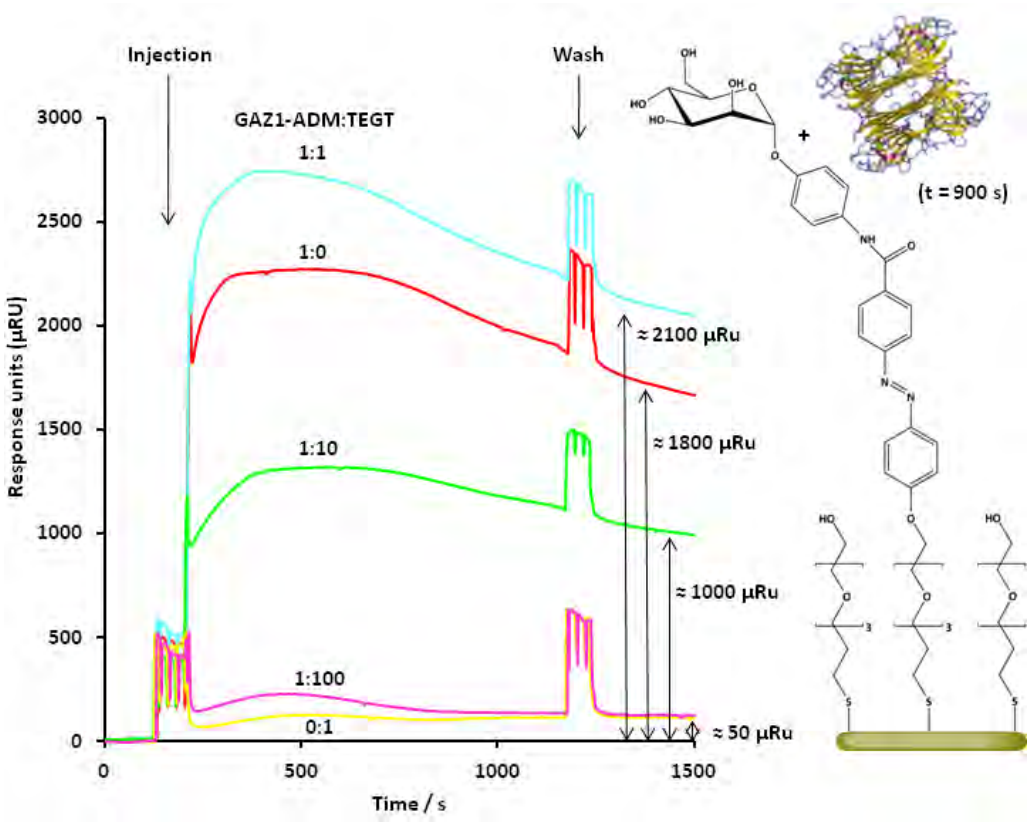

Figure 5.28 SPR sensorgram traces showing the response of all mixed SAMs, functionalised with ADM, to ConA injected over 900 s at a concentration of 0.005 mg ml^{-1}.

5.3.2.3.2 Ellipsometry at determined parameters

Ellipsometry was also employed to investigate the immobilisation of ConA on GAZ1-ADM SAMs. Using the concentration and time established by SPR, the degree of immobilisation on all ratios of GAZ1-ADM:TEGT SAMs was investigated (**Figure 5.29**).

The increases in ellipsometric thickness from the respective unfunctionalised surfaces were: Pure GAZ1 ≈ 4.5 nm, 1:1 GAZ1-ADM:TEGT ≈ 3 nm, 1:10 GAZ1-ADM:TEGT ≈ 2 nm, 1:100 GAZ1-ADM:TEGT ≈ 1 nm and pure TEGT showed no appreciable change.

The degree of immobilisation was of the order GAZ1-ADM:TEGT 1:0>1:1>1:10>1:100>0:1. Overall this order is in agreement with SPR results above (**Figure 5.28**) apart from the discrepancy between the degree of immobilisation on 1:0 and 1:1 GAZ1-ADM:TEGT SAMs.

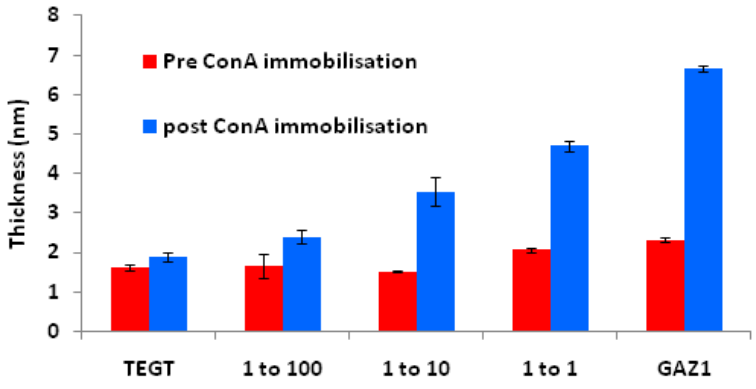

Figure 5.29 Ellipsometry of ConA immobilisation, thickness measured pre (red) and post (blue) ConA immobilisation**.**

It was envisaged that the differences in results, between the two techniques, might be due to the different protocols of ConA immobilisation. During SPR the ConA solution flows, *in-situ*, across the surface and in ellipsometry the surface is incubated with a static ConA solution, pre-analysis. Hence, the time dependence of ConA immobilisation on GAZ1 and 1:1 GAZ1-ADM:TEGT SAMs was investigated by ellipsometry and compared to SPR.

Within 300 s the increase in ellipsometric thickness relative to the non functionalised SAM was ≈ 3 nm. There was a slight increase to ≈ 4 nm by 900 s which was approximately the same for 1800 s. This result suggests that immobilisation was complete between 300 – 900 s (**Figure 5.30**). In close agreement with SPR of GAZ1 which showed immobilisation to take 900 s.

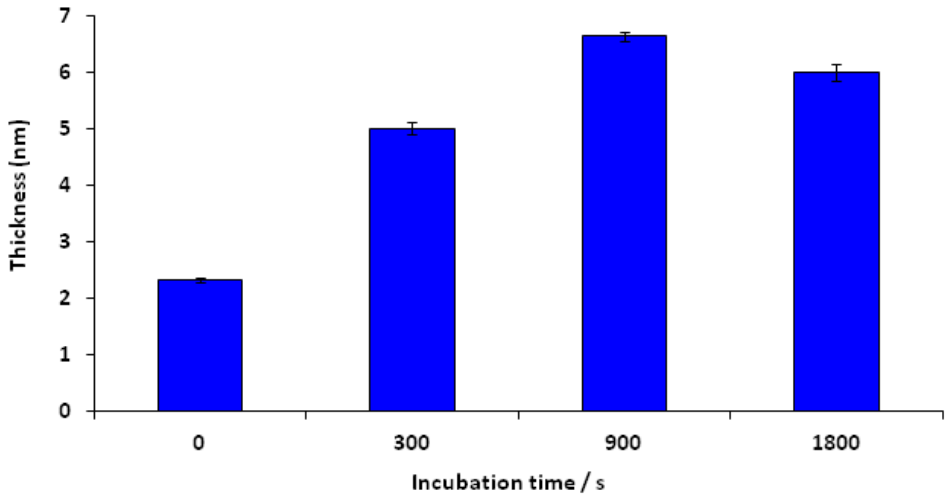

Figure 5.30 Ellipsometry results of ConA immobilisation at different incubation times on pure GAZ1 SAMs

5.3.3 Objective three - "*On/off*" switching of GAZ1-ADM SAMs

The *'on'/'off'* switchability of 1:1 GAZ1-ADM:TEGT SAMs was investigated by SPR, ellipsometry and *UV/Vis* spectroscopy. 1:1 GAZ1-ADM:TEGT SAMs were chosen as they exhibited the largest *UV/Vis* response.

SPR and ellipsometry were used to indirectly investigate *'on'/'off'* switchability with respect to ConA immobilisation. If SAMs successfully switched *'off'*, by exposure to *UV* light at 360 nm, then immobilisation of ConA would not occur. If SAMs were then successfully switched back *'on'*, by exposure to *Vis* at 440 nm, then immobilisation of ConA would occur. Three different SAMs were investigated. The first SAM was in its *'on'* state. The second SAM was switched '*off*' by exposure to 3 mins *UV* at 360 nm, pre ConA immobilisation. The third SAM was switched '*off*' and switched back '*on*' by exposure to 3 mins *UV* at 360 nm followed by 3 mins *Vis* at 440 nm, pre ConA immobilisation. An irradiation time of 3 minutes was used in accordance with GAZ1:TEGT SAM isomerisation/formation studies (section **5.3.1.3**)

5.3.3.1 SPR "*on/off*" switching studies of GAZ1-ADM SAMs

Switchability of the system was first investigated by SPR. The ADM functionalised SAM was irradiated in situ, post baseline stabilisation, using an SPR cell with a quartz window.

Exposing 1:1 GAZ1-ADM:TEGT SAMs to *UV* at 360 nm, for 3 mins (pre exposure to ConA) gave a SPR response of ≈ 300 µRU, 14 % of the non-irradiated sample which was ≈ 2100 µRU (**Figure 5.31**). Exposure of the 1:1 GAZ1-ADM:TEGT SAMs to 3 mins *UV* at 360 nm followed by 3 mins *Vis* at 400 nm, gave a SPR response of ≈ 600 µRU, which is 29% of the non-irradiated SAM.

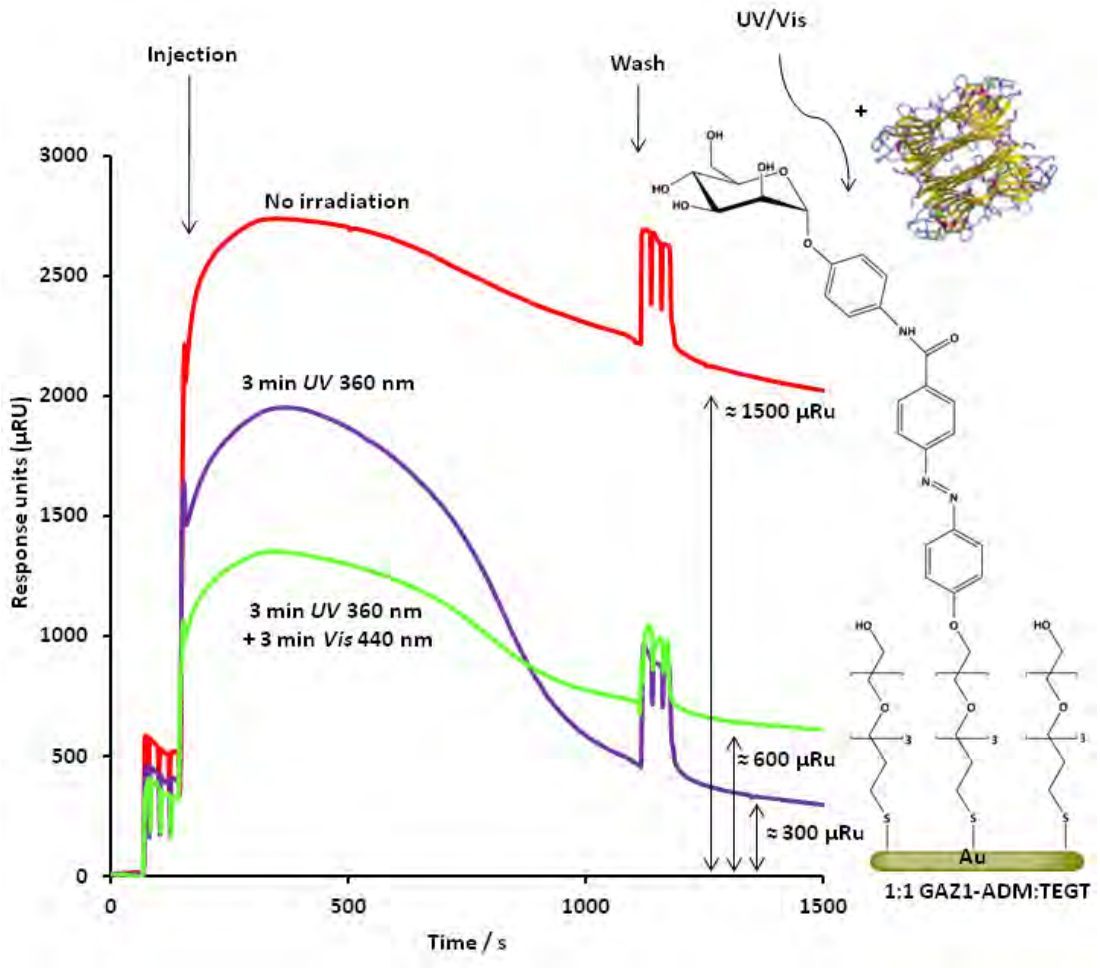

Figure 5.31 SPR sensorgram traces showing the response of 1:1 GAZ1-ADM:TEGT SAMs functionalised with ADM to ConA injected over 900 s at a concentration of 0.005 mg ml^{-1} with 3 mins *in-situ* irradiation of *UV* at 360 nm, and *UV/Vis* at 360/440 nm, compared to a non irradiated sample.

The significant reduction in the SPR response of the 1:1 GAZ1-ADM:TEGT SAM irradiated with *UV* at 360 nm, suggests that the system had been successfully switched *'off'*. Exposure of the 1:1 GAZ1-ADM:TEGT SAM to 3 mins *UV* at 360 nm followed by 3mins *Vis* at 400 nm, did not return the SPR response to its original value. However, it was double that of the 1:1 GAZ1-ADM:TEGT SAM exposed to *UV* at 360 nm only. This result suggests that the exposure to *Vis* light had not fully turned the SAM back *'on'*.

It is hypothesised that this could be due to either too short an irradiation time, photo-degradation of SAMs, or lack of space for *cis-trans* isomerisation.

If the irradiation time was too short the work done at the surface may not be sufficient to induce complete isomerisation. The irradiation time of 3 mins was chosen because it was shown to be sufficient to isomerise TAZ1 SAMs (**appendix II**) however, in hindsight it may not have been sufficient for GAZ1.

In comparison to the literature the work applied to the surface for the isomerisation of GAZ1 SAMs is intermediate of the wide spread values, used for azobenzene SAM isomerisation. Protocols for isomerisation of azobenzene SAMs within the literature vary, as do the analytical methods, surfactants, light sources and irradiation power/time. Furthermore some papers do not always provide irradiation times[134] or the lamps power ratings,[201] or give only the light sources nominal power.[134, 135] These differences make intergroup comparison difficult.

When the actual power of light at the surface, and irradiation time are given there are large differences between groups. These differences translate into massive differences in work done at the surface when inducing isomerisation, for example: W = 4.5 J,[191] W = 115.2 J,[161] W = 99 J.[203] The work done (W) at our surface is intermittent of these values: W_{UV} = 50.4 J and W_{Vis} = 37.8 J. The work done at our surface is much greater than the first two examples, but less than the last two. Considering this and the fact that *UV/Vis* of our (dry) unfunctionalised SAM was reversible, we conclude that the lack of *cis-trans* isomerisation is unlikely to be due to too short an irradiation time. However, in

order to prove that we used a sufficient irradiation time further investigation is required.

Thiol SAMs have been shown to undergo photooxidation upon exposure to UV light at 190nm.[204] It is speculated that *UV* light causes hot spots in the gold substrate, thus facilitating photo-oxidation. However, the work done at the surface is 240 J which is nearly five times greater than the work done at our surface. But photo-degradation of azobenzene itself, within SAMs has been speculated by SPR.[136] The speculation was used to interpret the diminishing change in reflectance between the *trans* and *cis* isomers upon repeated exposure to *UV* and *Vis*. Reversible isomerisation was observed before degradation started, which is not the case for the system investigated here. Furthermore, comparison is hard, because the paper gives only the nominal power of the lamps used and not the actual power of light at the surface. Considering that not only was reversible isomerisation observed before degradation, but also, that the *UV/Vis* absorption spectra of the (dry) 1:1 GAZ1:TEGT SAM was reversible, we conclude that although degradation maybe occurring, it does not fully explain our results which seem more attributable to lack of space. However, to completely rule out *UV* induced degradation further investigation is required.

When lack of space for the *cis* – *trans* isomerisation is concerned, two main mechanisms, rotation and inversion, have been shown to operate. The different mechanisms require different free volumes. Rotation requires a free volume of 0.28 nm^3 and inversion requires a free volume of 0.12 nm^3.[119] The actual mechanism is dependent on substitution pattern and the nature of substitutions about the benzene rings. However, without investigation we cannot stipulate which mechanisms operate. Furthermore, the mechanism of the *trans* - *cis* isomerisation maybe different from the *cis* – *trans* as seen in non-functionalised azobenzene. If the two mechanisms are

different the above result might suggest that isomerisation of the cis isomer maybe inhibited by a lack of space. This hypothesis seems to be the most likely.

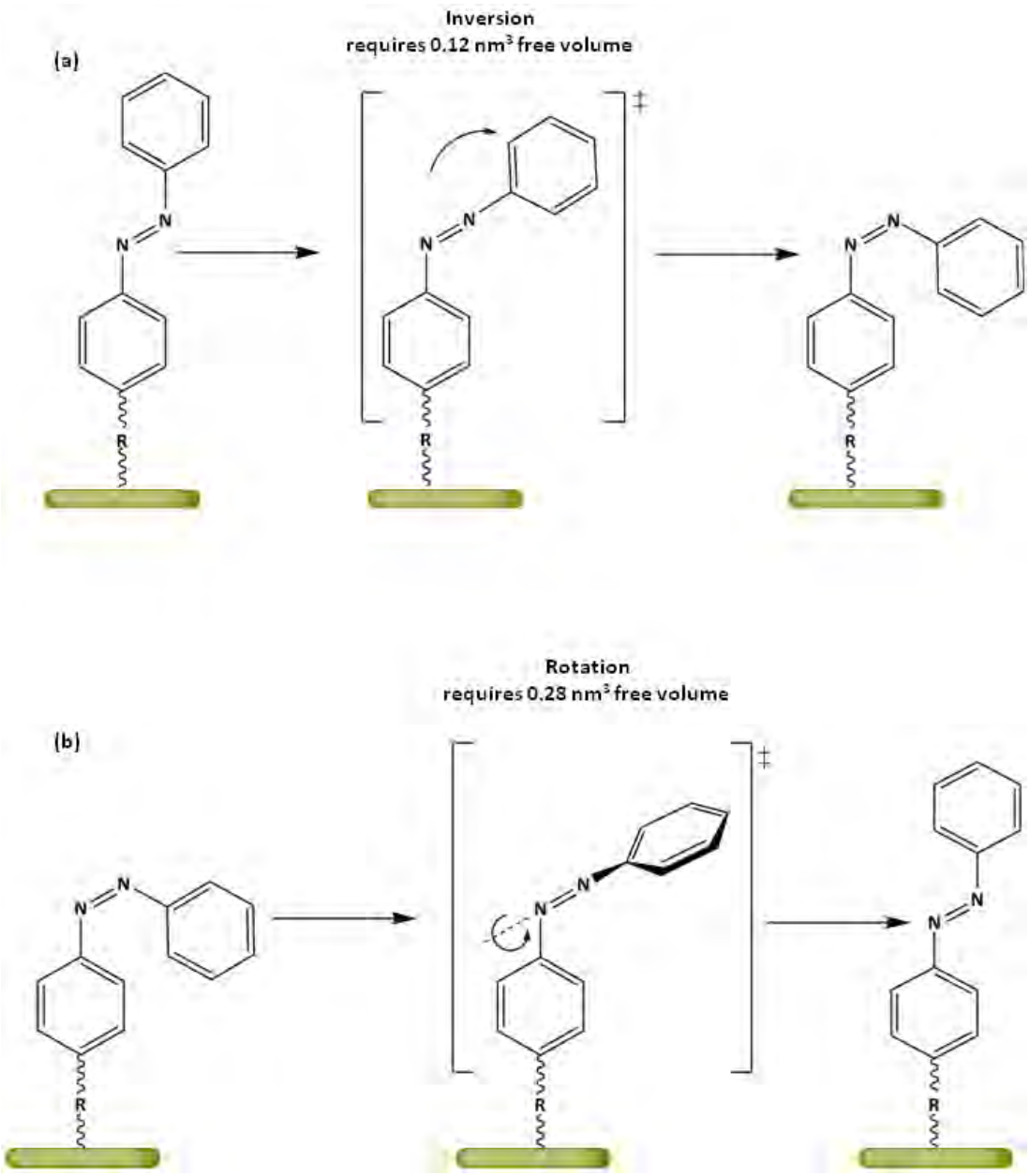

Figure 5.14 Isomerisation is known to proceed through two main mechanisms, rotation and inversion, both of which require different free volumes. Considering *UV/Vis* results we propose that the (a) *trans-cis* isomerisation occurs through inversion while (b) *cis - trans* isomerisation occurs through rotation.

5.3.3.2 Ellipsometry "*ON/OFF*" switching studies of GAZ1-ADM SAMs

Switchability of the system was investigated by ellipsometry. Again an irradiation time of 3 mins was used. GAZ1-ADM:TEGT samples were isomerised pre immersion in the ConA solution. Both isomerisation and immobilisation was performed in the dark, in order to prevent *Vis* induced relaxation of the *cis* isomer. The results are reported in **Figure 5.32**.

The non irradiated sample had an ellipsometric thickness of ≈ 5 nm and the irradiated sample ≈ 4 nm. This small difference suggests that irradiation of the respective surfaces pre-incubation was insufficient to completely turn SAMs *'off'*.

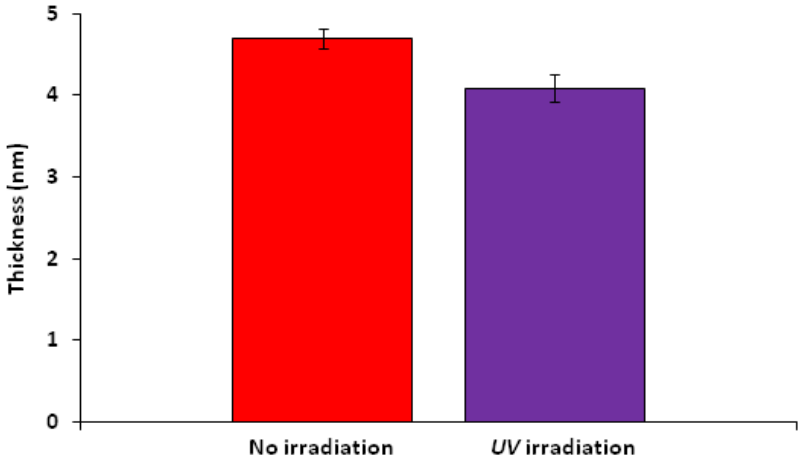

Figure 5.32 Ellipsometry of 1:1 GAZ1-ADM:TEGT SAMs comparing the SAM irradiated with *UV* to a non-irradiated sample.

There is a difference between these results and that of SPR, which showed the majority of the SAM to be switched '*off*'. It is believed that this difference could be attributed to the differences in the ConA immobilisation protocols between the two techniques, as discussed in section **5.3.2.2**. The result of these differences being that the

immobilisation of ConA is promoted through the static solution immobilisation protocol used pre-ellipsometric analysis.

Hence the immobilisation of ConA on 1:1 GAZ1-ADM SAMs was further investigated as a function of time, using ellipsometry. The results are reported in **Figure 5.33**. ConA immobilisation was shown to be complete within 300 s, with an increase in ellipsometric thickness, relative to the non functionalised SAM, of ≈ 3 nm. This result suggests that the immobilisation time of 900 s is perhaps too long when analysing SAMs by ellipsometry.

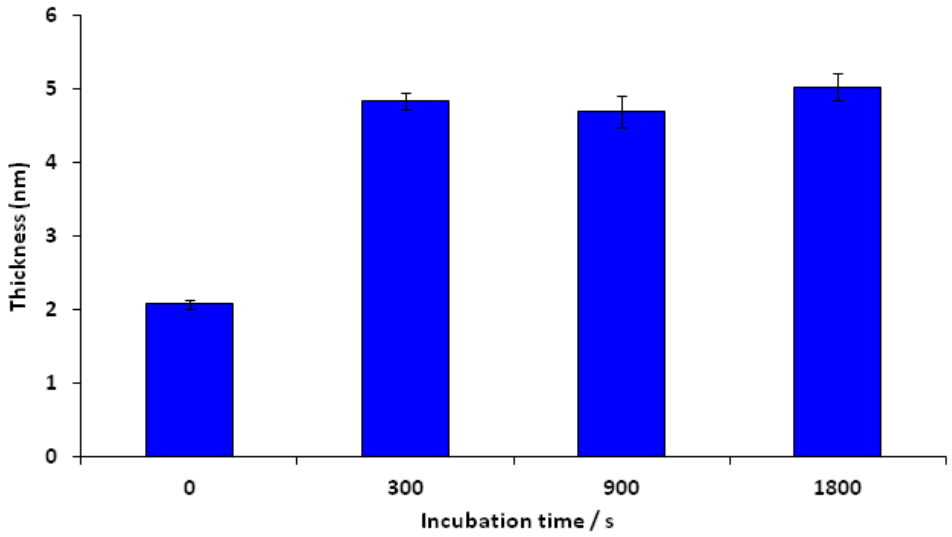

Figure 5.33 Ellipsometry results of ConA immobilisation at different incubation times 1:1 GAZ1-ADM SAMs.

5.3.3.3 *UV/Vis* "*ON/OFF*" switching studies of GAZ1-ADM SAMs

UV/VIS absorption spectroscopy was employed in order to further investigate the switching behaviour, of the GAZ1-ADM:TEGT 1:1 SAMs. A second SAM, the Glycol-ADM SAM, which conatins no azobenzene was used as a control.

λ_{max} of the 1:1 GAZ1-ADM:TEGT SAM was found to be hypsochromically shifted to ≈ 270 nm (**Figure 5.34a**). Exposure of the SAM to *UV* at 360 nm, caused a depletion of the peak as would be expected for *UV* induced isomerisation. However, irradiation with *Vis* at 440 nm had little effect on the peak.

λ_{max} of the non-azobenzene Glycol-ADM SAM also occurred at 270 nm, but at a relatively lower absorption (**Figure 5.34b**). Irradiation with *UV* at 360 nm increased the absorption of λ_{max} while irradiation with *Vis* at 440 nm resulted in no further change. This response is opposite to the azobenzene containing SAM and is presumably due to the aromatic nature of ADM.

UV/Vis absorption spectra of the Glycol-ADMSAM confirms that the response of 1:1 GAZ1-ADM:TEGT SAMs is attributable to azobenzene and not ADM itself. This lack of reversible isomerisation is in agreement with SPR studies.

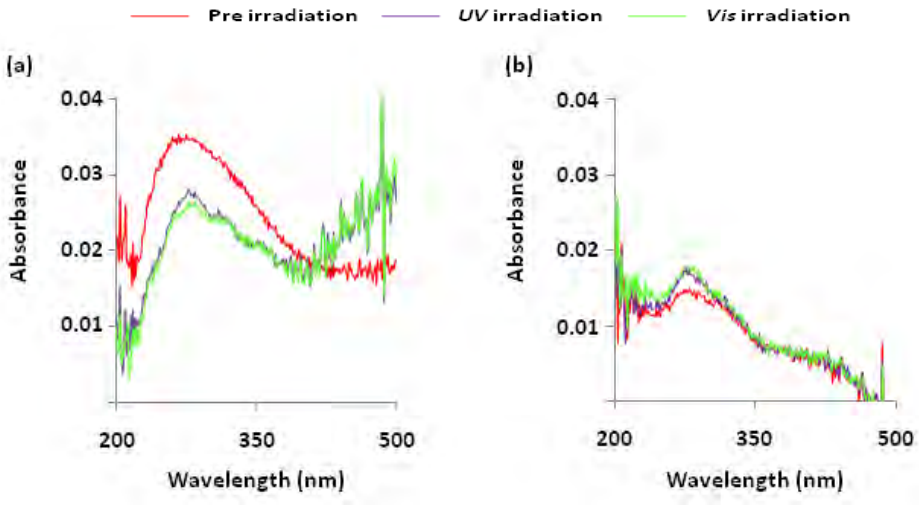

Figure 5.34 *UV/Vis* absorption spectra of SAMs (a) 1:1 GAZ1-ADM:TEGT SAM (b) Glycol acid-ADM SAM. Three different absorption spectra of both SAMs were recorded (1) pre irradiation (2) post irradiation with *UV* at 360 nm (3) post irradiation with *Vis* at 440 nm, which was subsequent to *UV* irradiation.

5.4 Conclusions

The formation of mixed SAMs of GAZ1:TEGT was confirmed by contact angle and ellipsometry. Formation required the presence of a small amount of TFA in order to circumvent bi-layer formation. For pure GAZ1 SAMs formation was complete within 0.5 hr, for pure TEGT SAMs 1 hr and for mixed SAMs 2 hr. However, UV/Vis spectra of 1:1 GAZ1:TEGT SAMs suggests further ordering occurs.

The optical activity of mixed SAMs of GAZ1:TEGT at ratios of 1:0, 1:1, 1:100 formed over 24 hours was determined by surface *UV/Vis* spectroscopy. 1:1 SAMs exhibited the best optical activity.

Next the optical activity of 1:1 SAMs was measured as a function of time over 24 hr. At low formation times (1-6 hr) isomerisation of GAZ1 SAMs were seen to be inhibited by both H-aggregation, as indicated by a hyposchrmoic shift in λ_{max} and spatial inhibition, as indicated by the lack of reversible isomerisation. This shift in λ_{max} and increasing *UV/Vis* activity over 24 hours indicates that post SAM formation further ordering occurs which increases optical activity of SAMs.

The immobilisation of ConA to mixed SAMs of GAZ1-ADM:TEGT was investigated by SPR and ellipsometry. The immobilisation of ConA requires the functionalisation of the acid terminated GAZ1 with ADM. ADM functionalisation of GAZ1 followed a well established protocol. No protocol for the immobilisation of ConA could be found and so a protocol was devised and optimised, with respect to concentration and time. Optimal concentration of ConA was found to be 0.005 mg ml^{-1} and the immobilisation was seen to be complete within 15 minutes. The degree of ConA binding decreased in the order GAZ1-ADM:TEGT 1:1>1:0>1:10>1:100>0:1 as shown by SPR. Ellispometry showed the order to be GAZ1-ADM:TEGT 1:0>1:1>1:10>1:100>0:1 with the order of 1:0 and 1:1 being the opposite way around. We have concluded that this observation is due to the fundamental, and unavoidable differences, of the ConA immobilisation protocols used for each technique.

The *'on'*/*'off'* switchability of 1:1 GAZ1-ADM:TEGT SAMs was investigated by SPR and ellipsometry. SPR required the *in-situ* switching of SAMs through the employment of a cell with a quartz window. 1:1 GAZ1-ADM:TEGT SAMs could be switched off through exposure to *UV* at 360 nm for 3 minutes prior to injection with a reduction in SPR response. However, exposure to *Vis* at 440 nm for 3 mins was insufficient to completely turn the SAMs back *'on'*. The optical activity of GAZ1-ADM:TEGT SAMs, measured by UV/Vis spectroscopy, also showed non-reversible isomerisation. It is concluded that lack

of reversible isomerisation is due to spatial constraints which inhibit the more spatially demanding cis – trans isomerisation.

In summary we have developed a photo-switchable SAM for the study of carbohydrate-lectin interactions, which could also be used for other bio-molecular interactions.

5.5 Future Work

It would be desirable to further investigate the ratios of GAZ1-ADM:TEGT SAM, in particular those between 1:1 – 1:10. Furthermore, it would also be desirable to further investigate the immobilisation time and concentration of ConA. Further investigation of GAZ1-ADM:TEGT SAM ratio, as well as ConA immobilisation time and concentration, would allow the establishment of their respective optimum values.

Future work also needs to invetigate if the lack of reversible isomerisation is due to lack of free volume, rather than degradation or too short an irradiation time. Furthermore, investigation of the switchability of other GAZ1-ADM:TEGT SAM ratios, in particular those between 1:1 – 1:10, need to be investigated and may show reversible isomerisation, due to an increase in free volume coinciding with a decrease in GAZ1 concentration.

Finally if a ratio with reversibly switching is not found then a new surfactant needs to be investigated. This new surfactant would require a head group which creates sufficient free volume, for isomerisation, within SAMs. This could be done by combining this system with the surfactant TAZ1 used in chapter 4 (**Figure 5.32**) or one of the other

novel surfactants described in chapter 1, which were shown to make reversibly switchable SAMs.

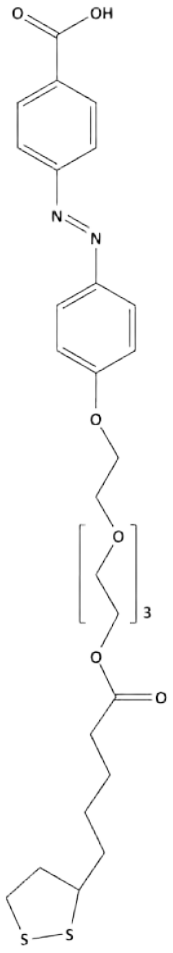

Figure 5.32 Possible surfactant to be used in future work.

6.0 Experimental

This chapter contains details on the general experimental protocols and analytical techniques used in this research. It is split into four sections. Firstly, molecular synthesis is described. Secondly, the specifications of equipment used in molecular characterisation are stated. Thirdly, SAM preparation protocols are described. Finally, the specifications of equipment used in SAM analysis are stated and the protocols described.

6.1 Molecular synthesis

The commercially available chemicals were purchased from either Sigma Aldrich or Fisher Scientific.

Thin-layer chromatography (TLC) was carried out on an aluminium plates coated with silica gel 60 F254 (Merck 5554). The TLC plates were either air-dried and analysed under a short wave *UV* lamp (254 nm) or developed in either permanganate solution or Jones's reagent and heat-dried. Column chromatographic separations were preformed silica gel 120 (ICN Chrom 32-63, 60 Å).

6.1.1 Synthesis of TAZ1, 4 -tert-butyl-ester, 4' thioctic acid, azobenzene

6.1.1.1 Compound 1

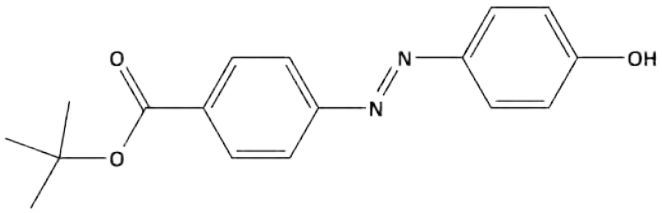

A solution of $NaNO_2$ (1.22 g, 17.68 mmol) in H_2O (3.4 ml) was added dropwise to a solution of 4-Aminobenzoic acid tert-butyl ester (3.40 g, 17.62 mmol) in 1 M HCl (10 ml) at 0 ^{0}C. The subsequent diazotised solution was added dropwise to a chilled solution of phenol (1.66 g, 17.66 mmol) and KOH (1.97 g, 35.18 mmol) in MeOH (21 ml). The resultant reaction mixture was further stirred for 4 h. The reddish/orange precipitate was collected through suction filtration to yield a reddish/orange solid (4.22 g, 85%).

^{1}H NMR (300 MHz, $CDCl_3$, Me_4Si, 25 ^{o}C) δ_H ppm 8.11 (d, 1H, *J* = 8.45 Hz, Ar*H*), 7.90 (d, 1H, *J* = 8.75 Hz, Ar*H*), 7.88 (d, 1H, *J* = 8.45 Hz, Ar*H*), 6.97 (d, 1H, *J* = 8.75 Hz, Ar*H*), 1.64 (s, 9H, ^{t}*Bu*); ^{13}C NMR (75 MHz, $CDCl_3$, Me_4Si, 25 ^{o}C) δ_C ppm 164.2, 157.1, 151.8, 144.0, 128.9, 124.0, 120.7, 114.5, 80.4, 26.7; m/z (ESMS): 321 ($[M + Na]^+$, 100%); m/z (HRMS): found 321.1217. Calc. Mass for $C_{17}H_{18}N_2O_3Na$: 321.1215.

6.1.1.2 Compound TAZ1

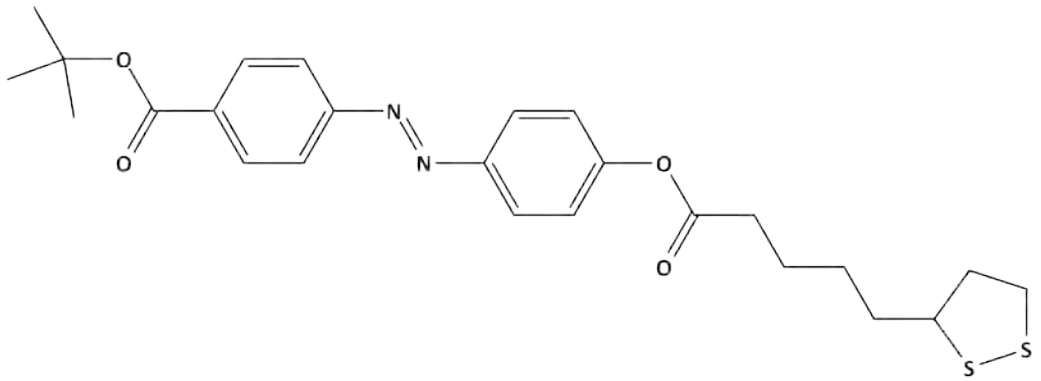

To a stirred solution of thioctic acid (2 g, 9.6 mM) and DMAP (0.06g, 0.48 mM) in anhydrous DCM, at room temperature AZ1 (0.72 g, 2.4 mM) was added. The reaction mixture was cooled to 0°C in an ice bath and DCC (1 g, 4.8 mM) added and stirred for 10 mins. The ice bath was then removed and the reaction mixture brought to room temperature and stirred overnight. The crude reaction mixture was washed with HCl (1M) (1 x 100 ml) followed by 5% $NaHCO_3$ (1 x 100 ml) and finally with water (1 x 100 ml). The organic layer was then dried ($MgSO_4$) filtered and concentrated in *vacuo*. The crude product was purified by column chromatography (1 % MeOH in DCM) to yield a orange solid (0.70 g, 60%).

Elemental analysis found: C, 61.88 %; H, 5.97 %; N, 5.52 %. Calc. for $C_{25}H_{30}N_2O_4S_2$: C, 61.7 %; H, 6.2 %; N, 5.8 %. ^{1}H NMR (300 MHz, $CDCl_3$): δH 8.41 (d, *J*= 8.6 Hz, 2H, H-?), 8.27 (d, *J*= 8.6 Hz, 2H, H-?), 8.19 (d, *J*= 8.6 Hz, 2H, H-?), 7.54 (d, *J*= 8.6 Hz, 2H, H-?), 3.89 (m, 1H, H-17), 3.45 (m, 2H, H-19), 2.90 (t, 2H, H-13), 2.05 (m, 4H, H-14 and H-16), 1.90 (s, 9H, H-1);^{13}C NMR (75 MHz, $CDCl_3$): δC 174.0, 156.7, 135.8, 134.5, 152.6, 132.3, 126.2, 124.4, 124.2, 58.1, 42.1, 40.4, 36.5, 36.0, 30.6, 30.1, 26.4; m/z (Es) 509.2 ([M + Na^+]$^+$, 100%).

6.1.2 Synthesis of thioctic methoxy-ester (TME)

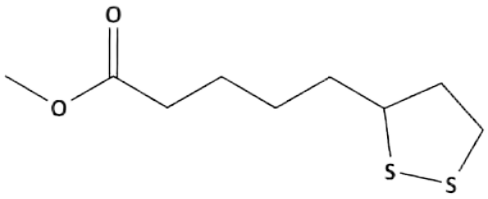

Synthesis followed the same general procedure as TAZ1 using methanol (0.08g, 2.4 mM) instead of AZ1. The crude product was purified by HPLC to yield a colourless solid (70 %).

Elemental analysis found: C, 49.55 %; H, 7.30 %. Calc. for $C_9H_{16}O_2S_2$: C, 49.05 %; H, 7.32 %. ^{1}H NMR (300 MHz, $CDCl_3$): δH 3.69 (s, 3H, H-1), 3.58 (m, 1H, H-7), 3.16 (m, 2H, H-9), 2.34 (t, *J* = 7.4 Hz, 2H, H-3), 1.94 (m, 1H, H-7), 1.71 (m, 5H, H-7 + H-4), 1.49 (qu, *J* = 8.0 Hz 2H, H-5); ^{13}C NMR (75 MHz, $CDCl_3$): δC 173.8, 56.3, 51.4, 40.2, 8.5, 34.5, 33.8, 28.7, 24.6 ; m/z (Es) 243.4 ($[M + Na^+]^+$, 100%) 259.4 ($[M + K^+]^+$, 10%).

6.1.3 Synthesis of SAZ1, 4 -tert-butyl-ester, 4’ oxyhexyl-6-thiol, azobenzene

6.1.3.1 Compound 2

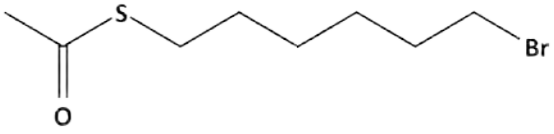

A solution of 6-bromohexene (2.00 g, 12.27 mmol), thioacetic acid (1.87 g, 24.61 mmol) and AIBN (catalytic amount) in PhMe (20 ml) was refluxed for 2 h. The resultant reaction mixture was allowed to cool to room temperature and saturated $NaHCO_3$ aqueous solution was added and the organic layer was extracted with DCM (3 x 20 ml). The

combined organic layers were dried ($MgSO_4$), filtered and concentrated *in vacuo*. The crude product was purified by column chromatography (eluent: hexane) to yield a colourless oil (2.00 g, 68 %).

^{1}H NMR (300 MHz, $CDCl_3$, Me_4Si, 25 ^oC) δ_H ppm 3.34 (t, 2H, *J* = 6.14 Hz, -*CH*$_2$Br), 2.80 (t, 2H, *J* = 7.56 Hz, -*CH*$_2$SAc), 2.26 (s, 3H, -S*Ac*), 1.83-1.75 (m, 2H, -C*H*$_2$CH$_2$Br), 1.58-1.48 (m, 2H, -*CH*$_2$CH$_2$SAc), 1.44-1.29 ((m, 4H, -*C*$_2$*H*$_4$C$_2$H$_4$SAc); ^{13}C NMR (75 MHz, $CDCl_3$, Me_4Si, 25 ^oC) δ_C ppm 195.9, 33.7, 32.6, 30.6, 29.3, 28.9, 27.9, 27.6; m/z (ESMS): 261 ([M + Na]$^+$, 100%), 263 ([M + Na]$^+$, 100%); m/z (HRMS): found 260.9923. Calc. Mass for $C_8H_{15}OSBrNa$: 260.9925.

6.1.3.2 Compound 3

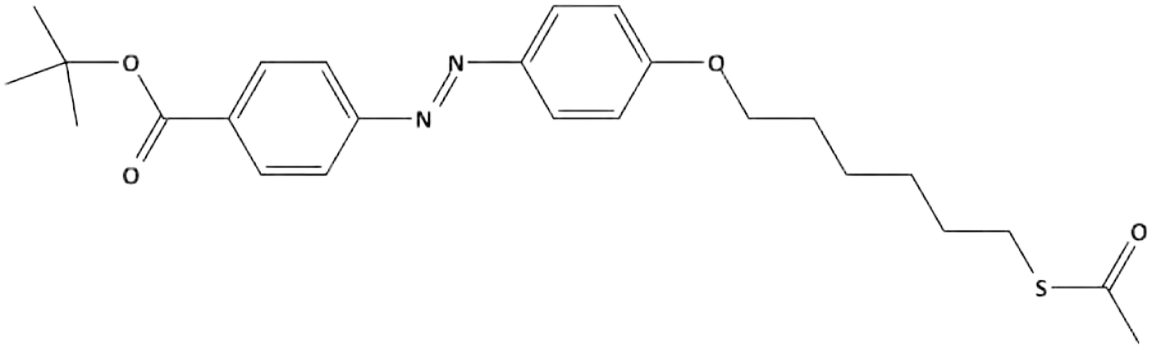

A slurry of **1** (1.00 g, 3.34 mmol), **2** (1.20 g, 5.02 mmol) and K_2CO_3 (0.92 g, 6.67 mmol) in acetone (50 ml) was refluxed for 16 h. The resultant reaction mixture was allowed to cool to room temperature and K_2CO_3 was filtered off and the solvent removed *in vacuo*. The crude solid was adsorbed onto silica and purified by column chromatography (gradient elution; 0 to 20 % EtOAc in hexane, increase in increments of 10 % after 100 ml of eluent) to yield a reddish orange solid (1.00 g, 66%).

^{1}H NMR (300 MHz, $CDCl_3$, Me_4Si, 25 ^{o}C) δ_H ppm 8.04 (d, 2H, *J* = 8.76 Hz, Ar*H*), 7.87 (d, 2H, *J* = 8.99 Hz, Ar*H*), 7.81 (d, 2H, *J* = 8.76 Hz, Ar*H*), 6.94 (d, 2H, *J* = 8.99 Hz, Ar*H*), 3.98 (t, 2H, *J* = 6.69 Hz, -*CH*$_2$Br), 2.83 (t, 2H, *J* = 7.86 Hz, -*CH*$_2$SAc), 2.26 (s, 3H, -S*Ac*), 1.81-1.69 (m, 2H, -*CH*$_2$CH$_2$Br), 1.55 (s, 9H, ^{t}*Bu*), 1.50-1.34 (m, 6H, -*C*$_3$*H*$_6$CH$_2$SAc); ^{13}C NMR (75 MHz, $CDCl_3$, Me_4Si, 25 ^{o}C) δ_C ppm 165.3, 162.2, 155.1, 146.9, 133.1, 130.4, 125.1, 122.2, 114.8, 81.3, 68.2, 30.7, 29.5, 29.0, 28.5, 28.2, 25.6; m/z (ESMS): 479 ([M + Na]$^{+}$, 100%); m/z (HRMS): found 479.1972. Calc. Mass for $C_{25}H_{32}N_2O_4SNa$: 479.1980.

6.1.3.3 Compound SAZ1

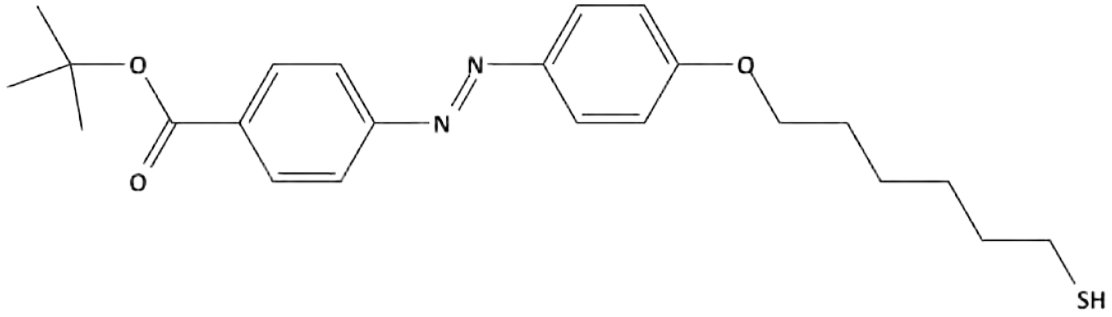

A solution of **3** (1.00 g, 2.19 mmol) in 0.1 M HCl methanoic solution (100 ml) was refluxed for 4 h under N_2 atmosphere. The resultant reaction mixture was concentrated *in vacuo* and the crude solid was adsorbed onto silica and purified by column chromatography (gradient elution; 0 to 20 % EtOAc in hexane, increase in increments of 10 % after 100 ml of eluent). The solvent was removed and the resultant solid was recrystallised from EtOH to yield reddish orange solid (0.65 g, 71 %).

Elemental analysis found: C, 66.35 %; H, 7.31 %; N, 6.77 %. Calc. for $C_{23}H_{30}N_2O_3S$: C, 66.64 %; H, 7.29 %; N, 6.79 %; ^{1}H NMR (300 MHz, $CDCl_3$, Me_4Si, 25 ^{o}C) δ_H ppm 8.04 (d, 2H, *J* = 8.07 Hz, Ar*H*), 7.87 (d, 2H, *J* = 9.00 Hz, Ar*H*), 7.81 (d, 2H, *J* = 8.07 Hz, Ar*H*), 6.94 (d, 2H, *J* = 9.00 Hz, Ar*H*), 3.98 (t, 2H, *J* = 6.42 Hz, -*CH*$_2$Br), 2.80 (q, 2H, *J* = 7.49 Hz, -*CH*$_2$SH),

1.82-1.73 (m, 2H, -*CH*$_2$CH$_2$Br), 1.55 (s, 9H, ^{t}*Bu*), 1.55-1.48 (m, 2H, -*CH*$_2$CH$_2$SAc), 1.44-1.42 (m, 4H, -*C*$_2$*H*$_4$C$_2$H$_4$SH), 1.28 (t, 2H, *J* = 7.49 Hz, -CH$_2$*SH*); ^{13}C NMR (75 MHz, $CDCl_3$, Me_4Si, 25 ^oC) δ_C ppm 165.3, 162.2, 155.1, 146.9, 133.1, 130.4, 125.1, 122.2, 114.8, 81.3, 68.2, 33.9, 29.1, 28.2, 28.1, 25.5, 24.5; m/z (ESMS): 415 ([M + H]$^+$, 100%); m/z (HRMS): found 415.2048. Calc. Mass for $C_{23}H_{31}N_2O_3S$ 415.2055.

6.1.4 Synthesis of TEGT, tri-ethylene glycol thiol

6.1.4.1 Compound 4

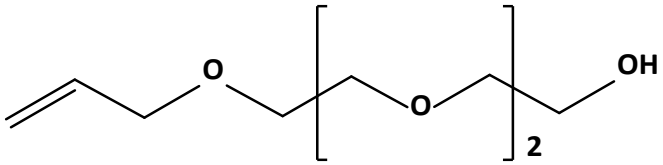

A solution of triethylene glycol (24.17 g, 16.11 mmol), 50 % NaOH (0.64 ml) and ally bromide (1.95 g, 16.11 mmol) was refluxed overnight. The organic layer was extracted with EtOAc (3 x 100 ml), dried ($MgSO_4$), filtered and concentrated *in vacuo*. The crude orange oil was purified by column chromatography (gradient elution; from 0 to 75 % EtOAc in hexane, increase in increments of 25 % per 100 ml of eluent) to yield a pale yellow oil (2.06 g, 60 %).

^{1}H NMR (300 MHz, $CDCl_3$, Me_4Si, 25 ^oC) δ_H ppm 6.01-5.84 (m, 1H, -CH$_2$*CH*CH$_2$), 5.33-5.15 (m, 2H, -CH$_2$CH*CH$_2$*), 4.02 (d, *J* = 5.67 Hz, 2H, -*CH*$_2$CHCH$_2$), 3.76-3.58 (m, 12H, -O*CH*$_2$*CH*$_2$O-), 2.56 (s, 1H, -*OH*); ^{13}C NMR (75 MHz; $CDCl_3$; Me_4Si, 25 ^oC) δ_C ppm 134.7, 117.2, 72.5, 72.3, 70.6, 70.4, 69.4, 61.8; (ESMS): 213 ([M + Na]$^+$, 100%); HRMS: found 213.1098. Calc. mass for $C_9H_{18}O_4Na$: 213.1103.

6.1.4.2 Compound 5

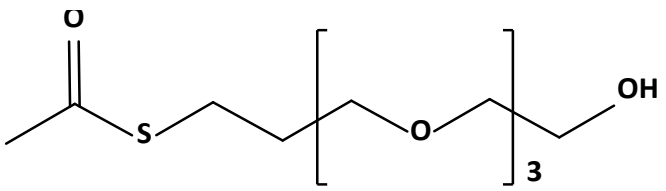

A solution of **4** (2.00 g, 11.43 mmol), thioacetic acid (1.30 g, 17.11 mmol) and AIBN (catalytic amount) in PhMe (10 ml) was refluxed for 2 h. Saturated $NaHCO_3$ (25 ml) was added to the reaction mixrture and the organic layer was extracted with DCM (3 x 25 ml). The combined organic layers were dried ($MgSO_4$), filtered and concentrated *in vacuo*. The crude oil was purified by column chromatography (gradient elution; from 0 to 75 % EtOAc in hexane, increase in increments of 25 % per 100 ml of eluent) to yield a colourless oil (1.84 g, 61 %).

^{1}H NMR (300 MHz, $CDCl_3$, Me_4Si, 25 ^{o}C) δ_H ppm 3.74-3.55 (m, 12H, -O*CH*$_2$*CH*$_2$O-), 3.50 (t, *J* = 6.20 Hz, 2H, -O*CH*$_2$(CH$_2$)$_2$SAc), 2.94 (t, *J* = 7.20 Hz, 2H, -O(CH$_2$)$_2$*CH*$_2$SAc), 2.31 (s, 3H, -*SAc*), 1.89-1.80 (m, 2H, -OCH$_2$*CH*$_2$CH$_2$SAc); ^{13}C NMR (75 MHz; $CDCl_3$; Me_4Si, 25 ^{o}C) δ_C ppm 196.0, 72.2, 70.3, 70.2, 70.0, 69.8, 68.8, 61.3, 30.2, 29.2, 25.6; (ESMS): 289 ([M + Na]$^+$, 100%); HRMS: found 289.1082. Calc. mass for $C_{11}H_{22}O_5SNa$: 289.1086.

6.1.4.3 Compound TEGT

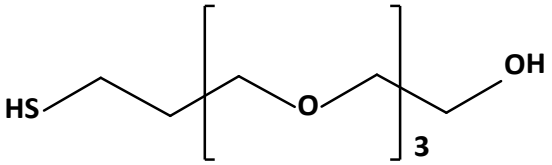

A solution of **5** (1.35 g, 5.40 mmol) in 0.1 M HCl (1.00 ml) made up in MeOH (100 ml) was heated under reflux under N2 atmosphere for 4 h. The reaction was concentrated *in vacuo*. The crude product was purified by column chromatography on silica gel (eluent: EtOAc) to yield a pale yellow oil (1.03 g, 90%).

Elemental analysis found: C, 47.89%; H, 9.23%. Calc. for C9H20O4S: C, 48.18%; H, 8.99%; vmax/cm-1 (film): 3454brm, 2871m; ^{1}H NMR (300 MHz; CDCl3; Me_4Si) δH 3.80-3.56 (m, 14H, -O*CH2CH2*O-, -O*CH2*(CH2)2SH), 2.65 (q, *J* = 7.51 Hz, 2H, - (CH2)2*CH2*SH), 1.92-1.82 (m, 2H, -OCH2*CH2*CH2SH), 1.42 (t, *J* = 7.51, 1H, -*SH*); ^{13}C NMR (75 MHz; $CDCl_3$; Me_4Si) δC 72.4, 70.5, 70.4, 70.2, 70.01, 69.0, 61.6, 33.5, 21.2; (EIMS): 247 ([M+ Na]+, 100%); HRMS: found 247.0977. Calc. mass for $C_9H_{20}O_4SNa$: 247.0980.

6.1.5 Synthesis of GAZ1, 4(benzoic acid)-4'(oxy-tri-ethylene glycol-propyl thiol)-azobenzene

6.1.5.1 Compound 6

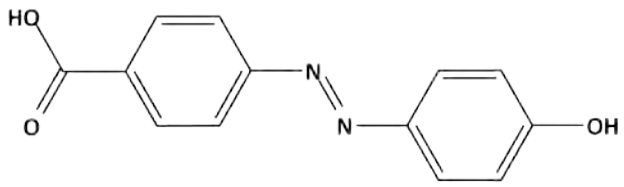

A solution of $NaNO_2$ (5.10 g, 73.91 mmol) in H_2O was added dropwise to a slurry of 4-aminobenzoic acid (10.00 g, 72.99 mmol) in HCl aqueous solution at 0 ^oC. The diazonium chloride solution was adjusted to pH 8 with saturated K_2CO_3 solution and phenol (6.90 g, 73.40 mmol) and NaOH (2.90 g, 72.50 mmol) in H_2O (40 ml) was added. The reaction mixture was further stirred for 30 min at 0 ^oC, followed adjusting pH to 6 with 1 M HCl solution. The red precipitate was filtered and washed with H_2O (100 ml). The solid was recrystallised from EtOH to yield a orange reddish precipitate (16.01 g, 90 %).

^1H NMR (300 MHz, $CDCl_3$, Me_4Si, 25 ^oC) δ_H ppm 8.09 (d, 2H, *J* = 7.92 Hz, Ar*H*), 7.85 (d, 2H, *J* = 9.36 Hz, Ar*H*), 7.83 (d, 2H, *J* = 7.92 Hz, Ar*H*), 6.94 (d, 2H, *J* = 9.36 Hz, Ar*H*); ^{13}C NMR (75 MHz, $CDCl_3$, Me_4Si, 25 ^oC) δ ppm 174.6, 162.5, 155.3, 147.6, 140.5, 131.2, 126.1, 122.7, 116.8; m/z (ESMS): 241 ($[M - H]^+$, 100%); m/z (HRMS): found 241.0609. Calc. Mass for $C_{13}H_9N_2O_3$: 241.0613.

6.1.5.2 Compound 7

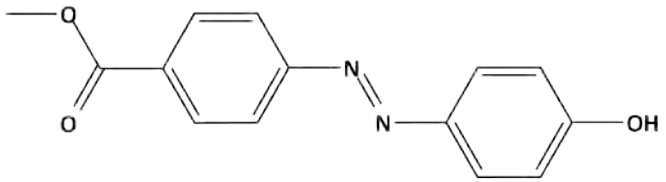

A solution of **6** (5.00 g, 20.58 mmol) and conc. H_2SO_4 (0.5 ml) in MeOH (100 ml) was refluxed overnight. The reaction mixture was allowed to cool to room temperature and concentrated *in vacuo* to ~20 ml. The organic layer was extracted with DCM (3 x 100 ml). The combined organic layers were dreied (MgSO4), filtered and solvent removed *in vacuo*. The crude product was purified by column chromatography (gradient elution; 0 to 5 % MeOH in DCM, increase in increments of 1 % after 100 ml of eluent) to yield a red solid (4.00 g, 76 %).

8.09 (d, 2H, *J* = 7.92 Hz, Ar*H*), 7.85 (d, 2H, *J* = 9.36 Hz, Ar*H*), 7.83 (d, 2H, *J* = 7.92 Hz, Ar*H*), 6.94 (d, 2H, *J* = 9.36 Hz, Ar*H*), 3.83 (s, 3H, -O*Me*); ^{13}C NMR (75 MHz, $CDCl_3$, Me_4Si, 25 ^{o}C) δ_C ppm 195.9, 166.6, 161.9, 155.3, 147.1, 131.2, 130.6, 125.2, 122.4, 115.0, 52.3; m/z (ESMS): 279 ([M + Na]$^+$, 100%); m/z (HRMS): found 279.0689. Calc. Mass for $C_{14}H_{12}N_2O_3Na$: 279.0746.

6.1.5.3 Compound 8

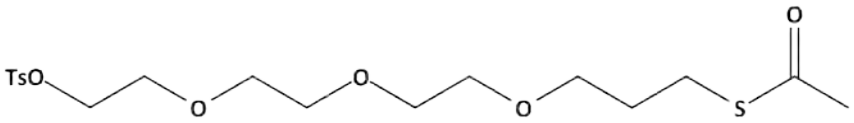

A solution of tosyl chloride (1.89 g, 9.95 mmol) in DCM (6 ml) was added dropwise to a solution of **5** (1.50 g, 6.64 mmol) and Et_3N (0.91 g, 1.25 ml, 10.00 mmol) in DCM (20 ml) at 0 ^oC and further, stirred at this temperature for 1 h, followed further stirred at room temperature overnight. The resultant mixture was allowed to cool to room temperature and washed with 1 M HCl (10 ml), 1 M $NaHCO_3$ (10 ml) and H_2O (10 ml). The organic layer was dried ($MgSO_4$), filtered and concentrated *in vacuo*. The crude oil was purified by column chromatography (gradient elution; from 0 to 25 % EtOAc in hexane, increase in increments of 5 % per 200 ml of eluent) to yield a colourless oil (1.88 g, 75 %).

^1H NMR (300 MHz, $CDCl_3$, Me_4Si, 25 ^oC) δ_H ppm 7.73 (d, 2H, *J* = 9.59 Hz, Ar*H*), 7.27 (d, 2H, *J* = 9.59 Hz, Ar*H*), 4.11-4.08 (m, 2H, -ArO*CH*$_2$-), 3.64-3.61 (m, 2H, -ArOCH$_2$*CH*$_2$O-), 3.55-3.47 (m, 8H, -O*C*$_2$*H*$_4$O-), 3.43 (t, 2H, *J* = 5.76 Hz, -O*CH*$_2$C$_2$H$_4$SAc), 2.87 (t, 2H, *J* = 7.28 Hz, -*CH*$_2$SAc), 2.38 (s, 3H, -S*Ac*), 1.82-1.74 (m, 2H, -*CH*$_2$CH$_2$SAc); ^{13}C NMR (75 MHz, $CDCl_3$, Me_4Si, 25 ^oC) δ_C ppm 195.9, 165.9, 144.8, 129.8, 128.0, 70.8, 70.6, 70.2, 69.6, 69.2, 68.7, 30.6, 29.6, 26.0, 21.6; m/z (ESMS): 443 ($[M + Na]^+$, 100%); m/z (HRMS): found 443.1160. Calc. Mass for $C_{18}H_{28}O_7S_2Na$: 443.1174.

6.1.5.4 Compound 9

A slurry of **7** (0.84 g, 3.29 mmol), **8** (1.50 g, 3.95 mmol) and K_2CO_3 in dry MeCN (50 ml) was refluxed overnight under N_2 atmosphere. The reaction mixture was allowed to cooll to room temperature and K_2CO_3 was filtered off and the filtrate was concentrated *in vacuo*. The crude product was purified by column chromatography (gradient elution; 0 to 5 % MeOH in DCM, increase in increments of 2 % after 100 ml of eluent) to yield a orange reddish solid (1.50 g, 94 %).

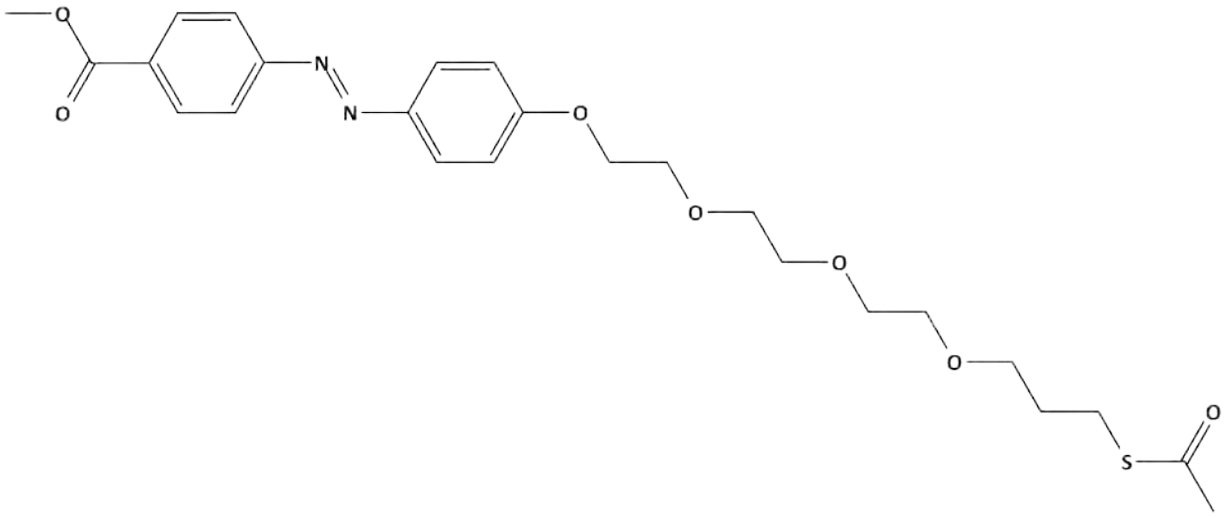

^{1}H NMR (300 MHz, $CDCl_3$, Me_4Si, 25 ^oC) δ_H ppm 8.10 (d, 2H, *J* = 8.63 Hz, Ar*H*), 7.87 (d, 2H, *J* = 9.98 Hz, Ar*H*), 7.83 (d, 2H, *J* = 8.63 Hz, Ar*H*), 6.97 (d, 2H, *J* = 9.98 Hz, Ar*H*), 4.18-4.14 (m, 2H, -ArO*CH*$_2$-), 3.88 (s, 3H, -O*Me*), 3.85-3.82 (m, 2H, -ArOCH$_2$*CH*$_2$O-), 3.70-3.55 (m, 8H, -O*C*$_2$*H*$_4$O-), 3.44 (t, 2H, *J* = 6.63 Hz, -O*CH*$_2$C$_2$H$_4$SAc), 2.87 (t, 2H, *J* = 7.23 Hz, -*CH*$_2$SAc), 2.38 (s, 3H, -S*Ac*), 1.83-1.74 (m, 2H, -*CH*$_2$CH$_2$SAc); ^{13}C NMR (75 MHz, $CDCl_3$, Me_4Si, 25 ^oC) δ_C ppm ; ^{13}C NMR (75 MHz, $CDCl_3$, Me_4Si, 25 ^oC) δ_C ppm 195.9, 166.6, 161.9, 155.3, 147.1, 131.2, 130.6, 125.2, 122.4, 115.0, 70.9, 70.8, 70.7, 70.6, 70.2, 69.6, 69.2, 68.7, 67.8, 29.6, 26.0; m/z (ESMS): 527 ([M + Na]$^+$, 100%); m/z (HRMS): found 527.1828. Calc. Mass for $C_{25}H_{32}N_2O_7SNa$: 457.1828.

6.1.5.5 Compound 10

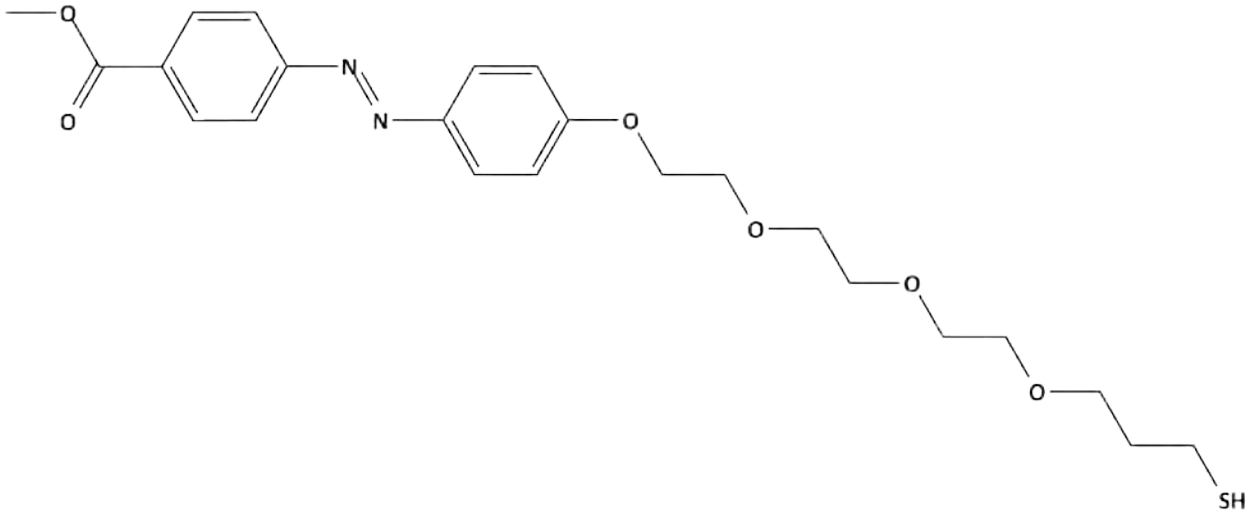

A solution of **9** (1.32 g, 2.73 mmol) and conc. HCl (1 ml) in MeOH (100 ml) was refluxed for 2 h under N_2 atmosphere. The solvent was removed *in vacuo* and purified by column chromatography (gradient elution; 0 to 20 % EtOAc in DCM, increase in increments of 5 % after 100 ml of eluent) to yield an orange reddish solid (1.00 g, 83 %).

^{1}H NMR (300 MHz, $CDCl_3$, Me_4Si, 25 ^oC) δ_H ppm 8.10 (d, 2H, *J* = 9.27 Hz, Ar*H*), 7.87 (d, 2H, *J* = 9.22 Hz, Ar*H*), 7.83 (d, 2H, *J* = 9.27 Hz, Ar*H*), 6.97 (d, 2H, *J* = 9.22 Hz, Ar*H*), 4.18-4.12 (m, 2H, -ArO*CH*$_2$-), 3.88 (s, 3H, -O*Me*), 3.85-3.82 (m, 2H, -ArOCH$_2$*CH*$_2$O-), 3.70-3.42 (m, 10H, -O*C*$_2$*H*$_4$O-, O*CH*$_2$C$_2$H$_4$SAc), 3.42 (t, 2H, *J* = 6.63 Hz, -O*CH*$_2$C$_2$H$_4$SAc), 2.55 (q, 2H, *J* = 7.75 Hz, -*CH*$_2$SH), 1.85-1.74 (m, 2H, -*CH*$_2$CH$_2$SH), 1.30 (t, 1H, *J* = 7.75 Hz, -*SH*); ^{13}C NMR (75 MHz, $CDCl_3$, Me_4Si, 25 ^oC) δ_C ppm 166.6, 161.9, 155.4, 147.1, 131.2, 130.6, 125.2, 122.4, 115.0, 70.9, 70.8, 70.7, 70.2, 69.7, 69.2, 67.8, 52.3, 33.7, 21.4; m/z (ESMS): 485 ([M + Na]$^+$, 100%); m/z (HRMS): found 485.1724. Calc. Mass for $C_{18}H_{28}N_2O_7S_2Na$: 485.1722.

6.1.5.6 Compound GAZ1

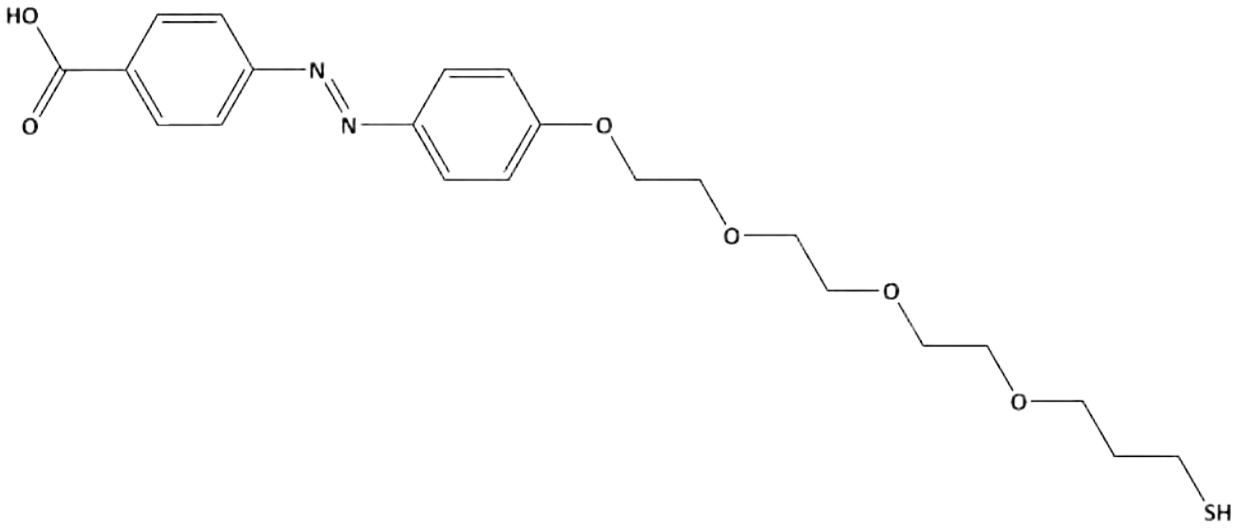

An aqueous solution of NaOH (0.14 g, 3.50 mmol) was added to a solution of **10** (0.80 g, 1.80 mmol) in MeOH (20 ml) and the resultant reaction mixture was refluxed overnight. After allowing the reaction to cool to room temperature, it was acidified with 0.1 M HCl. The resultant precipitate was collected by suction filtration and purified by column chromatography (gradient elution; 0 to 2 % EtOAc in DCM, increase in increments of 0.5 % after 100 ml of eluent) to yield an orange reddish solid, which was further recrystallised from EtOH (0.40 g, 52 %).

Elemental analysis found: C, 58.99 %; H, 6.42 %; N, 6.34 %. Calc. for $C_{22}H_{28}N_2O_6S$: C, 58.91 %; H, 6.29 %; N, 6.25 %; ^{1}H NMR (300 MHz, $CDCl_3$, Me_4Si, 25 ^oC) δ_H ppm 8.14 (d, 2H, *J* = 8.52 Hz, Ar*H*), 7.84 (d, 2H, *J* = 9.90 Hz, Ar*H*), 7.83 (d, 2H, *J* = 8.52 Hz, Ar*H*), 6.96 (d, 2H, *J* = 9.90 Hz, Ar*H*), 4.18-4.14 (m, 2H, -ArO*CH*$_2$-), 3.86-3.82 (m, 2H, -ArOCH$_2$*CH*$_2$O-), 3.71-3.49 (m, 10H, -O*C*$_2$*H*$_4$O-, -O*CH*$_2$C$_2$H$_4$SH), 2.55 (q, 2H, *J* = 7.67 Hz, -*CH*$_2$SH), 1.85-1.74 (m, 2H, -*CH*$_2$CH$_2$SAc), 1.30 (t, 1H, *J* = 7.67 Hz, -S*H*);^{13}C NMR (75 MHz, $CDCl_3$, Me_4Si, 25 ^oC) δ_C ppm 170.8, 162.0, 155.8, 147.1, 131.2, 130.4, 125.2, 122.4, 114.9, 70.9, 70.7,

70.6, 70.2, 69.6, 69.3, 67.8, 33.7, 21.4; m/z (ESMS): 447 ($[M - H]^+$, 100%); m/z (HRMS): found 447.1582. Calc. Mass for $C_{22}H_{27}N_2O_6S$: 447.1590.

6.2 Characterisation of synthesised molecular materials

The synthesised molecules were characterised by several methods which were ^1H and ^{13}C nuclear magnetic resonance (NMR) spectroscopy, mass spectrometry, infra red spectroscopy and elemental analysis.

6.2.1 Nuclear magnetic resonance spectroscopy

^1H Nuclear Magnetic Resonance (NMR) spectra were recorded on a Bruker AC 300 (300.13 MHz) spectrometer.

^{13}C NMR spectra were recorded on a Bruker AV 300 (75.5 MHz) using the pendent pulse sequences.

In both techniques all chemical shifts are calibrated to the $SiMe_4$ peak and quoted in ppm upfield of the reference. Analysis was performed in either deuterated chloroform ($CDCl_3$) or deuterated acetone $(CD_3)_2CO$. The coupling constants of ^1H NMR are expressed in Hertz (Hz) with multiplicities abbreviated as follows; s = singlet, d = doublet, t = triplet and m = multiplet.

6.2.2 Mass Spectroscopy

Mass Spectrometry was carried out by two techniques depeding on molecule: electron impact Mass Spectrometry (EI); preformed on VG Prospec and Electrospray Mass Spectrometry (ES); preformed on a Micromass Time of Flight (TOF) using methanol as the running solvent.

6.2.3 Elemental analysis

Samples were dried under vaccum for 2days pre elemental analysis. Analysis was carried out on a Carlo Erba EA 1110 (C, H, N) instrument. Reported results are an average of two samples, each composing of three experimental runs.

6.2.4 High performance liquid chromatography

Some compounds required purification by high performance liquid chromatography (HPLC). Analysis was performed using a Dionex Summit system, with a Summit UVD 170s *UV/VIS* multi-channel detector and Chromeleon software. The running solvent system was a MeCN/H_2O gradient. Analytical HPLC runs were preformed on a Luna (Phenomenex), C_{18} 250 mm x 4.6 mm ID, with a 10µm pore size column and same software/detector.

6.3 SAM preparation

SAMs were prepared on clean Au substrates from solutions of synthesied surfactants. The details of substrate preparation, as well as the general SAM formation protocol, are described below.

6.3.1 Substrate

Three different substrates were used in accordance to the requirements of each analytical technique.

Poly crystalline gold substrates employed in ellipsometry, contact angle and XPS were purchased from Georg Albert PVD, Germany. These substrates consisted of a 30nm gold layer deposited on mica covered with a thin (5 nm) titanium adhesion layer.

Poly crystalline gold substrates employed in *UV/VIS* spectroscopy were also purchased from Georg Albert PVD. These substrates were cutom made to order and consisted of a transparent 20 nm gold layer, deposited on schott NEXTERION® Glass B borosilicate glass slides, with a thin (5 nm) titanium adhesion layer.

Poly crystalline gold substrates employed in SPR were purchased from Reichert Technologies, USA. These substrates consisted of a 49 nm gold layer deposited on glass covered with a 1 nm chromiunm adhesion layer.

6.3.2 SAMs

Prior to SAM preparation all glassware and gold substrates were thoroughly cleaned, in order to remove any contaminants, using piranha solution. Piranha solution is an extremely reactive oxidising agent, which is known to spontaneously explode upon contact with organic material, making it very dangerous. Furthermore, its formation involves a highly exothermic reaction. Due to the potential danger of piranha solution, it was made in a cleaned, dried and cooled vessel, contained within an ice/water bath. Furthermore, significant care and vigilance was taken whilst using it.

6.3.2.1 Piranha solution

Piranha solution was prepared from 70% sulphuric acid by volume (Fisher scientific, analytical grade) to which 30% hydrogen peroxide was added (Fisher scientific, analytical grade)within a vessel cooled and contained within an ice/water bath.

6.3.2.2 Cleaning glassware

Glassware was cleaned using the following protocol

1. Immersion in piranha solution for 30 minutes
2. Rinsing with a large amount of ultra high quality (UHQ) water (18Ω)
3. Sonication in UHQ H_2O for 30min
4. Dried in an oven at 140°C for 1 hour
5. Sonication in EtOH for 30min
6. Dried in an oven at 140°C for 1 hour
7. Wrapped in aluminum foil in order to prevent exposure to air borne contaminants and used within 24 hours

6.3.2.3 Cleaning plastic equipment

Plastic vial lids were cleaned by rinsing with UHQ H_2O, sonicated in UHQ H_2O for 30 minutes then rinsed with HPLC EtOH and sonicated in HPLC EtOH for 30 minutes.

6.3.2.4 Substrate cleaning

Substrates were cleaned prior to use by immersion in cold piranha solution. Substrates were immersed in cooled piranha solution for 10mins. Next substrates were washed twice with ≈ 50ml of UHQ water followed by ≈ 50ml of EtOH (HPLC) before immersion in the SAM forming solution. It was ensured than substrates remained wet throughout cleaning, as to avoid contamination from the ambient laboratory environment.

6.3.2.5 General procedure for SAM formation

Immediately after cleaning in piranha solution substrates were immersed in 2.5 cm^3 of freshly prepared ethanolic (HPLC grade) surfactant solutions of 0.0625 mM concentration (made from a freshly prepared 1 mM solution). Both solutions (stock and SAM forming solution) were contained in piranha cleaned glassware. Post immersion in the SAM forming solution, SAMs were rinsed thoroughly with EtOH (HPLC grade) and dried with a stream of N_2.

6.3.2.6 Functionalisation of GAZ1 SAM with ADM.

Functionalisation of SAMs with ADM followed a well established procedure for the amidification of carboxylic acid terminated surfaces. Post SAM preparation SAMs were

washed with HPLC ethanol (100 ml) followed by UHQ H_2O (200 ml). Next they were placed immediately into a freshly prepared aqueous solution (UHQ H_2O) of NHS and EDC for 10mins, after which they were washed with UHQ H_2O (100 ml) and placed immediately into a solution of ADM for 30mins. Next SAMs were washed with UHQ H_2O (100 ml) and either dried for SPR or immersed in a ConA immobilizing solution for ellipsometry.

6.3.2.7 Immobilization of ConA on GAZ1-ADM SAM.

The protocol for ConA immobilisation depended on whether SAMs were analysed by SPR or ellipsometry. However, in both techniques SAMs were exposed to the same ConA immobilizing solution. The ConA immobilizing solution contained 0.05 mg ml^{-1} of ConA and was made up in UHQ H_2O, containing TRIS buffer, Ca^{2+} and Mn^{2+}. It was made fresh, on the day, from dry components.

For SPR, SAMs were washed and dried with a stream of $N_{2(g)}$ post ADM functionalisation. Next SAMs were immediately loaded into the SPR, for in-situ ConA immobilization studies. During SPR immobilisation SAMs were exposed to the ConA solution, for time T mins, using the general SPR protocol described in section **6.4.5**.

For ellipsometry, post SAMs were washed and dried with a stream of $N_{2(g)}$ post ADM functionalisation. Next SAMs were immediately immersed in a ConA immobilizing solution. SAMs were immersed for T mins. Next SAMs were washed with UHQ H_2O (100 ml) dried with a stream of $N_{2(g)}$ and analysed immediately, using the general SPR protocol described in section **6.4.1**.

6.4 SAM characterisation

The analytical techniques used to analyse SAMs were ellipsometry, contact angle, XPS, *UV/Vis* spectroscopy and SPR. The specifications of the equipment used are stated below along with the experimental protocols. The techniques are described in detail in chapter two.

6.4.1 Ellipsometry

Ellipsometry provided information thickness and indirect measure of tilt angle

6.4.1.1 Ellipsometry specification

The ellipsometer used is a Jobin Yvon UVISEL with a broadband xenon light source. The light source's angle of incidence and wavelength range, throughout the experiment, was 70° and 280-820nm respectively. Calibration of the ellipsometer and alignment of the polariser and detector was preformed through employment of an aluminium reference sample, with a thermally grown aluminium oxide (Al_2O_3) layer.

6.4.1.2 Ellipsometry experimental

The ellipsometric parameters, Δ and ψ, were recorded for both the clean bare substrates and for the substrates on which SAMs were formed. All measurements were made under conditions of ambient temperature, pressure and humidity.

DeltaPsi software was used to determine the film thickness. Raw data was modelled using a Cauchy transparent model over the whole data range (280-820nm). Reliability of

the model was tested/calibrated using SAMs formed from tetra-, hexa- and octa-decanethiols.

Measurements reported are an average of two independently prepared samples (or four if not in good agreement) with an average of six readings per sample, taken in different places ensuring not to take measurements on visibly defective sites.

6.4.2 Contact angle

Contact angle: provided information on surface wettability and roughness.

6.4.2.1 Contact angle specification

Measurements were preformed with UHQ H_2O on a homemade manually operated goniometer. A 25 µL gas tight syringe (Hamilton) was used to add and remove droplets to the surface, droplets were typically ≈ 15 µL. The drop was recorded with Hitachi™ Charged Coupled Device (CCD) camera, connected to a personal computer by USB in order to capture a video of the advancing and receding angles. Angles were analysed at the three phase boundary using the commercially available video analysis software FTÅ (First Ten Amstrongs) version 1.96.

6.4.2.2 Contact Angle experimental

Contact angles were determined by the dynamic Sessile drop method, using UHQ H_2O. The frame rate of video capture was 4 frames per second and 50 frames were collected. Measurements reported are an average of two independently prepared samples (or four if not in good agreement) with an average of five readings per sample, taken in

different places ensuring not to take measurements on visibly defective sites. All measurements were taken under ambient conditions of temperature, pressure and humidity. The errors reported are the standard errors of the mean.

6.4.3 X-Ray photoelectron

XPS provided information on surface composition.

6.4.3.1 X-Ray photoelectron specification

XPS spectra were obtained on the Scienta ESCA300 instrument based at the Council for the Central Laboratory of the Research Councils (CCLRC) in The National Centre for Electron Spectroscopy and Surface Analysis (NCESS) facility at Daresbury, UK. XPS experiments were carried out using a monochromatic Al Kα X-ray source (1486.7 eV) and a take-off angle of 150.

6.4.3.2 X-Ray photoelectron experimental

High-resolution scans of N (1s), S (2p), O (1s), C (1s) and Au (4f) were recorded using a pass energy of 150 eV at a step size of 0.05 eV.

Fitting of XPS peaks was performed using the *Avantage* V*2.2* processing software. Peaks were de-convoluted using the XPS spectra processing software. All peaks were fitted using a 30% Lorentzian: 70% Gaussian peaks. The sensitivity factors used were N 1s = 1.73, S 2p = 2.08, C 1s = 1.00, O 1s = 2.8, Au $4f_{7/2}$ = 9.58, Au $4f_{5/2}$ = 7.54.

6.4.4 Surface *UV/VIS* spectroscopy

UV/VIS spectroscopy provided information on absorption properties and isomerisation of azobenzene within SAMs

6.4.4.1 Surface *UV/VIS* specification

The *UV/Vis* spectrometer is a Carry 5000 with dual beam, a tungsten halogen *Vis* light source and a deuterium arc *UV* light source. The *UV/Vis* detector is a high performance R928 photomultiplier tube. Surface UV/Vis studies were performed using the

6.4.4.2 Surface *UV/VIS* experimental

Analysis was done in double beam mode using a clean gold background. Samples were prepared on purchased Au substrates. SAMs were analysed immediately after formation and subjected to a cycle of irradiation of 3 minute exposures to *UV* or *VIS* light. Between exposure to light and spectroscopic readings the samples were kept in the dark as much as possibly viable in the day.

6.4.5 Surface plasmon resonance spectroscopy

SPR provided information on absorption of ConA to the ADM fucntionalised surface

6.4.5.1 Surface Plasmon Resonance specification

The SPR used was a Reichart SR7000DC Dual Channel Spectrometer (Buffalo, NY, USA) with a 3700 Pixel linear CCD array image sensor to analyse refracted light. Data was analysed by SPR_V4017 Data Acquisition and Alignment Program.

6.4.5.2 Surface Plasmon Resonance experimental

Prior to ConA immobilization studies the baseline was equilibrated firstly with degassed ethanol (HPLC) at a rate of 100 µL min^{-1} for 15 mins, in order to remove and air bubbles. Followed by equilibration with degassed TRIS buffer at a rate of 100 µL min^{-1} for another 15mins . ConA solution (**6.3.2.7**) was injected over the SAM surface for 10 s at a 1500 µL min^{-1} and then a flow rate of 8 µL min^{-1} for the respective time (5, 15 and 30 min). The flow rate of ensures sufficient exposure time for binding to occur between the ADM SAM surface and ConA in solution. Finally and in order to remove any unbound ConA SAMs were washed with degassed TRIS buffer for 10 s at a 1500 µL min^{-1} followed by 10 mins at a flow rate of 100 µL min^{-1}. The SPR signal measured in micro response units.

7.0 Refernces

[1] J. C. Love, L.K. Estroff, J. K. Kriebel, R. G. Nuzzo, G. M. Whitesides, Self-assembled monolayers of thiolates on metals as a form of nanotechnology. *Chem. Rev.* (**2005**) 104, 1103.

[2] R. P. Feynman, There's Plenty of Room at the Bottom, An Invitation to Enter a New Field of Physics. Engineering and Science magazine, vol. XXIII, no. 5, February 1960.

[3] P. Werner, W. Zwerger, macroscopic quantum effects in nanomechanical systems, *Europhys. Lett*., (**2004**) 65, 158.

[4] C. A. Mirkin, The Beginning of a Small Revolution, *Small* (**2005**) 1, 14.

[5]B. Franklin, W.Brownrigg, Of the stilling of waves by means of Oil, *Philosophical Transactions* (**1774**), 64, 445.

[6] C. Tanford, "Ben Franklin Stilled the Waves: An Informal History of Pouring Oil on the on Water with Reflections on the Ups and Downs of Scientific Life in General." Duke University Press, Durham, NC, 1989.

[7] J. W. S. Rayleigh, On the relative contamination of the water-surface by equal quantities of different substances, *Philos. Mag*., (**1899**) 48, 321.

[8] C. P. Poole, F. J. Owens, introduction to nanotechnology (**2003**) Wiley-interscience

[9] F. Schreiber, Structure and growth of self-assembling Monolayers, *Prog. Surf. Sci.* (**2000**) 65, 151

[10] W. C. Bigelow, D. L. Pickett, W. A. Zisman, Oleophobic monolayer films adsorbed from solution in non-polar liquids, *J. Coll. Int. Sci.,* (**1946**) 1, 513.

[11] L. C. F. Blackman, M. J. S. Dewar, Promoters for the Dropwise Condensation of Steam, parts 1-4, *J. Chem. Soc.,* (**1957**) 162.

[12] J. Sagiv, Organized Monolayers by Adsorption, I . Formation and Structure of Oleophobic Mixed Monolayers on Solid Surfaces. *J. Am. Chem. Soc*., (**1980**) 102, 92.

[13] L. Netzer, J. Sagiv, A New Approach to Construction of Artificial Monolayer Assemblies, *J. Am. Chem. Soc.* (**1983**) *105,* 674.

[14] Y. Liu, L. Mu, B. Liu, J. Kong, Controlled Switchable Surface, *Chem. Eur. J.* (**2005**) 11, 2622.

[15] A. Ulman, An introduction to organic thin films from Langmuir-Blodgett to Self-Assembly (**1991**) Academic Press INC.

[16] W. A. Zisman, Relation of the Equilibrium Contact Angle to Liquid and Solid Constitution, *Adv. Chem. Ser.*, (**1964**) 43, 1.

[17] J. Lahann, S. Mitragotri, T. N. Tran, H. Kaido, J. Sundaram, I. S. Choi, S. Hoffer, G. A. Somorjai, R. Langer, A Reversibly Switching Surface, *Science,* (**2003**) *299*, 371.

[18] P.E. Laibiris, G. M. Whiteside, Self-Assembled Monolayers of *n*- Alkanethiolates on Copper are Barrier Films That Protect the Metal against Oxidation by Air, *J. Am. Chem. Soc.,* (**1992**) 114, 9022.

[19] N. Tillman, A. Ulman, J. S. Schildkraut, T. L. Renner, Incorporation of Phenoxy Groups in Self-Assembled Monolayers of Trichlorosilane Derivatives: Effects on Film Thickness, Wettability, and Molecular Orientation, *J. Am. Chem. Soc.,* (**1998**) 110, 6136.

[20] I. Markovich, D. Mandler, Preparation and characterization of octadecylsilane monolayers on indium–tin oxide (ITO) surfaces, *J. Electroanal. Chem.,* (**2001**) 500, 453.

[21] E. G. Shafrin, W. A. Zisman, The adsorption on platinum and wettability of monolayers of terminally fluorinated octadecyl derivatives, *J. Phys. Chem.*, (1957) 61, 1046.

[22] K. Oberg, P. Persson, A. Shchukarev, B. Eliasson, Comparison of monolayer films of stearicac id and methyl stearate on an Al_2O_3 surface, *Thin Solid Films,* (**2001**) 397, 102.

[23] C. Chung, M. Lee, Self-Assembled Monolayers of Mercaptoacetic Acid on Ag Powder: Characterization by FT-IR Diffuse Reflection Spectroscopy, *Bull. Korean Chem. Soc.,* (**2004**) 25, 10 1461.

[24] M.G. Badin, A. Bashir, S. Krakert, T. Strunskus, A. Terfort, C. Woll, Kinetically stable, flat-lying thiolate monolayers, *Angew. Chem. Int. Ed.* (**2007**) 46, 3762.

[25] A. Bashir, D.Käfer, J. Müller, C. Wööll, A. Terfort, G. Witte, Selenium as a Key Element for Highly Ordered Aromatic Self- Assembled Monolayers, *Angew. Chem. Int. Ed.* (**2008**) 47, 5250

[26] R. Gerlach, G. Polanski, H.-G. Rubahn, Growth of ultrathin organic films on Au (111) surfaces, *Thin Solid Films,* (**1998**) 318, 270.

[27] M. Kind, C. Woll. Organic surfaces exposed by self-assembled organothiol, monolayers: Preparation, characterization, and application. *Prog. Surf. Sci.* (**2009**) 84, 230.

[28] M. D. Porter, T. B. Bright, D. L. Allara, C. E. D. Chidsey, Spontaneously Organized Molecular Assemblies. 4. Structural Characterization of n-Alkyl Thiol Monolayers on Gold by Optical Ellipsometry, Infrared Spectroscopy, and Electrochemistry, *J. Am. Chem. Soc.,* (**1987**) 109, 3559.

[29] C. Pale-Grosdemange, E. S. Simon, K. L. Prime, G. M. Whitesides, Formation of Self-Assembled Monolayers by Chemisorption of Derivatives of Oligo(ethylene glycol) of Structure HS(CH_2)(OCH_2CH_2),0H on Gold, *J. Am. Chem.* Soc., (**1991**) *113, p*

[30] C. D. Bain, E. B. Troughton, Y. T. Tao, J. Evall, G. M. Whitesides, R. G. Nuzzo, Formation of monolayer films by the spontaneous assembly of organic thiols from solution onto gold, *J. Am. Chem. Soc.,* (**1989**) 111, 321.

[31] M. Kind, C. Wöll, Organic surfaces exposed by self-assembled organothiol monolayers: Preparation, characterization, and application, *Prog. Surf. Sci.* (**2009**), 84, 230.

[32] H. Wolf , E. Delamarche, T. Takami, H. Kang, B. Michel, Ch. Gerber, M. Jaschke, H. J. Butt, E. Bamberg, H. Ringsdorf, End-Group-Dominated Molecular Order in Self-Assembled Monolayers, *J. Phys. Chem.* (**1995**) *99,* 7102.

[33] T. M. Willey, A. L. Vance, C. Bostedt, T. van Buuren, R. W. Meulenberg, L. J. Terminello, C. S. Fadley, Surface Structure and Chemical Switching of Thioctic Acid Adsorbed on Au(111) As Observed Using Near-Edge X-ray Absorption Fine Structure, *Langmuir* (**2004**) 20, 4939.

[34] J.Lahann, R. Langer, Smart Materials with Dynamically Controllable Surfaces, *MRS bulletin* (**2005**) 30, 185.

[35] J.-P. Sauvage, Molecular Machines and Motors (Structure and Bonding), Springer publishing, 2001.

[36] L.H. Dubois, R.G. Nuzzo, Synthesis, Structure, and Properties of Model Organic Surfaces, *Annu. Rev. Phys. Chem.* (**1992**) 43, 437.

[37] P. Harder, M. Grunze, R. Dahint, G. M. Whitesides, P. E. Laibinis, Molecular conformation in Oligo (ethylene glycol) -Terminated Self-Assembled Monolayers on Gold and Silver Surfaces Determines Their Ability To Resist Protein Adsorption, *J. Phys. Chem.B.,* (**1998**) 102, 426.

[38] S.-C. Chang, I. Chao, Y.-T. Tao, Structure of Self-Assembled Monolayers of Aromatic-Derivatized Thiols on Evaporated Gold and Silver Surfaces: Implication on Packing Mechanism, *J. Am. Chem. Soc.,* (**1994**) 116, p???

[39] P. E. Laibinis, G. M. Whitesides, D. L. Allara, Y. Tao, A. N. Parikh, R. G. Nuzzo, Comparission ot the structures and wetting properties of self-assembled monolayers of n-alkanethiols on the coinage metal surfaces, Cu, Ag, Au. *J.Am. Chem. Soc.* (**1991**) 113, 7152.

[40] M. A. Bryant, J. E. Pemberton, Surface Raman scattering of self-assembled monolayers formed from 1-alkanethiols: behavior of films at Au and comparison to films at Ag. *J.Am. Chem. Soc.* (**1991**) 113, 8284.

[41] G. M. Whitesides, X. Jiang, E. Ostuni, R. G. Chapman, M. Grunze, SAMs and Biofunctional Surfaces: the “Inert Surface” problem, Polymer Preprints, (**2004**) 45, 90.

[42] P. Harder, M. Grunze, and R. Dahint, G. M. Whitesides, P. E. Laibinis, Molecular Conformation in Oligo(ethylene glycol)-Terminated Self-Assembled Monolayers on Gold and Silver Surfaces Determines Their Ability To Resist Protein Adsorption, *J. Phys. Chem. B* (**1998**) *102,* 426.

[43] S. Herrwerth, W. Eck, S. Reinhardt, M. Grunze, Factors that Determine the Protein Resistance of Oligoether Self-Assembled Monolayers - Internal Hydrophilicity, Terminal Hydrophilicity, and Lateral Packing Density, *J. Am. Chem. Soc.* (**2003**) 125, 9359.

[44] C. Vericat, M.E. Vela, G.A. Benitez, J.A.M Gago, X. Torrelles, Surface characterization of sulfur and alkanethiol self-assembled monolayers on Au (111), *J. Phys. Condens. Matter*. (**2006**) 18, R867.

[45] R. Doering, Y. Nishi, Handbook of semiconductor manufacturing technology, 2 nd ed. (**2007**) CRC press: Dallas, USA,

[46] H. 0. Finklea, L. R. Robinson, A. Blackburn, B. Richter, D. Allara, T. Bright, Formation of an Organized Monolayer by Solution Adsorption of Octadecyltrichlorosilane on Gold: Electrochemical Proper ties and Structural Characterization, *Langmuir* (**1986**) 2, 239

[47] S. Onclin, B. J. Ravoo, D. N. Reinhoudt, Engineering silicon oxide surfaces using self-assembled monolayers, *Angew. Chem. Int. Ed.* (**2005**) 44, 6282.

[48] D. L. Allara, A. N. Parikh, F. Rondelez, Evidence for a Unique Chain Organization in Long Chain Silane Monolayers Deposited on Two Widely Different Solid Substrates, *Langmuir* (**1995**) 11, 2357.

[49] F. Schreiber, Self-assembled monolayers: from 'simple' model systems to biofunctionalized interfaces, *J. Phys. Condens. Matter.* (**2004**) 16, R881.

[50] Y, Han, K, Uosaki, Effects of concentration and temperature on the formation process of decanethiol self-assembled monolayer on Au(111) followed by electrochemical reductive desorption, *Electrochimica. Acta.* (**2008**) 53, 6196.

[51] T. W. Schneider, D. A. Buttry, Electrochemical Quartz Crystal Microbalance Studies of Adsorption and Desorption of Self-Assembled Monolayers of Alkyl Thiols on Gold, *J. Am. Chem. Soc*. (**1991**),*115,* 12391.

[52] H.Wang, S. Chen, L. Li, S. Jiang, Improved Method for the Preparation of Carboxylic Acid and Amine Terminated Self-Assembled Monolayers of Alkanethiolates, *Langmuir*, (**2005**) 21,
2633

[53] A. Ulman, Formation and Structure of Self-Assembled Monolayers, *Chem. Rev*. (**1996**) 96, 1533.

[54] M. C. Leopold, E. F. Bowden, Influence of Gold Substrate Topography on the Voltammetry of Cytochrome *c* Adsorbed on Carboxylic Acid Terminated Self-Assembled Monolayers, *Langmuir,* (**2002**)18, 2239-2245

[55] R. H. Terrill, T. A. Tanzer, P. W. Bohn, Structural Evolution of Hexadecanethiol Monolayers on Gold during Assembly: Substrate and Concentration Dependence of Monolayer Structure and Crystallinity, *Langmuir* (**1998**)14, 845.

[56] H. Min, J. –W. Park, H. K. Shon, D. W. Moon, T. G. Lee, ToF-SIMS study on the cleaning methods of Au surface and their effects on the reproducibility of self-assembled monolayers, *Appl. Surf. Sci*., (**2008**) 255, 1025.

[57] C. Vericat, M. E. Vela, G. Benitez, P. Carrob and R. C. Salvarezza, Self-assembled monolayers of thiols and dithiols on gold: new challenges for a well-known system, *Chem. Soc. Rev*., (**2010**) 39, 1805.

[58] E. Torres, A. T. Blumenau,* and P. U. Biedermann, Mechanism for phase transitions and vacancy island formation in alkylthiol/Au(111) self-assembled monolayers based on adatom and vacancy-induced reconstructions, *Physical Review B* (**2009**) 79, 075440.

[59] E. Torres, A. T. Blumenau, and P. U. Biedermann, Steric and Chain Length Effects in the (√3 X √3) R30° Structures of Alkanethiol Self-Assembled Monolayers on Au(111), *ChemPhysChem* (**2011)** 12, 999.

[60] J. C. Love, L.K. Estroff, J. K. Kriebel, R. G. Nuzzo, G. M. Whitesides, Self-assembled monolayers of thiolates on metals as a form of nanotechnology. *Chem. Rev.* (**2005**) 104, 1103.

[61] B. Lussem, L. Muller-Meskamp, S. Karthauser, and R. Waser, A New Phase of the c(4 x 2) Superstructure of Alkanethiols Grown by Vapor Phase Deposition on Gold. *Langmuir* (**2005**) 21, 5256.

[62] R. L. Whetten, R. C. Price, Nano-Golden Order, *Science* (**2007**) 318, 407 – 408.

[63] D. Losic, J. G. Shapter, J. J. Gooding, Mapping of defects in self-assembled monolayersby polymer decoration, *J. Solid State Electr*. (**2005**) 9, 512.

[64] D. Losic, J.G. Shapter, J. J. Gooding, Integrating polymers with alkanethiol self-assembled monolayers (SAMs): blocking SAM defects with electrochemical polymerisation of tyramine, *Electrochem. Commun.* (**2002**) 4, 953.

[65] V. T. Moy, D. J. Keller, H. E. Gaub, H. M. McConnell, Long-Range Molecular Orientational Order in Monolayer Solid Domains of Phospholipid *J. Phys. Chem.* (**1986**) *90,* 3202.

[66] N. Aubry, P. Singh, M. Janjua, S. Nudurupati, Micro- and nanoparticles self-assembly for virtually defect-free, adjustable monolayers, *P. Natl. Acad. Sci. USA,* (**2008**) 105, 3711.

[67] F. Shi, P. Sharma, D. J. Kouri, F. Hussain, G.H. Gunaratne, Nanostructures with long-range order in monolayer self-assembly, *Phys. Rev.* (**2008**) 78, 25203.

[68] H. Kang, N.-S. Lee, E. Ito, M. Hara, J. Noh, Formation and Superlattice of Long-Range-Ordered Self-Assembled Monolayers of Pentafluorobenzenethiols on Au(111), *Langmuir* (**2010**) 26, 2983.

[69] C. D. Bain, G. M. Whitesides, Modelling Organic Surfaces with Self-Assembled Monolayer, Angew. Chem. Int. Ed Engl. (**1989**)28, 506.

[70] R. G. Chapman, E. Ostuni, L. Yan, G. M. Whitesides, Preparation of Mixed Self-Assembled Monolayers (SAMs) That Resist Adsorption of Proteins Using the Reaction of Amines with a SAM That Presents Interchain Carboxylic Anhydride Groups *Langmuir* (**2000**) *16,* 6927.

[71] Y. Montagut, J. Vi. García, Y. Jiménez, C. March, Á. Montoya, A. Arnau, Biosensors – Emerging Materials and Applications, chapter 9: QCM technology in bio sensors, InTech publishing, (**2001**) 167.

[72] J. P. Folkers, P. E. Laibinis, G. M. Whitesides, Self-Assembled Monolayers of Alkanethiols on Gold:Comparisons of Monolayers Containing Mixtures of Shortand Long-chain Constituents with CH3 and CH_2OH Terminal Groups, *Langmuir* (**1992**) 8, 133

[73] D. Bu, T. J. Mullen, G.-Y. Liu, Regulation of Local Structure and Composition of Binary Disulfide and Thiol Self-Assembled Monolayers Using Nanografting., ACS Nano, (**2010**) 4, 6863.

[74] M. Mrksich, Using self-assembled monolayers to model the extracellular matrix, Acta Biomater. (**2009**) 5, 832.

[75] Herrwerth, Sascha, Eck, Wolfgang. Reinhardt, Sven. Grunze, Michael. Factors that Determine the Protein Resistance of Oligoether Self-Assembled Monolayers - Internal Hydrophilicity, Terminal Hydrophilicity, and Lateral Packing Density, *J. Am. Chem. Soc.,* (**2003**) 125, 9359.

[76] Y.-Y. Luk, M. Kato, M. Mrksich, Self-Assembled Monolayers of Alkanethiolates Presenting Mannitol Groups Are Inert to Protein Adsorption and Cell Attachment, *Langmuir* (**2000**) *16,* 9604.

[77] E. Ostuni, R. G. Chapman, M. N. Liang, G. Meluleni, G. Pier, D. E. Ingber, G. M. Whitesides, Self-Assembled Monolayers That Resist the Adsorption of Proteins and the Adhesion of Bacterial and Mammalian Cells, *Langmuir* (**2001**) *17,* 6336-.

[78] R. L. C. Wang, H. J. Kreuzer, M. Grunze, Molecular Conformation and Solvation of Oligo(ethylene glycol)-Terminated Self-Assembled Monolayers and Their Resistance to Protein Adsorption, *J. Phys. Chem. B* (**1997**) *101,* 9767.

[79] Benjamin T. Houseman and Milan Mrksich, The Role of Ligand Density in the Enzymatic

Glycosylation of Carbohydrates Presented on Self-Assembled Monolayers of alkanethiolates on Gold, *Angew. Chem. Int. Ed*. (**1999**) 38, 782.

[80] P. M. Mendes, Stimuli-responsive surfaces for bio-applications, Chem. Soc. Rev., (**2008**) 37, 2512.

[81] R. Valiokas, M. Östblom, S. Svedhem, S. C. T. Svensson, B. Liedberg, Temperature-Driven Phase Transitions in Oligo(ethylene glycol)-terminated Self-Assembled Monolayers, *J. Phys. Chem. B,* (**2000**) 104, 7565.

[82] Prime, K. L.; Whitesides, G. M. Adsorption of Proteins onto Surfaces Containing End-Attached Oligo(ethylene oxide): A Model System Using Self-Assembled Monolayers, *J. Am. Chem. Soc.* (**1993**) *115*, 10714.

[83] S. Balamurugan, L. K. Ista, J. Yan, Gabriel P. Lopez, J. Fick, M. Himmelhaus, M. Grunze, Reversible Protein Adsorption and Bioadhesion on Monolayers Terminated with Mixtures of Oligo(ethylene glycol) and Methyl Groups. *J. Am. Chem. Soc*., (**2005**) 127, 14548.

[84] K. L. Prime, G. M. Whitesides, Adsorption of Proteins onto Surfaces Containing End-Attached Oligo(ethylene oxide): A Model System Using Self-Assembled Monolayers *J. Am. Chem. Soc.* (**1993**) 115, 10714.

[85] H. M. Zareie, C. Boyer, V. Bulmus, E. Nateghi, T. P. Davis, Temperature-Responsive Self-Assembled Monolayers of Oligo(ethylene glycol): Control of Biomolecular Recognition, ACS nano (**2008**) 2, 757.

[86] F. Auer, B. Sellergren, A. Swietlow, A. Offenhäuser, Self-Assembled Layers of Bisbenzamidines on Gold, *Langmuir* (**2000**) 16, 5936.

[87] J. H. Collier, M. Mrksich, Engineering a biospecific communication pathway between cells and electrodes, Proc. Natl. Acad. Sci. U. S. A., (**2006**) 103, 2021.

[88] P. M. Mendes, K. L. Christman, P. Parthasarathy, E. Schopf, J. Ouyang, Y. Yang, J. A. Preece, H. D. Maynard, Y. Chen and J. F. Stoddart, Electrochemically Controllable Self-Assembly of Proteins : Spatial Surface Bioconjugation, *Bioconjugate Chem.,* (**2007**) 18, 1919.

[89] W. S. Yeo, M. Mrksich, Electroactive Substrates that Reveal Aldehyde Groups for Bio-Immobilization, Adv. Mat., (**2004**) 16, 1352.

[90] M. N. Yousaf, B. T. Houseman, M. Mrksich, Turning On Cell Migration with Electroactive
Substrates, *Angew. Chem. Int. Ed.* (**2001**) 40, 1093.

[91] M. N. Yousaf, M. Mrksich, Diels-Alder Reaction for the Selective Immobilization of Protein to Electroactive Self-Assembled Monolayers *J. Am. Chem. Soc.* (**1999**) *121,* 4286.

[92] M. N. Yousaf, B. T. Houseman, M. Mrksich, Using electroactive substrates to pattern the attachment of two different cell populations, *Proc. Natl. Acad. Sci. U. S. A*., (**2001**) 98, 5992.

[93] W. S. Yeo, C. D. Hodneland, M. Mrksich, Electroactive monolayer substrates that selectively release adherent cells. *Chembiochem*., (**2001**) 2, 590.

[94] M. Curreli, C. Li, Y. H. Sun, B. Lei, M. A. Gundersen, M. E. Thompson and C. W. Zhou, Selective functionalization of In_2O_3 Nanowire Mat Devices for Biosensing Applications, *J. Am. Chem. Soc.,* (**2005**) 127, 6922.

[95] E. W. L. Chan, M. N. Yousaf, Immobilization of Ligands with Precise Control of Density to Electroactive Surfaces, *J. Am. Chem. Soc.,* (**2006**) 128,15542.

[96] W.-S. Yeo, M. N. Yousaf, M. Mrksich, Dynamic Interfaces between Cells and Surfaces: Electroactive Substrates that Sequentially Release and Attach Cells, *J. Am. Chem. Soc.,* (**2003**) 125, 14994.

[97] J. Lahann, S. Mitragotri, T.-N. Tran, H. Kaido, J. Sundaram, I. S. Choi, S. Hoffer, G. A. Somorjai, R. Langer, A Reversibly Switching Surface, Science, (**2003**) 299, 371.

[98] L. Mu, Y. Liu, S. Y. Cai and J. L. Kong, A Smart Surface in a Microfluidic Chip for Controlled Protein Separation, *Chem. Eur. J*., (**2007**) 13, 5113.

[99] C. L. Yeung, P. Iqbal, M. Allan, M. Lahkor, J. A. Preece, P.M. Mendes, Tuning specific biomolecular interactions using electro-switcahble oligopeptide surfaces, Adv. Funct. Mater. (**2010**) 20, 2657.

[100] U. Rant, K. Arinaga, S. Scherer, E. Pringsheim, S. Fujita, N. Yokoyama, M. Tornow, G. Abstreiter, Switchable DNA interfaces for the highly sensitive detection of label-free DNA targets, *Proc. Natl. Acad. Sci. USA*., (**2007**) 104, 17364.

[101] R. Blonder, E. Katz, I. Willner, V. Wray, A. F. Bückmann, Application of a Nitrospiropyran-FAD-Reconstituted Glucose Oxidase and Charged Electron Mediators as Optobioelectronic Assemblies for the Amperometric Transduction of Recorded Optical Signals: Control of the "*On*"-"*Off*" Direction of the Photoswitch, *J. Am. Chem. Soc.* (**1997**) 119, 11747.

[102] N. Katsonis, T. Kudernac, M. Walko, S. J. van der Molen, B. J. van Wees, B. L. Feringa, Reversible Conductance Switching of Single Diarylethenes on a Gold Surface, *Adv. Mater.* (**2006**) *18*, 1397.

[103] M. O. Wolf, M. A. Fox, Photochemistry and Surface Properties of Self-Assembled Monolayers of cis- and trans-4-Cyano-4'-(10-thiodecoxy)stilbene on Polycrystalline Gold, J. . Am. Chem. Soc., (1995) 117, 1845.

[104] F. Hamelmanna, U. Heinzmanna, U. Siemelingb, F. Bretthauerb, J. Vor der Brüggen, Light-stimulated switching of azobenzene-containing self-assembled monolayers, *Appl. Surf. Sci*., (**2004**) 222, 1.

[105] H. Akiyama, K. Tamada, J. Nagasawa, K. Abe, T. Tamaki, Photoreactivity in Self-Assembled Monolayers Formed from Asymmetric Disulfides Having para-Substituted Azobenzenes, *J. Phys. Chem. B.*, (**2003**) 107, 130.

[106] S. Sortino, S. Petralia, S. Conoci, S. Di Bella, Monitoring photoswitching of azobenzene-based self-assembled monolayers on ultrathin platinum films by UV/Vis spectroscopy in the transmission mode, *J. Mater. Chem*., (**2004**) 14, 811.

[107] K. Tamada, H. Akiyama, T.-X. Wei, S.-A. Kim, Photoisomerization Reaction of Unsymmetrical Azobenzene Disulfide Self-Assembled Monolayers: Modification of Azobenzene Dyes to Improve Thermal Endurance for Photoreaction, *Langmuir* (**2003**) *19,* 2306.

[108] M. Han, D. Ishikawa, T. Honda, E. Ito, M. Hara, Light-driven molecular switches in azobenzene self-assembled monolayers: effect of molecular structure on reversible photoisomerization and stable cis state, *Chem. Commun*., (**2010**) 46, 3598.

[109] T. Weidner, F. Bretthauer, N. Ballav, H. Motschmann, H.Orendi, C. Bruhn, U.Siemeling, M. Zharnikov, Correlation between the Molecular Structure and Photoresponse in Aliphatic Self-Assembled Monolayers with Azobenzene Tailgroups, *Langmuir,* (**2008**) *24,* 11691.

[110] U. Siemeling, C. Bruhn, F. Bretthauer, M. Borg, F. Träger, F. Vogel, W. Azzam, M. Badin, T. Strunskus, C. Wöll, Photoresponsive SAMs on gold fabricated from azobenzene-functionalised asparagusic acid derivatives, *Dalton Trans.*, (**2009**) 40, 8593.

[111] S. Zarwell, K. Rück-Braun, Synthesis of an azobenzene-linker-conjugate with tetrahedrical shape, *Tetrahedron Lett.* (**2008**) 49, 4020.

[112] M. Ito, T. X. Wei, P.-L. Chen, H. Akiyama, M. Matsumoto, K. Tamadab, Y. Yamamoto, A novel method for creation of free volume in a one-component self-assembled monolayer. Dramatic size effect of para-carborane, *J.Mater.Chem.,* (**2005**) 15, 478.

[113] F. Callari, S. Petraliab, S. Sortino, Highly photoresponsive monolayer-protected gold clusters by self-assembly of a cyclodextrin–azobenzene-derived supramolecular complex, *Chem. Commun.,* (**2006**) 42, 1009.

[114] F. L. Callari, S. Sortino, ‘‘Catch-and-release’’ of porphyrins by photoswitchable self-assembled monolayers*, J.Mater.Chem.,* (**2007**) 17, 4184.

[115] F. L. Callari, S. Petralia, S. Conoci and S. Sortino, Light-triggered DNA release by dynamic monolayer films, *New J. Chem.,* (**2008**) 32, 1899.

[116] D. Liu, Y. Xie, H. Shao, X. Jiang, Using Azobenzene-Embedded Self-Assembled Monolayers To Photochemically Control Cell Adhesion Reversibly, *Angew. Chem. Int. Ed*. (**2009**) 48, 4406.

[117] K. G. Yager, C. J. Barrett, Novel photo-switching using azobenzene functional materials*. J. Photochem. Photobio. A.* (**2006**) 182, 250.

[118] L. Ahlström, S. Amon, L. Mathiasson, Standard addition - A way of improving quantification of banned azo dyes in leather *J. Sep. Sci*. (**2005**) 28, 2407.

[119] K. Ichimura, S. –K. Oh, M. Nakagawa, Light-driven motion of liquids on a photoresponsive surface. *Science*, (**2000**) 288, 1624.

[120] V. Ferri, M. Elbing, G. Pace, M. D. Dickey, M. Zharnikov, P. Samor, M. Mayor, M. A. Rampi, Light-Powered Electrical Switch Based on Cargo-Lifting Azobenzene Monolayers, *Angew. Chem. Int. Ed.* (**2008**) 47, 3407 –3409

[121] G. Füchsel, T. Klamroth, J. Dokić, P. Saalfrank, On the Electronic Structure of Neutral and Ionic Azobenzenes and Their Possible Role as Surface Mounted Molecular Switches, *J. Phys. Chem. B* (**2006**) *110,* 16337.

[122] G. Tiberio, L. Muccioli, R. Berardi, and C. Zannoni, How Does the Trans–Cis Photoisomerization of Azobenzene Take Place in Organic Solvents? *ChemPhysChem*, (**2010**) 11, 1018.

[123] N. Tamai, and H. Miyasaka, Ultrafast Dynamics of Photochromic Systems, *Chem. Rev.,* (**2000**) 100, 1875.

[124] H. Satzger, C. Root, and M. Braun, Excited-State Dynamics of trans- and cis-Azobenzene after UV Excitation in the Band, *J. Phys. Chem. A*, (**2004**) 108, 6265.

[125] P. Cattaneo and M. Persico, An abinitio study of the photochemistry of azobenzene, *Phys. Chem. Chem. Phys.,* (**1999**) 1, 4739.

[126] Christina R. Crecca and Adrian E. Roitberg, Theoretical Study of the Isomerization Mechanism of Azobenzene and Disubstituted Azobenzene Derivatives *J. Phys. Chem. A,* (**2006**) 110, 8188.

[127] Y. Douab, Y. Hua, S. Yuanac, W. Wua, H. Tanga, Detailed mechanism of trans–cis photoisomerization of azobenzene studied by semiclassical dynamics simulation, Molecular Physics (2009)107, 181.

[128] C. M. Stuart, R. R. Frontiera, R. A. Mathies, Excited-State Structure and Dynamics of *cis*- and *trans*-Azobenzene from Resonance Raman Intensity Analysis, *J. Phys. Chem. A*, (**2007**) 111, 12072.

[129] A. Shaabani, M. Zahedi, Semiempirical molecular orbital calculation of azobenzene: stability study of isomers and mechanism of E/Z isomerization, J. Mol. Struct-Theochem., (**2000**) 506, 257.

[130] E. W.-G. Diau. A New Trans-to-Cis Photoisomerization Mechanism of Azobenzene on the S1(n,ð*) Surface. *J. Phys. Chem. A* (**2004**) 108, 950.

[131] A. Cembran, F. Bernardi, M. Garavelli, L. Gagliardi, G. Orlandi, On the Mechanism of the *cis-trans* Isomerization in the Lowest Electronic States of Azobenzene: S0,S1, and T1, *J. Am. Chem. Soc* (**2004**) 126, 3234.

[132] R. Cimiraglia, H. J. Hofmann, Rotation and inversion states in thermal *E/Z* isomerization of aromatic azo compounds, chem. phys. Let. (**1994**) 217, 430.

[133] F. Hamelmann, U. Heinzmann, U. Siemeling, F. Bretthauer, J. Vor der Brüggen, Light-stimulated switching of azobenzene-containing self-assembled monolayers, Applied Surface Science (**2004**) 222, 1.

[134] W. Freyera, D. Bretea, R. Schmidta, C. Gahla, R. Carleya, M. Weinelt, Switching behavior and optical absorbance of azobenzene-functionalized alkanethiols in different environments. . *J. Photochem. Photobio. A.* (**2009**) 204, 102.

[135] R. Schmidt, E. McNellis, W. Freyer, D. Brete, T. Gießel, C. Gahl, K. Reuter, M. Weinelt Azobenzene-functionalized alkanethiols in self-assembled monolayers on gold. Appl. Phys. A. (**2008**) 93, 267.

[136] S. D. Evans, S. R. Johnson, H. Ringsdorf, L. M. Williams, H. Wolf, Photoswitching of Azobenzene Derivatives Formed on Planar and Colloidal Gold Surfaces, *Langmuir*, (**1998**) 14, 6436.

[137] C. Gahl, R. Schmidt, D. Brete, E. R. McNellis, W. Freyer, R. Carley, K. Reuter, M. Weinelt, Structure and Excitonic Coupling in Self-Assembled Monolayers of Azobenzene-Functionalised Alkanethiols, *J. Am. Chem. Soc.* (**2010**) 132, 8131.

[138] H. G. Tompkins, E. A. Irene, Handbook of Ellipsometry, (**2005**) Springer-Verlag GmbH & Co. publishing

[139] D. Gonçalves, E. A. Irene, fundamentals and applications of spectroscopic ellipsometry, *Quin. Nova,* (**2002**) 25, 794.

[140]R. J. Good, Contact angle, wetting, and adhesion: a critical review, *J. Adhes. Sci. Technol.*, (**1992**) 6, 1269.

[141] M. Strobel, C. S. Lyons , An Essay on Contact Angle Measurements*, Plasma Process. Polym*., (**2011**) 8, 8.

[142] M. Müller, C. Oehr, Comments on ‘‘An Essay on Contact Angle Measurements’’ by Strobel and Lyons, *Plasma Process. Polym*. (**2011**) 8, 19.

[143] J.Drelich, J. D. Miller, R. J. Good, The Effect of Drop (Bubble) Size on Advancing and Receding Contact Angles for Heterogeneous and Rough Solid Surfaces as Observed with Sessile-Drop and Captive-Bubble Techniques, J. Colloid Interf. Sci.(**1996**) 179, 37.

[144] L. M. Lander, L. M. Siewierski, W.J. Brittain, E. A. Voglert, A Systematic Comparison of Contact Angle Methods, *Langmuir* (**1993**) 9, 2237.

[145] J. F. Moulder, W. F.Stickle, P. E. Sobol, K. D. Bomben, Handbook of X-ray Photoelectron Spectroscopy, (**1992**) Perkin-Elmer Corp, Eden Prairie, MN, USA.

[146] A. S. Duwez, Exploiting electron spectroscopies to probe structure and organization of self-assembled monolayer: a review, *J. Electron Spectrosc*., (**2004**) 134, 97.

[147] P. Atkins, the elements of physical chemistry, (**2001**), Oxford University Press, chapter 14.

[148] P. Atkins, the elements of physical chemistry (**2001**), Oxford University Press, chapter 18.

[149] C. – W. Li , M. Benjamin, G. korshin, Use of UV Spectroscopy To Characterize the Reaction between NOM and Free Chlorine, *Environ. Sci. Technol*. (**2000**) 34, 2570.

[150] S. Attal, R. Thiruvengadathan, O. Regev. Determination of the Concentration of Single-Walled Carbon Nanotubes in Aqueous Dispersions Using UV-Visible Absorption Spectroscopy, *Anal. Chem.* (**2006**) 78, 8098.

[151] I. K. Lednev,T,. –Q. Ye, R. E. Hester, J. N. Moore, Femtosecond Time-Resolved UV-Visible Absorption Spectroscopy of *trans*-Azobenzene in Solution, *J. Phys. Chem.* (**1996**) *100,* 13338.

[152] Mitsuo Kira,* Toyotaro Maruyama, Chizuko Kabuto, Keisuke Ebata, and Hideki Sakurai* Stable Tetrakis(trialkylsily1)disilenes; Synthesis, X-Ray Structures, and UV/VIS Spectra. *Angew. Chem. Int. Ed* (**1994**) 33, 1489.

[153] S. B. Nielsen, A. Lapierre, J. U. Andersen, U.V. Pedersen, S. Tomita, L. H. Andersen, Absorption Spectrum of the Green Fluorescent Protein Chromophore Anion *In Vacuo,* Phys Rev Lett., 87, 228102.

[154] IUPAC Compendium of chemical terminology, (**1997**) 2nd edition

[155] J. Homola, S. S. Yee, G. Gauglitz, Surface Plasmon resonance sensors: review, Sensor actuator B-Chem, (**1999**) 54, 3.

[156] K. Tamada, H. Akiyama, T. X. Wei, Photoisomerization Reaction of Unsymmetrical Azobenzene Disulfide Self-Assembled Monolayers Studied by Surface Plasmon Spectroscopy: Influences of Side Chain Length and Contacting Medium, *Langmuir* (**2002**) *18,* 5239.

[157] J. Matsui, K. Akamatsu, N. Hara, D. Miyoshi, H. Nawafune, K. Tamaki, N. Sugimoto, SPR Sensor Chip for Detection of Small Molecules Using Molecularly Imprinted Polymer with Embedded Gold Nanoparticles, *Anal. Chem.* (**2005**) 77, 4282.

[158] J. M. Brockman, B. P. Nelson, R. M. Corn, Surface Plasmon Resonance Imaging Measurements of Ultrathin Organic Films, *Annu. Rev. Phys. Chem*. (**2000**) 51, 41.

[159] K. Lee, F. Pan, G. T. Carroll, N. J. Turro, J. T. Koberstein, Photolithographic Technique for Direct Photochemical Modification and Chemical Micropatterning of Surfaces, *Langmuir* (**2004**) *20,* 1812.

[160] P. Iqbal, K. Critchley, J. Bowen, D. Attwood, D. Tunnicliffe, S. D. Evans, J. A. Preece, Fabrication of a nanoparticle gradient substrate by thermochemical manipulation of an ester functionalized SAM, J. Mater. Chem., (**2007**) 17, 5097.

[161] A. S. Kumar, T. Ye, T. Takami, B. –C. Yu, A. K. Flatt, J. M. Tour, P. S. Weiss, Reverisible Photo-Switching of Single Azobenzne Molecules in Controlled Nanosacle Environments, *Nano Lett*., (**2008**) 8, 1644.

[162] F. Hamelmanna, U. Heinzmanna, U. Siemeling, F. Bretthauerb, J. Vor der Brüggen, Light-stimulated switching of azobenzene-containing self-assembled monolayers, *Appl. Surf. Sci*. (2004) 222, 1.

[163] X. Song, J. Perlstein, D.G. Whitten**,** Supramolecular Aggregates of Azobenzene Phospholipids and Related Compounds in Bilayer Assemblies and Other Microheterogeneous Media: Structure, Properties, and Photoreactivity, *J. Am. Chem. Soc.* (**1997**) *119,* 9144.

[164]K. Taniike, T. Matsumoto, T. Sato, Y. Ozaki, K. Nakashima, K. Iriyama, Spectroscopic studies on phase transitions in Langmuir-Blodgett films of a azobenzene-containing long-chain fatty acid: dependence of phase transitions on the number of monolayers and transistion cycles among H-, J-, and J'-aggregates inn multilayer films. *J. Phys. Chem*., (**1996**) 100, 15508.

[165] K. Tamada, J. Nagasawa, F. Nakanishi, K. Abe, T. Ishida, M. Hara, and W. Knoll, Structure and Growth of Hexyl Azobenzene Thiol SAMs on Au(111), *Langmuir* (**1998**) *14,* 3264.

[166] T. W. Schneider, D. A. Buttry, Electrochemical Quartz Crystal Microbalance Studies of Adsorption and Desorption of Self-Assembled Monolayers of Alkyl Thiols on Gold*, J. Am. Chem. Soc.* (**1993**) 115, 12391.

[167] D. J. Lavrich, S. M. Wetterer, S. L. Bernasek, G. Scoles, Physisorption and Chemisorption of Alkanethiols and Alkyl Sulfides on Au(111), *J. Phys. Chem. B* (**1998**) *102,* 3456.

[168] E. R. McNellis, J. Meyer, K. Reuter, Azobenzene at coinage metal surfaces: Role of dispersive van der Waals interactions, *Phys. Rev. B*,. (**2009**) 80, 205414.

[169] H. –L. Zhang, J. Zhang, H.-Y. Li, Z.-F. Liu, H.-L. Li, Structural investigation of a new series of azobenzene-containing self-assembled monolayers on gold, Mat. Sci. Eng. C., (**1999**) 9, 179.

[170] X. Wen, R. W. Linton, F. Formaggio, C. Toniolo, E. T. Samulski, Self-Assembled Monolayers of Hexapeptides on Gold: Surface Characterization and Orientation Distribution Analysis, *J. Phys. Chem. A* (**2004**) *108,* 9673.

[171] M. D. Porter, T. B. Bright, D. L. Allara, C. E. D. Chidseyi, Spontaneously Organized Molecular Assemblies. 4. Structural Characterization of n-Alkyl Thiol Monolayers on Gold by Optical Ellipsometry, Infrared Spectroscopy, and Electrochemistry, *J. Am. Chem. Soc.,* (**1987**) 109, 3559.

[172] C. D. Bain, E. B. Troughton, Y.-T. Tao, J. Evall, G. M. Whitesides, R. *G.* Nuzzo, Formation of Monolayer Films by the Spontaneous Assembly of Organic Thiols from Solution onto Gold, *J. Am. Chem. Soc.,* (**1989**) 111, 321.

[173] C. Yan, A. Golzhauser, M. Grunze, Ch. Woll, Formation of alkanethiolate self-assembled monolayers on oxidised gold surfaces, *Langmuir*, (**1999**) 15, 2414.

[174] M. Onoue, M.R. Han, E. Ito, M. Hara, Step-wise decomposition process of azobenzene self-assembled monolayers, *Surf. Sci*. (**2006**) 600, 3999.

[175] T. M. Willey, A. L. Vance, C. Bostedt, T. van Buuren, R. W. Meulenberg, L. J. Terminello, C. S. Fadley, Surface Structure and Chemical Switching of Thioctic Acid Adsorbed on Au(111) As Observed Using Near-Edge X-ray Absorption Fine Structure, *Langmuir* (**2004**) 20, 4939.

[176] P. Mendes, M. Belloni, M. Ashworth, C.Hardy, K.Nikitin, D. Fitzmaurice, K. Critchley, S. Evans, J. Preece, A Novel Example of X-Ray-Radiation-Induced Chemical Reduction of an Aromatic Nitro-Group-Containing Thin Film on SiO_2 to an Aromatic Amine Film, ChemPhysChem, (2003) 4, 884.

[177] M. Zharnikov, S. Frey, K. Heister, M. Grunze, Modification of Alkanethiolate Monolayers by Low Energy Electron Irradiation: Dependence on the Substrate Material and on the Length and Isotopic Composition of the Alkyl Chains, *Langmuir* (**2000**) *16,* 2697.

[178] T. Laiho, J.A. Leiro, J. Lukkari, XPS study of irradiation damage and different metal–sulfur bonds in dodecanethiol monolayers on gold and platinum surfaces, Appl. Surf. Sci. (**2003**) 212, 525.

[179] M. Himmelhausa, I. Gaussa, M. Bucka, F. Eiserta, C. Wöll, M. Grunze, Adsorption of docosanethiol from solution on polycrystalline silver surfaces: an XPS and NEXAFS study, *J. Electron. Spectrosc*.(**1998**) 92, 139.

[180] J. Polčák, J. Čechal, P. Bábor, M. Urbánek, S. Průša, T. Šikola, Angle-resolved XPS depth profiling of modeled structures: testing and improvement of the method, *Surf. Interface Anal.* (**2010**) *42*, 649.

[181] D. J. Lavrich, S. M. Wetterer, S. L. Bernasek, G. Scoles, Physisorption and Chemisorption of Alkanethiols and Alkyl Sulfides on Au(111), *J. Phys. Chem. B*, (**1998**) 102, 3456.

[182] M. W. J. Beulen, B. –H. Huisman, P. A. van der Heijden, F. C. J. M. van Veggel, M. G. Simons, M. E. F. Biemond, P. J. de Lange, D. N. Reinhoudt, Evidence for Nondestructive Adsorption of Dialkyl Sulfides on Gold, *Langmuir*, (**1996**) 12, 6170.

[183] H.A. Biebuyck, C. D. Bain, G. M. Whitesides, Comparison of Organic Monolayers on Polycrystalline Gold Spontaneously Assembled from Solutions Containing Dialkyl Disulfides or Alkanethiols, *Langmuir*, (**1994**) 10, 1825.

[184] P. Fenter, A. Eberhardt, P. Eisenberger, Self-Assembly of n-Alkyl Thiols as Disulfides on Au (111), *Science*, (**1994**) 266, 1216.

[185] D. G. Castner , B. D. Ratner, Biomedical surface science: Foundations to frontiers, Surf. Sci. (**2002**) 500, 28.

[186] M. Mrksich, G. M. Whitesides, Using self-assembled monolayers to understand the interactions of man-made surfaces with proteins and cells, Annu. Rev. Biophys. Biomol. Struct. (**1996**) 25, 55.

[187] N. J. Sniadecki, R. A. Desai, S. A. Ruiz, C. S. Chen, Nanotechnology for Cell–Substrate Interactions, Annals of Biomedical Engineering (**2005**).

[188] W. Senaratne, L. Andruzzi, C. K. Ober, Self-Assembled Monolayers and Polymer Brushes in Biotechnology: Current Applications and Future Perspectives, Biomacromolecules (**2005**) 6, 2427.

[189] L. Ding, W. Cheng, X. Wang, S. Ding, H. Ju, Carbohydrate Monolayer Strategy for Electrochemical Assay of Cell Surface Carbohydrate. *J.Am. Chem. Soc.* (**2008**) 130, 7224.

[190] C.R. Bertozzi, L.L. Kiessling, Chemical Glycobiology**,** *Science* (**2001**) 291, 2357.

[191] M. Inatani, F. Irie, A. S. Plump, M, Tessier-Lavigne, Y. Yamaguchi, Mammalian Brain Morphogenesis and Midline Axon Guidance Require Heparan Sulfate, *Science* (**2003**) *302*, 1044.

[192]K. T. Pilobello, L. K. Mahal, *Curr. Opin. Chem. Biol.* (**2007**) *11*, 1.

[193] H. Lis, N. Sharon, Lectins: Carbohydrate-Specific Proteins That Mediate Cellular Recognition, *Chem. Rev*. (**1998**) 98, 637.

[194] A. Pashov, S. MacLeod, R. Saha, M. Perry, T. C. VanCott, T. Kieber-Emmons, Concanavalin A binding to HIV envelope protein is less sensitive to mutations in glycosylation sites than monoclonal antibody 2G12, *Glycobiology* (**2005**) 15, 994.

[195] J. Lahann, S. Mitragotri, T. –N. Tran, H. Kaido, J. Sundaram, I. S. Choi, S. Hoffer, G. A. Somorjai, R. Langer, A Reversibly Switching Surface, *Science*, (**2003**) 299, 371.

[196] N. Faucheux, R. Schweiss, K. Lützow, C. Werner, T. Groth, Self-assembled monolayers with different terminating groups as model substrates for cell adhesion studies Biomaterials (**2004**) 25, 2721.

[197] C. D. Bain, G. M. Whitesides, A study by contact angle of the acid-base behavior of monolayers containing .omega.-mercaptocarboxylic acids adsorbed on gold: an example of reactive spreading, *Langmuir* (1989) 5, 1370.

[198] K. R. Yoon, Y. S. Chi, K –B. Lee, J. K. Lee, D. J. Kim, Y. –J. Koh, S. –W. Joo, W. S. Yund, I. S. Choi, Surface-initiated, ring-opening polymerization of *p*-dioxanone from gold and silicon oxide surfaces, *J. Mater. Chem*., (**2003**) 13, 2910.

[199] M. D. Porter, T. B. Bright, D. L. Allara, C. E. D. Chidsey, Spontaneously Organized Molecular Assemblies. 4. Structural Characterization of n-Alkyl Thiol Monolayers on Gold by Optical Ellipsometry, Infrared Spectroscopy, and Electrochemistry, *J. Am. Chem. Soc.,*(**1987**) 109, 3559.

[200] X. Qian, S. J. Metallo, I. S. Choi, H. Wu, M. N. Liang, G. M. Whitesides, Arrays of Self-Assembled Monolayers for Studying Inhibition of Bacterial Adhesion, *Anal. Chem.* (**2002**) 74, 1805.

[201] G. Pace, V. Ferri, C. Grave, M. Elbing, C. von Hänisch, M. Zharnikov, M. Mayor, M. A. Rampi, P. Samorı, Cooperative light-induced molecular movements of highly ordered azobenzene self-assembled monolayers, *P. Natl. Acad. Sci. USA* (**2007**) 104, 9937.

[202] D. Gustina, E. Markava,I. Muzikante, B. Stiller, L. Brehmer, Photoisomerisation Process of Selfassembled Monolayers of Some Novel Azobenzenes, *Adv. Mater. Opt. Electron.*(**1999**) 9, 245.

[203] N. Delorme, J.-F. Bardeau, A. Bulou, F. Poncin-Epaillard, Azobenzene-Containing Monolayer with Photoswitchable Wettability, *Langmuir* (**2005**) 21, 12278.

[204] J. Huang, J. C. Hemminger, Photooxidation of thiols in self-assembled monolayers on gold, *J. Am. Chem. Soc* **1993**, 115, 3342.

Oh my days…finally finished, what a experience this was….

8.0 Appendix

8.1 Appendix I - Solution *UV/Vis* spectra

UV/Vis spectra of TAZ1 and SAZ1 in solution

The solution *UV/VIS* spectra TAZ1 and SAZ1 (**Figure 8.1**) were conducted in order to establish λ_{max}, isobestic points and the reversibility (with respect to trans-cis isomerisation) of both surfactants. TAZ1 was shown to have an absorption corresponding to the *trans* $\pi - \pi^*$ excitation at λ_{max} =328 nm and SAZ1 at λ_{max} = 358 nm, the difference in λ_{max} may be attributed to the different substitution patterns between surfactants. Both peaks were depleted upon *UV* radiation (360 nm) to give the characteristic *cis* spectra. Upon irradiation with *vis* radiation (440 nm) TAZ1 spectra returned to its non-irradiated state, while SAZ1 did not completely, indicating that some of the *cis* isomer remains populated.

The solution *UV/Vis* absorption spectra of GAZ1 at a solution concentration of 0.0625 mM was also conducted and compared to TAZ1 and SAZ1. λmax was found to be 356 nm, 328 and 358 nm respectively (**Figure 8.2**)

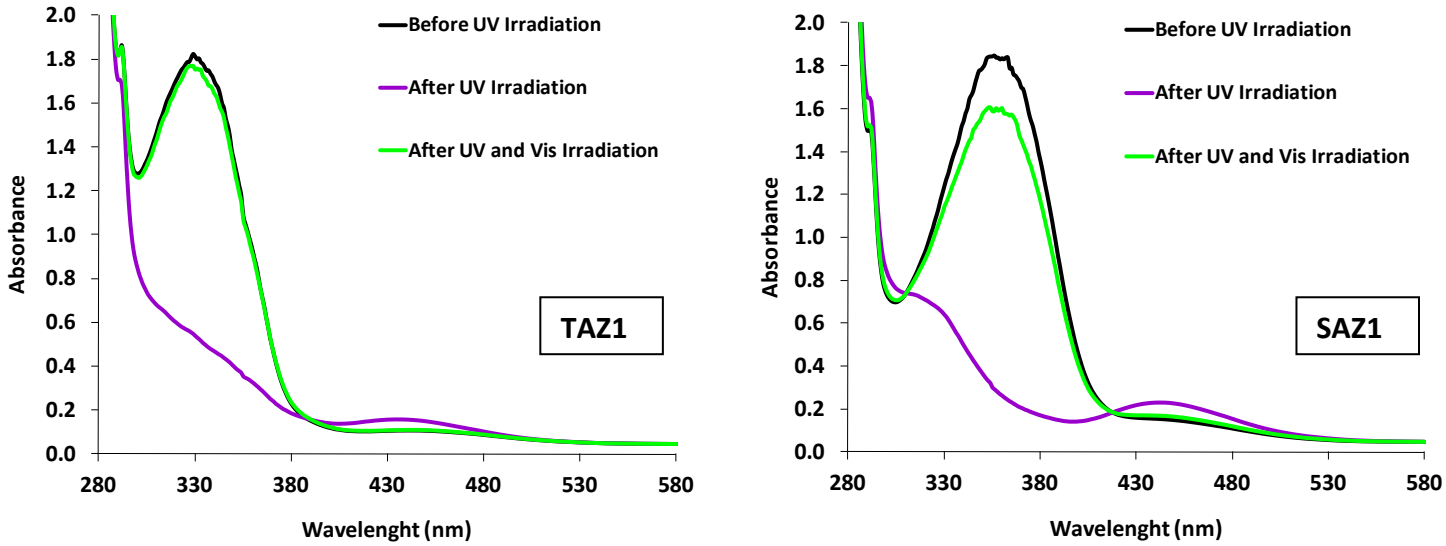

Figure 8.1 Solution *UV/Vis* spectra of TAZ1 and SAZ1 showing spectra pre irradiation and post irradiation with *UV* (360 nm) and *vis* (440 nm) respectively.

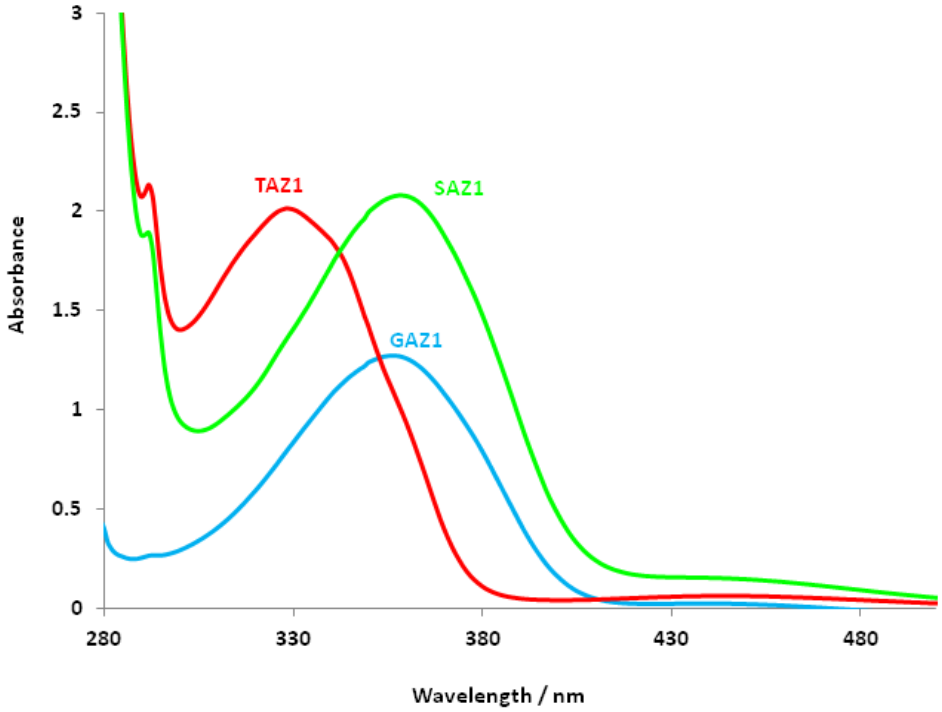

Figure 8.2 Solution *UV/Vis* spectra of SAM surfactants TAZ1, SAZ1 and GAZ1.

8.2 Appendix II - SAM irradiation time

The irradiation time used was 3 mins, this was found to be sufficient to isomerise azobenzene SAMs (**Figure 8.3**).

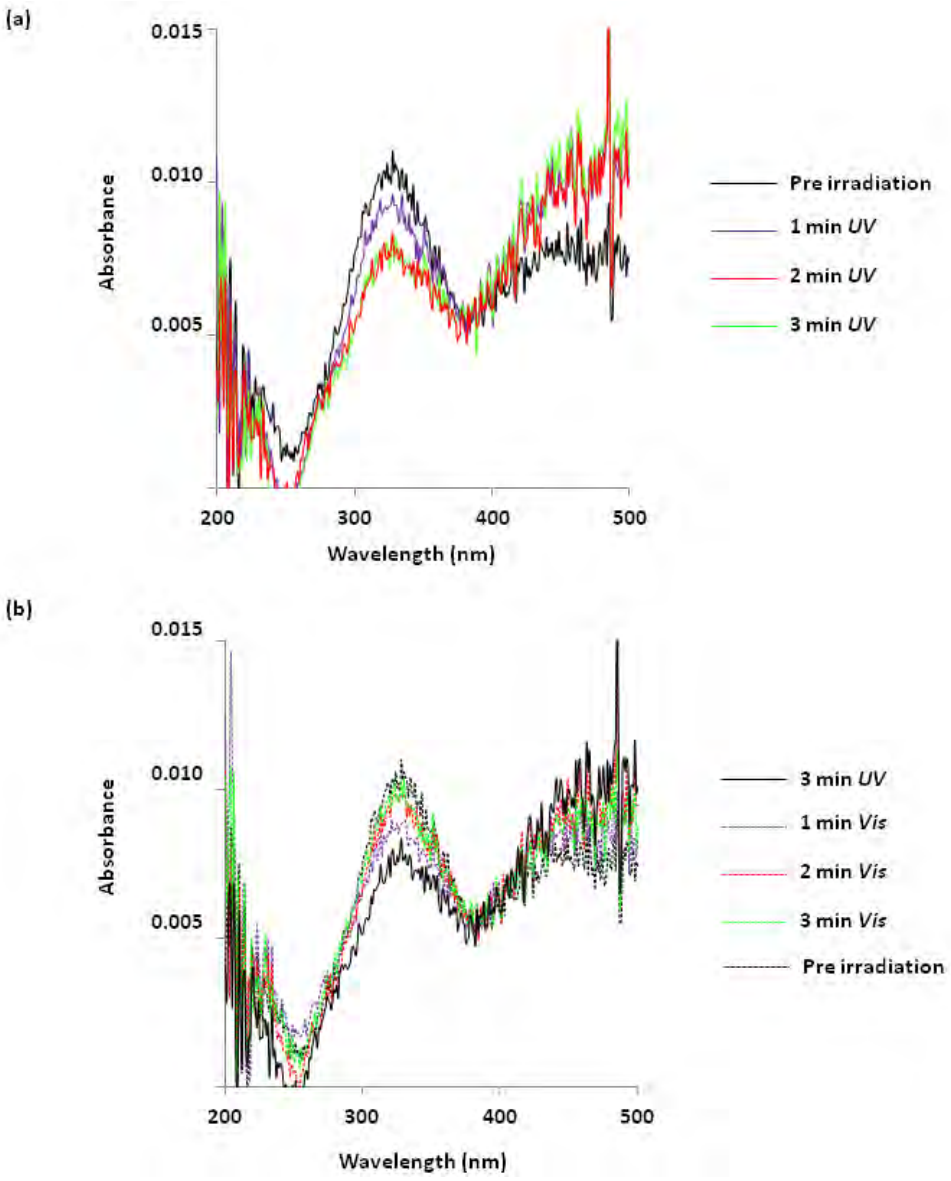

Figure 8.3 Surface UV/Vis spectra of TAZ1 SAMs formed over 24 hrs (a) irradiation with UV light at 360 nm (b) irradiation with Vis light at 440 nm.

8.3 Appendix III – The surface *UV/Vis* spectra of TAZ1 and SAZ1 SAMs as a function of SAM formation time.

The surface UV/Vis spectra of TAZ1 SAMs as a function of time can be seen below in **Figure 8.4** (0.5 – 3 hrs) and **8.5** (6 – 24 hrs). The spectra exhibit three formation regions, defined by formation time, and corresponding to the regions seen in contact angle and ellipsometry.

Region I: Corresponds to the formation times 0.5 – 6 hrs. Generally samples within region I showed optical activity atypical of azobenzene. λ_{max} was hypsochromically shifted and irradiation with *UV* increased absorption, while exposure to *Vis* light had little further effect, suggesting that irradiation induces aggregation.

Region II: Corresponds to the formation times 6 -21 hrs. Three spectra were recorded at 12hrs. At 12hrs, two samples exhibited a small degree of isomerisation while the third did not. All λ_{max} was hypsochromically shifted.

Region III: Corresponds to the formation time over 21 hrs. Three spectra were recorded at 24 hrs. At 24 hours, all spectra exhibited reversible isomerisation and λ_{max} was equal to the solution value (328nm **appendix I**). However, azobenzene does not undergo complete isomerisation, suggesting that there are still spatial constraints restricting isomerisation of some surfactants.

Overall the optical activity of TAZ1 SAMs increases with increasing formation time. Increase in optical activity is accompanied by a loss of aggregation, as is reflected in the

shifts in λ_{max}. However, despite the loss of aggregation not all surfactants are able to isomerise due to reaming spatial constraints.

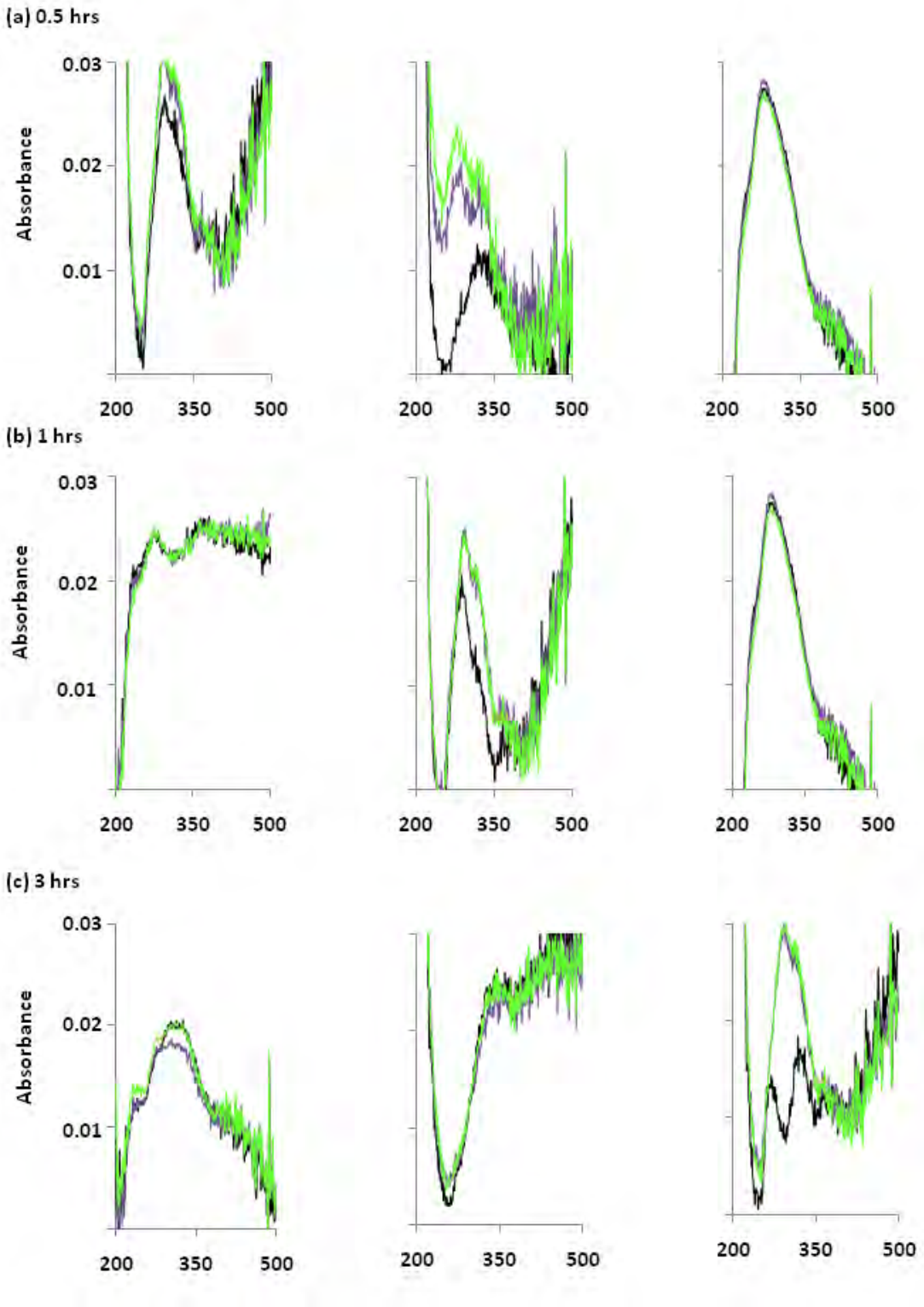

Figure 8.4 TAZ1 SAM UV/Vis spectra as a function of time 0.5 – 3 hrs.

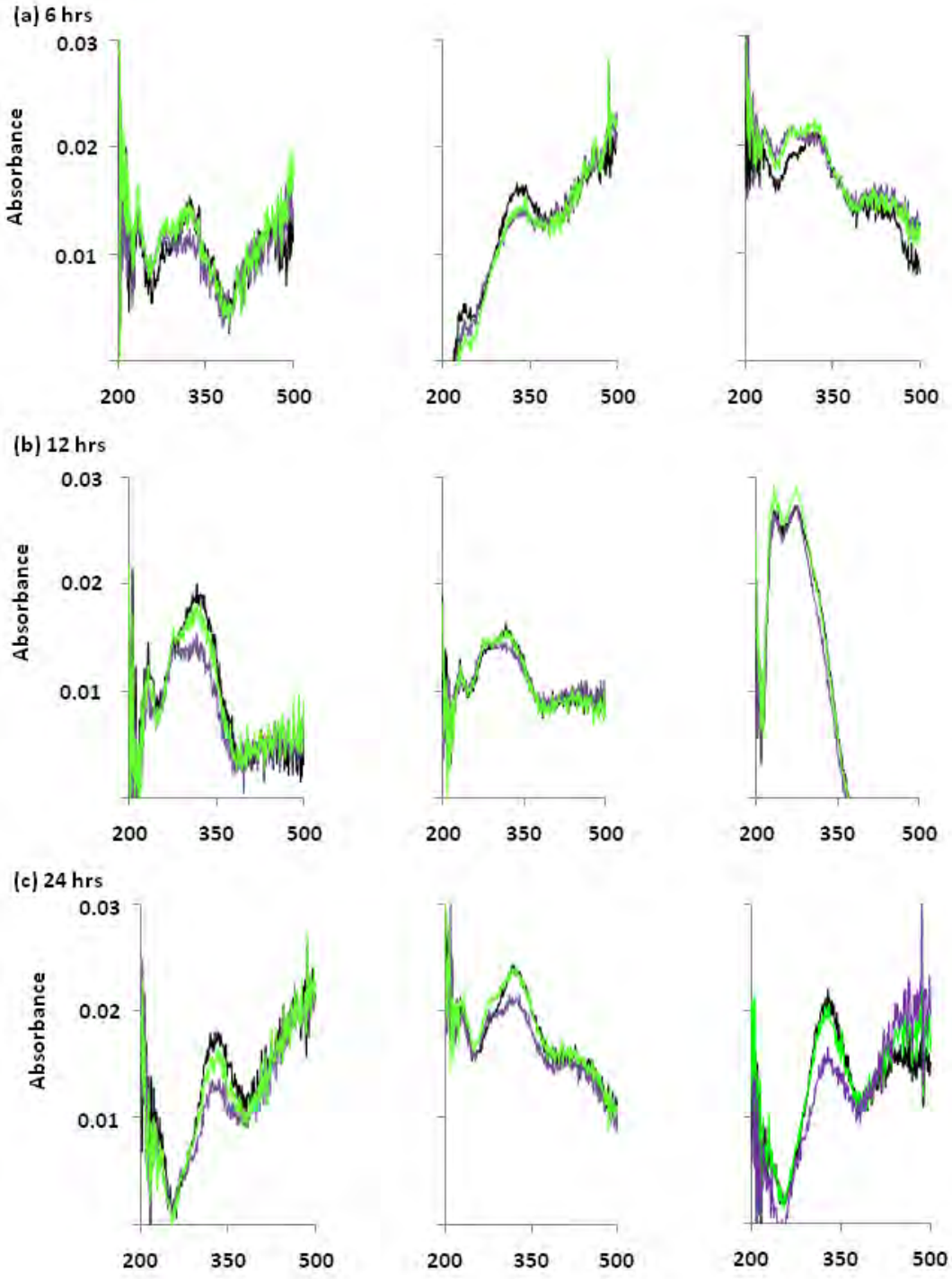

Figure 8.5 TAZ1 SAM UV/Vis spectra as a function of time 6 – 24 hrs.

The surface UV/Vis spectra of SAZ1 SAMs as a function of time can be seen below in **Figure 8.6** (0.5 – 3 hrs) and **8.7** (6 – 24 hrs).The SAZ1 *UV/Vis* spectra generally exhibit two absorption peaks one corresponding to the aggregated surfactants at ≈ 270 nm and non-aggregated surfactants at ≈ 360 nm.

At formation times 0.5 – 3 hr λ_{max} was generally ≈ 270 nm . SAMs showed optical activity non typical of azobenzene isomerisation, with an increase in absorption about λ_{max} upon exposure to UV light and exposure to *Vis* light having little further effect. Although, some samples did show typical behaviour at ≈ 360 nm corresponding to non-aggregated surfactants, however it was accompanied by an increase in absorption at ≈ 270 nm.

Between 6 - 24 hrs formation time, λ_{max} was generally ≈ 360 nm and exposure to *UV* resulted in a decrease in the absorption of this peak which was reversible by irradiation with *Vis*. However, irradiation also caused a non-reversible increase in absorption at ≈ 270 nm, corresponding to aggregated surfactants, which consequently became λ_{max}. This non-reversible increase in absorption at ≈ 270 nm suggests that SAZ1 SAMs are unstable with respect to *UV* irradiation, which induces aggregation of surfactants.

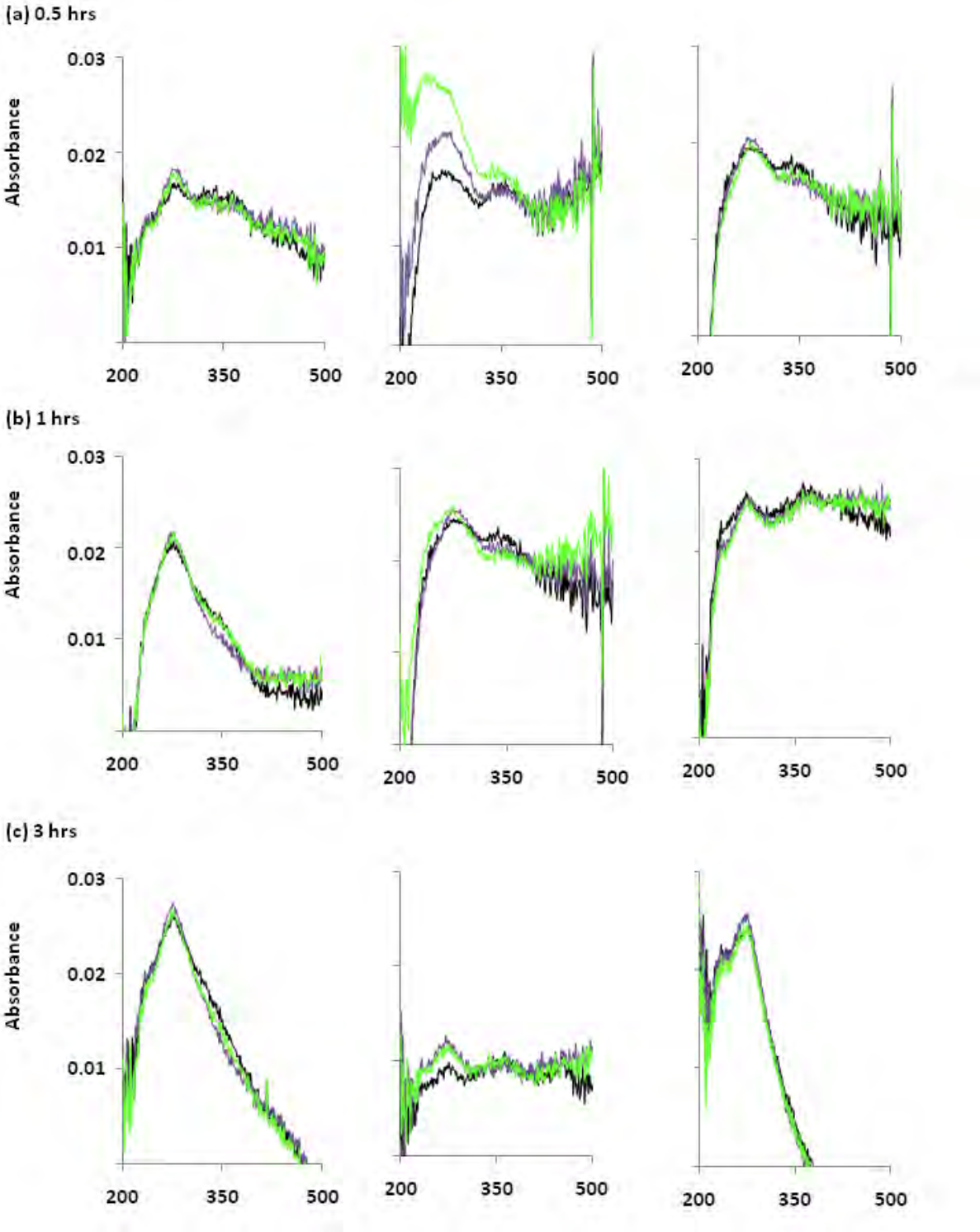

Figure 8.6 TAZ1 SAM UV/Vis spectra as a function of time 0.5 – 3 hrs.

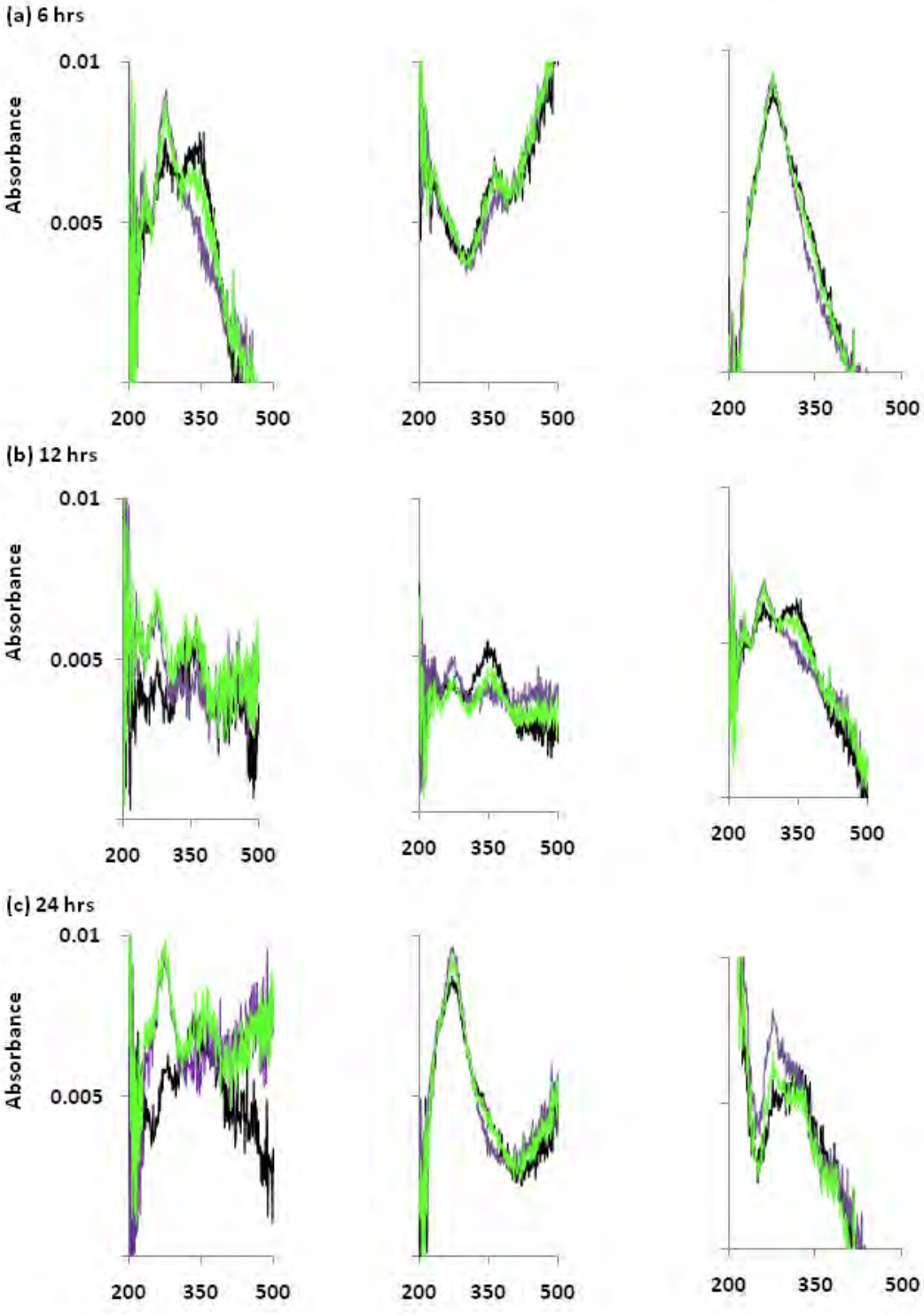

Figure 8.7 SAZ1 SAM UV/Vis spectra as a function of time 6 – 24 hrs.